SCIENCE & TECHNOLOGY

ARS JOURNAL

A PUBLICATION OF THE AMERICAN ROCKET SOCIETY

FORMERLY JET PROPULSION

LOS ANGELES PUBLIC LIBRARY

APR 22 1959

BIND

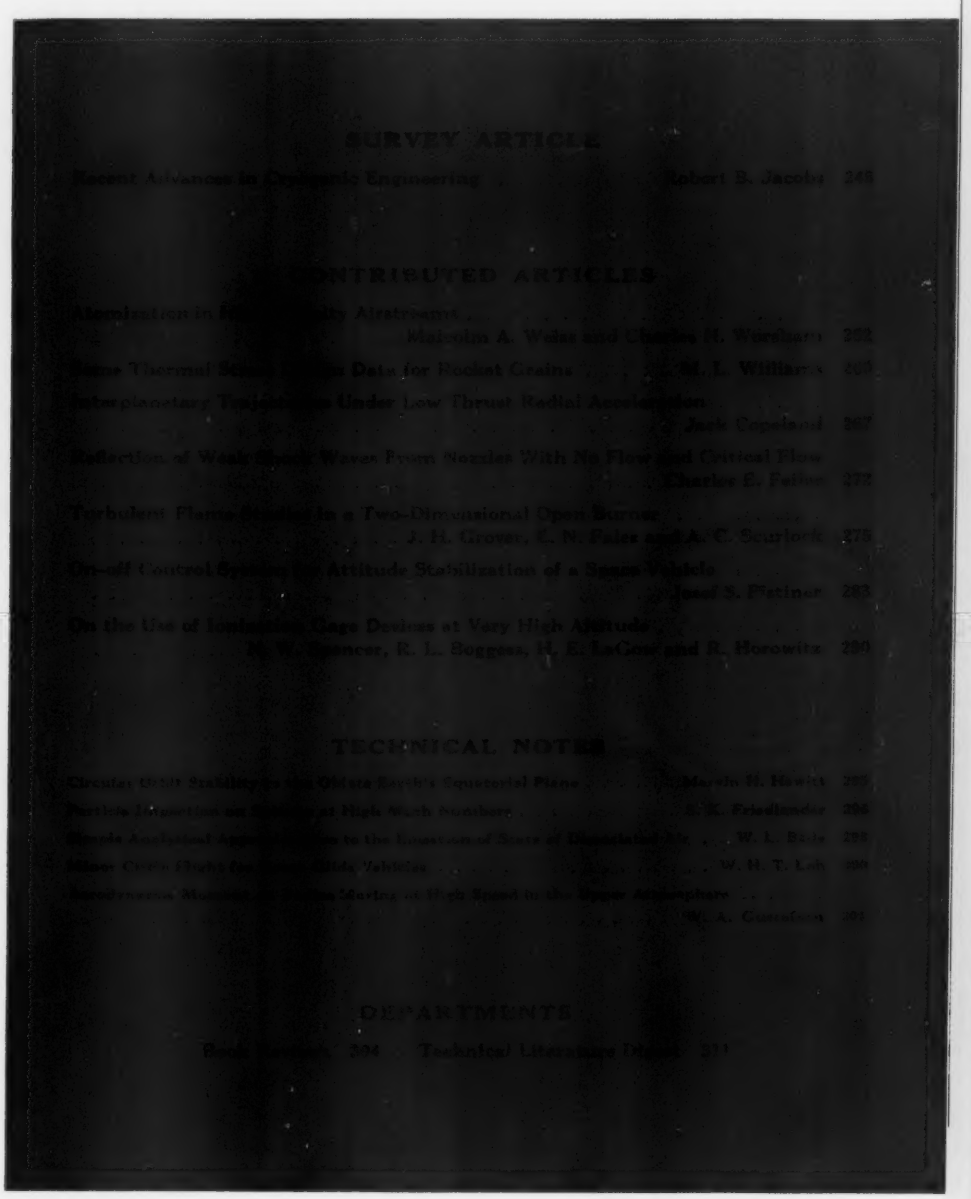

SURVEY ARTICLE

Recent Advances in Cryogenic Engineering ..... Robert B. Jacobs 243

CONTRIBUTED ARTICLES

Atomization in Rocket Gravity Airstream ..... Malcolm A. Weiss and Charles H. Worsham 252

Some Thermal Safety Design Data for Rocket Grains ..... M. L. Williams 267

Interplanetary Trajectories Under Low Thrust Radial Acceleration ..... Jack Copeland 267

Reflection of Weak Shock Waves From Nozzles With No Flow and Critical Flow ..... Charles E. Feiler 272

Turbulent Flame Spreading in a Two-Dimensional Open Burner ..... J. H. Grover, E. N. Fales and A. C. Scurlock 275

On-off Control Systems for Attitude Stabilization of a Space Vehicle ..... Josef S. Pfeiffer 283

On the Use of Ionization Gage Devices at Very High Altitudes ..... M. W. Spencer, R. L. Boggess, H. E. LaGow and R. Horowitz 290

TECHNICAL NOTES

Circular Orbit Stability in the Orbital Equatorial Plane ..... Marvin H. Hewitt 295

Particle Trajectories on Slender Cones at High Mach Numbers ..... S. C. Freidlander 296

Missile Aerodynamic Appendages Applied to the Limitation of Skew of Dispersion Ellipse ..... W. L. Black 298

Minor Orbit Perturbations of Satellite Vehicles ..... W. H. T. Loh 300

Spectroscopic Measurements of Shock Waves at High Speed in the Upper Atmosphere ..... W. A. Gustafson 301

DEPARTMENTS

Book Reviews 304 Technical Literature Digest 311

April 1959 Volume 29 Number 4

THIOKOL AT ELKTON MARYLAND

ROCKETS FOR SAFETY · ROCKETS FOR DEFENSE · ROCKETS FOR RESEARCH

On a 300 acre site in Maryland, Thiokol's Elkton Division pursues advanced programs of basic and applied rocket research, development and production.

In current production are rockets for low altitude cockpit ejection systems. One such device — powered with a Thiokol rocket — has been instrumental in saving life in two emergencies.

Nucleus of Thiokol's rocket team was organized at Elkton in 1948. *Recruit*, solid propellant rockets for "Operation Farside" and *Cajun*, for upper atmosphere research, are marked milestones in Elkton's progress.

Equipped with the most modern laboratory, production and testing facilities...the Elkton Division is engaged in the development of advanced rocket motors of diversified size and type, of high energy fuels—and their adaptation to military and civilian use.

Scientists, Engineers: perhaps there's a place for you in Thiokol's expanding organization. Our new projects present challenging problems and a chance for greater responsibility.

Thiokol®

CHEMICAL CORPORATION

TRENTON, N. J. · ELKTON, MD. · HUNTSVILLE, ALA.
MARSHALL, TEXAS · MOSS POINT, MISS. · BRIGHAM CITY, UTAH
DENVILLE, N. J. · BRISTOL, PA.

*Registered trademark of the Thiokol Chemical Corporation for its liquid polymers, rocket propellants, plasticizers and other chemical products

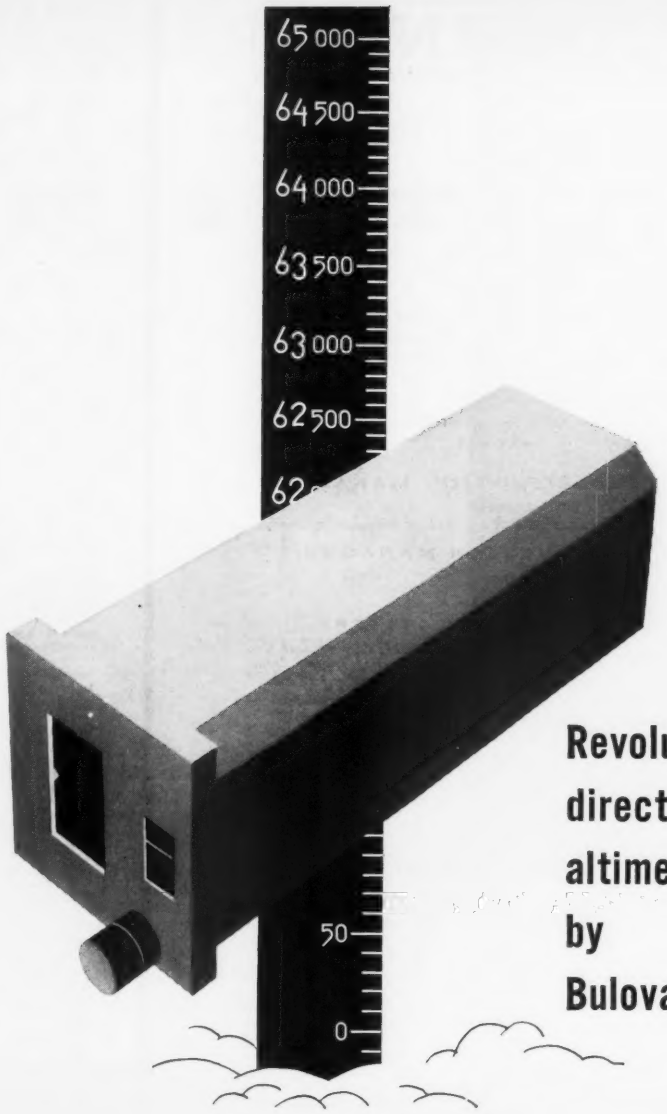

Revolutionary direct-reading altimeter... by Bulova

A major break-through in flight safety

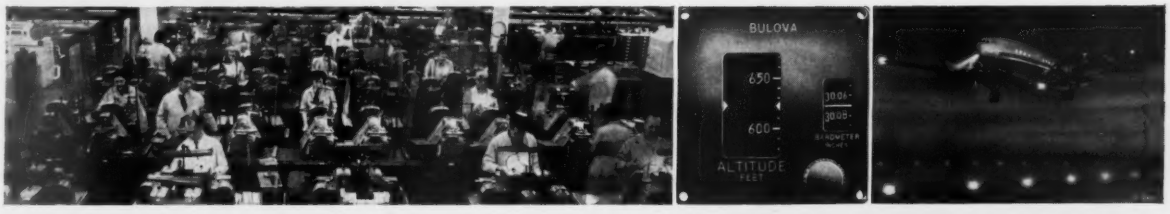

Test pilots flying high-performance craft enthusiastically responded to the new Bulova Altimeter. No difficulty was experienced in making accurate, split-second readings even when altitude changes exceeded 25,000 fpm.

Bulova tape presentation ends ambiguous readings... ends pointer scanning... increases reading speed and accuracy. These features, coupled with an instrument error of less than 10 ft. at sea level, 50 ft. at 40,000, make the Bulova Altimeter an important *advance* in flight safety.

Experience in precision design, in precision manufacture, is the Bulova tradition, the Bulova capability. Has been for over 80 years. For more information write —

Industrial & Defense Sales, Bulova, 62-10 Woodside Ave., Woodside 77, N.Y.

BULOVA

ARS JOURNAL

A PUBLICATION OF THE AMERICAN ROCKET SOCIETY

FORMERLY JET PROPULSION

EDITOR **Martin Summerfield**

ASSISTANT EDITOR **Barbara Nowak**

ART EDITOR **John Culin**

ASSOCIATE EDITORS

Ali Bulent Cambel *Northwestern University*
Irvin Glassman *Princeton University*
M. H. Smith *Princeton University*

CONTRIBUTORS

Marshall Fisher *Princeton University*
George F. McLaughlin

ADVERTISING AND PROMOTION MANAGER

William Chenoweth

ADVERTISING PRODUCTION MANAGER

Walter Brunke

ADVERTISING REPRESENTATIVES

D. C. Emery and Associates
155 East 42 St., New York, N. Y.
Telephone: Yukon 6-6855

James C. Galloway and Co.
6535 Wilshire Blvd., Los Angeles, Calif.
Telephone: Olive 3-3223

Jim Summers and Associates
35 E. Wacker Dr., Chicago, Ill.
Telephone: Andover 3-1154

R. F. Pickrell and Associates
318 Stephenson Bldg., Detroit, Mich.
Telephone: Trinity 1-0790

Louis J. Brosnick
304 Washington Ave., Chelsea 50, Mass.
Telephone: Chelsea 3-3335

John W. Foster
239 4th Ave., Pittsburgh, Pa.
Telephone: Atlantic 1-2977

American Rocket Society

500 Fifth Avenue, New York 36, N. Y.

Founded 1930

OFFICERS

President	**John P. Stapp**
Vice-President	**Howard S. Seifert**
Executive Secretary	**James J. Harford**
Treasurer	**Robert M. Lawrence**
Secretary and Asst. Treasurer	**A. C. Slade**
General Counsel	**Andrew G. Haley**
Director of Publications	**Irwin Hersey**

BOARD OF DIRECTORS

Terms expiring on dates indicated

James R. Dempsey	**1961**	**Simon Ramo**	**1960**
Alfred J. Eggers Jr.	**1959**	**H. W. Ritchey**	**1959**
Krafft Ehricke	**1959**	**William L. Rogers**	**1959**
Samuel K. Hoffman	**1960**	**David G. Simons**	**1961**
J. Preston Layton	**1960**	**John L. Sloop**	**1961**
A. K. Oppenheim	**1961**	**Martin Summerfield**	**1959**
William H. Pickering	**1961**	**Wernher von Braun**	**1960**
		Maurice J. Zucrow	**1960**

TECHNICAL COMMITTEE CHAIRMEN

Lawrence S. Brown, Guidance and Navigation
Milton U. Clauser, Hydromagnetics
Kurt H. Debus, Logistics and Operations
William H. Dorrance, Hypersonics
Herbert Friedman, Instrumentation and Control
George Gerard, Structures and Materials
Milton Greenberg, Physics of the Atmosphere and Space
Stanley V. Gunn, Nuclear Propulsion
Andrew G. Haley, Space Law and Sociology
Samuel Herrick, Flight Mechanics
Max Hunter, Missiles and Space Vehicles
David B. Langmuir, Ion and Plasma Propulsion
Y. C. Lee, Liquid Rockets
Max Lowy, Communications
Harold W. Norton, Test Facilities and Support Equipment
Paul E. Sandorff, Education
William Shippen, Ramjets
John L. Sloop, Propellants and Combustion
Ivan E. Tuhy, Solid Rockets
Stanley White, Human Factors
George F. Wislicenus, Underwater Propulsion
Abe Zarem, Non-Propulsive Power

Scope of ARS JOURNAL

This Journal is devoted to the advancement of astronautics through the dissemination of original papers disclosing new scientific knowledge and basic applications of such knowledge. The sciences of astronautics are understood here to embrace selected aspects of jet and rocket propulsion, space flight mechanics, high-speed aerodynamics, flight guidance, space communications, atmospheric and outer space physics, materials and structures, human engineering, overall system analysis, and possibly certain other scientific areas. The selection of papers to be printed will be governed by the pertinence of the topic to the field of astronautics, by the current or probable future significance of the research and by the importance of distributing the information to the members of the Society and to the profession at large.

Information for Authors

Manuscripts must be as brief as the proper presentation of the ideas will allow. Exclusion of dispensable material and conciseness of expression will influence the Editors' acceptance of a manuscript. In terms of standard-size double-spaced typed pages, a typical maximum length is 22 pages of text (including equations), 1 page of references, 1 page of abstract and 12 illustrations. Fewer illustrations permit more text, and vice versa. Greater length will be acceptable only in exceptional cases.

Short manuscripts, not more than one quarter of the maximum length stated for full articles, may qualify for publication as Technical Notes or Technical Comments. They may be devoted to new developments requiring prompt disclosure or to comments on previously published papers. Such manuscripts are usually published within two months of the date of receipt.

Sponsored manuscripts are published occasionally as an ARS service to the industry. A manuscript that does not qualify for publication, according to the above-stated requirements as to subject, scope or length, but which nevertheless deserves widespread distribution among jet propulsion engineers, may be printed as an extra part of the Journal or as a special supplement, if the author or his sponsor will reimburse the Society for actual publication costs. Estimates are available on request. Acknowledgment of such financial sponsorship appears as a footnote on the first page of the article. Publication is prompt since such papers are not in the ordinary backlog.

Manuscripts must be double spaced on one side of paper only with wide margins to allow for instructions to printer. Include a 100 to 200 word abstract. State the authors' positions and affiliations in a footnote on the first page. Equations and symbols may be handwritten or typewritten; clarity for the printer is essential. Greek letters and unusual symbols should be identified in the margin. If handwritten, distinguish between capital and lower case letters, and indicate subscripts and superscripts. References are to be grouped at the end of the manuscript and are to be given as follows: For journal articles: authors first, then title, journal, volume, year, page numbers for books: authors first, then title, publisher, city, edition and page or chapter numbers. Line drawings must be clear and sharp to make clear engravings. Use black ink on white paper or tracing cloth. Lettering should be large enough to be legible after reduction. Photographs should be glossy prints, not matte or semi-matte. Each illustration must have a legend; legends should be listed in order on a separate sheet.

Manuscripts must be accompanied by written assurance as to security clearance in the event the subject matter lies in a classified area or if the paper originates under government sponsorship. Full responsibility rests with the author.

Submit manuscripts in duplicate (original plus first carbon, with two sets of illustrations) to the Editor, Martin Summerfield, Professor of Aeronautical Engineering, Princeton University, Princeton, N. J. Preprints of papers presented at ARS national meetings are automatically considered for publication.

ARS JOURNAL is published monthly by the American Rocket Society, Inc. and the American Interplanetary Society at 20th & Northampton Sts., Easton, Pa., U. S. A. Editorial offices: 500 Fifth Ave., New York 36, N. Y. Price: $12.50 per year, $2.00 per single copy. Second-class mail privileges authorized at Easton, Pa. This Publication is authorized to be mailed at the special rates of postage prescribed by Section 132.122. Notice of change of address should be sent to the Secretary, ARS, at least 30 days prior to publication. Opinions expressed herein are the authors and do not necessarily reflect the views of the Editors or of the Society.

© Copyright 1959 by the American Rocket Society, Inc.

Storable and Powerful Rocket Fuel Oxidizer

CTF

Chlorine Trifluoride (ClF_3)

Much is expected of Chlorine Trifluoride as a rocket fuel oxidizer. That's because it combines good handling and storage properties with very high performance. To be specific:

CTF is not difficult to handle! Boiling point of Chlorine Trifluoride is 53.15°F. Freezing point is −105.4°F. Vapor pressure at 140°F is 80 psia.

CTF may be stored conveniently! Chlorine Trifluoride is storable over a very wide range of temperatures. You can count on years of storage life!

CTF has excellent stability! Shock resistance of pure CTF is very high. And it is thermally stable to high temperatures.

CTF offers high performance! The high density of Chlorine Trifluoride (1.825 at 68°F) leads to outstanding density impulse values. An important plus—CTF is hypergolic with hydrogenic fuels over a wide range of pressures and temperatures.

Fluorine and other Fluorine-Based Oxidizers

CTF is one of several fluorine-based chemicals produced by General Chemical which are now considered as excellent rocket-fuel oxidizers for various missions. Another is Bromine Pentafluoride which shares many of CTF's desirable physical and chemical properties. General Chemical, the sole producer of elemental liquid fluorine, has extensive technical data available on Fluorine and Halogen Fluorides. Write today for further information on these high-energy oxidizers.

Typical test stand of Rocketdyne, a division of North American Aviation, Inc.

BAKER & ADAMSON® Products

Allied Chemical

GENERAL CHEMICAL DIVISION
40 Rector Street, New York 6, N. Y.

measure control... without contact...

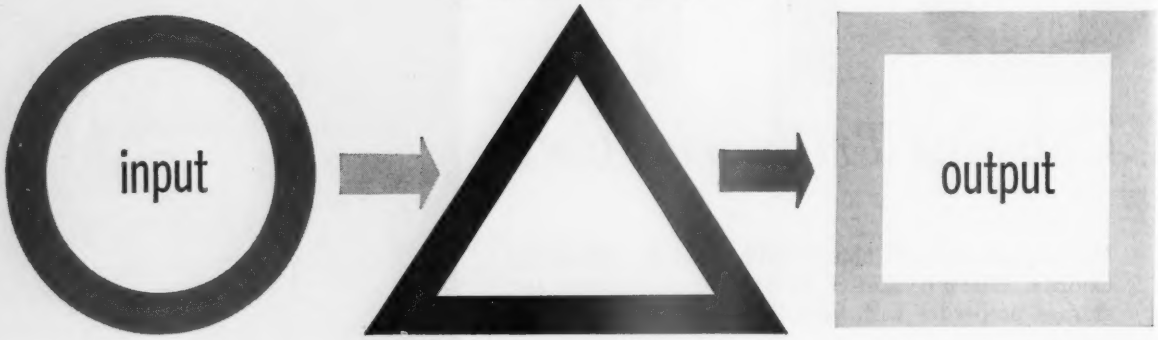

Now—measure pressure, temperature, vibration . . . any physical quantity you can convert to a change in capacitance . . . without fuss, muss, or bother. Decker's Delta Unit takes the output from the simplest △ capacitance sensors you can devise, converts it to an analagous phase sensitive differential DC voltage for indication and recording.

The new 902-1 Delta Unit is based on Decker's patented T-42 Ionization Transducer. It provides all the advantages of the T-42 ready to use in a simple, compact package as versatile and flexible as your own imagination.

Accepting initial capacitances from 1 to 50 μμF, the 902-1 provides maximum signals of ±30 VDC. Sensitivity in the 5-20 μμF initial capacitance range is approximately 0.2V/% △ C. Unit is provided with a single measuring probe and cable assembly; however, two measuring probes may be operated simultaneously. Complete information is provided in Instrument Data Sheet 902-1, available on request.

THE DECKER CORPORATION *Bala Cynwyd, Pennsylvania.*

Recent Advances in Cryogenic Engineering

ROBERT B. JACOBS

National Bureau of Standards
Boulder, Colo.

Dr. Jacobs is Chief of the Cryogenic Equipment Section, National Bureau of Standards. He received his B.S. from the University of California and his M.S. from MIT, both in Mechanical Engineering, and his Ph.D. in Applied Science from Harvard. The author has taught in the Mechanical Engineering Department at MIT where he did research in cryogenic engineering. Since 1951, he has been at the Cryogenic Engineering Laboratory working on problems of handling, storage and transportation of liquefied gases; his work includes research on two-phase fluid flow, pumping and cavitation, boiling heat transfer, flow measurement, pressurization and stratification, insulation and equipment optimization.

THE IMPORTANCE of cryogenic engineering to rocketry stems from the desirability of using liquefied gases as propellants. This importance will probably increase because the use of liquefied gases appears mandatory for the more ambitious missions in the not-too-distant future. It is well to realize that the large effort put into, and the consequent rapid growth of, the field of cryogenic engineering is in large part due to the importance of rocket propulsion. Because of the relatively short time in which the major growth of the field has occurred, an exposition of the recent advances of cryogenic engineering should cover the whole field of cryogenics which is of importance to propulsion. In addition, because of security restrictions, proprietary considerations and a definitely limited interest, a large part of the literature in cryogenic engineering has had very limited distribution. Finally, there has been a tendency to ignore the cryogenic aspects of the problems facing the rocket engineer; in some cases the problems resolve themselves, but too frequently the neglected problem remains to plague the engineer with malfunction and failure.

Perhaps the most important point to stress is that cryogenic problems can generally be solved through application of the same basic principles which have been successfully employed for many years in mechanical, chemical and electrical engineering. Situations in which new principles (e.g., super conductivity) arise are very rare. Normally, the significant deviations of cryogenic problems from the more familiar ones are caused by changes in emphasis or differences in order of magnitude; design difficulties are usually the result of insufficient knowledge of properties of materials. For example, if the basic phenomena occurring in a centrifugal pump are adequately understood, prediction of the performance and cavitation characteristics of a liquid hydrogen pump will be just as reliable as the predictions for a cold water pump. As a matter of fact, because of the gaseous and solid contaminants usually present in cold water, the hydrogen problem may be easier. An engineer who has experience designing valves for operation at ordinary temperatures will notice that the relative importance of some of his problems will change; whereas hydraulic efficiency and leak tightness across the seat and through stem packing may have been primary considerations in the past, problems concerned with differential contraction, freezing of packing materials, icing of movable parts, impact strength, seat materials with satisfactory room and low temperature properties, and insulation may be more important in the cryogenic application. Perhaps the most striking example of a specification which is of different order of magnitude in cryogenic engineering compared with ordinary practice is permissible heat leak; insulations with mean effective thermal conductivities of less than 0.0002 Btu/hr ft F are common in cryogenic equipment, whereas for the same temperature range one of the best conventional insulations has a mean thermal conductivity of about 0.02 Btu/hr ft F.

Received Jan. 14, 1959.

The cryogenic problems encountered in rocket propulsion can arbitrarily be segregated into those associated with ground handling and those associated with equipment and processes aboard the vehicle. The differences in these two groups are not due solely to weight and space limitations imposed upon the one, but also to requirements pertaining to permissible propellant loss, acceptable flow rates, readiness conditions, cooldown requirements, etc. (The secondary uses of liquefied gases for rocket propelled vehicles, such as refrigeration of instrumentation and power for pneumatic controls, will not be discussed here; they do not involve any basic problems not encountered in the propellant system. Also, the field of gas liquefaction will not be discussed here.)

Ground handling equipment is that required to convey the propellants from the liquefiers to the final vehicle: Storage and transport containers; piping systems including valves, couplings, filters, etc.; both low and high capacity, moderate head transfer pumps; pressurization equipment, such as tank farms, gas generators and compressors; instrumentation for measuring, controlling and recording flow rate, temperature, pressure, liquid-vapor composition, and liquid level. Examples of equipment found aboard the vehicle are: Storage tanks; piping, valves and other fittings; high capacity, high head pumps; heat exchangers involving boiling as well as convective heat transfer; instrumentation. In addition to the problems associated with the equipment, there are problems associated with procedures and techniques. Should propellants be stored at low or high pressure? Should pressurization or pumping be used for a certain transfer operation? Should transport containers or piping systems be used? Should equipment be evacuated and purged, or just purged? Adequate solutions to these problems require information concerning, for example, properties of materials, insulation techniques, pumping, tank and piping system design, single- and two-phase fluid flow, heat transfer and instrumentation techniques.

Properties of Materials

It is obvious from the preceding discussion that data concerning all of the properties required for equipment design at room temperature and above are also required for the de-

sign of equipment to operate at low temperatures. In order to make all pertinent information and data available to those concerned with cryogenic problems, the Cryogenic Engineering Laboratory, National Bureau of Standards, Boulder, Colo., maintains the Cryogenic Data Center. Although it is estimated that the Center will not be completely up-to-date for another two years, its services are currently available.

In addition to the mechanical properties commonly used in the design of equipment, the design of cryogenic equipment requires a particular awareness of thermal expansion coefficients and specific heats. A knowledge of the former is required so that, after equipment is cooled to its operating temperature, the required clearances are attained and thermal stress limitations are obeyed; specific heat data are required for prediction of cooldown characteristics of equipment. Thermal conductivity is another property which the cryogenic designer should bear in mind: If heat leak through metallic members is to be minimized, a stainless steel, monel or other poorly conducting alloy should be used; if temperature stratification in liquid containers is desirable, the inner tanks should be stainless steel, whereas if stratification is to be inhibited, aluminum or copper alloys may be desirable.

A series of articles by Corruccini (1)[1] presents data and general discussion concerning thermodynamic, transport and mechanical properties of solids, including metals, plastics, glass and insulating materials, at low temperatures; a selected list of useful references pertaining to the properties is given in part one of the series. Chelton and Mann (2) have assembled a very useful compilation of thermodynamic, transport, mechanical, electrical and miscellaneous properties of solids, liquids, gases, insulations, etc. Besides (1 and 2) and the Data Center, useful collections of cryogenic data apparently exist only in the private files of those who have been working in the field.

A rather complete bibliography of references on mechanical properties of solids below zero deg C has been assembled by Kropschot and McColm (3). This report covers the literature from 1945 to 1955, and includes an abstract for each reference. As with other materials, the strengths of austenitic stainless steels, copper alloys and some aluminum alloys increase greatly with decreasing temperature; however, even at liquid hydrogen temperature these specific materials possess sufficient ductility to permit their use under essentially the same impact and vibration specifications as at normal temperatures. It follows that equipment fabricated of these materials, which is to be operated at all temperatures from room temperature down, should be designed using room temperature strength data; it is also apparent that if weight and space specifications are not severe, equipment can be conservatively designed by utilizing room temperature data. If weight limitations are severe and equipment is to be subjected to working stresses only after cooldown, appreciable weight saving can be realized by designing to the mechanical strength available at the operating temperatures. Because of the wide use of welding as a method of joining in cryogenic equipment, information concerning the mechanical properties of weldments at low temperatures is required by the designer. Unfortunately, work in this area is very limited (see Mikesell and Reed (4)).

Because of their light weight, low thermal conductivity and adequate mechanical properties, plastics have found wide use in cryogenic equipment as insulating supports, gasketing material, valve seats, insulation, tank material, etc. However, adequate information is not available for optimum design in this area; results have been reported by Reed and Mikesell (5), McClintock (6) and Corruccini (1). Epoxy resins have been successfully used as structural adhesives in cryogenic equipment for use at temperatures down to 20 K; McClintock and Hiza (7) have reported work in this area. Information pertaining to the electrical and magnetic properties of solids at low temperatures is meager, and consequently optimal design of electric and magnetic equipment to operate at these temperatures is difficult. As most measurements are made with the purpose of investigating basic behavior, materials which are not of interest to the designer are studied. Examples of the type of work which is useful to the engineer are afforded by Hall et al. (8), and Brown and Brennand (9).

Although much information about the properties of fluids is still needed, especially in the high pressure liquid and the high density gas regions, sufficient information is available to produce nonoptimum design. Knowledge of essentially all of the thermodynamic (pressure, density, temperature, specific heat, etc.) and transport (viscosity, thermal conductivity, etc.) properties is necessary for the desired fluid flow, heat transfer, pumping, etc., calculations which must be made by the rocket engineer. Although the effort is apparently not yet intensive enough, programs to determine some of the necessary information are now under way. The paper of Woolley, Scott and Brickwedde (10) is probably still the best compilation of the properties of hydrogen. Although comparable compendia for the other propellants do not exist, it is the intention of the Cryogenic Data Center to issue such documents as soon as possible. As there is insufficient space here to list even a token sample of the available references, the reader is advised to obtain necessary information from (2), from the Cryogenic Data Center or directly from the literature.

Insulation Techniques

The effectiveness of thermal insulations required for cryogenic equipment runs the gamut from no insulation whatsoever (except that afforded by condensates which may form) to the best vacuum-type insulations. Perhaps the major reason for using insulation is to prevent the vaporization, and consequent loss, of liquefied gas. However, there are other reasons for using insulation which, for certain applications, may be more important; two of these are to prevent cooling of adjacent equipment and to minimize pressure drops by preventing two-phase flow.

Uninsulated Equipment

The greatest, and perhaps only widespread, use of uninsulated ground handling equipment is at rocket engine test sites. The storage tanks are usually well-insulated, but the transfer systems and run tanks are not; consequently, as much as 75 per cent of the liquid oxygen purchased by a site may be lost. For a transfer system of any permanence, there seems to be no economic justification for not using insulation; in many cases, high vacuum insulation can be justified. There may be good reasons for leaving run tanks uninsulated; however, the one usually given is that insulation would alter the dynamic characteristics of the test stand and thus render the test results less applicable. Inasmuch as run tanks are not flight tanks anyway, the reasoning appears to be faulty. It therefore appears that the use of uninsulated equipment at test sites could be reduced. However, as the loss of liquefied gas due to heat leak is a function of the heat leak per unit mass of fluid flowing (11), transfer systems with high flow rates can tolerate poor insulation. In fact, high capacity propellant loading systems should be uninsulated, since the loading operation would be complete before an insulation could be effective.

The use of insulation aboard the vehicle, where the weight and space limitations are severe, may be determined primarily by these limitations. It is probable that in-flight insulation of liquid oxygen equipment in present missions is not justified except in situations where piping passes through fuel tanks, etc.

The use of uninsulated equipment, including tankage, with liquid hydrogen is not such a clear-cut issue. It is probable that for very rapid loading, uninsulated transfer systems can

[1] Numbers in parentheses indicate References at end of paper.

be used. The problems of using uninsulated equipment with liquid hydrogen are currently being investigated. Possibly the most challenging insulation problem in cryogenic engineering is that of developing tankage which will carry liquid hydrogen on the more ambitious missions.

The factors determining the steady-state heat transfer rate to liquefied gases in uninsulated equipment depend upon the liquid as well as ambient conditions. With liquid oxygen a loose frost or snow normally forms. The presence of this layer can halve the heat transfer rate (12); however, since it is easily blown off, it should not be relied upon to provide insulation. Some investigators have reported that rain bounces off uninsulated liquid oxygen containers, while others have reported that the rain adheres, building up thick layers of ice. It is obvious that controlled investigation should be carried out; some work of this nature is being done. With liquid nitrogen, air (as well as water) condenses on the equipment. Because the normal boiling point of liquid nitrogen is above the triple point temperature of air, liquid air continuously runs off of the equipment, washing the ice with it. Consequently, the outside film coefficient, which may be the rate determining factor, should be computed from condensing information. Because the normal boiling point of fluorine is below the condensing temperature of air, we would expect uninsulated fluorine equipment to condense air, and thus the heat transfer computations would be similar to those for nitrogen equipment. Experience with uninsulated liquid hydrogen equipment has shown that solid air does not adhere to the exposed surfaces to form a layer of solid, but is continuously washed off by liquid air. Therefore, heat transfer computations should involve film condensation considerations. Available information indicates that, if the hydrogen is boiling, in some cases the condensing heat transfer coefficient may be the rate controlling factor, while in others the boiling coefficient may be controlling. If the liquefied gas in uninsulated equipment is sufficiently pressurized (or subcooled), boiling will not occur, and although the phenomena occurring on the outside surfaces may not change appreciably, the heat transfer rate in these cases may be controlled by the film coefficient in the liquefied gas.

Conventional Insulations

Whether or not insulation, and especially non-vacuum type insulation, is used depends upon the length of time that the equipment is in use for each operation. It is obvious that if the use time is extremely short, the equipment will not have time to cool, much less transfer energy from the environment. Also, if complete cooldown of metallic parts does occur, the thermal diffusivities of conventional insulations (e.g., fiber glass) are usually small enough so that a fraction of an inch insulation thickness is adequate. For example, a $1\frac{3}{16}$-in. thickness of fiber glass insulation on a 4-in. liquid oxygen line does not reach steady state for almost 2 hr (13). The use of conventional insulations, with liquid oxygen transfer lines for example, can reduce the steady-state heat link by 96 per cent (12).

The primary problem connected with the use of conventional insulations is the vapor barrier; this problem is automatically circumvented with vacuum insulations. The objective is, of course, to prevent water, air, etc., from condensing in the insulation, thereby materially decreasing the insulating quality; either the condensate can solidify and produce an insulating layer with the thermal conductivity of the solid, or it can liquefy, flow to warmer parts of the insulation and evaporate, causing a high rate, regenerative-type heat transfer mechanism. There are plastic and glass foam-type insulations which are unicellular and can be preformed; with these it is only necessary to seal along the joints with a suitable mastic. Programs to develop satisfactory "foamed-in-place" plastic insulations are under way; these will not have any joints to be sealed; the primary difficulty with these materials is failure due to thermal stresses. With the open, or porous, insulations, a covering sheath is generally used. This covering can operate in one of three ways:

1 It can be gas tight; because the pressure in the insulation space will drop when the equipment is cooled, this type of installation must be able to withstand external pressure.

2 The covering can be gas tight but will be allowed to "breathe" gas that does not condense at the operating temperature; in this way the insulation need not withstand external pressure.

3 The covering need not be gas tight, but a sufficient quantity of suitable gas is fed into the insulation so that it maintains a positive gage pressure therein.

The second method is most desirable. Besides the difficulty experienced in truly sealing a vapor barrier, especially around valve bodies, supports, etc., there is the problem of ruggedness with respect to both mechanical and environmental abuse. The designer should be aware of the possibility that, in providing a vapor barrier with the necessary ruggedness, he may end with equipment that is as expensive as and heavier than vacuum-insulated equipment.

The thermal design of cryogenic equipment with conventional insulation involves conventional heat transfer calculations. The determination of the transient characteristics will require a knowledge of specific heat, density and thermal conductivity, whereas a determination of the steady-state characteristics requires a knowledge of thermal conductivity only (12 to 16).

Vacuum Insulations

Although vacuum-type insulations have been used for many years to insulate tanks, there has been a strong reaction to their use with transfer systems and other components. The reason has been the almost universal lack of knowledge and technique concerning high vacuum systems; however, the situation is changing. Once the suspicion of unreliability had been overcome and enough fabrication experience had been obtained so that realistic cost estimates could be made, it was possible to demonstrate that, in many cases, vacuum insulated systems are economically as well as technically desirable (17). With the use of liquid hydrogen as a propellant, and the increased handling of helium in liquid form (18, 19), the place of vacuum-type insulation in rocketry cannot be denied.

Vacuum-type insulations can be divided into three classes: High-vacuum, evacuated powder, and so-called "superinsulations" or "breakthroughs" which have "apparent mean thermal conductivities" that are an "order of magnitude" lower than the usual designs in the first two classes. The details of these insulations are rather well-guarded proprietary information. Vacuum-type insulations can be permanently sealed (static), continuously pumped (dynamic), periodically pumped and sealed, or of the condensing type. In the last, the vacuum jacket is filled with a gas (e.g., carbon dioxide) which solidifies on the cold surfaces when the equipment is put into operation, producing a high vacuum; this system has an advantage with respect to long storage life.

The advantages of evacuated powder over nonshielded high vacuum are that, for larger equipment, the heat transfer is less and only rough vacua are required; the disadvantages are greater insulation thickness, some added fabrication problems and more cooldown mass. In the past, high vacuum has been made very effective in larger equipment for use with hydrogen and helium by employing liquid nitrogen cooled radiation shields. It appears that the "superinsulations" mentioned above will replace liquid nitrogen shielding in many applications. The "superinsulations" of which the author is aware are all vacuum-type. It is probable that at least some of them are high vacuum, but with clever methods of shielding.

The methods for calculating heat transfer through vacuum-

type insulations are straightforward. In high vacuum, only radiant energy is significant, and so only information concerning geometry and optical absorptivities is needed (11, 20). If, for some reason, the pressure in a high vacuum insulation becomes too high, the energy transport due to gas conduction will have to be computed (21). The energy transport through evacuated powder occurs by means of radiation, gas conduction and solid conduction; the powder absorbs and reflects radiation and reduces the gas conduction. Although investigators are currently studying the three mechanisms separately, engineering design computations are based upon mean apparent thermal conductivities (11). As these numbers are derived from the experiments by means of the Fourier conduction equation, conventional heat conduction calculations are used; the values used for the conductivities must, of course, apply to the temperature range in question. Values of apparent mean thermal conductivities have been reported by Fulk et al. (22); however, more data are needed, especially down to liquid hydrogen and helium temperatures.

Flow Considerations

The fluid mechanical design of transfer systems for liquefied gases does not require the use of new principles. However, it will be useful to put down some thoughts and references. (Pumping of liquefied gases will be discussed in a later section.)

Systems which involve single-phase (liquid) flow and systems which involve two-phase (liquid and vapor), single-component flow are encountered. It is generally desirable to have single-phase flow; pressure drops, equipment size and costs can be smaller; design computations are simpler and more accurate; flow measurement is easier; undesirable compressiblity effects, such as choking are reduced (or eliminated), etc. Single-phase flow can be achieved by assuring that the static pressure is always greater than the vapor pressure. A fairly thorough presentation of the single-phase problem has been given by Jacobs (11).

The design procedures for two-phase systems are still relatively crude and inaccurate. Although the results may have an error of more than 50 per cent, the most widely used empirical correlation is that of Lockhart and Martinelli (23). This correlation is based upon data obtained for isothermal, two-component flow with no mass transfer between the phases; it has been shown, however, that the correlation can be used with single-component systems, with appreciable vaporization, if a simple correction is made to account for the variation in the axial component of momentum (24, 25, 26). Harvey and Foust (27) set up a system of equations for one-dimensional flow of two-phase, single-component fluids utilizing the correlation of Lockhart and Martinelli to account for the frictional pressure drop. However, since the labor connected with numerical computations based upon these equations is very great and the errors inherent in the equations (due to shortcomings of the Lockhart and Martinelli correlation) may be large, design calculations based upon the simple momentum correction (26) may be preferred. An insight into the complexity of the method of Harvey and Foust can be obtained from the work of Rogers (28), who made some calculations for the two-phase flow of hydrogen; Rogers' results have not been compared with experimental results.

The extreme complexity of the two-phase flow problem has prevented appreciable progress through more theoretical approaches; although the work of Linning (56) is less empirical than that in the preceding references, numerical calculation depends upon an appreciable amount of experimental information. There are at least two groups carrying out theoretical work on annular-type, two-phase flow, but results have not yet been published.

The flow problem about which least is quantitatively known is that concerned with the transient phenomena that occur when cryogenic equipment is cooled from atmospheric temperature down to operating conditions. The two questions which arise are: How fast can systems be cooled, and what pressures occur during the various possible cooldown procedures. In many cases, sufficient time is available and the equipment can be sufficiently well designed so that cooldown offers no difficulty. However, if one is not aware of potential pitfalls, he can lay out a transfer system that could never be cooled.

In their most detailed aspects, cooldown problems involve consideration of unsteady flows of highly compressible fluids, two-phase flows, convective and boiling heat transfer, etc. Because of the extremely low critical velocities of two-phase systems, the flow is readily choked; because of the rapid vaporization which occurs when liquid contacts a relatively warm wall, there are large pressure surges which can reverse the direction of liquid flow. A common technique for decreasing the cooldown time of relatively long transfer systems is to provide vent valves through which the large amounts of vapor can be bypassed, thereby eliminating the necessity of having to push large volumes through the whole system.

Apparently all of the investigations, to date, of the cooldown of cryogenic systems have been oriented toward the prediction of cooldown time. Only the work of Burke et al. (29) appears in the open literature; they report reasonable correlation between theoretical predictions and experimental results for transfer systems in which the flow is controlled by a choking orifice near the exit; the experiments were carried out with liquid oxygen. Macinko (30) has developed a method for the prediction of the cooldown time for transfer systems without restrictions and has obtained good agreement between his predicted cooldown times and those actually measured with both hydrogen and nitrogen.

Pumping Equipment

There is a wide range of specifications for pumping equipment which may be used in connection with cryogenic propellants. Besides the obvious differences in weight and bulk between ground handling and spaceborne equipment, head specifications can cover the whole range up to 50,000 ft and capacity specifications can cover the whole range to more than 10,000 gpm; high shaft speeds will be necessary. It is apparent that positive displacement, centrifugal and axial pumps have their places. Also, with hydrogen and helium, compressibility effects are appreciable. It should be stressed that the fundamental concepts and methods, which are adequate for the fluid-mechanical design of pumps for common fluids, are just as applicable to liquefied gases. The performance characteristics will differ because of such things as greater leakage due to lower viscosity; the efficiency may be lower due to the fact that a smaller density will require less total power input, but the fixed losses (such as bearing) will not decrease appreciably. The cavitation characteristics will differ because of differences in thermodynamic and transport properties, but the same fundamental considerations apply in all cases.

The centrifugal-type pump has been most widely used with liquefied gases although turbine-type transfer pumps are common. Reciprocating pumps have long been used to compress liquefied gases for the production of high pressure gases; of course, this type of equipment has low capacity, but pressures up to 10,000 psia are achieved, and development of equipment for pressures to over 13,000 psia is under way (31). Some work has been done on vane-type cryogenic pumps, but no results have been published. Work is also progressing on airborne multicylinder pumps (32) for providing high pressure gas for purging, pneumatic control, cooling, etc. (33, 34).

The work done on the pumping of liquefied gases with centrifugal pumps indicates that, as far as performance characteristics are concerned, no extraordinary behavior is to be expected. The years of experience with liquid oxygen ground handling and rocket engine pumps, as well as the work

of Jacobs, Martin et al. (35) with water, oxygen, nitrogen and hydrogen, and the work of Caine et al. (36) with hydrogen, substantiate this. However, studies into cavitation characteristics are still needed. Substantial progress has been made in this area recently by analyzing cavitation characteristics through consideration of the thermodynamic properties of the fluids (35, 36, 37, 38). For example, it was predicted theoretically and shown experimentally (35) that the minimum required net positive suction head (NPSH) for hydrogen is only about $\frac{1}{4.2}$ that required for nitrogen in the same pump; in a water pump with a specific speed of 1930 (at 3450 rpm) only $2\frac{1}{2}$ in. NPSH were required to prevent cavitation with hydrogen (35), whereas a booster-type pump that was designed for hydrogen and had a specific speed of about 800 (at 12,000 rpm) required an NPSH of only 6 in. (36). The measurement of these NPSH's with adequate accuracy requires vapor-pressure instrumentation (39).

Besides the low NPSH requirement, hydrogen pumps are different from others because the low density requires very high heads for high pressures. Where weight and space limitations are severe, it is necessary to use high speeds. One development along this line is the radial-vane pump described by Bosco and Carter (40).

Two problem associated with pumps and which have not been mentioned previously concern bearings and seals. The bearing problem is frequently solved by using shafts which are so long that frictional energy dissipation, heat transfer from the atmosphere, or heaters can keep the bearings warm; in these cases, no exceptional bearing problems arise, but the disadvantages of long shafts and the possibility of appreciable heat transfer into the pump are present.

The advantages of submerging the bearings in the liquid which is being pumped have stimulated work along this line. This can be achieved by either using a sump configuration or by bleeding some of the liquid from the pump discharge through the bearings. All of the work on submerged bearings reported to date has been with thoroughly cleansed and degreased ball bearings; this work indicates that the separator is the critical item in the performance of ball bearings submerged in liquefied gases. Bearings have been evaluated in pumps operating from 3000 to 22,000 rpm in hydrogen and nitrogen and in a test rig from 3000 to 10,000 rpm in nitrogen (41). The most successful separator material has been fabric-reinforced phenolic. Satisfactory performance has been achieved with angular contact bearings with balls and races made of both 52100 steel and 400-C stainless; the stainless is preferable, however, because of its greater resistance to corrosion in the event that water condenses on the bearings. Running times of hundreds of hours have been achieved in tests up to 12,300 rpm. Long lives may also be attainable to higher speeds, but tests have not yet been run; the tests at 22,000 rpm in hydrogen were terminated after about 6 hr, but not because of bearing failure.

Small ball bearings have been run successfully in gaseous hydrogen from room temperature down to liquid hydrogen temperature at 10,000 rpm (42). These bearings had 440 stainless steel balls and races, used micarta ribbon retainers, and ran successfully both with and without oil.

As in the case of bearings, the problems arising from the operation of shaft seals at low temperatures have been circumvented by putting the seals in ambient temperature regions. The author is not aware of any literature on low temperature liquid seals except for the limited and undetailed comments in (35 and 40). One reason low temperature shaft seal development has lagged is because sump-type pump configurations do not require cold shaft seals; if the pump is driven by an extension shaft with the drive in the atmosphere, only a seal to hold the sump pressure is needed; if the driver is in the sump as an integral part of the pumping unit, no seals whatsoever are needed. It has been thoroughly demonstrated that electric motors can be designed for operation submerged in any liquefied gas (36). There is no apparent reason why submerged turbine drives cannot be developed for the larger power requirements.

Heat Transfer

Although heat transfer considerations in cryogenic equipment do not involve new principles, it should be pointed out that there is a definite lack of heat transfer data and that some of the published results are contradictory. Many convective heat transfer calculations for cryogenic equipment are based on the accepted correlations obtained from data with more common fluids. Of course, when new geometries are used, the designer should be most skeptical in extrapolating data. Much heat exchange in cryogenic equipment involves boiling and/or condensing. Most of the information available has been obtained with simple geometries (43, 44, 45) (wires, cylinders, etc.) or with special geometries (46), and so is not directly applicable to most heat exchanger designs. Although investigations concerned with heat transfer with liquefied gases flowing through actual heat exchanger configurations are in progress, no results have appeared in the open literature.

Instrumentation

The instrumentation with which the cryogenic engineer is concerned and which is important in the evaluation and operation of propulsion systems is related to pressure, temperature, flow, liquid level and static mass measurement. As is generally the case with other equipment, instrumentation in cryogenics is not significantly different from conventional instrumentation except that the low temperature, and possibly high vacuum, requirements may effect the details of some of the sensing elements.

Pressure

Static (i.e., steady-state) pressure measurement offers no difficulty in cryogenic equipment. The geometry of the pressure tubing should be such that liquid cannot continuously drain or percolate into it, and if heat conduction is to be minimized, the tubing should be stainless steel. All of the normal procedures, such as the use of piezometer rings and prevention of unknown hydrostatic heads should be followed. Of course, all contaminants which can freeze and block the pressure taps and connecting tubing must be removed before cooldown.

Dynamic (i.e., unsteady) pressure measurement offers no difficulty if the transducer can be located so that its temperature is known. This can usually be accomplished by having the transducer in the atmosphere and connecting it to the pressure tap with a piece of stainless steel tubing; the only reason it may be inadvisable to do this is that the dynamic response of the system, with the connecting tubing, may be unsatisfactory. There are transducers on the market which are made and calibrated for use down to about −350 F and possibly lower. As the zero shift with temperature of these units is quite large, the temperature of the transducer must be known. Thus transducers can be connected directly to equipment if the pressure data are needed only when the transducer temperature is known. However, if pressure transients are to be measured during the cooldown of equipment, a transducer connected directly to the equipment will not yield accurate pressure information directly. The signals or records will have to be manipulated to account for an effective transducer temperature at each instant.

Temperature

The problems of temperature measurement can also be divided into those associated with static and those associated

with dynamic situations. The former can be adequately handled, but for the latter better response characteristics are desired. For a comprehensive exposition of the field of thermometry, the reader is referred to (47 and 48).

Five types of thermometers are commonly used in cryogenic applications: Thermocouples, vapor-pressure bulbs, gas thermometers, platinum resistance thermometers and semiconductor thermometers. The choice of system to be used depends upon the conventional considerations, such as accuracy and sensitivity, cost and dynamic characteristics.

Thermocouples have wide use in cryogenic engineering, their main assets being adequate accuracy, good response time and moderate cost. A primary disadvantage seems to to be a drift in calibration (or instability) due to thermal cycling. Of course, as is true with all thermometers, the installations must be such that the junctions are adequately tempered; that is, heat conduction through the leads and well to the junction must be made negligible. As the thermoelectric power of thermocouples decreases at low temperatures (for copper-constantan it is only 6 μv per deg K at 20 K), junctions with higher powers are continually being sought; a junction which has found wide use, and which has a power of 15 μv per deg K at 20 K, is gold with a 2.1 atomic per cent cobalt impurity vs. copper (49). Because the instability is believed to be due to the copper, work is now being done on a junction of the gold-cobalt, mentioned above, vs. silver with an 0.37 per cent gold impurity.

Vapor bulbs have the advantages of extremely high accuracy and simplicity, but have limited ranges. Tests indicate that vapor bulb systems can have time responses that are about as fast as those of thermocouples made with 30 gage wire. In equipment where the measured temperature range is between the triple and critical points of a suitable substance, the use of vapor pressure thermometers should be seriously considered.

Gas thermometers have the serious disadvantages of being difficult to fabricate and difficult to use. They are therefore probably undesirable for use in engineering equipment.

Platinum resistance thermometers have the advantages of stability of calibration, accuracy, linearity (down to 40 K) and a large temperature range. Their primary disadvantages are cost and procurement time; the author is not aware of any data concerning the response characteristics of platinum resistance thermometers, but they are relatively sluggish.

Semiconductor thermometers are resistance thermometers, employing semiconductors, such as carbon, germanium, silicon or metallic oxides as the sensing elements. Their advantages include relative simplicity, accuracy and, in some cases (50), stability when subjected to thermal cycling. They have the disadvantage of nonlinear calibration curves, and in some cases (e.g., carbon) they are unstable. The large changes in the resistance of the units which occur over appreciable temperature ranges require that special consideration be given to the circuitry if the measurements are to be optimized (51). Because these sensors can be made rather small, their response characteristics can be fast.

Flow

One of the major instrumentation problems in the cryogenic aspects of rocketry is flow measurement. Once again, it can be said that the basic considerations with liquefied gases do not differ from those with the more common fluids. Some development work of mass flow meters for use with liquefied gases is now in progress, but essentially all flow measurement has been volumetric. Turbine-type meters have been most extensively used; however, their superiority over other types of meters is not apparent. One of their major difficulties is that if two-phase flow inadvertently occurs, the turbines can be wrecked. Based upon work with hydrogen, nitrogen and water, Richards (52) concludes that sharp edged orifices are reliable flow measuring devices for use with liquefied gases; the results were reliable except when two-phase flow was known to enter the orifice.

The primary difficulty in flow measurement is encountered if two-phase flow exists. This problem, which is common to all volumetric flow meters, will disappear if a mass flow meter is developed, but until then, the development of an instrument to determine the liquid-vapor composition of a flowing fluid is needed. There are several programs under way which aim to perfect equipment for detecting the presence of vapor in liquid (53), but the adequacy of the instruments so far developed for the quantitative measurement of the composition of two-phase flows is questionable.

Tank Contents

Another type of instrumentation important in handling liquefied gases is that required for determining the amount of liquid in a tank. Several adequate systems are available for use with ground handling equipment, but attainment of the desired accuracy in uninsulated tanks still presents problems. The instruments can be classified as direct weighing, hydrostatic and liquid level. The direct weighing of cryogenic tanks is not different from other tanks; load cells using strain gages, inductance, capacitance or resistance principles, or some other sensing device can be used along with conventional circuitry.

The use of hydrostatic pressure systems is widespread; depending upon what the pressure signal is to be used for, either electrical or mechanical sensors, recorders, etc., may be used. The location of the pressure taps and their layout is important. In many installations the taps have been placed in the vent and liquid lines; consequently, when there is liquid or vapor flow, the instrumentation cannot be used. The system must be such that the location of the liquid-vapor interfaces in the pressure lines is known. In some systems, the high pressure tap has been taken directly from the bottom of the tank, permitting percolation; this produces a disturbance in the signal. In a relatively well-insulated tank, the mass of liquid can be obtained from a hydrostatic system if the tank geometry is known. However, if there are appreciable convection currents, there may be appreciable error in a mass determination.

Liquid level devices are widely used for control as well as indication of liquid level. As these are simply height measuring devices, information concerning tank geometry as well as fluid density must be known if fluid volumes and masses are to be determined. The capacitance liquid level device (54) has been used successfully for many years for the indication, control and recording of the liquid level of liquefied gases; it is a continuously indicating device and has a fast time response. For point (and multipoint) indication, control and recording, the carbon resistor liquid level device has been successfully used for years. Because the properties of carbon resistors drift under thermal cycling, the associated circuity should be made relatively insensitive to this. With proper circuit design, the carbon-resistor level indicator can respond in 2 to 3 sec. Some work has been done on ultrasonic-type indicators, vibrating paddle-type indicators and radiation-type indicators, but no information is available in the open literature.

Summary

The point to be emphasized is that cryogenic engineering is a synthesis of the older branches of engineering (mechanical, chemical, electrical), and therefore does not involve new basic principles. The discussion presented here has avoided those areas where usual engineering experience is directly applicable. An attempt has been made to discuss situations where the unwary may go astray and where the cryogenic engineer has evolved new techniques. In addition, an attempt has been made to indicate the location of data and information applicable to new materials and situations, as

well as that applicable to the familiar materials and situations in the low temperature regions. Finally, it should be pointed out that a comprehensive treatise on cryogenic engineering (55) is to be published early in 1959.

References

1 Corruccini, R. J., "Properties of Materials at Low Temperatures," *Chem. Engng. Prog.*, vol. 53, nos. 6, 7 and 8, June, July and Aug. 1957, pp. 262–267, 342–346, and 397–402.

2 Chelton, D. B. and Mann, D. B., "Cryogenic Data Book," Rep. UCRL-3421, Univ. of Calif. Radiation Laboratory, Berkeley.

3 Kropschot, R. H. and McColm, D. W., "A Bibliography on the Effect of Low Temperature on the Mechanical Properties of Materials," unpublished report, Nat. Bur. Standards, Boulder, Colo.

4 Mikesell, R. P. and Reed, R. P., "The Tensile and Impact Strength to 20° K of Annealed and Welded 5086 Aluminum," Proc. 1958 Cryogenic Engineering Conf., K. D. Timmerhaus, ed., Univ. of Colo., Boulder.

5 Reed, R. P. and Mikesell, R. P., "Some Mechanical Properties of Mylar and Dacron Polyester Strands at Low Temperatures," *Rev. Sci. Instr.*, vol. 29, no. 8, Aug. 1958, p. 734.

6 McClintock, R. M., "Mechanical Properties of Insulating Plastic Foams at Low Temperatures," *Soc. Plastics Engrs. J.*, vol. 14, no. 11, Nov. 1958.

7 McClintock, R. M. and Hiza, M. J., "Epoxy Resins as Cryogenic Structural Adhesives," *Modern Plastics*, vol. 35, no. 10, June, 1958.

8 Hall, W. J., Roder, H. M. and Powell, R. L., "Thermal and Electrical Conductivity of Aluminum and Aluminum Alloys," Proc. Fifth International Conf., Low Temperature Physics and Chemistry, Joseph R. Dillinger, ed., Univ. of Wisc. Press, Madison, 1958.

9 Brown, E. H. and Brennand, J. R., Jr., "Magnetic Losses at Low Temperatures," Proc. 1958 Cryogenic Engineering Conf., K. D. Timmerhaus, ed., Univ. of Colo., Boulder.

10 Woolley, H. W., Scott, R. B. and Brickwedde, F. G., "Compilation of Thermal Properties of Hydrogen in its Various Isotopic and Ortho-Para Modifications," *J. Res., Nat. Bur. Standards*, vol. 41, Nov. 1948, p. 379.

11 Jacobs, R. B., "Single-Phase Transfer of Liquefied Gases," Nat. Bur. Standards Circular no. 596, U. S. Government Printing Office, Washington 25, D. C.

12 Van Grundy, D. A. and Jacobs, R. B., "Characteristics of Some Insulations for Liquid Oxygen Transfer Lines," Proc. 1956 Cryogenic Engineering Conf., K. D. Timmerhaus, ed., Univ. of Colo., Boulder.

13 Van Gundy, D. A., unpublished data, Nat. Bur. Standards, Boulder.

14 Wilkes, G. B., "Thermal Conductivity, Expansion and Specific Heat of Insulators at Extremely Low Temperatures," *Refrig. Engng.*, vol. 54, no. 37, July 1946.

15 Chow, C. S., "The Thermal Conductivity of Some Insulating Materials at Low Temperatures," Proc. Phys. Soc. London, vol. 61, Sept. 1948, pp. 206–216.

16 Verschoor, J. D., "Thermal Conductivity of Commercial Insulations at Low Temperature," *Refrig. Engng.*, vol. 62, Sept. 1954, p. 35.

17 Fuller, P. D. and Peavy, W. R., "Economic and Design Considerations for a 650 Lineal Foot Liquid Oxygen Transfer Line," Proc. 1958 Cryogenic Engineering Conf., K. D. Timmerhaus, ed., Univ. of Colo., Boulder.

18 Brown, R. E., "Economic and Other Aspects of the Distribution of Navy Helium in Liquid Form," Proc. 1957 Cryogenic Engineering Conf., K. D. Timmerhaus, ed., Univ. of Colo., Boulder.

19 Mann, D. B., Birmingham, B. W. and Vander Arend, P. G., "Technical Aspects of Large Scale Liquid Helium Liquefaction and Transportation," Proc. 1957 Cryogenic Engineering Conf., K. D. Timmerhaus, ed., Univ. of Colo., Boulder.

20 American Institute of Physics Handbook, D. E. Gray, Coordinating Editor, McGraw-Hill Book Co., Inc., New York, 1957, Table 6g-3, pp. 6–68 through 6-71.

21 Corruccini, R. J., "Calculation of Gaseous Heat Conduction in Dewars," Proc. 1957 Cryogenic Engineering Conf., K. D. Timmerhaus, ed., Univ. of Colo., Boulder.

22 Fulk, M. M., Corruccini, R. J., Devereux, R. J. and Schrodt, J. E., "Heat Transfer Through Foams and Powders," Proc. 1956 Cryogenic Engineering Conf., K. D. Timmerhaus, ed., Univ. of Colo., Boulder.

23 Lockhart, R. W. and Martinelli, R. C., "Proposed Correlation of Data for Isothermal Two-Phase, Two-Component Flow in Pipes," *Chem. Engng. Prog.*, vol. 45, no. 1, Jan. 1949, p. 39.

24 Martinelli, R. C. and Nelson, D. B., "Prediction of Pressure Drop During Forced-Circulation Boiling of Water," *Trans. ASME*, vol. 70, Aug. 1948, p. 695.

25 Isbin, H. S., Moen, R. H., Wickey, L. O., Mosler, D. R. and Larson, H. C., "Two-Phase Steam-Water Pressure Drops," Preprint 147, Nuclear Engineering and Science Conf., March 17–21, 1958, Chicago, A.I.Ch.E.

26 Hatch, M. R., Jacobs, R. B., Richards, R. J., Boggs, R. N. and Phelps, G. R., "Prediction of Pressure Drop in Two-Phase, Single-Component Fluid Flow," Proc. 1958 Cryogenic Engineering Conf., K. D. Timmerhaus ed., Univ. of Colo., Boulder.

27 Harvey, B. F. and Foust, A. S., "Two-Phase One-Dimensional Flow Equations and Their Application to Flow in Evaporator Tubes," Heat Transfer Symposium, A.I.Ch.E., Dec. 1951.

28 Rogers, J. D., "Two-Phase Flow of Hydrogen in Horizontal Tubes," *J. AIChE*, vol. 2, Dec. 1958, p. 536.

29 Burke, J. C., Byrnes, W. R., Post, A. H. and Ruccia, R. E., "Cooldown of Cryogenic Transfer Systems," Proc. 1958 Cryogenic Engineering Conf., K. D. Timmerhaus, ed., Univ. of Colo., Boulder.

30 Macinko, J., unpublished work, Nat. Bur. Standards, Boulder, Colo.

31 Holcombe, A. H. and Gottzman, C. F., "High Pressure Pumping Equipment for Cryogenic Liquids," Proc. 1958 Cryogenic Engineering Conf., K. D. Timmerhaus, ed., Univ. of Colo., Boulder.

32 Ball, R. and Anderson, R., "Piston Type High Pressure Aircraft Cryogenic Pumps," Proc. 1957 Cryogenic Engineering Conf., K. D. Timmerhaus, ed., Univ. of Colo., Boulder.

33 Ball, R. H., "An Airborne Cryogenic System for Pneumatic Power Generation, Cooling and Other Uses," Proc. 1958 Cryogenic Engineering Conf., K. D. Timmerhaus, ed., Univ. of Colo., Boulder.

34 Patterson, W. and Hokmann, C., "Cryogenic Systems As Auxiliary Power Sources for Aircraft and Missile Applications," Proc. 1958 Cryogenic Engineering Conf., K. D. Timmerhaus, ed., Univ. of Colo., Boulder.

35 Jacobs, R. B., Martin, K. B., Van Wylen, G. J. and Birmingham, B. W., "Pumping Cryogenic Liquids," unpublished report, Nat. Bur. Standards, Boulder. *See also* Martin, K. B., Jacobs, R. B. and Hardy, R. J., "Performance of Pumps With Liquefied Gases," Proc. 1956 Cryogenic Engineering Conf., K. D. Timmerhaus, ed., Univ. of Colo., Boulder.

36 Caine, G. H., Burgeson, D. A. and Shafer, L. J., "Pumping of Liquid Hydrogen," Proc. 1958 Cryogenic Engineering Conf., K. D. Timmerhaus, ed., Univ. of Colo., Boulder.

37 Stahl, H. A. and Stepanoff, A. J., "Thermodynamic Aspects of Cavitation in Centrifugal Pumps," paper no. 55-A-136, 1955 Annual Meeting ASME, Chicago.

38 Salemann, V., "Cavitation and NPSH Requirements of Various Liquids," Paper no. 58-A-82, 1958 Annual Meeting ASME, N. Y., to appear in *Trans. ASME*.

39 Jacobs, R. B., Martin, K. B. and Hardy, R. J., "Direct Measurement of Net Positive Suction Head," Paper No. 58-A-38, 1958 Annual Meeting ASME, N. Y., to appear in *Trans. ASME*.

40 Bosco, G. B., Jr. and Carter, T. A., Jr., "Liquid Hydrogen Pumping Systems," Proc. 1956 Cryogenic Engineering Conf., K. D. Timmerhaus, ed., Univ. of Colo., Boulder.

41 Martin, K. B. and Jacobs, R. B., "Testing and Operation of Ball Bearings Submerged in Liquefied Gases," Preprint no. 58LC-13, ASLE/ASME Lubrication Conference, Los Angeles, Calif., Oct. 13–15, 1958, to appear in *Trans. ASLE*, vol. 2, no. 1. Reprinted in Proc. 1958 Cryogenic Engineering Conf., K. D. Timmerhaus, ed., Univ. of Colo., Boulder.

42 Tanza, G. F., "Development Program for a Non Lubricated 10,000 rpm Bearing Operating Over a Temperature Range From 40° R to 560° R," Proc. 1956 Cryogenic Engineering Conf., K. D. Timmerhaus, ed., Univ. of Colo., Boulder.

43 Haselden, G. G. and Peters, J. I., "Heat Transfer to Boiling Liquid Oxygen and Liquid Nitrogen," *Trans. Inst. Chem. Engrs.*, London, vol. 27, 1949, p. 201.

44 Bromley, L. A., "Heat Transfer in Stable Film Boiling," *Chem. Engng. Prog.*, vol. 46, no. 5, 1950, pp. 221–227.

45 Monroe, A. G., Bristow, H. A. S. and Newell, J. E., "Heat Transfer to Boiling Liquids at Low Temperatures and Elevated Pressures," *J. Appl. Chem.*, vol. 2, 1952, pp. 613–624.

46 Richards, R. J., Robbins, R. F., Jacobs, R. B. and Holten, D. C., "Heat Transfer to Boiling Liquid Nitrogen and Hydrogen Flowing Axially Through Narrow Annular Passages," Proc. 1957 Cryogenic Engineering Conf., K. D. Timmerhaus, ed., Univ. of Colo., Boulder.

47 "Temperature. Its Measurement and Control in Science and Industry." Reinhold Publishing Corp., New York, third ed., 1952.

48 "Temperature. Its Measurement and Control in Science and Industry," vol. 2, Reinhold Publishing Corp., New York, 1955.

49 Bunch, M. D., Powell, R. L. and Corruccini, R. J., "Thermal EMF of Some Thermometric Alloys," in "Low Temperature Physics and Chemistry," J. R. Dillinger, ed., The Univ. of Wisc. Press, Madison, 1958.

50 Geballe, T. H., Morin, F. J. and Maita, J. P., "Some Low Temperature Thermometric Properties of Germanium," Conf. de Physique des Basses Temperatures, Paris, Sept. 2–8, 1955, Annexe 1955-3, Supplement au Bulletin de l'Institut International du Froid, Paris.

51 Goodwin, R. D., "Design of Simple Resistance Thermometer Bridges for Wide-Range Control of Low Temperatures," *Rev. Sci. Instr.*, vol. 29, no. 6, June, 1958, pp. 497–501.

52 Richards, R. J., Jacobs, R. B. and Pestalozzi, W. G., "Measurement of the Flow of Liquefied Gases With Sharp-Edged Orifices," Proc. 1958 Cryogenic Engineering Conf., K. D. Timmerhaus, ed., Univ. of Colo., Boulder.

53 Clark, J., "A New Method for Detecting Cavitation and Turbulence in Cryogenic Fluids," Proc. 1958 Cryogenic Engineering Conf., K. D. Timmerhaus, ed., Univ. of Colo., Boulder.

54 Williams, W. E., Jr. and Maxwell, E., "Liquid Level Indicator for Condensed Gases at Low Temperatures," *Rev. Sci. Instr.*, vol. 25, Feb. 1954, p. 111.

55 Scott, R. B., "Cryogenic Engineering," D. Van Nostrand Co., Inc., Princeton, 1959.

56 Linning, D. L., "The Adiabatic Flow of Evaporating Fluids in Pipes of Uniform Bore," Inst. of Mech. Engrs., Proc., B, vol. 1B, no. 2, 1952, p. 64.

Atomization in High Velocity Airstreams

MALCOLM A. WEISS[1] and CHARLES H. WORSHAM[2]

Esso Research and Engineering Co.
Linden, N. J.

An experimental study was made of the drop sizes obtained on injecting a liquid into large hot airstreams of sustained high velocity. The liquid, a molten synthetic wax, was injected contrastream or costream through simple cylindrical tubes. Downstream, a traversing probe withdrew a representative sample of the stream, cooled it and froze the droplets. The collected solid particles were analyzed by sedimentation and by sieving. The results were correlated empirically by the dimensionless equation

$$\left(\frac{X\rho_A V^2}{\sigma_L}\right) = 0.61\left(\frac{V\mu_L}{\sigma_L}\right)^{2/3}\left(1+\frac{10^3\rho_A}{\rho_L}\right)\left(\frac{W\rho_L\sigma_L\mu_A}{\mu_L{}^4}\right)^{1/12}$$

Mass median diameter (X), air density (ρ_A), relative velocity (V), liquid viscosity (μ_L) and mass injection rate (W) were changed over 4- to 25-fold ranges. Surface tension (σ_L), liquid density (ρ_L) and air viscosity (μ_A) were not changed significantly.

AN EXPERIMENTAL study was made of the drop size distributions resulting from spraying liquids into large airstreams of sustained high velocity. The intent of this study was to simulate fuel injection in turbojet afterburners and in ramjets. Although there are much data on drop size for liquids atomized by small, rapidly expanding airjets, there are very little data on atomization in large, steady flow airstreams of high velocity. The latter is the physical system in jet engines, and it is different enough from the systems studied to warrant investigation.

A survey of possible techniques for measuring drop size distributions led to the choice of a modified "substitute-fluid" method for this work. The substitute-fluid method injects a liquid which is solid under normal conditions. However, when molten under injection conditions, the liquid has physical properties similar to those of the real liquid fuels of interest. The molten drops can be frozen after atomization, collected as solid particles and analyzed for drop size distribution.

In order to obtain meaningful results, Longwell (1)[3] (and preliminary experiments here) showed that there must be no marked change in temperature until atomization is completed. If a hot molten material is sprayed into cold air, liquid temperature can drop, and freezing can begin while drop breakup is still occurring. At the least, rapid cooling of the liquid leads to an ambiguity in temperature (and thus in liquid physical properties) during atomization. Therefore, in all of this work the molten liquid was sprayed into hot air at the same temperature as the liquid, and the drops were not cooled and frozen until drop breakup was completed.

Experimental Methods

The liquid injected in all tests was molten Acrawax C, a synthetic wax manufactured by the Glyco Products Co. It melted at 284 to 290 F and was not volatile; the vapor pressure was estimated to be 10^{-5} mm Hg at 300 F. Added to the wax was 4 per cent of alcohol-soluble nigrosine black dye; the dye made the solid drops opaque for photomicrographic calibrations. The dyed wax had the following physical properties

	300 F	350 F	400 F
specific gravity	0.828	0.811	0.806
surface tension (dyne/cm)	22.0	20.1	18.2
viscosity (centipoise)	11.3	5.86	3.25

Except for the study of liquid viscosity effects, all runs were made at 300 F.

Dyed wax was melted in a heated blowcase containing a large spherical float (to minimize diffusion of the pressuring inert gas into the liquid). The liquid was piped through heated lines to a turbine flowmeter, then through a high surface heat exchanger (to match air and liquid temperatures), and finally to the injector.

The injectors themselves consisted of cylindrical tubes, $\frac{3}{64}$-, $\frac{3}{32}$- and $\frac{3}{16}$-in. ID. Each tube was supported and fed by a thin strut of flattened tubing, welded in a ring of 6-in. pipe (see Fig. 1). Injector axis always coincided with the air duct axis, but the orientation could be either costream or contrastream.

The air duct consisted of 6-in. pipe. Two perforated plates and a straight run of about 14 ft preceded the flanges between which the injector ring was clamped. The length of pipe downstream of the injector could be varied as the sampling distance required. The air compressor available allowed velocities up to about 1000 ft per sec in the duct at atmospheric pressure; at higher pressures, maximum velocities were proportionately lower.

For tests at atmospheric pressure, the length of duct downstream of the injector simply exhausted to the atmosphere. The entrance to the sampling probe then was located in the exit plane of the duct, and samples could be taken at fixed points or while the probe was moving in a traverse path across the exit plane. For tests at pressures above atmospheric, the duct exhausted into a 12-in. pipe section with a variable exit area. The sampling probe was contained within this section, and the sampling probe entrance was again located in the duct exit plane. However, the probe could not be moved during high pressure tests, and all samples were taken at a single point 0.5-in. above the duct axis.

Received Aug. 4, 1958.

[1] Section Head.

[2] Research Engineer.

[3] Numbers in parentheses indicate References at end of paper.

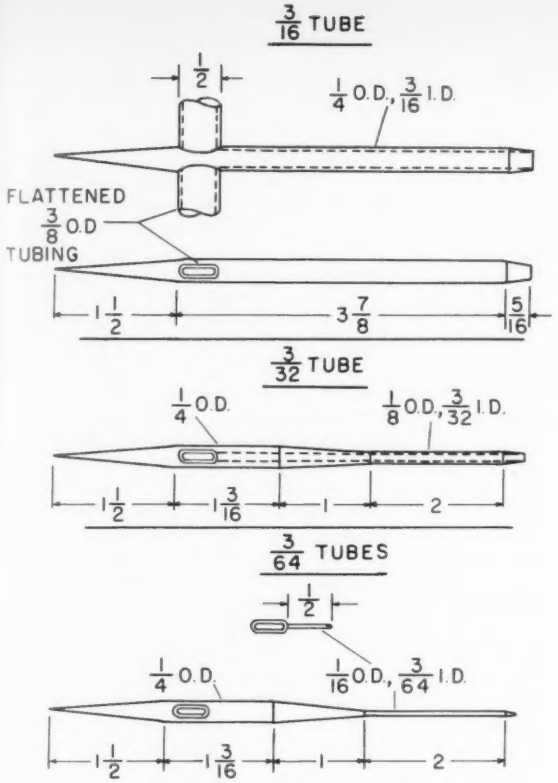

Fig. 1 Geometry of cylindrical injectors, in.

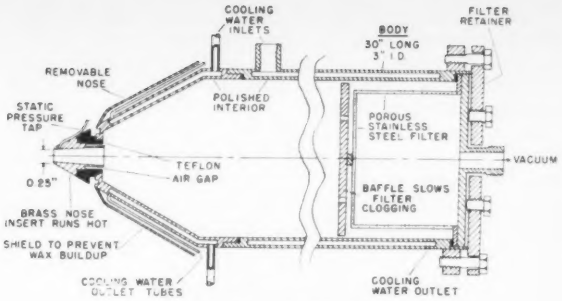

Fig. 2 Droplet sampling probe

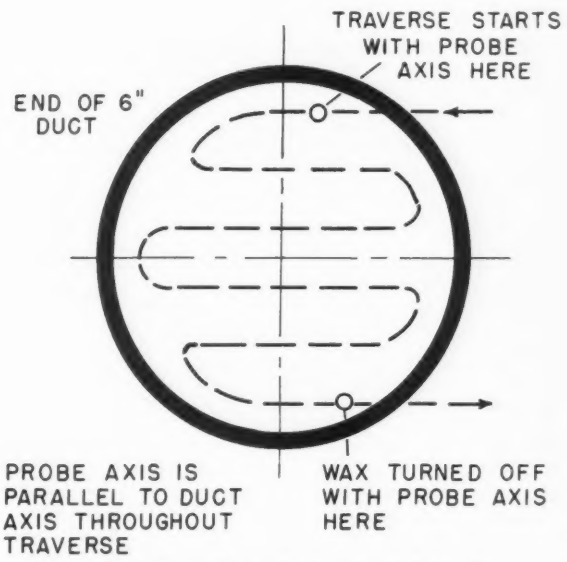
TRAVERSE STARTS WITH PROBE AXIS HERE
END OF 6" DUCT
PROBE AXIS IS PARALLEL TO DUCT AXIS THROUGHOUT TRAVERSE
WAX TURNED OFF WITH PROBE AXIS HERE

Fig. 3 Path of sampling probe traverse at duct exit

The sampling probe used is shown in Fig. 2. This design was developed in order to:

1 Sample at stream velocity to prevent size discrimination while collecting.

2 Collect and freeze droplets without distortion.

3 Collect a reasonable amount of sample in a reasonable length of time.

4 Enable measurements at fixed locations or across the traverse path.

In order to traverse, the entire probe was mounted in a counterbalanced assembly with a follower which tracked in a slotted template. The path described by the probe axis is shown in Fig. 3. During normal operation, air was withdrawn through the probe filter at a rate which equalized static pressure in the probe tip and static pressure in the airstream; this procedure is the most convenient way to obtain sampling at approximately stream velocity. The solid particles collected in the probe were flushed out after a run, dried and analyzed.

Evaluation of Analysis and Sampling

The solid spheres removed from the probe were analyzed for drop size distribution in the Micromerograph—a commercial sedimentation-in-air analyzer. Two sets of five replicate runs were made to determine reproducibility of the analysis; one set used a sample with a mass median diameter of 22 μ, and the other set used a median of 87 μ. For both sets, the rms error was less than 5 per cent of diameter, at a given volume percentage, for cumulative volumes between 5 and 95 per cent. (Particles larger than 150 μ were always separated from the Micromerograph feed and were analyzed by sieving.)

Absolute calibrations of the analyses were made by comparing the results with manual sizing and counting of images from enlarged photomicrographs of 11 different samples ranging in mass median diameter from 13 to 95 μ. From 1700 to 11,000 images were counted for each sample. At the mass median diameter (50 per cent cumulative volume), there was an rms difference in diameter between the two types of analyses of about 8 per cent. Comparisons were also made at 15.9 and 84.1 per cent cumulative volumes; these percentages represent variations of one geometric standard deviation from the mass median for a log-probability drop size distribution. At the 84 per cent level, the rms difference in diameters was about 6 per cent; but at the 16 per cent level, it was about 24 per cent with the Micromerograph usually showing larger particles. It was interesting that this error—in sizing the smallest part of a sample—was not much affected by the absolute level of diameter. A given particle diameter was measured more accurately if it occurred at the 50 per cent point rather than at the 16 per cent point.

Attributing all of the error to the sedimentation analysis probably exaggerates the defects of that analysis. There were also variations from one photomicrograph to another of a given sample. Therefore, because of the speed and simplicity of the Micromerograph (and sieve) analyses, they were used throughout for the data reported here. Unless the smallest drops in a given spray are of critical importance, as they might be in some ignition phenomena for example, the overall accuracy of the analyses is considered adequate for any likely application of the data.

Development of analytical techniques made possible an assessment of the sampling probe. First, particles collected from the probe were found to be almost uniformly spherical.

There was no consistent distortion of the largest drops, which are most difficult to freeze before impaction. On the average, less than 5 per cent of the total sample weight collected was found as a film on the probe walls; a film would prove impact before freezing.

Air withdrawal rate through the probe was deliberately varied (unbalancing the probe nose and stream static pressures) in a series of runs. Only when the mismatch between probe nose and main stream velocities reached about 100 ft per sec was any significant shift observed in the size distribution of particles collected. Since a match within 10 to 30 ft per sec was easily obtained, sampling velocity was not critical.

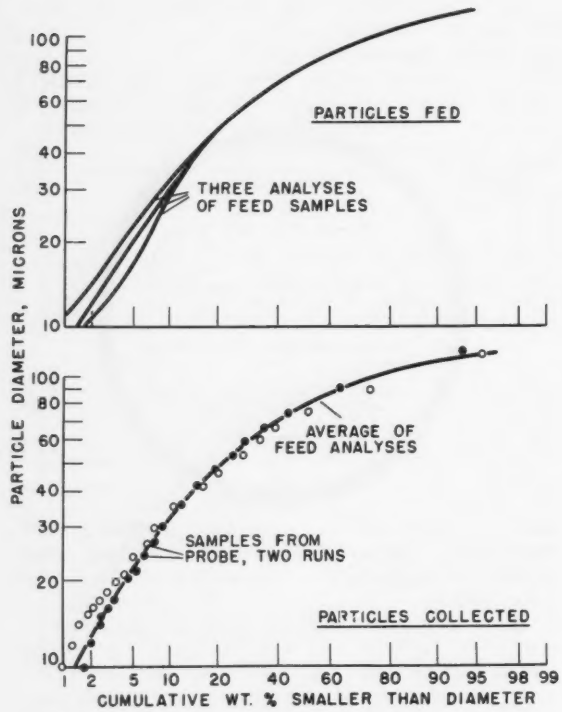

Fig. 4 Collection of solid particles by sampling probe

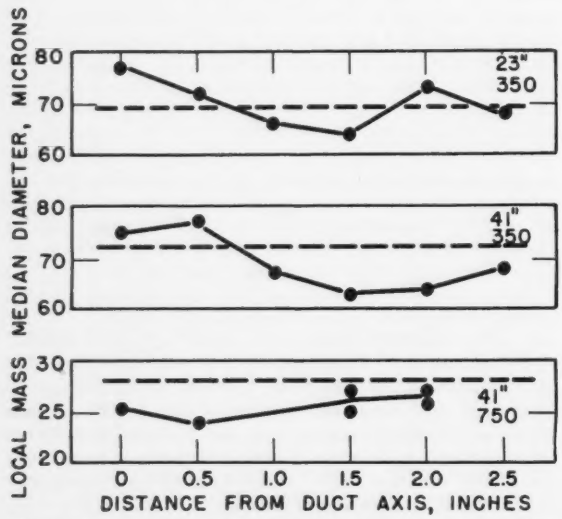

Fig. 5 Local mass median diameters. Dotted lines show average of full traverses. Sampling distances, in., relative velocity, ft per sec

The presence of the probe did not greatly distort the velocity profile upstream of the probe. A small ($\frac{1}{4}$-in. long) Kiel tube was mounted on the duct axis, and the sampling probe was moved across a diameter in a plane just downstream of the Kiel tube. For the complete sample probe travel (from directly behind the Kiel tube to completely clearing it), the maximum change in air velocity at the axis was less than 1 per cent.

There was no preference for any particular particle size during sampling. This was demonstrated by injecting a "spray" of solid spherical particles and collecting a sample in the normal way used for liquid drops. Three analyses of the particles fed are compared in Fig. 4 with analyses from two runs in which the solid particles were collected. Within analytical error, the results were identical.

Finally, the adequacy of the traverse path chosen was assessed. An error in average particle size for the total spray would exist only if *both* (a) local particle size distribution varied appreciably from point to point in the spray, and (b) the sampling probe did not collect for an approximately equal time at all equivalent points in the cross section.

Local samples were taken from three sprays, each resulting from a $\frac{3}{16}$-in. tube injecting contrastream at 1 gpm. Two sampling distances were tested—23 and 41 in. between injector tip and sampling plane—and two air velocities—350 and 750 ft per sec. The results are plotted in Fig. 5. They show that in none of the three sprays did any local median diameter vary by more than 10 per cent from the average between maximum and minimum local median diameters.

The total mass collected by the probe during spray traverses was 100 per cent of the theoretical collection with a standard deviation of about 20 per cent. Considering that local liquid mass velocities varied by as much as 100 to 1 in a given spray, this indicates that the traverse used did give a reasonably weighted sample of the entire spray.

Experimental Results

Using the experimental methods outlined above, a study was made of the sprays from simple cylindrical tubes. The variables studied and the approximate ranges covered were as follows: Relative air velocity (V, 200 to 1000 ft per sec), liquid injection velocity (v, 4 to 100 ft per sec), injector inside diameter (D, $\frac{3}{64}$ to $\frac{3}{16}$ in.), liquid viscosity (μ_L, 3.2 to 11.3 centipoise), air static pressure (P, 1 to 5 atm—corresponding to an overall air density, ρ_A, change of 0.046 to 0.26 lb per ft^3) and both costream and contrastream injection. The liquid injection rate varied from 0.1 to 3 gpm. Resulting mass median diameters (X) ranged from 19 to 118 μ. The experimental data, summarized in the following sections, are presented in detail in (5).

Effect of Relative Air Velocity

Velocity was the variable with the largest effect, by far, on drop diameter. The most useful velocity to consider was relative velocity between liquid- and airstreams (i.e., air velocity plus liquid injection velocity for contrastream injection or minus liquid injection velocity for costream injection). At a given relative velocity—with other parameters also constant—the same drop sizes were obtained when injecting either costream or contrastream.

Most of the data obtained are shown in Fig. 6; the results are separated by injector diameter and direction of injection; liquid injection velocity is the parameter. If all of the slopes of the sixteen lines of Fig. 6 are considered, the average velocity exponent is 1.33 with a standard deviation of 0.13. Two of the lines have markedly low slopes, both resulting from the $\frac{3}{64}$ tubes at low liquid injection velocity (and both

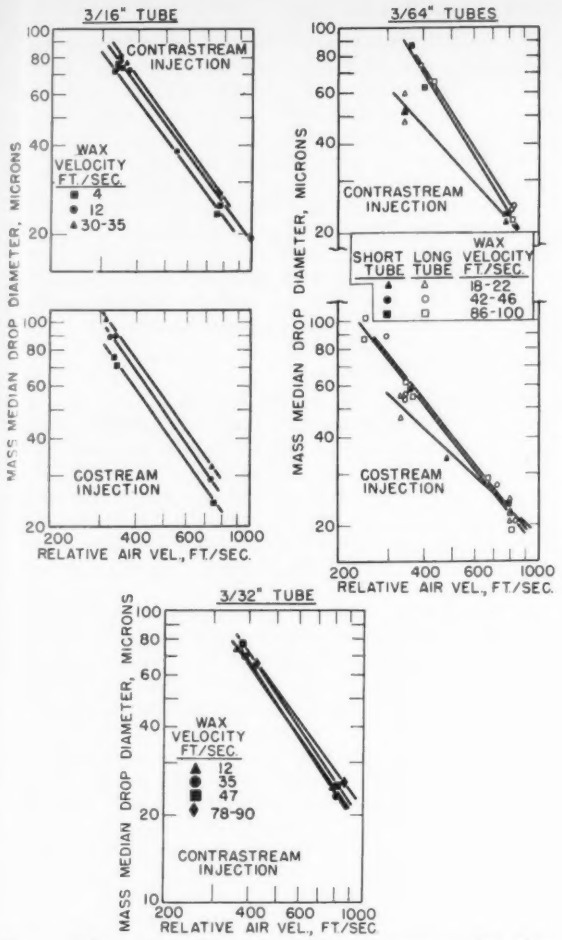

Fig. 6 **Effect of relative air velocity on mass median drop diameter**

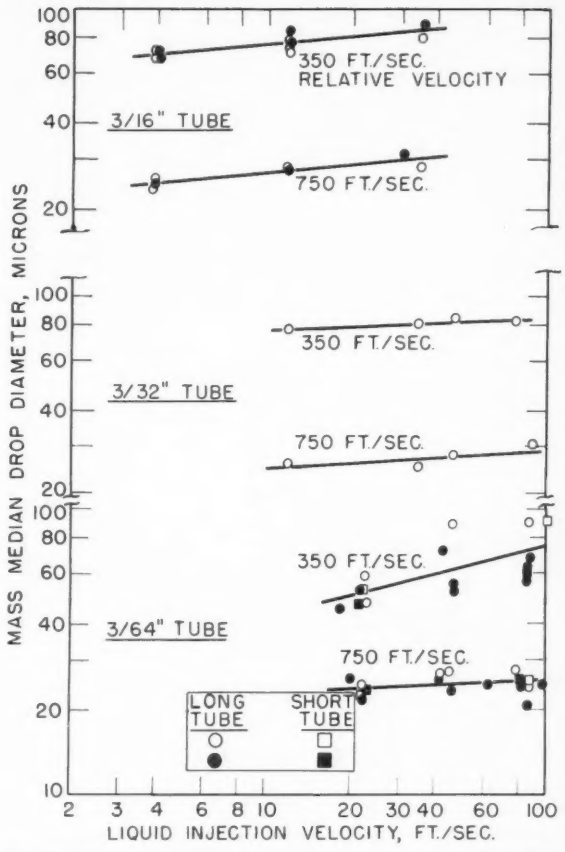

Fig. 7 **Effect of liquid injection velocity on mass median drop diameter. Open points are contrastream, solid points costream**

evidently caused by unexpectedly small drops at low relative velocity). Excluding these two slopes, the average exponent becomes 1.37 with a standard deviation of 0.10. Therefore, the difference in precision offered little justification for eliminating these two slopes, and an average velocity exponent was taken as 1.33, i.e., $X \sim V^{-1.33}$. This velocity exponent compares to the value of 1.0 found by Nukiyama and Tanasawa (4) for small pneumatic atomizers, and to the value of 1.11 for a metal alloy and 1.68 for a wax found by Marshall (2) for large venturi atomizers.

There was no consistent change of relative velocity exponent with injector diameter, direction of injection or liquid injection velocity.

Effect of Liquid Injection Velocity

Fig. 6 makes it clear that liquid injection velocity per se affects drop size in addition to its contribution to relative velocity between liquid and air. This effect is shown in Fig. 7 for each injector diameter, combining the costream and contrastream injection points. The data are grouped at the two levels of relative velocity, 350 and 750 ft per sec, at which most of the results were obtained. When a run was not made at exactly these relative velocity levels, the diameter was corrected by the relative velocity exponent read from the appropriate individual line in Fig. 6.

As liquid injection velocity increases, there is an increase in drop diameter under all conditions. The effect is small except in one case; again, the $\frac{3}{64}$ tubes produce drops smaller than expected at low relative velocities and low liquid injection velocities. Excluding this case, the average liquid velocity exponent is 0.07 with a standard deviation of 0.02. Including it, the average exponent is 0.09 with a standard deviation of 0.07. If less weight is given to the single high value, a reasonable compromise exponent would be 0.08.

Effect of Injector Diameter

The curves of Fig. 7 are crossplotted in Fig. 8 to establish the effect of injector diameter. Thus, different injectors can be compared at constant relative velocity and at constant liquid injection velocity.

At 750 ft per sec, the results are quite regular; drop size increases slowly and consistently as injector diameter increases at all liquid injection velocities. The line slopes range from 0.12 to 0.18, averaging 0.15. However, at 350 ft per sec, the results for the smallest tube are again spread—as would be expected from the high liquid velocity exponent observed for this tube in Fig. 7. The lines in Fig. 8 connect the data points directly. If an attempt is made to draw "best straight lines" through all corresponding points, the slopes range from zero to about 0.35, averaging about 0.19. Giving a slight weight to this higher average value, a compromise exponent for diameter would be about 0.16.

The unusual behavior of the $\frac{3}{64}$ tube at low relative velocity and low liquid injection velocity is not unique to one par-

ticular geometry of injector. Both the "long" and "short" $\frac{3}{64}$ tubes shown in Fig. 1 gave about the same results (see Fig. 7). Therefore, it is likely that a different mechanism of atomization begins to become important for these small tubes at low liquid and air velocities. Drops produced by such tubes will not be accurately predicted by results from the same tubes under other conditions, or from other tubes under similar conditions.

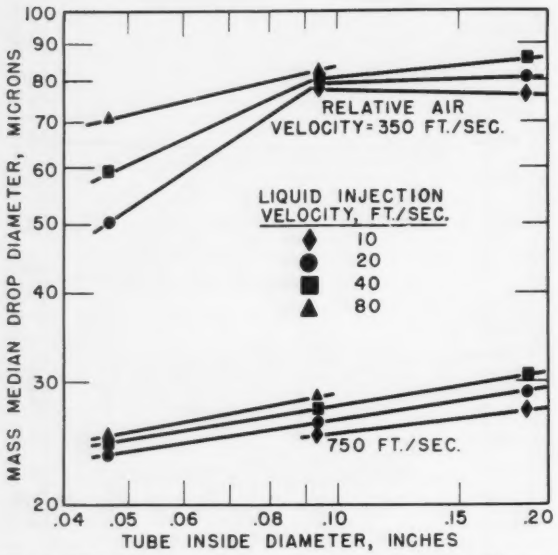

Fig. 8 Effect of injector diameter on mass median drop diameter

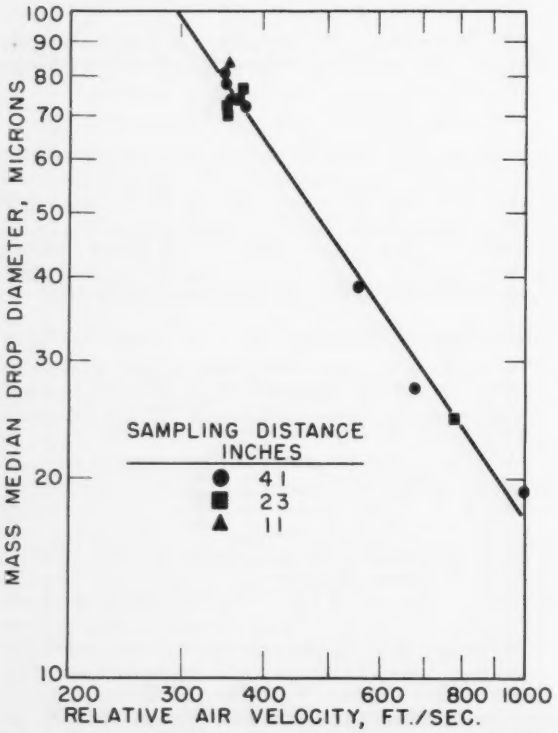

Fig. 9 Effect of sampling distance between injector and probe tips

Effect of Sampling Distance

The results discussed up to this point were obtained sampling at distances of 33 to 41 in. from the injector tip. Several runs were made to determine the effect of sampling closer to the injector. All of these tests used the $\frac{3}{16}$-in. tube injecting contrastream at a liquid velocity of 12 ft per sec.

Fig. 9 shows that a reduction in sampling distance from 41 to 23 in. had no observable effect. In one run there was a further reduction, to 11 in. The resulting median diameter was slightly higher than the mean of the other points, but the difference, based on this single run, is not regarded as significant. Therefore, one can conclude that no important changes in drop size distribution occur at distances greater than about 1 ft for conditions similar to those tested.

Effect of Air Density

The effect of air density was studied by varying static pressure of the air stream while sampling at a fixed location. All of the tests were run with wax injected contrastream at about $\frac{1}{3}$ gpm (16 ft per sec) through the $\frac{3}{32}$-in. tube. Static pressure was varied from 1 to 5 atm abs with maximum air velocity limited by compressor capacity. The minimum air velocity was about 200 ft per sec; lower velocities resulted in gravitational classification of particles between injection and sampling points.

In the first tests, results at atmospheric pressure for point sampling in the "pressure duct" were compared to results at atmospheric pressure in the normal duct with full sampling traverses. The data, in Fig. 10, show no evident differences.

All of the pressure data obtained are plotted in Fig. 11 (in two parts to minimize confusion of data points). For each set of points at a given pressure level, a best straight line was drawn and the slope measured. No slope but one differed by more than 6 per cent from the average of 1.33 determined for all data at atmospheric pressure. The single exception, at 3 atm, could be shifted greatly by change of one point. Therefore, the effect of relative velocity on drop diameter

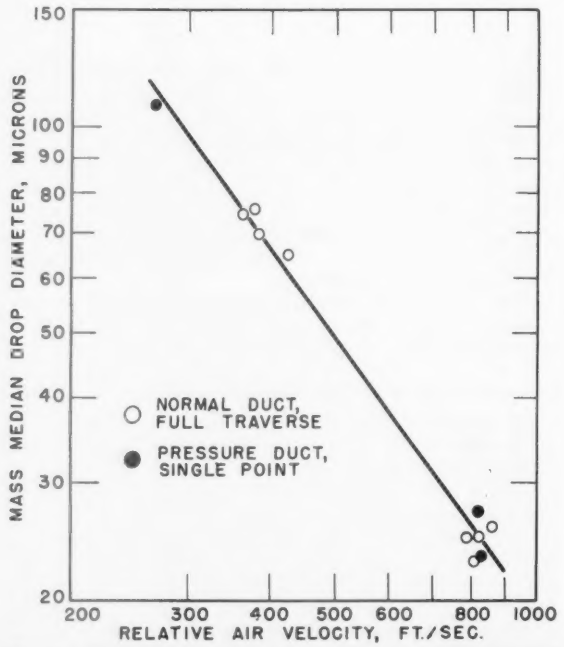

Fig. 10 Comparison of sprays from pressure duct and normal traverses

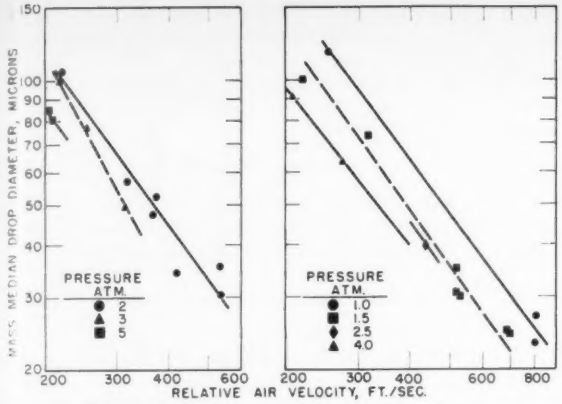

Fig. 11 **Effect of relative air velocity at several air pressure levels**

seems to be unaffected by pressure in the pressure range covered.

The effect of pressure at given velocity levels was determined by crossplotting points from the lines of Fig. 11. Fig. 12 shows that a fairly uniform pressure effect was found when diameter was plotted against $(1 + 1/P)$. The slopes of the lines in Fig. 12 vary from about 1.0 to 1.2, averaging 1.1.

Because of the scatter of original data points in Fig. 11, the exponent of 1.1 was simplified to 1.0. Original pressure duct data were then correlated by the group $(1 + 1/P)/V^{4/3}$. The correlation showed that the equation $X = K(1 + P)/V^{4/3}$ (with K a constant) described the 25 pressure duct median diameters with a standard deviation of 6 per cent of diameter.

Effect of Liquid Viscosity

Seven tests were conducted in order to determine the effect of lowered liquid viscosity on median drop size. This was done by spraying wax at temperatures up to 400 F into airstreams of the same temperature. The results are shown in Fig. 13 for comparison with earlier data at 300 F. There is a marked reduction in drop diameter as temperature increases.

Points from the lines of Fig. 13 are crossplotted in Fig. 14 to determine the viscosity exponent. An average for the three lines shown is 0.34. The same exponent was found for a pair of runs at 300 and 350 F using a smaller ($\frac{3}{32}$-in.) injector.

On increasing temperature, properties other than liquid viscosity also change, and these changes can be expected to affect drop diameter. However, the effects are small compared to the overall effect observed. For example, assuming the influences of surface tension and liquid density to be those reported by Nukiyama and Tanasawa (4), and assuming the influence of air density to be the same as reported in the previous section, a temperature increase from 300 to 400 F would cause an overall drop diameter change of less than 3 per cent if there were no effect of liquid or air viscosity. This compares to the 35 per cent changes observed.

Correlation of Results

The results described can be summarized briefly by the following proportion

$$X \sim V^{-1.33}\mu^{0.08}D^{0.16}\mu_L^{0.34}\left(1 + \frac{\rho_{A0}}{\rho_A}\right)$$

where ρ_{A0} is the density of air at 300 F and atmospheric pressure. Three other properties, not studied here, can be ex-

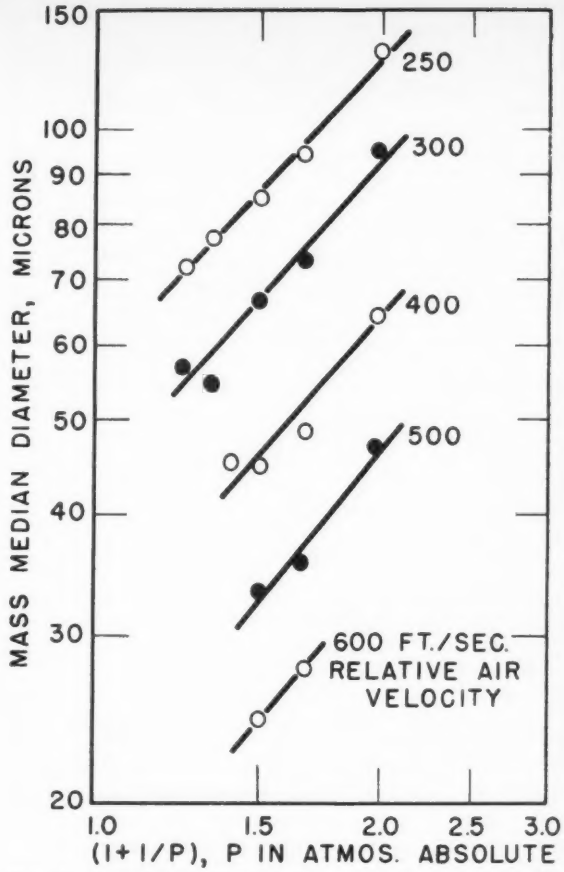

Fig. 12 **Crossplotted effect of air pressure at several velocity levels**

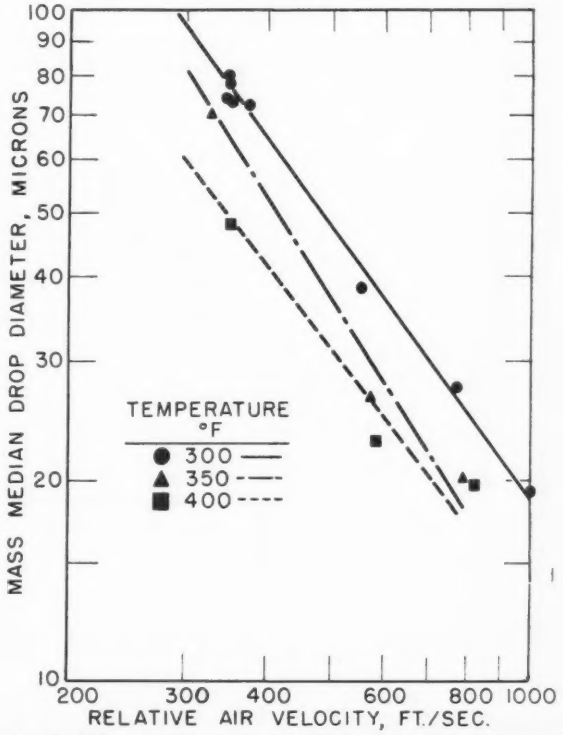

Fig. 13 **Effect of temperature on mass median drop diameter $\frac{3}{16}$-in. contrastream tube, 1 gpm**

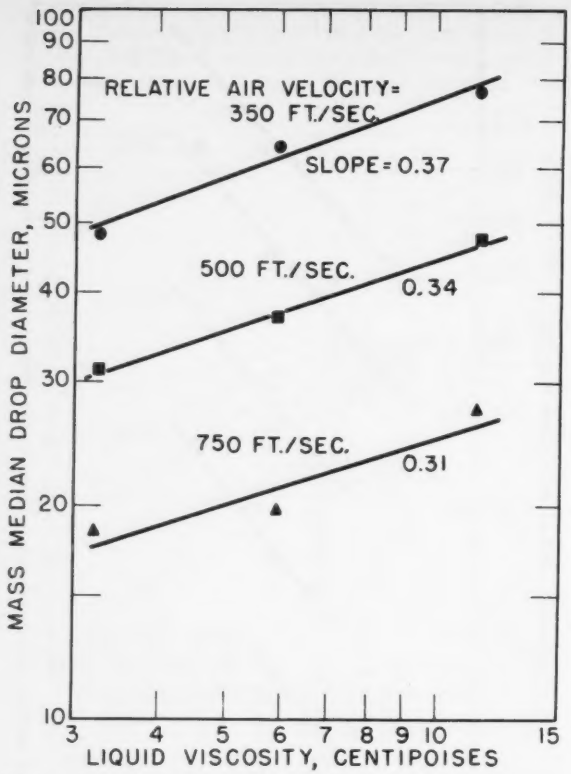

Fig. 14 Effect of liquid viscosity on mass median drop diameter

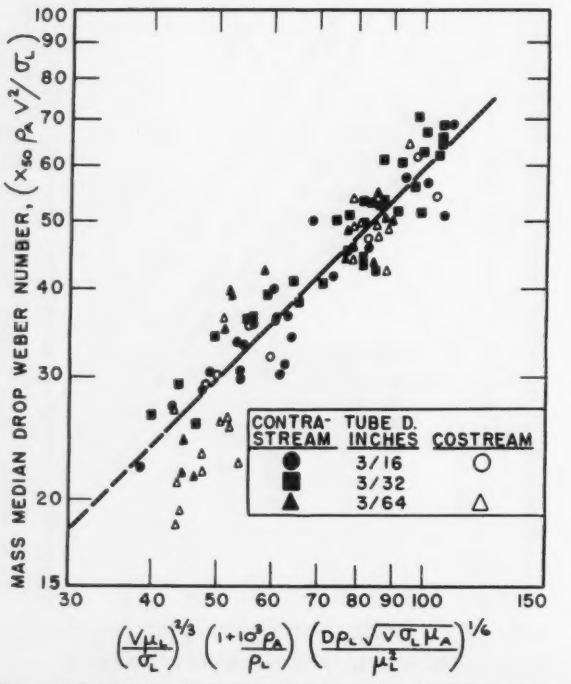

Fig. 15 Correlation of mass median drop diameters from tube injectors

pected to affect drop size: Surface tension, air viscosity and liquid density. Assuming that drop diameter is proportional to each property raised to some simple exponent, the exponents can be determined uniquely by elementary dimensional analysis (since there are three exponents and three dimensions). The result is

$$X \sim \sigma_L^{0.41}\,\mu_A^{0.09}\,\rho_L^{-0.84}$$

Combining this proportion with the preceding one, the mass median drop Weber number (the ratio of air dynamic pressure forces to surface tension forces) can be separated to give

$$\frac{X\rho_A V^2}{\sigma_L} = K_1\,\frac{V^{0.67}\mu_L^{0.24}}{\sigma_L^{0.59}}\,v^{0.08}D^{0.16}\mu_A^{0.09}\,\frac{\rho_A}{\rho_L^{0.84}}\left(1+\frac{\rho_{A_0}}{\rho_A}\right)$$

In the experiments, ρ_L was 0.828 (at 300 F) and ρ_{A_0} was 0.000838. It is a convenient approximation to substitute $\rho_L/10^3$ for ρ_{A_0}. If this is done, and if variables with like exponents are collected, one reasonable grouping of the variables is

$$\frac{X\rho_A V^2}{\sigma_L} = K_2\left(\frac{V\mu_L}{\sigma_L}\right)^{2/3}\left(1+\frac{10^3\rho_A}{\rho_L}\right)\left(\frac{D\rho_L\sqrt{v\sigma_L\mu_A}}{\mu_L^2}\right)^{1/6}$$

with all variables in consistent units.

One final substitution can be made which eliminates D and v explicitly. Letting W be the mass rate of injection of liquid (e.g., lb/sec), then

$$\frac{X\rho_A V^2}{\sigma_L} = K_3\left(\frac{V\mu_L}{\sigma_L}\right)^{2/3}\left(1+\frac{10^3\rho_A}{\rho_L}\right)\left(\frac{W\rho_L\sigma_L\mu_A}{\mu_L^4}\right)^{1/12}$$

This equation, with $K_3 = 0.61$, was tested against all of the experimental data, including all air and liquid velocities for both costream and contrastream injection, all injectors, and all air densities and liquid viscosities. The only runs excluded were those point samples designed to measure local spray variations.

Fig. 15 shows the results for 101 runs about equally divided among the $\frac{3}{16}$-, $\frac{3}{32}$- and $\frac{3}{64}$-in. injectors. For the two larger tubes, the standard deviation between observed and correlated median drop diameters was 9.3 and 9.6 per cent. For the 35 points for the $\frac{3}{64}$-in. injector, the standard deviation was 20 per cent. However, Fig. 15 shows clearly that there are large and consistent deviations for the nine $\frac{3}{64}$ tube data points at Weber numbers lower than 25. Excluding these nine points, the standard deviation drops to 12 per cent.

All nine of the excluded points resulted from $\frac{3}{64}$-in. tubes operating at relative velocities below 350 ft per sec. Earlier data showed repeatedly that the smallest injector did not fall into the general pattern at low relative velocities. Therefore, the failure of these points to fit the correlation is not surprising.

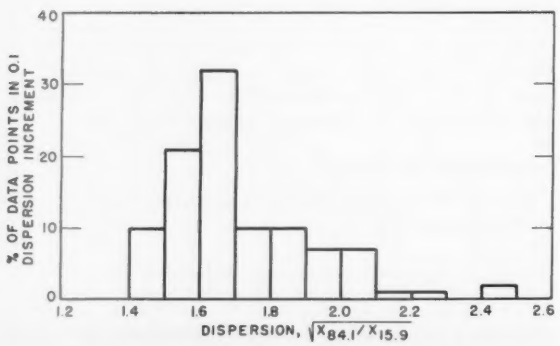

Fig. 16 Distribution of dispersions

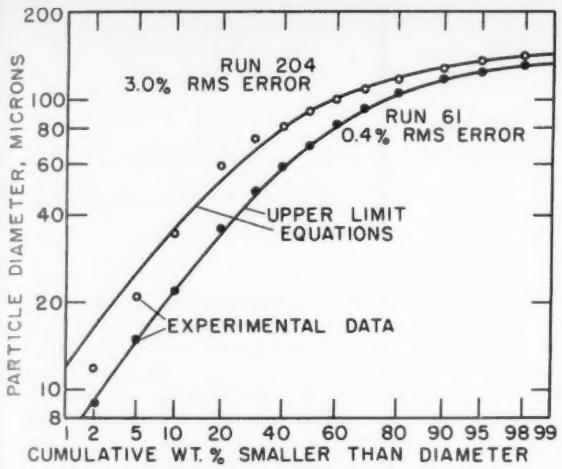

Fig. 17 Examples of data matching for contrastream injectors, log-probability coordinates

Run	Air veloc.	Wax veloc.	Tube diam.	Air press.
61	335	12	$\frac{3}{16}$	1.0
204	199	18	$\frac{3}{32}$	4.0

The drop diameters observed in this study were 35 to 100 per cent larger than predicted by Nukiyama and Tanasawa (4) from their work in small pneumatic atomizers. However, there was much better agreement (less than about 30 per cent difference) with results cited by Marshall (2) for larger venturi atomizers.

Other Spray Properties

Because the entire drop size distribution was measured in each run, properties of the spray other than mass median diameter were also determined.

The distribution of dispersions is shown in Fig. 16. Dispersion is defined here as $\sqrt{X_{84.1}/X_{15.9}}$, where $X_{84.1}$ and $X_{15.9}$ are the drop diameters at cumulative volume percentages of 84.1 and 15.9, respectively. No significant correlation could be found between dispersion and any of the variables or their simple interactions. The median dispersion was 1.66, and the average was 1.71. About two-thirds of the data points lie within 10 per cent of 1.7, and 97 per cent lie within 25 per cent of 1.7.

As would be expected, the ratio of Sauter mean diameter (the diameter of a drop with the same surface-to-volume ratio as the total spray) to mass median diameter decreased as dispersion increased. An empirical value for this ratio was $(1.43 - 0.43\,q)$ where q is the dispersion. The average Sauter mean diameter was about 70 per cent of the mass median, but the range extended from 36 to 87 per cent.

Each drop size distribution was matched by a best fitting upper limit equation. The latter was proposed by Mugele and Evans (3) and is a modification of the log-probability equation that assumes a maximum drop size. By adjusting two constants of the upper limit equation (the third constant was the mass median diameter, and the equation was constrained to pass through the observed value), very good data matching was obtained. In only 2 per cent of the runs did the rms difference between predicted and observed volume percentage (at any given drop diameter) exceed 4 per cent absolute. Two typical matches between the upper limit equation and the experimental data are shown in Fig. 17. One match illustrates a very good fit with an rms error of 0.4 per cent. The other illustrates a relatively poor fit with an rms error of 3.0 per cent. However, even the "poor" fit does a reasonably good job of describing the data. The experimental data were obtained as continuous traces on the Micromerograph; discrete data points from these traces are shown in Fig. 17 to distinguish more clearly between the data and the matching curves.

A "maximum diameter" was one of the two constants selected to give the best fitting equation. In some cases, this maximum diameter was larger and in some cases smaller than the largest drops actually observed; however, the analytical data were quite erratic in measuring the last few per cent of the spray containing the largest drops. In general, the maximum diameter varied in the same way that the median diameter did, but the ratio of maximum to median showed a great deal of scatter.

Since only three constants are required to define the upper limit equation, the maximum diameter is a unique function of the dispersion if the Sauter mean diameter is also specified as a function of dispersion. Assuming the Sauter mean to vary with dispersion as defined above, the ratio of maximum diameter to median diameter is approximately equal to $(2.66q - 0.56q^2 - 1.10)$. This is an empirical expression useful for q up to about 2.5.

Conclusions

The atomization of liquids by large high velocity airstreams occurs by direct action of the airstream on the exposed liquid surface. Therefore, relative velocity between liquid- and airstreams is of primary importance. Physical properties of the fluids do affect spray fineness, but their net influence is less critical. The exact way in which the liquid is introduced to the air, i.e., the geometry and operation of the injector, is of least importance, particularly at very high air velocities and for customary ranges of the variables.

Acknowledgment

This work was supported by the Bureau of Ordnance, Department of the Navy, as part of a program in cooperation with the Applied Physics Laboratory, The Johns Hopkins University. Robert J. Lang contributed greatly to the early phases of the experimental program.

References

1 Longwell, J. P., "Fuel Oil Atomization," D.Sc. Thesis, MIT, 1943.

2 Marshall, W. R., Jr., "Atomization and Spray Drying," *Chem. Engng. Prog. Monograph Series* no. 2, vol. 5, 1954.

3 Mugele, R. A. and Evans, H. D., "Droplet Size Distribution in Sprays," *Ind. and Engng. Chem.*, vol. 43, 1951, p. 1317.

4 Nukiyama, S. and Tanasawa, Y., "Experiments on the Atomization of Liquids in an Air Stream," *Trans. Soc. Mech. Eng.* (Japan), vol. 4, 1938, pp. 86, 138; vol. 5, 1939, pp. 62, 68; vol. 6, 1939, pp. II-7, II-15; vol. 6, 1940, p. II-18.

5 Weiss, M. A. and Worsham, C. H., "Atomization in High Velocity Air Streams," Bumblebee Report no. 277, Esso Research and Engineering Co., May 1958.

Some Thermal Stress Design Data for Rocket Grains

M. L. WILLIAMS[1]

California Institute of Technology
Pasadena, Calif.

Supplementing a previous paper (JET PROPULSION, June 1957) giving preliminary elastic stress concentration factors in internal burning star rocket propellant grains due to pressure differences across the web, similar design data for thermal stresses are presented for the particular case of a steady-state temperature difference across the grain, or for a specified heat flux. After determining the internal temperature using a voltage analogy, the Biot-Muskhelishvili analogy is employed to transform the thermal stress field into an equivalent temperature independent edge dislocation problem. The appropriate displacements are then applied to a series of photoelastic specimens of slotted grains, and the stress rise over that existing in a thick walled cylinder of the same web is evaluated experimentally. Following the previous procedure, the data are presented in design chart form.

IN A PREVIOUS paper (1),[2] some photoelastic data were presented for a series of internal burning star-shaped rocket grains subjected to pressure loadings. The design curves given were arranged in the form of stress concentration factors, normalized upon the stress which would exist in a thick walled cylinder in the same web fraction, as a function of the geometric proportions and number of star points. Inasmuch as thermal loadings contribute another major class of design problems in rocket grains, some exploratory investigations were conducted upon geometries similar to the pressure loaded case, for a steady-state temperature difference across the web of the elastic specimen. Although the simulated loading condition is, of course, restricted, it is believed that the quantitative information obtained will provide a firmer basis for the necessary design extrapolations.

In considering a typical model for elastic thermal stress analysis, it is found that the thick walled cylinder is the simplest configuration with which to work. With particular reference to rocket grains, Geckler's work (2) supplies the basis for a fairly comprehensive study of this problem. On the other hand, and similar to the pressure loading case, when the wall thickness is nonuniform, as in the case of an internal burning star, analytical solutions are not readily obtained. Furthermore, numerical methods are not easily applied in areas of high stress concentration, and one therefore naturally turns to experimental methods.

Biot (3) and Muskhelishvili (4) independently pointed out that certain classes of thermal stress problems, to which the usual grain configurations belong, are analogous to superimposing appropriate displacements on the boundary which are uniquely determinable by the prescribed steady-state temperature distribution or heat flux into the grain. In 1939 Weibel (5) exploited this analogy photoelastically and, after experimentally verifying the results by comparison with the analytical solution for the thick walled cylinder, evaluated the thermal stresses in a square thick walled tube. It required therefore only minor modifications to Weibel's experimental setup to test a rocket grain configuration. Preliminary tests on several slotted grains have been completed wherein the maximum thermal stress at the star point was found and then divided, for normalization, by the thermal stress which would exist in a thick walled cylinder for the same temperature difference. The resulting thermal stress concentration factors can then be presented as functions of the design parameters in charts for easy use.

More specifically, there are actually two concentrations present: (a) a geometric factor representing the difference in planar rigidity of the star from a thick walled cylinder of the same web fraction, and (b) a temperature factor due to the concentration of heat flux at the star points, which is of course not present in the cylinder. While the two effects can be combined, a comparison of the geometric factor with the (geometric) factor for pressure loading indicates they are quantitatively very similar. In order to explain this association, consider for example the hoop stress distribution through the web when the grain is loaded by internal pressure contrasted with a temperature loading, say hot outside and cold inside. The first case tends to produce a more or less uniform tensile stress across the web, whereas the latter will lead toward internal tensile and external compressive stresses, approximately linearly distributed across the wall.

If one next turns to Neuber's curves for stress concentration factors (6) for a flat rectangular bar notched on one side (Fig. 6)—with the notch associated with the star point at the minimum web section, it is found that when the bar is pulled in tension the factors are qualitatively similar to, but quantitatively lower than, those when the bar undergoes bending. As these loadings are characteristically those produced by pressure and temperature, respectively, in the web of the grain, one would expect the relative increase of stress at the star point to be in approximately the same relation. The experimental results substantiate this conjecture (1)—higher values for the geometric thermal factor.

It is perhaps worth emphasizing at this point that the temperature distribution is usually a requirement for the subsequent determination of thermal stress[3] with one possible

Received Nov. 4, 1958.

[1] Associate Professor, also Consultant, U. S. Naval Ordnance Test Station, China Lake, Calif. Member ARS.

[2] Numbers in parentheses indicate References at end of paper.

[3] Generally speaking, the three-dimensional classical thermal stress boundary value problem requires a simultaneous solution of four coupled linear partial differential equations in the three displacements and the temperature. It is only a consequence of the fact that thermal inputs do not, in most engineering problems, accelerate elements of the elastic body sufficiently for those displacements to affect the temperature distribution. Thus it is permissible to uncouple the four equations and solve the fourth (heat conduction) equation independently of the displacements, by hypothesis, and with the temperature field known, solve the remaining three equations for the displacements in three directions corresponding to the temperature. See the full equations for example in the Parkus paper (7). The only area in rocket grains where this separation might have to be further explored is under deflagration-detonation conditions, where the chemical energy terms would also have to be included in the above set.

photothermoelastic exception (8). Even presuming that the temperature or heat flux boundary conditions are known at the surface of the solid, it is not always an easy thing to determine the internal temperatures. Aside from analytical solutions which exist in certain cases either by direct quadrature or conformal mapping techniques for steady state, one again thinks of experimental determination or analogs. Thermocouples have frequently been used, particularly where transients are required, but for steady-state and relatively simple boundary conditions a voltage analogy works well. This technique, using Teledeltos conducting paper[4] rather than a fluid medium, was actually the one used in preparing to find the thermal stress concentration factors.

An alternate semi-analytical technique may also be used for determining approximate temperature distributions. Minimum principles have been determined for heat conduction by Biot (9), Chambers (10) and Parkus (7), that is, a functional representation of the temperature distribution may be assumed, say a power series with unknown coefficients for which the values are determined by setting the first variation of the heat conduction integral with respect to these unknowns to zero and solving the resulting algebraic equations. For those acquainted with structural analysis, the method is identical in principle with the Rayleigh-Ritz procedure.

Analogy

Consider the case of a hollow cylinder in plane strain, that is, the axial displacement is restrained to zero. Then, if steady-state temperature conditions exist and the temperature is symmetric and independent of the axial length, the problem can be formulated as one of plane stress. Specifically applied to rocket grains, one would have a thin slab of uniform thickness with outer and inner boundaries C_o and C_i, respectively (Fig. 1). The steady-state temperature distribution can then be calculated from a solution of $\nabla^2 T(x, y) = 0$ for the arbitrary boundary conditions on the temperature or heat flux upon C_o and C_i. Presuming a thermal field is the only loading, the stresses can then be calculated from the applicable equations of elasticity and the associated boundary conditions.

The principle of using a photoelastic technique to find thermal stress was first employed by Weibel (5), based upon the independent theoretical work of Muskhelishvili (4) and Biot (3). The essence of the matter has also been concisely summarized by Timoshenko and Goodier (11), whose treatment will be outlined for ready reference.

First, it can be shown that if the cross section of a cylinder is simply connected, i.e., without holes, then the steady-state thermal stresses in the plane are zero. Hence, it is concluded that in a cross section which is multiply connected, i.e., having one or more holes, thermal stresses present in this case can be completely relieved by making the cross section simply connected through the simple expedient of making cuts connecting the various inclusions. Reversing the argument then, the thermal stress distribution can be restored to the body by imposing the proper displacements and rotations in closing the various slits.

For the thermal stress in the singly connected cross section to be zero, $\sigma_x = \sigma_y = \tau_{xy} = 0$, the normal strain must be

$$\epsilon_x = \frac{\partial u}{\partial x} = (1 + \nu)\alpha\Delta T \equiv \epsilon \qquad [1a]$$

$$\epsilon_y = \frac{\partial v}{\partial y} = (1 + \nu)\alpha\Delta T \equiv \epsilon \qquad [1b]$$

and the shear strain

$$\gamma_{xy} = \frac{\partial v}{\partial x} + \frac{\partial u}{\partial y} = 0 \qquad [2]$$

[4] Such conducting paper is supplied by the General Electric Co., Schenectady, N. Y., under the trade name Teledeltos. The silver conducting paint was supplied by Micro-Circuits Co., New Buffalo, Mich.

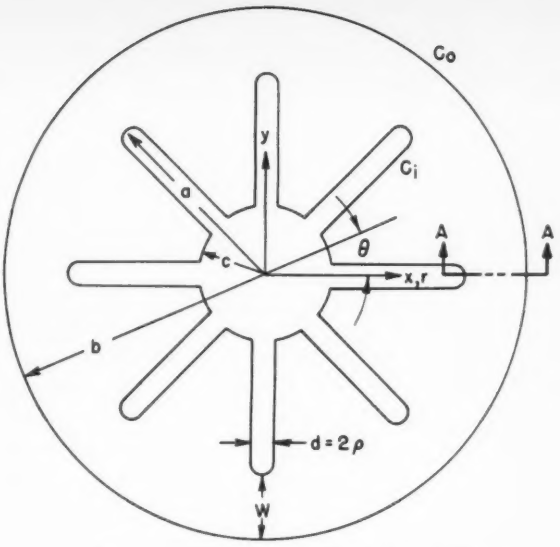

Fig. 1 Geometry of the grain configuration

The preliminary steps are completed upon recalling the definition of rotation at a point

$$\omega = \frac{1}{2}\left(\frac{\partial v}{\partial x} - \frac{\partial u}{\partial y}\right) \qquad [3]$$

From Equations [1 and 2] we have

$$\frac{\partial u}{\partial x} = \frac{\partial v}{\partial y} \qquad \frac{\partial v}{\partial x} = -\frac{\partial u}{\partial y}$$

which Cauchy-Riemann equations show that the u and v displacements in the x and y directions, respectively, are harmonic functions. Moreover the dilatation ϵ and rotation ω are themselves harmonic, which is easy to verify, e.g.

$$\frac{\partial \omega}{\partial y} = \frac{\partial}{\partial y}\left[\frac{1}{2}\frac{\partial v}{\partial x} - \frac{1}{2}\frac{\partial u}{\partial y}\right] = \frac{1}{2}\frac{\partial}{\partial x}\left[\frac{\partial v}{\partial y}\right] - \frac{1}{2}\frac{\partial}{\partial y}\left[-\frac{\partial v}{\partial x}\right] = \frac{\partial \epsilon}{\partial x}$$

Hence, one can form the complex function

$$\epsilon(x, y) + i\omega(x, y) \equiv F(x + iy) = F(z) \qquad [4]$$

From the property of line integrals along a path in the body, beginning at a point u_0, v_0, one can show that

$$(u - u_0) + i(v - v_0) = \int_{z_0}^{z} F(z)dz \qquad [5]$$

$$\omega - \omega_0 = \int_{z_0}^{z}\left(\frac{\partial \epsilon}{\partial x}\,dy - \frac{\partial \epsilon}{\partial y}\,dx\right) \qquad [6]$$

Now, whereas in a singly connected region these integrals must vanish when the contour is closed on itself, $z \to z_0$, in order that the thermal stress vanish, in a multiply connected region this is not necessarily true. The values of the integrals—which depend only upon the given temperature distribution—give the displacements Δu and Δv and the rotation $\Delta\omega$, which must be released at the cuts in order that the thermal stress vanish. Or, conversely, if these same dislocations were imposed on a cross section (at room temperature), they would produce stresses identical to those of the temperature distribution with which they are associated.

This means that if the original region is cut (say across AA, Fig. 1), then the thermal stresses may be simulated by im-

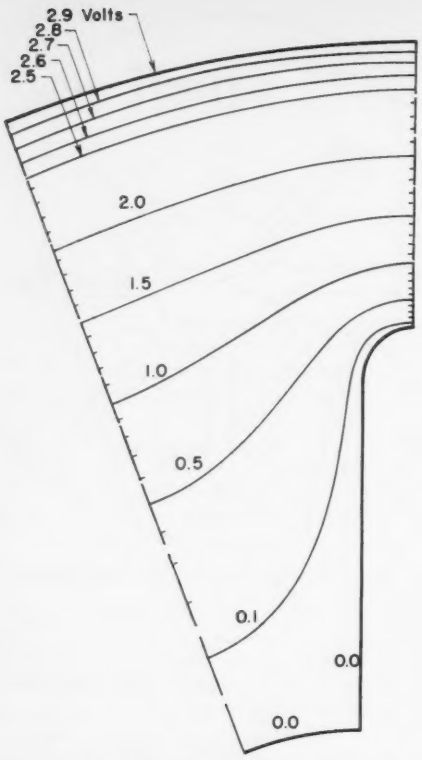

Fig. 2 Sectional thermal contour showing lines of constant voltage or temperature

posing the resulting translations and rotation as boundary displacements at the cut. Using a deformeter similar to that of Weibel's, a birefringent specimen in polarized light can be subjected to the dislocations, and resulting fringes interpreted in terms of principal stress by the Stress Optic law[6]

$$\sigma_1 - \sigma_2 = \frac{2f}{t} n \qquad [7]$$

where on the internal boundary, one of the principal stresses is zero. Thus the steady-state thermal stress variation along the boundary may be obtained relatively simply.

The model stresses obtained in this plane stress experiment are now transferred to an equivalent plane strain case for a long restrained cylinder of the model material by increasing the stresses by the factor $1/(1 - \nu^2)$, where ν is Poisson's ratio.

Finally, the stresses in a prototype grain material are obtained by multiplying the plane strain model stresses by the ratio (E_p/E_m) where E is Young's modulus, and the subscripts p and m indicate the prototype and model, respectively. The axial stress when the ends are restrained becomes

$$\sigma_{z_p} = -E_p\alpha_p T(x, y) + \nu_p(\sigma_{x_p} + \sigma_{y_p}) \qquad [8]$$

Determination of the Temperature Distribution

As most grain shapes have more or less irregular cross-sectional shapes, it is somewhat difficult to solve for the temperature distribution analytically. For the same reason, a numerical solution using relaxation methods is also somewhat cumbersome, because of the large number of irregular stars needed in the network. The method used in this particular case was to take advantage of the similarity between the steady-state heat and potential equations. By cutting out a geometrically similar contour from a piece of conducting paper and imposing arbitrary boundary voltages, the lines of constant voltage (or temperature) were easily found by running a probe, which was in series with a voltmeter, across the paper.

In applying this technique to a geometry of interest in this investigation, the shape shown in Fig. 1 was chosen. First, the temperature distribution was measured experimentally using the Teledeltos conducting paper. A nominal 3 v differential was imposed by a standard dry cell after painting the boundaries C_o and C_i with conducting silver paint to insure the same level of potential along each boundary. A typical set of experimental temperatures or voltage contours is shown in Fig. 2.

For grains which have a circumferentially periodic symmetry, it turns out that along any radial cut, the radial displacement is identically zero. The displacement therefore is only tangential and proportional to the radius from the center of the grain, or alternately, a pure rotation of the slit. Now in Equation [5], $F(z) = \epsilon + i\omega = (1 + \nu)\alpha\Delta T + i\omega$. However, the temperature must be an even function of θ with respect to AA, whereas the rotation must be odd. Thus, upon writing the line element dz along a constant radial path r_0 as $-r_0 \sin\theta\, d\theta + ir_0 \cos\theta\, d\theta$ the integral becomes in polar form

$$\Delta u_r + i\Delta v_\theta = \int_0^{2\pi} [(1+\nu)\alpha \sum \Delta T_n \cos n\theta + i \sum \omega_n \sin n\theta] \times (-r_0 \sin\theta\, d\theta + ir_0 \cos\theta\, d\theta)$$

which reduces by the orthogonality relations to

$$\Delta u_r + i\Delta v_\theta = ir_0 \int_0^{2\pi} [(1+\nu)\alpha \sum \Delta T_n \cos\theta \cos n\theta - \sum \omega_n \sin\theta \sin n\theta] d\theta$$

$$= 0 + ir_0 \text{ (constant)}$$

so that

$$\Delta u_r = 0 \qquad [9]$$

$$\Delta v_\theta = \beta r_0 \qquad \beta = \text{constant} \qquad [10]$$

Turning to Equation [6], one has

$$\Delta\omega = \int \left(\frac{\partial\omega}{\partial r} dr + \frac{\partial\omega}{\partial\theta} d\theta\right)_{r = r_0}$$

$$= \int_0^{2\pi} \frac{\partial\omega}{\partial\theta}\bigg|_{r = r_0} d\theta = \int_0^{2\pi} r \frac{\partial\epsilon}{\partial r}\bigg|_{r = r_0} d\theta$$

using the Cauchy-Riemann relation. The rotation then, $\beta \equiv \Delta\omega$, is

$$\beta = (1+\nu)\alpha r_0 \int_0^{2\pi} \frac{\partial\Delta T}{\partial r}\bigg|_{r = r_0} d\theta \qquad [11]$$

and the physical significance of the rotation is immediately evident. It is the amount of heat flow across a constant radius boundary. Specifically, if the arbitrary radius r_0 is chosen as the external surface of the grain, the analogy requires a rotational dislocation of the slit, proportional to the total heat flux into the grain.

For cases where the flux is prescribed or known on the boundary through fluid mechanics considerations or otherwise, evaluation of Equation [11] is straightforward. On the other hand, if a constant temperature condition is prescribed the boundary flux will, of course, vary if the cross-section geometry is other than constant wall thickness.

[6] The model constant $2f/t$ equaled 376 psi per fringe for the tests to be discussed presently: f is a property of the model material and t is the thickness of the specimen.

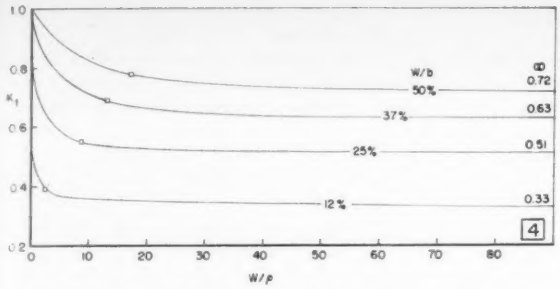

Fig. 3a Thermal concentration factor—four-slotted grain

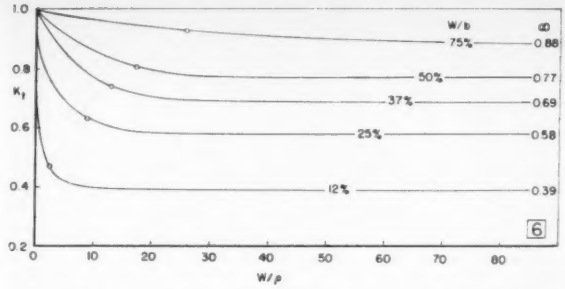

Fig. 3b Thermal concentration factor—six-slotted grain

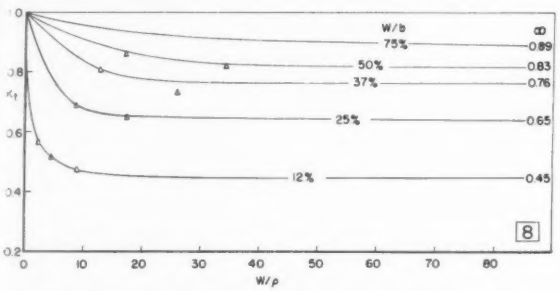

Fig. 3c Thermal concentration factor—eight-slotted grain

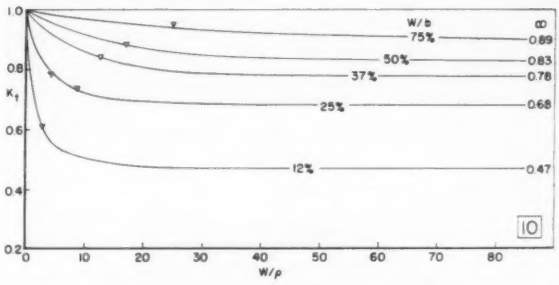

Fig. 3d Thermal concentration factor—ten-slotted grain

As a specific example useful in later normalization, the steady-state temperature distribution in a thick wall grain with web differential ΔT, such that, $T(a) = 0$, $T(b) = T_0$, is

$$\frac{\Delta T}{T_0} = \frac{\log (r/a)}{\log (b/a)} \qquad [12]$$

giving the heat flux as

$$\frac{\partial \Delta T}{\partial r} = \frac{T_0}{\log (b/a)} \cdot \frac{1}{r}$$

so that the associated reference rotation for the cylinder becomes, using Equation [11]

$$\beta^* = \frac{2\pi(1 + \nu)\alpha T_0}{\log (b/a)} \qquad [13]$$

For the grain of Fig. 1, Equation [11] was integrated numerically on the basis of the voltages measured and shown in Fig. 2

$$\begin{aligned} \beta &= (1 + \nu)\alpha T_0 \int_0^{2\pi} \frac{\partial(\Delta T/T_0)}{\partial(r/r_0)}\bigg|_{r = r_0} d\theta \\ &= (1 + \nu)\alpha T_0 \int_0^{2\pi} \frac{\partial(\Delta V/V_0)}{\partial(r/r_0)}\bigg|_{r = r_0} d\theta \end{aligned} \qquad [14]$$

by the similarity of the temperature and voltage distributions. In the tests, the flux was measured across several different control boundaries r_0 and averaged. It was convenient to measure the voltage drop across a fixed Δr_0 interval at N equal spaced intervals $\Delta\theta_0$.[6] The finite difference form of Equation [14] therefore becomes

$$\beta = (1 + \nu)\alpha T_0 \frac{r_0 N \Delta\theta_0}{V_0} \sum_{n=1}^{N} \Delta V_n \qquad [15]$$

In such a fashion, the thermal concentration factor K_t was obtained as the ratio of Equations [15] to [13]

$$K_t = \frac{\beta}{\beta^*} = \frac{r_0 \Delta\theta_0 \log (b/a)}{2\pi V_0} N \sum_{n=1}^{N} \Delta V_n \qquad [16]$$

The test results for a series of four-, six-, eight- and ten-slotted grains are given in Fig. 3.[7]

Alternate Methods

Before leaving the subject of temperature distributions, it may be remarked that analytical expressions for temperature distributions may sometimes be obtained. One case, for example, is a wedge of included angle ϕ with, say, zero temperature on the radial edges and a temperature $\overline{T}$ along the unit radius. Using the even cosine expansion in θ about the bisector of the wedge angle, one can easily find

$$\frac{T}{\overline{T}} = \frac{4}{\pi} \sum_{m=0}^{\infty} \frac{(-1)^n}{2m + 1} r^{(2m+1)\pi/\phi} \cos (2m + 1)\pi\theta/\phi \qquad [17]$$

Indeed a closed form solution can be obtained if $\phi = \pi/4$ (12)

$$\frac{T}{\overline{T}} = 1 - \frac{2}{\pi} \tan^{-1}\left[\frac{1 - r^8}{2r^4 \sin 4\theta}\right] \qquad [17a]$$

Such formulas may be useful in analyzing limit cases, although for the example chosen in Equation [17] the input heat flux is infinite because of the temperature discontinuity on the boundary.

Sometimes boundaries of interest can be obtained by conformal mapping techniques. In this case the mapping function $z = f(\zeta) = C\zeta\ (1 + m\zeta^n)$ deforms a circle into a wavy corrugated form with mean radius c, containing n waves or star points. The depth of the star point is mc measured from the mean radius (13). Thus this contour resembles an internal burning surface and, if the web fraction is not too small, can be used to represent the grain cross section for temperature or even for stress calculations.

As a final simple example, one can state a minimum principle for heat conduction by analogy with the Rayleigh-Ritz (14) procedure used in determining approximate deflections of a membrane whose governing equation is also of the Laplace

[6] If one is interested only in total flux, as opposed to the complete determination of internal temperature distribution, it proves adequate and simpler to measure the integrated flow, because the resistance of the conducting paper is constant over the interval Δr.

[7] In obtaining the experimental data for this investigation, it is a pleasure to acknowledge the assistance of R. R. Parmerter.

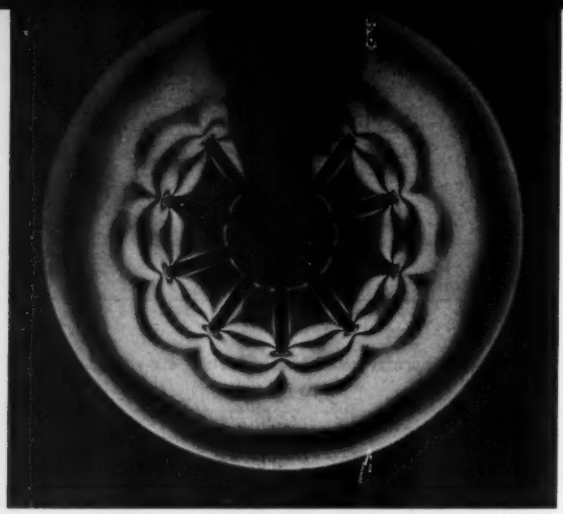

Fig. 4a Isochromatic fringe pattern simulating thermal stress in a rocket grain

Fig. 4b Isochromatic fringe pattern for a pressure loaded grain

type. Theorems in a broader form have already been discussed by various authors (7, 9, 10).

The Dislocation Stresses

Having determined the temperature, or more precisely the required rotation β, the problem of imposing the rotation upon the plane stress photoelastic specimen remains. This, however, is a straightforward procedure and can be accomplished without difficulty in the photoelastic laboratory. Using Weibel's deformeter (5) as the loading mechanism, fringe patterns, and specifically the maximum fringes at the points of maximum stress, were recorded for several values of β. A typical fringe pattern is shown in Fig. 4 along with a similar pattern for pressure loading from (1). Inasmuch as the stress is directly proportional to deformation, this permitted a (linear) curve to be drawn through the test data instead of relying on measurements at only one loading. The test data then became a plot of maximum fringe order at the point of the slot vs. β, from which the slope of the plotted curve could be readily obtained.

Again, the plane stress slice with a constant wall thickness was used for normalization. It can be shown (15) that wedge opening will cause a tangential stress σ_θ on the inside boundary of the model

$$\sigma_{\theta_m}{}^*(a) = \frac{\beta E}{4\pi}\left[1 - \frac{2\log(b/a)}{1-(a/b)^2}\right] \qquad [18]$$

Recall, however (17), that when the stress in the cylinder of the model material is desired, the plane strain solution is obtained from the plane stress solution Equation [18] by replacing E by $E/(1-\nu^2)$, so for the cylinder

$$\sigma_{\theta_c}{}^* = \frac{\beta E}{4\pi(1-\nu^2)}\left[1 - \frac{2\log(b/a)}{1-(a/b)^2}\right] \qquad [18a]$$

Inasmuch as the radial stress is zero, i.e., $\sigma_r(a) = 0$, by the boundary condition, and as σ_r and σ_θ are the principal stresses, the Stress Optic law (7) can be used to obtain

$$n^* = \frac{\beta E}{4\pi(2f/t)}\left[1 - \frac{2\log(b/a)}{1-(a/b)^2}\right] \qquad [19]$$

and

$$\frac{dn^*}{d\beta} = \frac{E}{4\pi(2f/t)}\left[1 - \frac{2\log(b/a)}{1-(a/b)^2}\right] \qquad [20]$$

From experimental data, however, we have a relation similar to Equation [19 or 18] for the actual contour; a geometric factor K_g, for identical β, can now be defined

$$K_g = \frac{\sigma_\theta}{\sigma_{\theta_m}{}^*} = \frac{n_{\max}}{n^*} = \frac{dn/d\beta}{dn^*/d\beta} = \frac{dn/d\beta}{\dfrac{E}{4\pi(2f/t)}\left[1 - \dfrac{2\log(b/a)}{1-(a/b)^2}\right]} \qquad [21]$$

The results for a series of slotted grains are presented in Fig. 5.

Thermal Stress—Constant Temperature Across Web

Returning to the thermal stress problem in the grains, the final stress concentration factor will depend upon both K_t and K_g. The data can be arranged for convenient design use in the form shown in Fig. 7, which illustrates the case of a constant temperature difference across the wall. The actual maximum thermal stress at the star point in the cylinder under plane strain is, using Equation [18a] and recalling that the negative wedge angle must be used to obtain the desired doubly connected region

$$\sigma_{\theta_c} = K_g \frac{E}{4\pi(1-\nu^2)}\left[1 - \frac{2\log(b/a)}{1-(a/b)^2}\right](-\beta) \qquad [22]$$

but from Equation [16], $\beta = K_t\beta^*$. Thereupon using the normalizing value of β^* from Equation [13]

$$\sigma_{\theta_c} = K_g K_t \frac{-E\alpha T_0}{2(1-\nu)\log(b/a)}\left[1 - \frac{2\log(b/a)}{1-(a/b)^2}\right] \qquad [23]$$

Upon setting $K_g = K_t = 1$, Equation [23] is found to yield the proper stress for a hollow thick walled cylinder (16), which normalizing value $\sigma_{\theta_c}{}^*$ is shown in Fig. 8a as a function of b/a for convenient reference.

Thermal Stress—Constant Heat Input

Suppose now an alternate problem is considered, namely that various slotted configurations of the same outside diameter are compared under the condition that the total heat flux

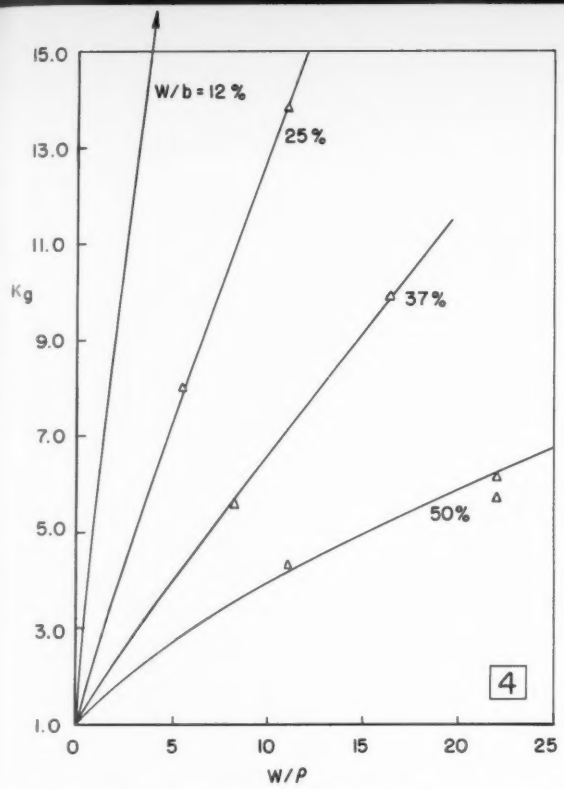

Fig. 5a Geometric concentration factor—four-slotted grain

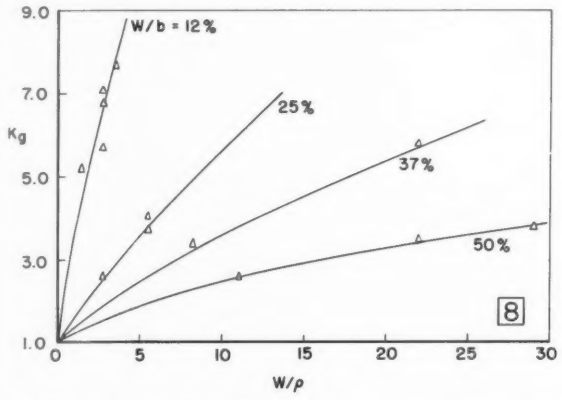

Fig. 5c Geometric concentration factor—eight-slotted grain

into the grain is the same. Thus if

$$\kappa \left.\frac{\partial T}{\partial r}\right|_{r=b} = -q_0(\theta) \qquad [24]$$

then

$$r_0 \int_0^{2\pi} \left.\frac{\partial \Delta T}{\partial r}\right|_{r=r_0} d\theta = -\frac{b}{\kappa}\int_0^{2\pi} q_0(\theta)d\theta \equiv 2\pi b\left(\frac{Q_0}{\kappa}\right) \qquad [25]$$

so that Equation [11] gives the rotation to be applied as

$$\beta = (1+\nu)\alpha 2\pi b Q_0/\kappa \qquad [26]$$

But, as Q_0 is constant for all shapes, it will specifically be the same for a thick walled cylinder, or $\beta^* = \beta$, which following the previous notation implies $K_t = 1$. In this fashion

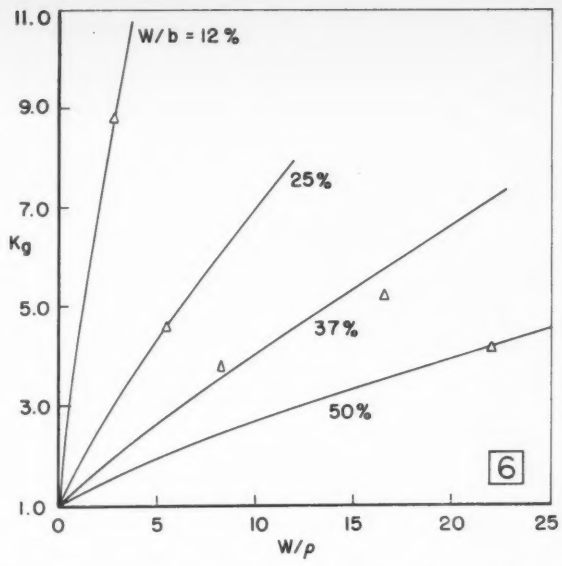

Fig. 5b Geometric concentration factor—six-slotted grain

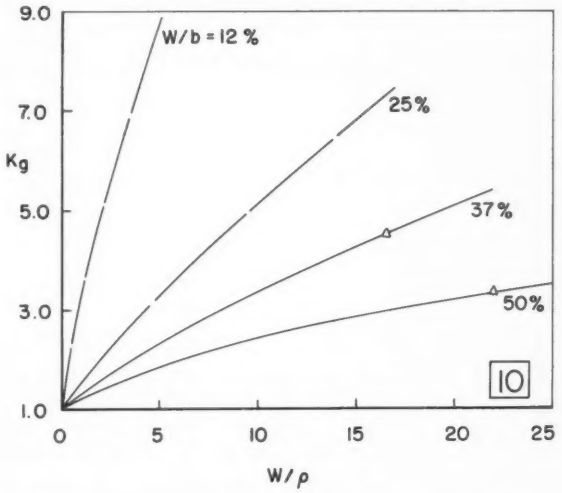

Fig. 5d Geometric concentration factor—ten-slotted grain

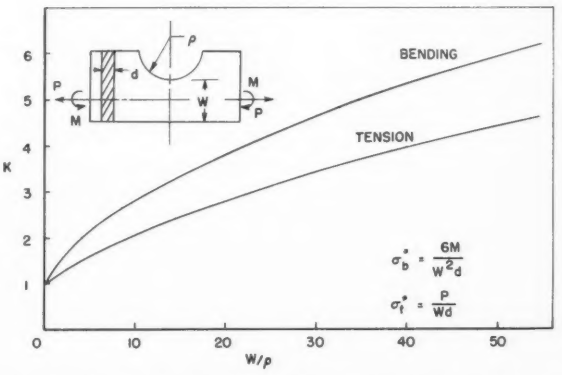

Fig 6. Stress concentration factors for notched bars, from Neuber (6)

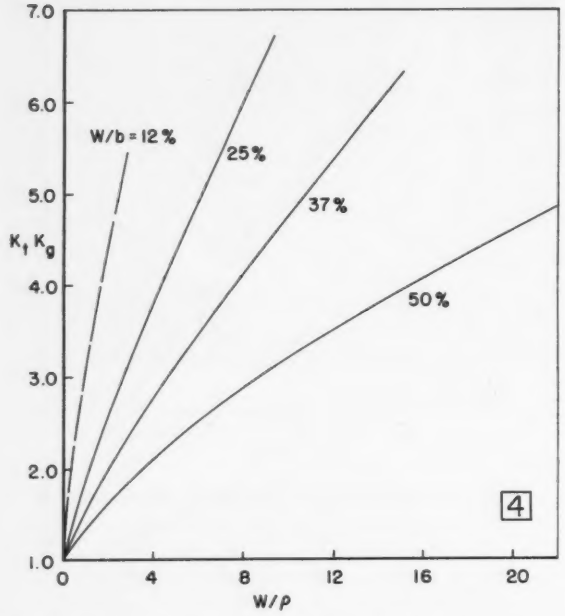

Fig. 7a Combined stress concentration factor—four-slotted grain

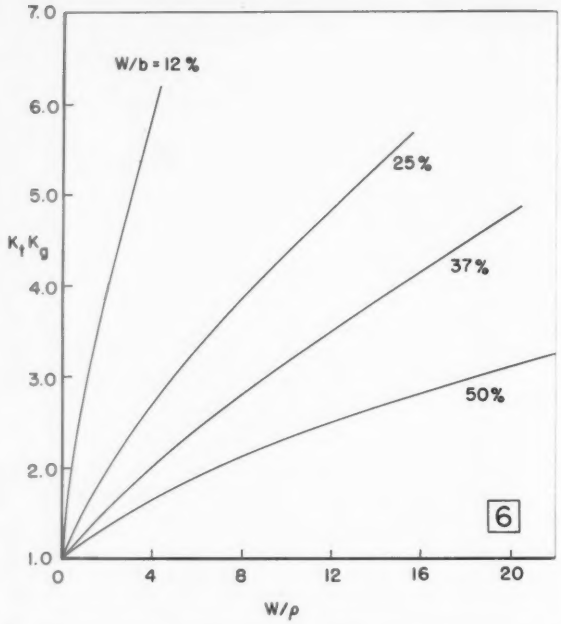

Fig. 7b Combined stress concentration factor—six-slotted grain

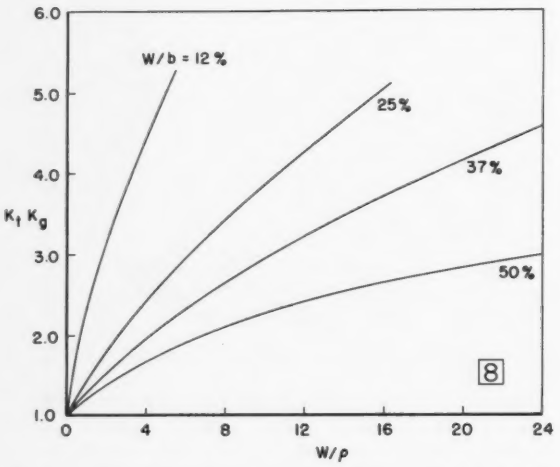

Fig. 7c Combined stress concentration factor—eight-slotted grain

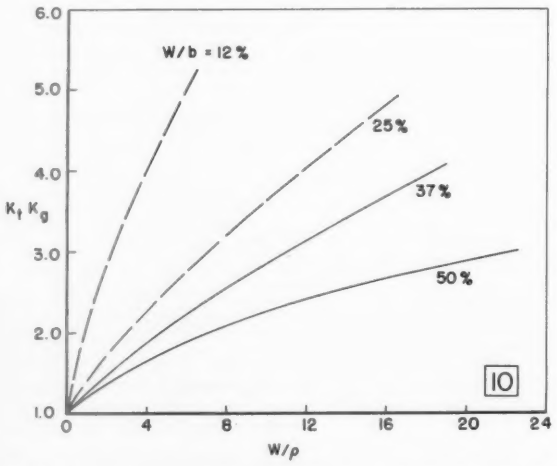

Fig. 7d Combined stress concentration factor—ten-slotted grain

Equation [22] may be used as before, but now substituting Equation [26] there results for the maximum stress in the slot

$$\sigma_{\theta c} = K_g \frac{-E\alpha Q_0/\kappa}{2(1-\nu)} \left[1 - \frac{2\log(b/a)}{1-(a/b)^2}\right] \qquad [27]$$

where, as before, K_g is taken from Fig. 5, and the normalized stress $\sigma_{\theta c}^* \equiv \sigma_{\theta c}/K_g$ is plotted in Fig. 8b.

As a final remark, the heat flux is often estimated in terms of film coefficients, $Q_0 \equiv h[T(b) - T_r]$, where T_r, is the (known) temperature at the medium surrounding the grain.

Conclusion

The question always arises as to the validity of applying elastic stress concentration factors to viscoelastic propellant grain materials. Although it is not the intent of this paper to dwell upon this important fact, it may be pointed out that there are many practical cases in which a direct association for an elastic and viscoelastic state can be made (18); hence one has an important reason for devoting time to elastic considerations which at first sight appear inappropriate.

Further development and engineering applications along these lines will be reported subsequently.

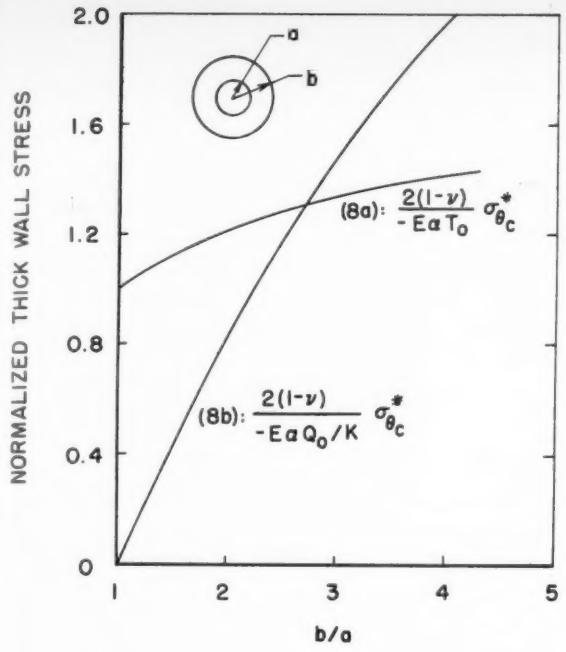

Fig. 8 Thermal stress in a thick walled cylinder, used as a normalizing quantity: 8a Constant temperature difference across web; 8b constant heat input to the web

References

1 Ordahl, D. D. and Williams, M. L., "Preliminary Photoelastic Design Data for Stresses in Rocket Grains," JET PROPULSION, vol. 27, June 1957, pp. 657–662.

2 Geckler, R. D., "Thermal Stresses in Propellant Grains," JET PROPULSION, vol. 26, Feb. 1956, p. 93.

3 Biot, M. A., "A General Property of Two-Dimensional Thermal Stress Distribution," *Phil. Mag.*, ser. 7, vol. 90, March 1935, p. 540.

4 Muskhelishvili, N. I., "On Thermal Stresses in the Plane Problem of the Theory of Elasticity," Bull., Elec. Tech. Inst., St. Petersburg, vol. 13, 1916, p. 23.

5 Weibel, E. E., "Thermal Stresses in Cylinders by the Photoelastic Method," in "Proc. Fifth Int. Congress Applied Mechanics," John Wiley and Sons, 1939, p. 213.

6 Neuber, H. "Theory of Notch Stresses," Edwards Brothers, Ann Arbor, Mich., p. 47 et seq. (Figs. 26, 28), p. 181 (Fig. 104).

7 Parkus, H., "On an Extension of Hamilton's Principle to Thermoelastic Phenomena," "Beitrage zur angewandten Mechanik, " F. Deuticke, Wein, 1950, p. 295; *see also* summary in *Applied Mechanics Reviews*, March 1952, p. 97.

8 Gerard, G. and Gilbert, A. C., "Photothermoelasticity. An Exploratory Study," *J. Appl. Mech.*, Sept. 1957; *see also* discussion by Williams, M. L., *J. Appl. Mech.*, March 1958.

9 Biot, M. A., "Thermoelasticity and Irreversible Thermodynamics," *J. Appl. Phys.*, vol. 27, no. 3, March 1956, pp. 240–253; *see also* Proc. 3rd Nat. Congress Applied Mechanics, June 1958.

10 Chambers, LL. G., "A Variational Principle for the Conduction of Heat," Reprinted from *Quart. J. Mech. and Appl. Math.*, vol. IX, part 2, June 1956.

11 Timoshenko, S. and Goodier, J. N., "Theory of Elasticity," McGraw-Hill Book Co., Inc., p. 429.

12 Churchill, R. V., "Introduction to Complex Variables and Applications," McGraw-Hill Book Co., 1948, p. 159.

13 Stevenson, A. C., "The Torsion of a Fluted Column," *Philosoph. Mag.*, series 7, vol. 34, 1943, p. 115.

14 Sechler, E. E., "Elasticity in Engineering," John Wiley and Sons, 1952, p. 193; *see also* Sokolnikoff, I. S., "Mathematical Theory of Elasticity," McGraw-Hill Book Co., 1956, p. 382.

15 Timoshenko, S. and Goodier, J. N., "Theory of Elasticity," McGraw-Hill Book Co., 1951, p. 66.

16 *Ibid.*, p. 413.

17 *Ibid.*, p. 408.

18 Lee, E. H., "Viscoelastic Stress Analysis," First Symposium on Naval Structural Mechanics, Stanford Univ., Aug. 1958.

Interplanetary Trajectories Under Low Thrust Radical Acceleration

JACK COPELAND[1]

Autonetics Div.,
North American Aviation, Inc.
Downey, Calif.

Interplanetary trajectories resulting from constant radial acceleration (toward or away from the sun) are obtained in terms of tabulated functions. For sustained acceleration greater than a critical value, the vehicle spirals to escape. For accelerations less than critical, the vehicle moves in precessing orbits with perihelion or aphelion on the initial orbit using outward or inward thrust, respectively. Some examples of trajectories are given and their implications discussed.

IN THE many discussions of space travel that have appeared in recent literature, it is generally agreed that interplanetary corrective maneuvers will have to be made if the space vehicle is to intercept and orbit the destination planet. Whether the corrections are made continuously or by impulses, the guidance and control equipment must perform their functions properly during months of unsupervised operation. The question of system reliability is clearly of paramount importance, even if the guidance equipment is aided by human intelligence.

One way to increase reliability is to make the guidance program so simple that a mistake is unlikely, or if a minor miscalculation is made, it will little affect the overall success of the mission. Since maneuvers must be made, the thrust must be changed at least in direction; however, an easily mechanized thrust program requiring a minimum of computer decisions for the major portion of the trip would allevi-

Received May 21, 1958.

[1] Senior Engineer, Inertial Navigation Preliminary Engineering Research.

ate the problem. It should be emphasized that we are concerned here with the interplanetary phase of the guidance program; that is, escape from the Earth has been effected by some means and we are now faced with the problem of guiding the vehicle so as to intercept the destination planet.

With simplicity a prime consideration, a constant radial acceleration, toward or away from the sun, looks quite attractive. From a mechanization standpoint, the thrust direction relative to the vehicle is easily determined. Momentum conservation will reduce the vehicle velocity relative to the destination planet, thereby facilitating the corrective maneuvers necessary to effect final planetary capture of the vehicle. Although perhaps not optimum, when such factors as fuel economy or transit time are considered, such a thrust program because of its simplicity deserves more than cursory consideration.

Fortunately, the equations of motion for this special case are not so intractable as to discourage further investigation. In the analysis that follows certain simplifying assumptions are made; consequently, the results are not exact, particularly in the region of the Earth and the destination planet. The general shape of the trajectories are given, however, along with the transit times, which are not prohibitive.

Analysis

A complete analysis of the problem would involve many variables among which are the effects of Earth and moon at departure, and of the destination planet at the end of the trip. For study purposes, however, it is sufficient to consider the problem reduced by the following assumptions:

1 The perturbations of Earth, moon and destination planet are ignored; that is, the general n-body problem has been reduced to a simple two-body problem involving the sun and the vehicle.

2 The vehicle is initially moving in what is essentially the Earth's orbit with approximately the Earth's orbital speed.

3 The orbits of the Earth and destination planet are considered circular and coplanar.

Although these assumptions cannot be used for actual trajectory calculations, they do not invalidate the general conclusions which result.

Let us locate the vehicle in a heliocentric coordinate system by a radius vector R and a polar angle ϕ. If the vehicle acceleration is constant and directed radially, the equations of motion are

$$\frac{d^2R}{dt^2} - R\left(\frac{d\phi}{dt}\right)^2 + g_0\left(\frac{R_0}{R}\right)^2 = A \qquad [1]$$

$$R^2\frac{d\phi}{dt} = \text{constant} \qquad [2]$$

where

R_0 = one astronomical unit
g_0 = sun's gravitational acceleration at R_0
A = the vehicle's acceleration

For convenience, we make the following changes of variable [1]

$$R = rR_0$$
$$A = \alpha g_0$$
$$t = \tau\left(\frac{R_0}{g_0}\right)^{1/2} \qquad [3]$$

In other words, the unit of distance is the astronomical unit, the unit of time $1/2\,\pi$ years, and the unit of acceleration g_0. Velocity is measured in units of the Earth's orbital velocity, 30 km/sec. With these changes, Equations [1 and 2] become

$$\ddot{r} - r\dot{\phi}^2 + \frac{1}{r^2} = \alpha \qquad [4]$$

$$r^2\dot{\phi} = r^2(0)\dot{\phi}(0) = 1 \qquad [5]$$

where the dots indicate differentiation with respect to τ. The use of Equation [5] to eliminate $\dot{\phi}$ from Equation [4] gives

$$\ddot{r} - \frac{1}{r^3} + \frac{1}{r^2} = \alpha \qquad [6]$$

Integration of Equation [6] assuming an initially circular orbit at $r = 1$, gives

$$\dot{r}^2 = \frac{2}{r} - \frac{1}{r^2} + 2\,\alpha\,(r-1) - 1 \qquad [7]$$

Except for one special case, the second integration to find $r(\tau)$ or $r(\phi)$ results in elliptic integrals; however, a great deal of information about the trajectory can be deduced from an examination of $\dot{r}(r)$.

It is apparent from Equation [7] that the radial velocity will be zero at those values of r that satisfy

$$2\,\alpha r^3 - (2\,\alpha + 1)r^2 + 2r - 1 = 0 \qquad [8]$$

Equation [8] is satisfied by $r = 1$ and

$$r = \frac{1 \pm \sqrt{1 - 8\,\alpha}}{4\,\alpha} \qquad [9]$$

It is clear that r is bounded for $\alpha < \frac{1}{8}$; however, if $\alpha > \frac{1}{8}$ no real roots exist, which means that escape from the solar system will be accomplished if the thrust can be maintained long enough. This behavior is well-known and has been mentioned in the literature (1, 4). A dimensionless acceleration of $\frac{1}{8}$ corresponds to an actual acceleration of about $0.8 \times 10^{-4}\,g$. Since the acceleration to be expected from the use of ion rockets may be of the order of $10^{-4}\,g$ (2), the trajectories for $\alpha < \frac{1}{8}$ are of more than academic interest.

To obtain the trajectory $\phi(r)$, Equation [7] must be integrated. We have

$$\frac{dr}{d\phi} = \frac{\dot{r}}{\dot{\phi}} = r\sqrt{(r-1)\,(2\,\alpha r^2 - r + 1)} \qquad [10]$$

$$\phi(r) = \int_1^r \frac{dx}{x\sqrt{(x-1)\,(2\,\alpha x^2 - x + 1)}} \qquad [11]$$

The time to r may be found as follows

$$\tau(r) = \int_1^r \frac{dr}{\dot{r}} = \int_1^r \frac{x\,dx}{\sqrt{(x-1)\,(2\,\alpha x^2 - x + 1)}} \qquad [12]$$

The radial speed is given by Equation [7]

$$V_r = \dot{r} = \sqrt{\frac{2}{r} - \frac{1}{r^2} + 2\,\alpha(r-1) - 1}$$

and the ϕ component by Equation [5]

$$V_\phi = \frac{1}{r}$$

Therefore the velocity at r is given by

$$V(r) = \sqrt{\frac{2}{r} + 2\,\alpha(r-1) - 1} \qquad [13]$$

There will be four different types[3] of trajectories (4) corre-

[2] Numbers in parentheses indicate References at end of paper.

[3] Reference (4) examines the complete elliptic integrals for our case 2, and considers $\alpha \ll \frac{1}{8}$.

sponding to: $\alpha < 0$; $0 < \alpha < \frac{1}{8}$; $\alpha = \frac{1}{8}$; $\alpha > \frac{1}{8}$.

Case 1: $\alpha < 0$

For $\alpha < 0$, $\dot{r} = 0$ has three real roots, two positive and one negative. The negative root has no physical significance. It may be noted that as $\alpha \to \infty$, the roots of $\dot{r} = 0$ are at zero and unity; that is, if the sun were a point mass, collision with the sun by means of a constant finite radical acceleration would be impossible.

It can be shown (3) that the transformation

$$r = \frac{a \sin^2 \theta + b}{c \sin^2 \theta + d}$$

reduces Equations [11 and 12] to

$$\phi = \frac{2\delta}{\gamma a}\left[\frac{\delta}{b}\,\Pi(\theta, a/b, k) + cF(\theta, k)\right] + \text{constant} \quad [14]$$

$$\tau = \frac{2\delta}{\gamma}\left[x_3 F(\theta, k) + (x_1 - x_3)\,E(\theta, k) + \frac{(x_1 - x_2)\sin 2\theta}{2\sqrt{1 - k^2 \sin^2 \theta}}\right] + \text{constant} \quad [15]$$

where

$$a = -x_3 k^2$$
$$b = x_2$$
$$c = -k^2 = -\frac{x_1 - x_2}{x_1 - x_3}$$
$$r = \frac{a \sin^2 \theta + b}{c \sin^2 \theta + 1}$$
$$\delta = (x_2 - x_3)k^2$$
$$\gamma = (x_2 - x_3)k^2\sqrt{-2\,\alpha(x_1 - x_3)}$$

and $x_1 > x_2 > x_3$ are roots of $\dot{r} = 0$. The constants of integration should be chosen so that ϕ and τ vanish at $r = 1$; however, this is not essential for plotting the trajectory.

The functions $F(\theta, k)$, $E(\theta, k)$ and $\Pi(\theta, a/b, k)$ are elliptic integrals of the first, second and third kind, respectively (3).

As an example let us take $\alpha = -\frac{2}{9}$. The three roots are

$$x_1 = 1 \qquad x_2 = 3/4 \qquad x_3 = -3 \quad [16]$$

$$\phi = 3\left[\Pi\left(\frac{\pi}{2}, \frac{1}{2}, \frac{1}{2}\right) - \Pi\left(\theta, \frac{1}{2}, \frac{1}{2}\right)\right] = \frac{3}{2}\left[F\left(\frac{\pi}{2}, \frac{1}{2}\right) - F\left(\theta, \frac{1}{2}\right)\right] + \frac{\pi}{2} - \arctan\frac{3}{2}\frac{\tan\theta}{\sqrt{1-(1/16)\sin^2\theta}} \quad [21]$$

$$\tau = 9\left[F\left(\frac{\pi}{2}, \frac{1}{2}\right) - F\left(\theta, \frac{1}{2}\right)\right] - 6\left[E\left(\frac{\pi}{2}, \frac{1}{2}\right) - E\left(\theta, \frac{1}{2}\right)\right] \quad [22]$$

where $r = \frac{1}{2}\sin^2\theta + 1$.

Fortuitously, $\alpha = -\frac{2}{9}$ results in perfect squares under the radicals and produces an x_2 near Venus' orbital distance.

Equations [14 and 15] become (3)

$$\phi = 8\left\{\frac{5}{16}\left[\Pi\left(\pi, \frac{1}{4}, \frac{1}{4}\right) - \Pi\left(\theta, \frac{1}{4}, \frac{1}{4}\right)\right] - \frac{1}{16}\left[F\left(\frac{\pi}{6}, \frac{1}{4}\right) - F\left(\theta, \frac{1}{4}\right)\right]\right\} \quad [17]$$

$$= \frac{3}{4}\left[F\left(\frac{\pi}{6}, \frac{1}{4}\right) - F\left(\theta, \frac{1}{4}\right)\right] + \arctan\frac{5}{4}\frac{\tan \pi/6}{\sqrt{1-(1/16)\sin^2\pi/6}} - \arctan\frac{5}{4}\frac{\tan\theta}{\sqrt{1-(1/16)\sin^2\theta}}$$

$$\tau = \frac{3}{2}\left\{4\left[E\left(\frac{\pi}{6}, \frac{1}{4}\right) - E\left(\theta, \frac{1}{4}\right)\right] - 3\left[F\left(\frac{\pi}{6}, \frac{1}{4}\right) - F\left(\theta, \frac{1}{4}\right)\right] + \frac{\sin \pi/3}{8\sqrt{1-(1/16)\sin^2\pi/6}} - \frac{\sin 2\theta}{8\sqrt{1-(1/16)\sin^2\theta}}\right\} \quad [18]$$

where $\sin^2\theta = 4(r - \frac{3}{4})/(r + 3)$.

The trajectory $\phi(r)$ is shown[4] in Fig. 1. The vehicle "spirals" in toward the sun, reaching $r = \frac{3}{4}$ after about 1.7 months. At this point $\dot{r}$ becomes positive and the vehicle returns to $r = 1$ after an additional 1.7 months at which time it leads the Earth by about 20 deg. If the vehicle were unperturbed by either Venus or the Earth, it would continue, oscillating between $r = 1$ and $r = \frac{3}{4}$ with a period of 3.4 months.

Case 2: $0 < \alpha < \frac{1}{8}$

Here, the three roots of $\dot{r} = 0$ are all real and positive. From (3) we find

$$\phi = \frac{2\delta^2}{\gamma a b}\,\Pi\left(\theta, \frac{a}{b}, k\right) + \text{constant} \quad [19]$$

$$\tau = \frac{2\delta}{\gamma}\left[x_1 F(\theta, k) - (x_1 - x_3)E(\theta, k)\right] + \text{constant} \quad [20]$$

where

$$a = x_2 - x_3$$
$$b = x_3$$
$$\gamma = (x_2 - x_3)\sqrt{2\,\alpha(x_1 - x_3)}$$
$$r = a \sin^2\theta + b$$
$$\delta = x_2 - x_3$$
$$k^2 = \frac{x_2 - x_3}{x_1 - x_3}$$

and $x_1 > x_2 > x_3$ are roots of $\dot{r}(r) = 0$.

In this case, $\alpha = \frac{1}{9}$ is convenient for an illustrative example. Equations [19 and 20] become

The trajectory $\phi(r)$ is shown in Fig. 2. The vehicle spirals outward reaching $r = 1.5$ after 12 months. At this point, $\dot{r}$ becomes negative and the vehicle spirals inward, reaching $r = 1$ after an additional 12 months at which time it leads the Earth by about 108 deg. As can be seen from the

[4] The author is indebted to one of the reviewers for calling his attention to the existence of errors in evaluating the complete integrals of case 2. This prompted a complete recomputation of the trajectories for $\alpha = -\frac{2}{9}$ and $\alpha = \frac{1}{9}$. Both trajectories differ significantly from those in the original paper.

figure, the unperturbed trajectory is a quasi-elliptical orbit whose perihelion rotates about 108 deg per period.

Case 3: $\alpha = \frac{1}{8}$

For this case the elliptic integrals degenerate into elementary functions. We get

$$\phi(r) = 2\int_1^r \frac{dx}{x(2-x)\sqrt{x-1}} \qquad [23]$$

The change of variable $\tan^2 \xi = x - 1$ permits easy integration. The result is

$$\phi = 2\left[\xi + \frac{1}{2}\log_e \tan\left(\frac{\pi}{4} + \xi\right)\right] \qquad [24]$$

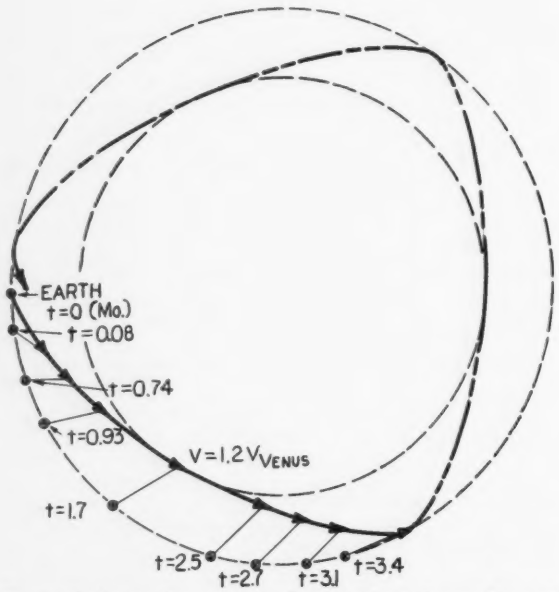

Fig. 1 Trajectory for $\alpha = -\frac{2}{9}$, showing the relative positions of Earth and vehicle. The heavy dashed curve is the path the vehicle follows if unperturbed by either Venus or Earth

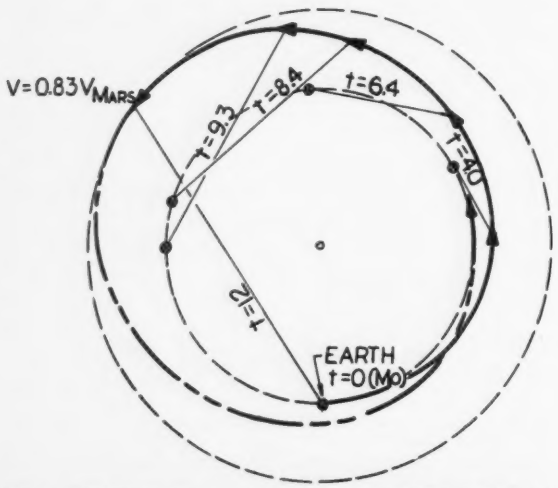

Fig. 2 Trajectory for $\alpha = \frac{1}{16}$, showing the relative positions of Earth and vehicle. The vehicle reaches $r = 1.5$ after 1 year and, if unperturbed by Mars, continues on a path shown by the heavy dashed line

The time to r is

$$\tau(r) = 2\int_1^r \frac{x\,dx}{(2-x)\sqrt{x-1}} \qquad [25]$$

Here the change of variable $\sin^2 \zeta = x - 1$ is convenient. We get

$$\tau = 4\left[2\log_e \tan\left(\frac{\pi}{4} + \frac{\zeta}{2}\right) - \sin\zeta\right] \qquad [26]$$

In this case $\dot{r} = 0$ has three positive real roots, two of which are equal; that is, one root is unity, and $r = 2$ is a double root. Inspection of Equation [4] reveals that $\ddot{r}\,(2) = 0$; therefore, r approaches 2 asymptotically. The time to $r = 1.5$ is 8.2 months. The trajectory $\phi(r)$ is shown in Fig. 3.

Case 4: $\alpha > \frac{1}{8}$

Here $\dot{r} = 0$ has only one real root, unity, and a pair of imaginary roots.

From (3) we get

$$\tau = \frac{2}{\sqrt{2\alpha}}\left[\frac{1+\cos\theta}{\sin\theta}\sqrt{1-k^2\sin^2\theta} - F(\theta, k) + E(\theta, k)\right] \qquad [27]$$

$$\phi = \arcsin(k\sin\theta) - \frac{1}{\sqrt{8\alpha}}F(\theta, k)\Bigg] \qquad [28]$$

where

$$r = \frac{2}{1-\cos\theta} \qquad k^2 = \frac{1}{8\alpha}$$

Fig. (4) shows $\phi(r)$ for $\alpha = \frac{1}{6}$.

The time to reach escape is perhaps of interest. The potential that must be overcome is $1/r$. When $1/r$ is equated to $\frac{1}{2}(\dot{r}^2 + r^2\dot{\phi}^2)$, it is found that escape velocity will be reached when $r = 1 + \frac{1}{2}\alpha$. For $\alpha = \frac{1}{6}$, escape velocity is reached at $r = 4$. The time to escape is 16 months.

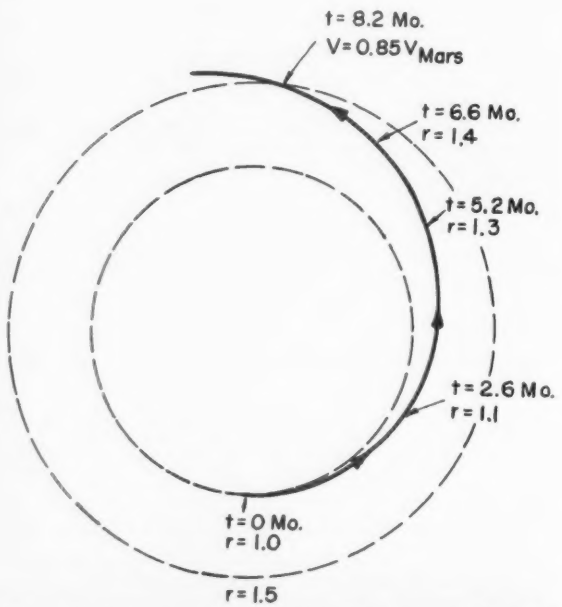

Fig. 3 Trajectory for $\alpha = \frac{1}{6}$ (although not apparent from the figure, the approach to $r = 2$ is asymptotic)

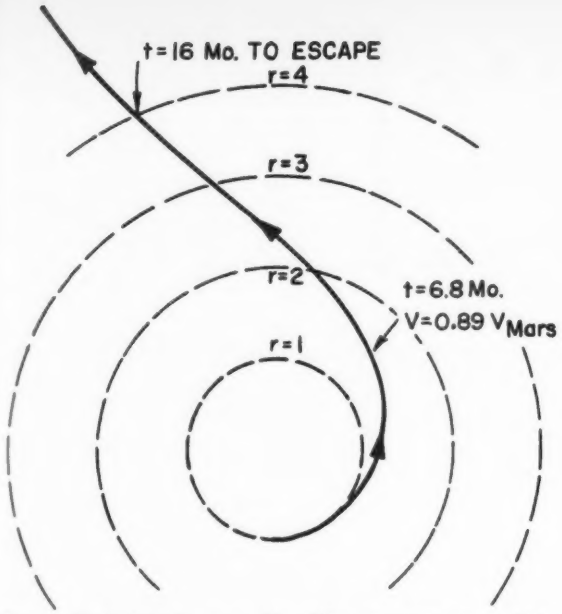

Fig. 4 Trajectory for $\alpha = \frac{1}{6}$. After 16 months the vehicle reaches escape velocity at $r = 4$

Discussion

The question of what terminal corrective maneuvers must be made remains unanswered, since the planets were ignored to facilitate analysis; however, the destination planet may be replaced for discussion purposes without substantially altering most of the vehicle trajectory. A qualitative discussion of the capture problem may then be made by assuming the interplanetary phase of the mission has been successful, so that near the nominal intercept point the vehicle is approaching the planet on what is approximately a collision course. Consider case 4, $\alpha = \frac{1}{6}$, as a first example. Under the assumption of circular planetary orbits, the velocity of the vehicle relative to Mars in the region of $r = 1.5$ would be about 8 km/sec. This is 3 km/sec in excess of escape velocity from the surface of Mars. Obviously, the vehicle in this case will either collide with Mars or orbit hyperbolically unless sufficient corrective impulse can be applied in the proper direction at the proper time.

For the case of $\alpha = \frac{1}{8}$, the situation is not quite so critical. The vehicle velocity relative to Mars at $r = 1.5$ would be only slightly greater than escape (5.5 km/sec). Corrective maneuvers must still be made; however, less impulse is needed, and, since the vehicle approaches Mars more slowly, there is more time in which to make the necessary corrections.

For $\alpha = \frac{1}{9}$, the velocity of the vehicle at $r = 1.5$ is only 4 km/sec relative to Mars at the same point. This is four-fifths of escape velocity from the surface of Mars. A very attractive approach trajectory is one with aphelion somewhat beyond 1.5, say 1.55, and crossing $r = 1.5$ perhaps 2 months in advance of Mars. Mars, moving more rapidly than the vehicle, would then come between the vehicle and the sun as the vehicle approached aphelion. The vehicle would spend about 3 months within some 5 million miles of Mars with a relative velocity of the order of 4 km/sec. Even at 5 million miles, however, the presence of Mars enters the problem only as a minor perturbation, since at that distance the gravitational acceleration of the sun exceeds that of Mars by four orders of magnitude. Whatever the approach trajectory, the terminal maneuver problem is a three-body one and can be discussed here only qualitatively.

The situation for capture by Venus ($\alpha \simeq \frac{2}{9}$) is not so favorable. The velocity of the vehicle relative to Venus is about 12 km/sec compared to 10 km/sec for escape from Venus, and only about $1\frac{1}{2}$ months are spent within 5 million miles of $r = 0.75$.

The bounded trajectories for $\alpha < \frac{1}{8}$ are interesting. In particular, a trajectory for $\alpha \simeq \frac{1}{9}$ with its orbital period of 2 years is practicable for a reconnaissance of Mars with subsequent recovery of the information from the vehicle upon its return near perihelion. Successful recovery would be a difficult problem but not manifestly more so than that, for example, of establishing the vehicle in a satellite orbit about Mars and transmitting the information there obtained to Earth, some 50 million miles distant. Reliable operation for a period of 2 years is indeed questionable; however, a minimum of guidance equipment would be required. Of course, the final feasibility of such a mission can only be determined after a more rigorous solution of the problem, including the effects of both Earth and Mars, has been made. Here, the assumption of coplanar orbits is not necessary or even desirable; advantage should be taken of the 4 million mile separation that would result to reduce the perturbation of the vehicle by Mars. A similar mission for reconnaissance of Venus (case 1) is of equal interest. It has two attractive features: Duration of only about $3\frac{1}{2}$ months, and an unobstructed communication range of less than some 75 million miles.

The results given here for heliocentric motion may be easily extended to geocentric motion by a simple change of scale. For example, a vehicle leaving a circular orbit above the Earth under a constant $\frac{1}{8}\ g$ radial acceleration would spiral outward approaching about 2 Earth radii asymptotically.

References

1 Tsien, H. S., "Take-off from a Satellite Orbit," JET PROPULSION, vol. 23, July-Aug. 1953, p. 233.

2 Stuhlinger, E., "Flight Path of an Ion-Propelled Space Ship," JET PROPULSION, vol. 27, April 1957, p. 410.

3 Grobner, W. and Hofreiter, H., "Integraltafel (Erster Teil, Unbestimmte Integrale)" Springer-Verlag, Wien and Innsbruck, 1949.

4 Dobrowolski, A., "Satellite Orbit Perturbations Under a Continuous Radial Thrust of Small Magnitude," JET PROPULSION, vol. 28, Oct. 1958, pp. 687–689.

Reflection of Weak Shock Waves From Nozzles With No Flow and Critical Flow

CHARLES E. FEILER[1]

National Aeronautics and Space Administration
Cleveland, Ohio

The reflection of weak shock waves from nozzles having contraction ratios of 16, 4 and 2, and convergence half-angles of 60, 30 and 15 deg was studied in a shock tube. The experiments were performed with no initial flow through the nozzle and also with critical flow, and the results compared with theory. Contraction ratio, as predicted by theory, had much less effect on reflected shock strength with critical flow through the nozzles than with no initial flow. Convergence angle had little effect on reflected shock strength for either flow condition.

HIGH-frequency combustion instability poses a serious problem in the development of liquid propellant rocket engines. The mechanism that sustains these oscillations is obscure. For the case of longitudinal oscillations, the pressure waves reflect directly from the engine nozzle, and the engine behaves acoustically as though it were a closed organ pipe (1, 2).[2] In (3), it has been reported that the severity of combustion instability is related to the nozzle convergence angle. It was also postulated that the nozzle might have an amplifying effect on the pressure wave associated with this instability.

The reflection of shock waves from the closed or open end of a shock tube has been studied both experimentally and analytically (4, 5). Methods of analysis applying to nozzles for both no initial flow and critical flow through the nozzle have also been determined (6, 7). This paper describes the results of an experimental study of the reflection of weak shock waves from nozzles having contraction ratios of 2, 4 and 16, and convergence half-angles of 15, 30 and 60 deg. Experiments were conducted for both no flow and critical flow initially through the nozzle, and the results compared with theory. The range of incident shock strengths (pressure ratio across the shock) varied from about 1.8 to 3.5.

Received May 29, 1958.

[1] Aeronautical Research Scientist, Lewis Research Center. Member ARS.

[2] Numbers in parentheses indicate References at end of paper.

Apparatus

The dimensions of the shock tube and locations of the pressure transducers, nozzle and injector are shown in Fig. 1. A pneumatically operated plunger was used to burst the diaphragm separating the high and low pressure sections. Driver pressure was measured with a Bourdon tube gage. The driver gas used was nitrogen; the gas in the low pressure or test section was air. Both gases were at room temperature. Diaphragm materials varied with the shock strength desired and were selected by trial.

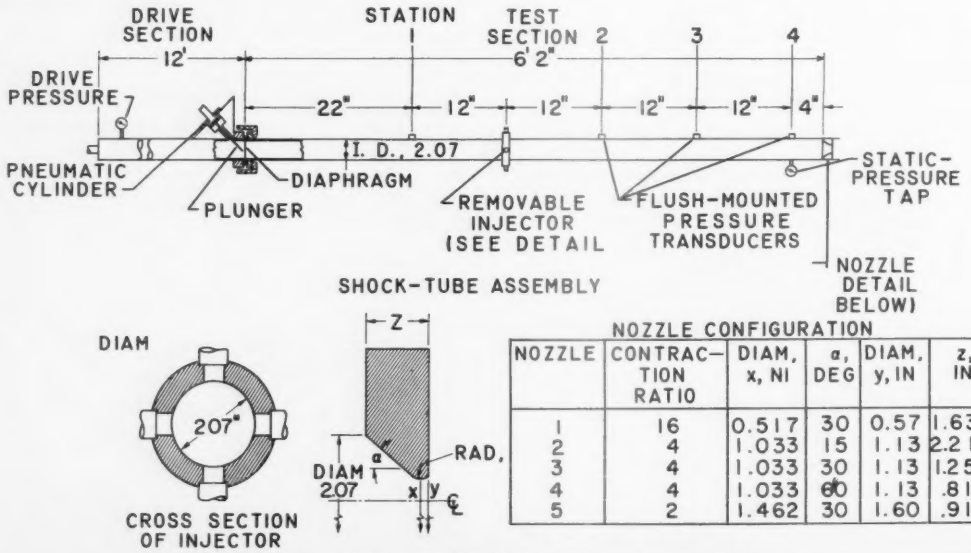

NOZZLE CONFIGURATION

NOZZLE	CONTRACTION RATIO	DIAM, x, IN	α, DEG	DIAM, y, IN	z, IN.
1	16	0.517	30	0.57	1.635
2	4	1.033	15	1.13	2.210
3	4	1.033	30	1.13	1.250
4	4	1.033	60	1.13	.810
5	2	1.462	30	1.60	.913

Fig. 1 Shock-tube assembly, injector and nozzle configuration

The configuration and dimensions of the nozzles are shown in Fig. 1. Contraction ratios (area shock tube/area nozzle throat) were 2, 4 and 16.

A sketch of the injector used to provide airflow into the test section is shown in Fig. 1. For the air supply pressure used, the pressure ratio across the entry holes was subcritical, and thus the flow velocity into the shock tube was subsonic.

Instrumentation

High-frequency-response pressure transducers were mounted flush at four stations along the test section, as shown in Fig. 1. The outputs of these transducers were amplified and fed into a four-channel oscilloscope. Pressure at these four stations was recorded continuously on film. Accuracy of the transducers was within ±1 per cent of full-scale deflection or about ±2 lb per in.^{2}. At the lower pressures, 25 to 30 lb per in.^{2}, this error could be of the order 6 to 8 per cent. Impact of the shock waves excited the natural frequency of the pick-up diaphragms. This effect, shown in the oscillogram of Fig. 2, increased the difficulty of measuring pressures accurately.

Shock velocity was determined from the transit time of the shock between stations. Accuracy of velocity measurements was limited largely by time resolution on the film. Velocities appeared to be accurate to within about ±3 per cent over the entire range (1500 to 1900 ft per sec).

Procedure

Data Recording

The oscillogram of Fig. 2 is typical of the data obtained. Deflection of the traces occurs as the shock wave passes each station. Incident shock strength P_I was obtained from the average value of pressure measured at all four stations. For no-flow tests, the initial pressure in the test section was atmospheric; for the flow tests, it was about 35 lb per in.^{2} abs. A typical x, t-plane diagram, as obtained from the oscillogram, is also shown in Fig. 2. The position or time of the interaction of the reflected shock with the contact surface varied with initial shock strength and usually occurred near station 3. As a result, reflected shock strength could be obtained from station 4 only.

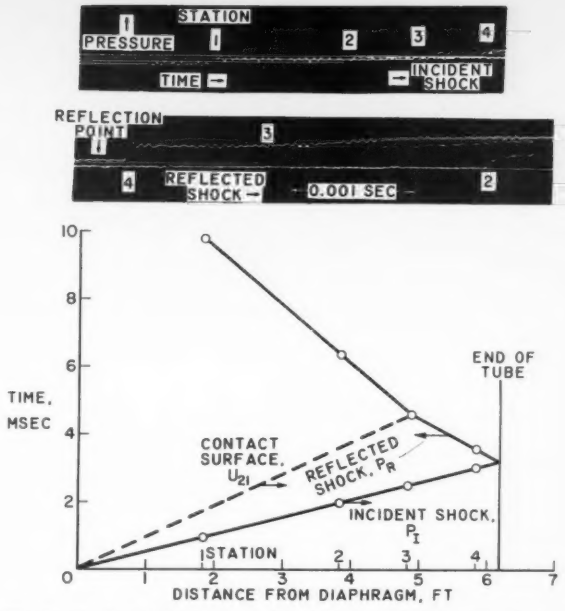

Fig. 2 Typical oscillogram and x, t-plane diagram. Nozzle 1: $P_1 = 3.19$; $P_R = 2.58$; $U_{21} = 0.93$

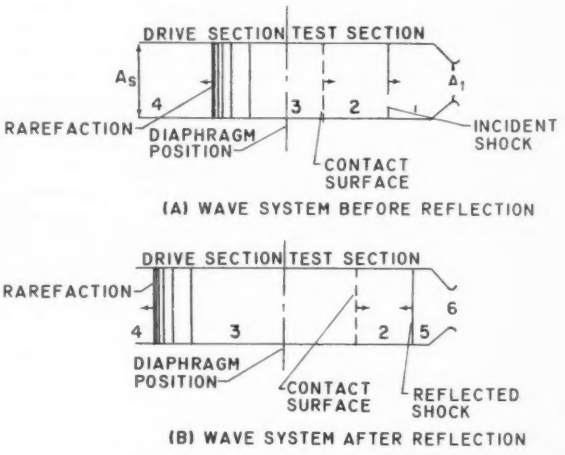

Fig. 3 Wave system in shock tube

Calculation of Reflected Shock Strengths*

The wave system set up by the shock waves is shown in Fig. 3. For the reflected wave (Fig. 3B) the following equations may be obtained for a gas of heat capacity ratio equal to 7/5

$$U_{51} = M_1 + \frac{5}{\sqrt{7}} \frac{1}{\sqrt{6P_I + 1}} \times \left[P_I - 1 - (P_R - 1) \sqrt{\frac{P_I (P_I + 6)}{6P_R + 1}} \right] \quad [1]$$

$$C_{51} = \sqrt{\frac{P_I(P_I + 6)}{6P_I + 1}} \sqrt{\frac{P_R (P_R + 6)}{6P_R + 1}} \quad [2]$$

$$A_s U_{51} C_{51}^5 = A_t U_{61} C_{61}^5 \quad [3]$$

$$5C_{51}^2 + U_{51}^2 = 5C_{61}^2 + U_{61}^2 \quad [4]$$

Equations [1 and 2] relate properties behind the reflected shock to the pressure ratios across the incident and reflected shock waves. Equations [3 and 4] relate flow properties (assumed to be steady-state) behind the reflected shock to those at the nozzle throat, that is, across the converging section of the nozzle. For no initial flow through the nozzle, $M_1 = 0$, calculation showed that for the weakest incident shock strength ($P_I = 2.0$) sonic flow occurs at the nozzle throat after shock reflection for contraction ratios of about 1.4 or larger. Thus for the range of contraction ratios and incident shock strengths studied, the nozzle was choked after reflection of the incident shock. The boundary condition was then $U_{61} = C_{61}$. For this boundary condition there results a reflected shock wave; however, for weaker incident shock strength or smaller contraction ratios the flow through the nozzle would be subsonic, and the reflected wave would be an expansion wave due to the different boundary condition.

For critical flow through the nozzle initially, the boundary condition was also $U_{61} = C_{61}$. In this case the value of M_1 is a function of the contraction ratio and can be calculated from stream-tube area relations. M_1 was also equal to M_5, where M_5 is the Mach number of the flow behind the reflected shock.

* A list of definitions of symbols appears at end of paper.

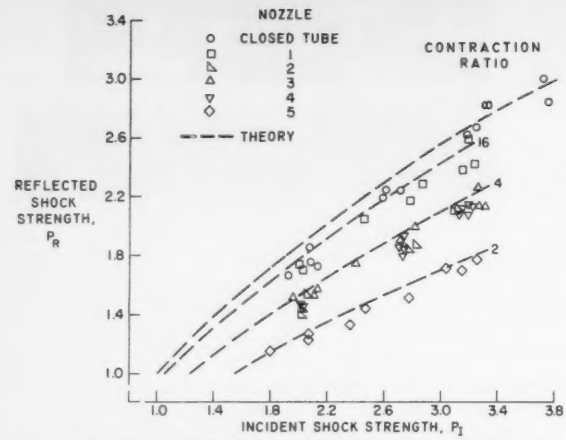

Fig. 4 Variation of reflected shock strength with incident shock strength for various nozzle configurations. No initial flow

The system of equations was solved by iteration. Values of P_R calculated for the two cases are shown in Table 1.

Table 1 Calculated values of reflected shock strength

A_s/A_t	M_s	P_I	No flow, $M_1 = 0$, P_R	Sonic flow, $M_1 = M_s$, P_R
2	0.305	1.5	...	1.40
		2.0	1.25	1.75
		2.5	1.49	2.04
		3.0	1.70	2.29
4	0.1466	1.5	1.20	1.44
		2.0	1.53	1.81
		2.5	1.83	2.14
		3.0	2.10	2.43
16	0.0363	1.5	1.39	1.46
		2.0	1.78	1.86
		2.5	2.13	2.21
		3.0	2.43	2.52

Experimental Results

Reflected shock strength is shown as a function of incident shock strength in Figs. 4 and 5 for the initial conditions of no flow and critical flow, respectively. No data were obtained for nozzle 5 with flow, since its critical flow rate considerably exceeded the capacity of the available system. Contraction ratio had a much greater effect on reflected shock strength with no initial flow than with critical flow initially, as predicted by the theoretical calculations. Convergence angle gave no observable effect for either flow condition.

The scatter in the data is of the same order as the experimental error previously discussed. Experimental data tended, in general, to fall below the corresponding theoretical curves. A recent study of the interaction of a reflected shock with the boundary layer created by the incident shock shows that for a closed-end tube the reflected shock is appreciably attenuated (8). This effect may partly account for the observed deviation.

The data of Fig. 4 are crossplotted in Fig. 6 to show the variation of reflected shock strength with contraction ratio. The curves terminate on the abscissa at the contraction ratio that just gives sonic flow for that particular incident shock strength.

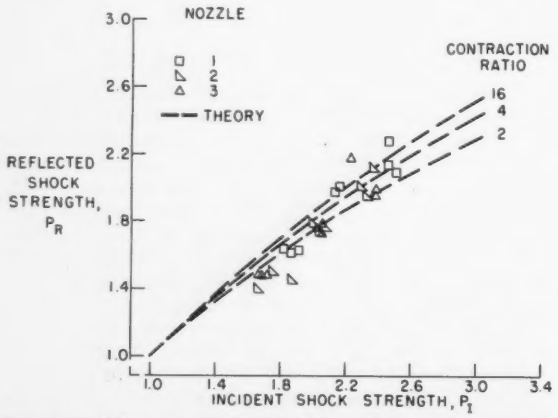

Fig. 5 Variation of reflected shock strength with incident shock strength for various nozzle configurations. Initial flow critical

Conclusions

The results show, as predicted by theory, that contraction ratio has much less effect on reflected shock strength when there is critical flow initially through the nozzle than when there is no initial flow. Also, convergence angle had no observable effect for either flow condition. The insensitivity of reflected shock strength to contraction ratio with critical flow also supports the observation that a rocket engine behaves acoustically as a closed organ pipe during longitudinal instability.

Acknowledgment

The help of Phillip R. Meng and Donald E. Seidel in the experimental and analytical parts of the program is gratefully acknowledged.

Nomenclature

A_s = area of shock tube
A_t = area of nozzle throat
c = speed of sound
M = Mach number
P_I = pressure ratio across incident shock
P_R = pressure ratio across reflected shock
u = particle velocity or contact surface velocity
$C_{ij} = c_i/c_j$ (e.g., $C_{s1} = c_s/c_1$), dimensionless quantity
$M_i = u_i/c_i$, dimensionless quantity
$U_{ij} = u_i/c_j$, dimensionless quantity

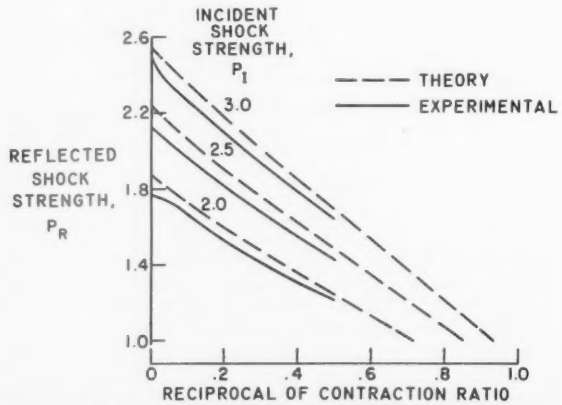

Fig. 6 Variation of reflected shock strength with contraction ratio. No initial flow

Subscripts

i, j = regions of constant flow properties (Fig. 3)
1 = low pressure or test section initially
2 = behind incident shock
3 = behind rarefaction wave
4 = high pressure or driver section initially
5 = behind reflected shock
6 = nozzle throat

References

1 Tischler, A. O., Massa, R. V. and Mantler, R. L., "An Investigation of High-Frequency Combustion Oscillations in Liquid-Propellant Rocket Engines," NACA RM E53B27, 1953.

2 Crocco, L. and Cheng, Sin-I, "Theory of Combustion Instability in Liquid Propellant Rocket Motors," AGARDograph No. 8, Butterworths Sci. Pub., London, 1956.

3 Berman, K. and Cheny, S. H., Jr., "Combustion Studies in Rocket Motors," JOURNAL OF THE AMERICAN ROCKET SOCIETY, vol. 23, no. 2, March-April 1953; *see also* discussion by Sin-I-Cheng.

4 Glass, I. I., Martin, W. and Patterson, G. N., "A Theoretical and Experimental Study of the Shock Tube," UTIA Rep. no. 2, Inst. Aerophysics, Univ. of Toronto, Nov. 1953.

5 Rudinger, G., "On the Reflection of Shock Waves from the Open End of a Duct," *J. Appl. Phys.*, vol. 26, 1955, p. 981.

6 Rudinger, G., "Wave Diagrams for Nonsteady Flow in Ducts," Van Nostrand Co., Inc., New York, 1955.

7 Jenny, E., "Unidimensional Transient Flow with Consideration of Friction, Heat Transfer and Change of Section," *Brown Boveri Review*, vol. 37, no. 11, Nov. 1950, p. 447.

8 Mark, H., "The Interaction of a Reflected Shock Wave with the Boundary Layer in a Shock Tube," NACA TM 1418, 1958.

Turbulent Flame Studies in a Two-Dimensional Open Burner[1]

J. H. GROVER,[2] E. N. FALES[3] and A. C. SCURLOCK[4]

Atlantic Research Corp.
Alexandria, Va.

A two-dimensional open burner has been developed for studying turbulent flames. Stoichiometric natural gas-air flames with inlet flow velocities of 15, 20, 30 and 40 ft per sec were investigated. Densitometer traverses of time exposures were used to locate the position of the mean flame front and its root-mean-square displacement. Flash tube exposures of the flame with one-micron magnesium oxide particles in the flow were taken to determine the flow lines into and through the flame front. The large reduction of brightness that occurred when the flow passed through the flame front, due to the reduction of particle concentration, shows clearly the outline of the instantaneously wrinkled flame front and the islands of unburned gas often present in the burned gas. From the intercepts of the flow lines and the mean flame front, the local turbulent flame velocity along the flame front was calculated. The turbulent flame velocity increased rapidly with distance above the burner rim. The flame velocity increase can be entirely accounted for by flame wrinkling. Both this result and the appearance of the flash tube photographs, showing the instantaneous flame front, support the wrinkled flame concept of turbulent flame propagation.

IN A REVIEW of the status of experimental turbulent flame studies prepared by two of the present authors and published in 1954 (12)[5] attention was directed to the inadequacy of the then existing experimental results for turbulent flames propagating in homogeneous mixtures (as distinguished from turbulent diffusion flames). It was pointed out that most of the earlier studies (1,3,13,16) with such flames were concerned with the overall effects of turbulence on the entire flame brush and had not attempted to follow the local development of the flame at various distances from the stabilizer. One notable exception was the work of Karlovitz and his associates (8) who measured turbulent flame velocity vs. distance from the burner rim for bunsen flames disturbed by pipe turbulence. No account was taken by Karlovitz, however, of the flow divergence in the unburned gases; and it now appears that this divergence is of considerable importance. Since the present authors in 1953 (11) outlined their concept of the role of eddy diffusion, and thus of flame exposure time or distance downstream from the stabilizer, on the development of the turbulent flame, it has been recognized that a better understanding of turbulent flames could be achieved from analysis of measurements of local turbulent flame velocity vs. distance from the stabilizer under various conditions of turbulence, mixture composition and flow. The recent work of several investigators has been directed toward this objective (2,10).

The purpose of the present investigation of turbulent flames propagating in homogeneous mixtures has been to determine the location of both the time-average and instantaneous flame fronts, to obtain measurements of the flow in the vicinity of these flame fronts, and from these data to determine accurately the local turbulent flame velocity point-by-point along the mean flame front. This has been accomplished through the use of a "two-dimensional" open burner.

Received Sept. 12, 1958.
[1] This work was supported by the U. S. Air Force through the Air Force Office of Scientific Research of the Air Research and Development Command, under Contract no. AF 49(638)-177.

[2] Head, Aerothermodynamics Group. Member ARS.
[3] Research Associate, Aerothermodynamics Group.
[4] President. Member ARS.
[5] Numbers in parentheses indicate References at end of paper.

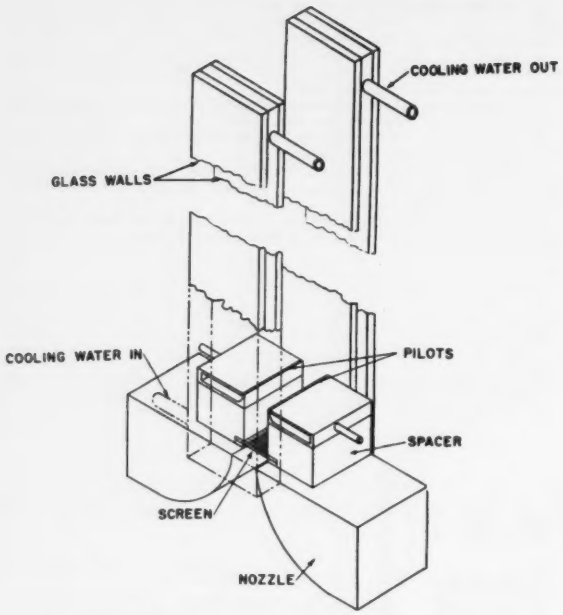

Fig. 1 Schematic of two-dimensional open burner

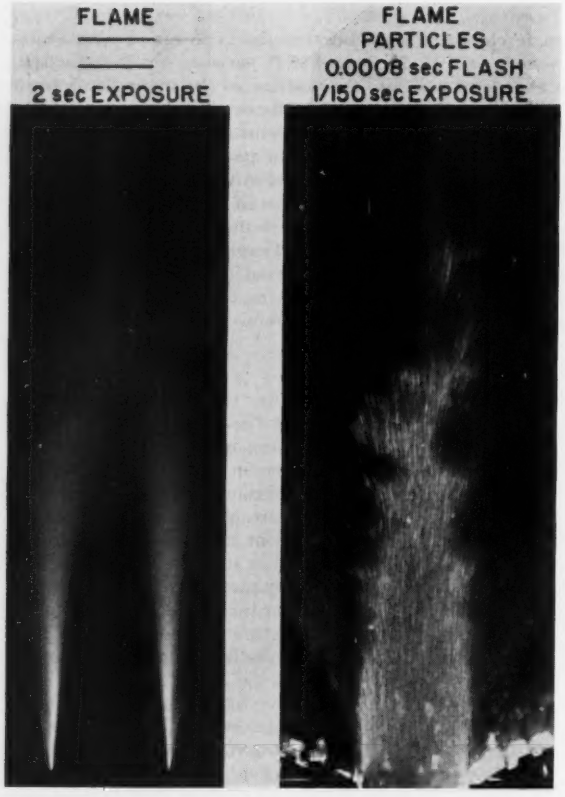

Fig. 2 Photographs of flame and flow in two-dimensional open burner (stoichiometric natural gas-air mixture; approach velocity, 20 ft per sec; four-mesh screen 2 in. upstream of burner rim)

Description of Apparatus

The 1 × 3-in. rectangular burner that was employed in these studies is shown schematically in Fig. 1. The 3-in. sides of the burner are open. Transparent confining walls extend along the 1-in. sides (the front and back of the burner). These serve to constrain the flow, causing it to be essentially two-dimensional and making it possible to view and photograph the flame.

Air is supplied from an oil-free compressor at a pressure of approximately 60 psi. The compressed air is dried by passage through a separator for removal of entrained moisture and through a silica gel bed for absorption of water vapor. The air is then metered by rotameter and passes through a control valve which regulates the flow rate and reduces the pressure. The air then enters an inspirator, as the primary stream, where the air pumps in low pressure natural gas (about 88 per cent methane), and the two streams are thoroughly mixed.

The natural gas, obtained from the Alexandria city main, is also metered by rotameter.

The air-fuel mixture proceeds from the inspirator into the calming section. The gases then pass through a nozzle with a contraction ratio of 25:1 where the turbulence intensity is reduced to less than 1 per cent. The 1 × 3-in. exit of this nozzle serves as the entrance to the burner.

Turbulence in the gases entering the burner was generated by placing a screen in the nozzle throat. Screens employed in this study were of stainless steel with a ratio of mesh width to wire diameter of 5:1.

As is shown in Fig. 1, removable spacers extend downstream for a short distance along the 3-in. sides of the burner, the purpose of the spacers being to make possible a variation of the distance between the flame and the turbulence generating screen. Immediately downstream of the spacers, propane-air pilots extend along the 3-in. sides of the burner.

To prevent the flame from stabilizing on the glass walls, it was necessary to maintain them at a relatively low temperature. This was accomplished by employing double plates with circulation of cooling water between the inner Vycor glass and the outer window glass.

For visualization of the flow into and through the flame, 1-μ particles of magnesium oxide were injected into the combustible mixture just prior to its entry into the calming section. These particles, which upon entering the burner are evenly distributed throughout the flow, are illuminated by a short-duration flash and photographed. The flash duration is regulated so that the individual particles appear in the photographs as short white streaks, which indicate the local instantaneous direction of flow.

Gilbert, Davis and Altman (6) concluded that 1-μ particles would correctly trace the streamline direction through a propane-air flame. It is thus believed safe to assume that the magnesium oxide particles follow the flow in these flames with at least the precision to which the direction of the particles are measured.

To obtain a photograph of these very small particles without obscuration by radiation from the flame, the particles were illuminated by the light of a cloud-chamber flash tube. The flash tube is powered by a bank of eight 25-μf capacitors. These capacitors are charged to a potential of 2000 v, and their discharge through the flash tube is synchronized with the camera shutter. The flash duration is about 0.8 millisec.

The light flux from the flash tube is intensified by focusing it at the center of the burner with a pair of cylindrical lenses. The lenses are focused so that a flat beam of light about $\frac{3}{8}$-in. thick slices through the center of the 3-in. wide flame.

The camera was constructed around an f8, 36-in.-focal-length, aerial-survey camera lens. The lens was equipped with a high speed between-the-lens shutter with a speed of about 7 millisec which was synchronized with the flash tube and used in obtaining the particle tracking exposures. In addition, a pneumatic shutter was installed back of the lens for obtaining time exposures.

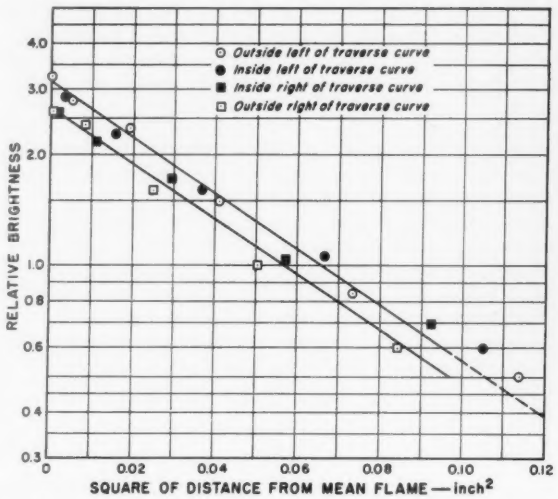

Fig. 3 Brightness distribution for the densitometer traverse 2.42 in. above the nozzle (stoichiometric natural gas-air flame with approach velocity of 20 ft per sec and four-mesh screen 2 in. upstream of burner rim)

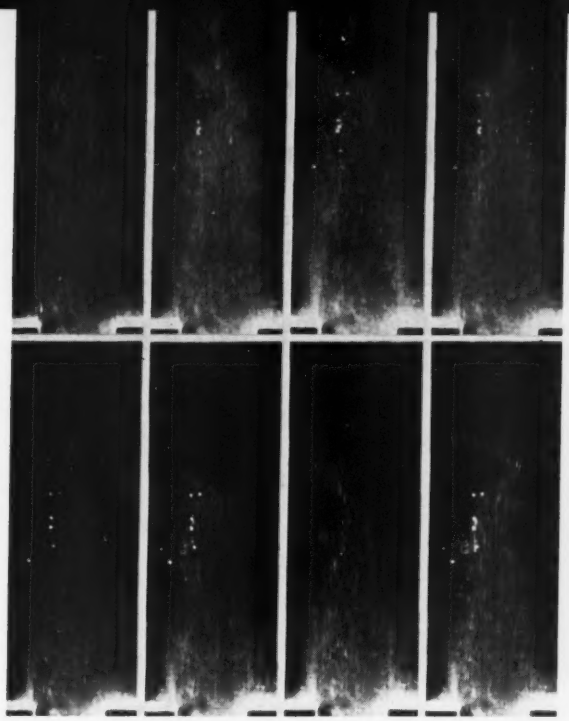

Fig. 4 Typical flash photographs of magnesium oxide particles in a stoichiometric natural gas-air flame with approach velocity 20 ft per sec (four-mesh screen 2 in. upstream of burner rim)

Experimental Results

All of the present work has been conducted with stoichiometric natural gas-air flames. The principal results were obtained with flow velocity at the entrance to the two-dimensional burner maintained at 20 ft per sec and with a four-mesh screen situated in the nozzle throat 2 in. upstream of the burner rim. Flame photographs and some limited results were also obtained at other approach flow velocities and with an eight-mesh screen in the nozzle throat.

Shown in Fig. 2 are examples of the two types of photographs employed for analysis in this study. The first is a time exposure of the turbulent flame with the flame itself as the sole source of light. The diffuse nature of the flame bush and its widening with distance from the burner rim are clearly observed. The second is a flash tube exposure with magnesium oxide particles in the flow.[6] Duration of the flash was chosen so that each particle would appear on the photograph as a short dash indicating the local instantaneous direction of flow. The instantaneous boundary between burned and unburned gases, assumed to be the flame front, is clearly shown. This results from the approximately eightfold (7.62) increase in specific volume of the gases associated with combustion and the attendant eightfold decrease in volumetric concentration of magnesium oxide particles upon passage through the flame front.

The flame front is observed to have a wrinkled appearance. At its top, a small island of unburned mixture has been pinched off by the flame propagation and is now surrounded by burned gases. The presence of a continuous sharply defined flame front in these and similar photographs (see also Fig. 4) lends support to the wrinkled flame concept of turbulent flame propagation as distinguished from the picture advanced by some (14) of a diffuse reaction zone. Since these photographs are essentially two-dimensional, depending for exposure only on the reflected light from small particles moving with the flow in a thin flame slice equidistant from the burner walls, they are less ambiguous than photographs obtained by shadow or Schlieren techniques which are dependent on refraction of light rays during their passage through the entire flame zone.

[6] Here the speed of the camera shutter is sufficient to prevent radiation from the flame itself from exposing the film and masking the light reflected from the particles.

Analysis of Time Exposure for Position of Mean Flame Front and Its rms Displacement

From the negative of the time-exposure photograph—the first photograph of Fig. 2—both the mean position of the flame front and the rms displacement of the flame front from its mean position have been determined from densitometer traverses across the flame. The mean flame front was taken as the locus of points of maximum density.

In order to determine the rms displacement of the flame front, it was necessary to relate the film density to the relative luminosity or brightness of the flame. Film density was found to be proportional to 0.64 times the logarithm of the luminosity over most of the range of density. Using this relationship and the density traverses, the distribution of flame luminosity was obtained. In Fig. 3, this distribution is shown for one of the density traverses. The logarithm of the relative brightness is plotted vs. the square of the distance from the mean flame front. Except for the dim regions of the flame where the background and reflected light are not negligible compared with the light of the flame, the data fall on a straight line. Thus the distribution of brightness is essentially Gaussian, and the rms displacement occurs at the point where the luminosity is 61 per cent of the maximum.[7]

[7] Since the distribution is Gaussian

$$b = \frac{1}{\sigma\sqrt{2\pi}} e^{-1/2\left(\frac{x-a}{\sigma}\right)^2}$$

where b is relative brightness, σ is a constant equal to the rms displacement; x is distance, and a is distance at the mean; and $b_{x=a\pm\sigma}/b_{x=a} = e^{-1/2} = 0.6065$.

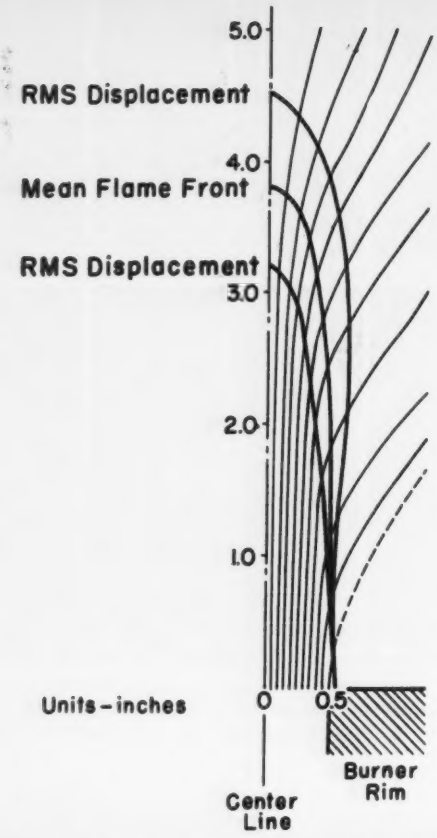

Fig. 5 Mean flow lines, mean flame front and rms displacement of the mean flame front (stoichiometric natural gas-air flame with approach velocity of 20 ft per sec and four-mesh screen 2 in. upstream of burner rim)

Since the density is proportional to 0.64 times the logarithm of the luminosity, the rms displacement occurs at the point where the film density is 0.139 below its maximum value;[8] and the rms displacement can be obtained directly from the densitometer traverses.

Analysis of Flash Tube Photographs for the Mean Flow

From a set of 20 flash tube exposures taken at different times under conditions corresponding to those for the second photograph of Fig. 2, the mean flow profile in the neighborhood of the flame has been obtained. A set of eight of these flash tube photographs used in the analysis are shown in Fig. 4. The photographs were projected one-by-one on a large grid, and the angle made by the particle tracks with the vertical was measured at 165 points in the flow. The readings for the right half of the flame were averaged with those for the left half, so that the average angle for each point was the average of 40 readings. From these data, curves of average angle vs. lateral distance from the center of the flame were drawn for each 0.5-in. increment of distance downstream from the burner inlet. From these results, mean flow lines have been constructed.

These mean flow lines, with the mean flame front and its rms displacement superimposed, are shown in Fig. 5. The rms displacement is observed to increase rapidly with distance from the burner rim. The flow divergence in the gases approaching the mean flame front is found to be substantial.

[8] $D\sigma - Da = \gamma \log (b\sigma/ba) = 0.64 \log 0.6065 = -0.139$, where $D\sigma$ and Da are the film densities at the rms displacement and the mean, respectively, and γ is the measured proportionality factor between the film density and the logarithm of the relative brightness.

Determination of Local Turbulent Flame Velocity

From the mean flow lines and position of the mean flame front, and assuming conservation of mass within any one mean stream tube, the local turbulent flame velocity S_T has been determined as a function of distance measured along the flame front from the burner rim.[9] The results are shown in Fig. 6. S_T is found to increase rapidly from 1.5 ft per sec at 1.5 in. above the burner rim to about 7 ft per sec at approximately 4 in. above the burner rim at the flame tip. These values may be compared with a laminar flame velocity S_L for the mixture of 1.2 ft per sec (9).

The time of exposure of a mean flame element or its age t has also been estimated from flow velocities obtained from the known divergence of the central stream tube and the assumption that, in the approach flow, the component of flow velocity parallel to the burner axis at any given distance downstream of the chamber entrance remains uniform. Flame element age is obtained by graphic integration of the relation

$$t = \int_0^h \frac{dh}{V}$$

where

h = the distance downstream of the chamber inlet
V = the local velocity in the central stream tube

A plot of V vs. h is shown in Fig. 7, and the Fig. 6 results replotted as S_T/S_L vs. t are shown in Fig. 8. From Fig. 7 the flow divergence in the gases above the burner inlet is found to result in a reduction in flow velocity parallel to the mean flame front from approximately 20 ft per sec at the burner entrance to about 8 ft per sec at the flame tip.

[9] For any one stream tube, the assumption of conservation of mass yields $\rho_u A_s U = \rho_u A_f S_T$, where ρ_u is the density of the unburned gases; A_s is the cross-sectional area of a stream tube at the chamber entrance (assumed to be uniform); A_f is area of the mean flame front through which the stream tube passes, and S_T is the local turbulent flame velocity (actually the local turbulent flame velocity averaged over the area A_f).

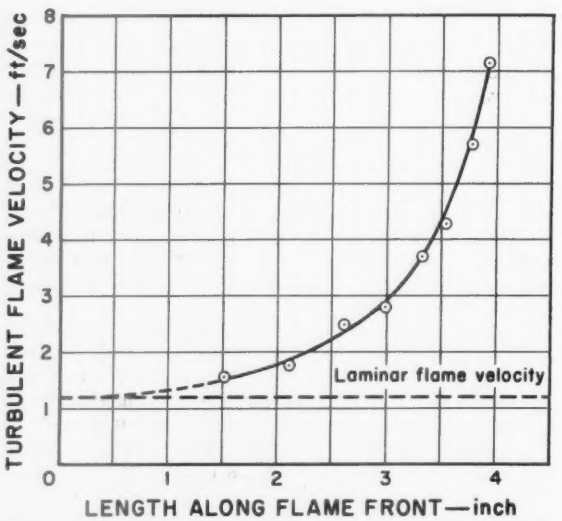

Fig. 6 Turbulent flame velocity vs. flame length (stoichiometric natural gas-air flame with approach velocity of 20 ft per sec and four-mesh screen 2 in. upstream of burner rim)

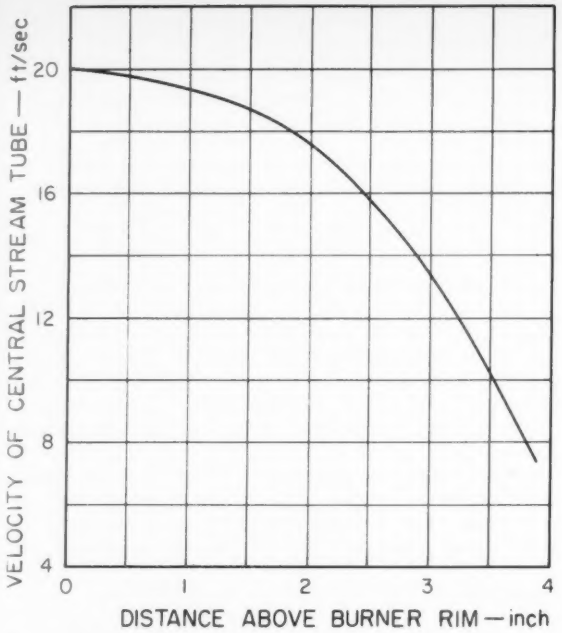

Fig. 7 Velocity along central stream tube (stoichiometric natural gas-air flame with inlet flow velocity of 20 ft per sec and four-mesh screen 2 in. upstream of burner rim)

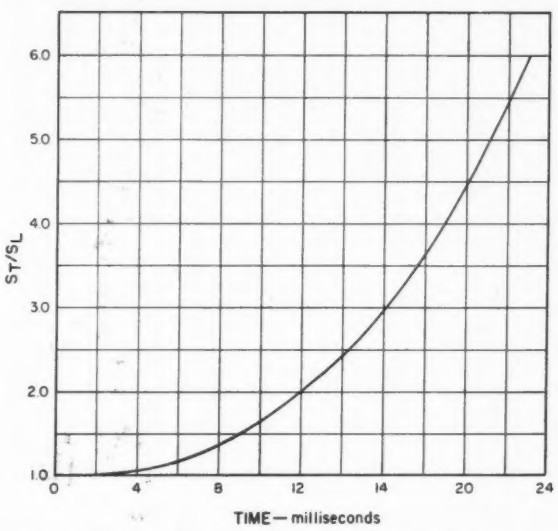

Fig. 8 S_T/S_L vs. time (stoichiometric natural gas-air flame with approach velocity of 20 ft per sec and four-mesh screen 2 in. upstream of burner rim)

Position of Mean Flame Front and Its rms Displacement From Flash Tube Photographs

As a check on the results obtained from the densitometer traverses of the time exposure photograph, the position of the mean flame front and its rms displacement were determined independently by analysis of a set of flash tube photographs. The outline of the instantaneous wrinkled flame front, as denoted by the rapid change in particle concentration, was traced for 18 flash exposures of this flame. At short intervals downstream from the inlet, measurements were obtained from each tracing of distance of the right and left flame fronts from the chamber center line. When flame wrinkling resulted in the presence of more than one flame front at any chosen height, a measurement for each individual flame front was taken. Flame symmetry was again assumed, and measurements from right and left flame fronts were grouped together for analysis.

The position of the mean flame front and its rms displacement determined for each interval from these measurements are plotted as points in Fig. 9. The results of the densitometer method are shown as the solid lines for comparison. Agreement is excellent on the position of the mean flame front and reasonably good on rms displacement. Since the densitometer method is dependent for flame front location on light from the luminous flame zone, whereas the flash tube photograph method is dependent for flame front location on the rapid change in concentration of suspended particles, the excellent agreement of the two methods on location of the mean flame front gives strong support to the assumption that the steep gradient in suspended particle concentration does, in fact, correspond to the luminous flame front. Since the flash tube photographs are of a thin slice of flame in the center of the burner, whereas the time exposure photographs are of the entire flame including that adjacent to the front and rear walls, this excellent agreement is also interpreted as evidence that, under the conditions studied, the boundary effects of the confining walls are relatively small.

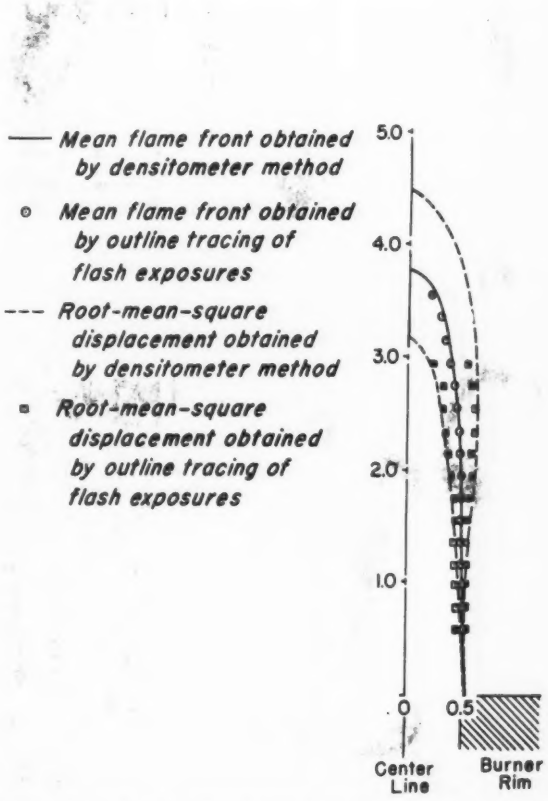

Fig. 9 Mean flame front and rms displacement as obtained by two methods (stoichiometric natural gas-air flame with approach velocity of 20 ft per sec and four-mesh screen 2 in. upstream of burner rim)

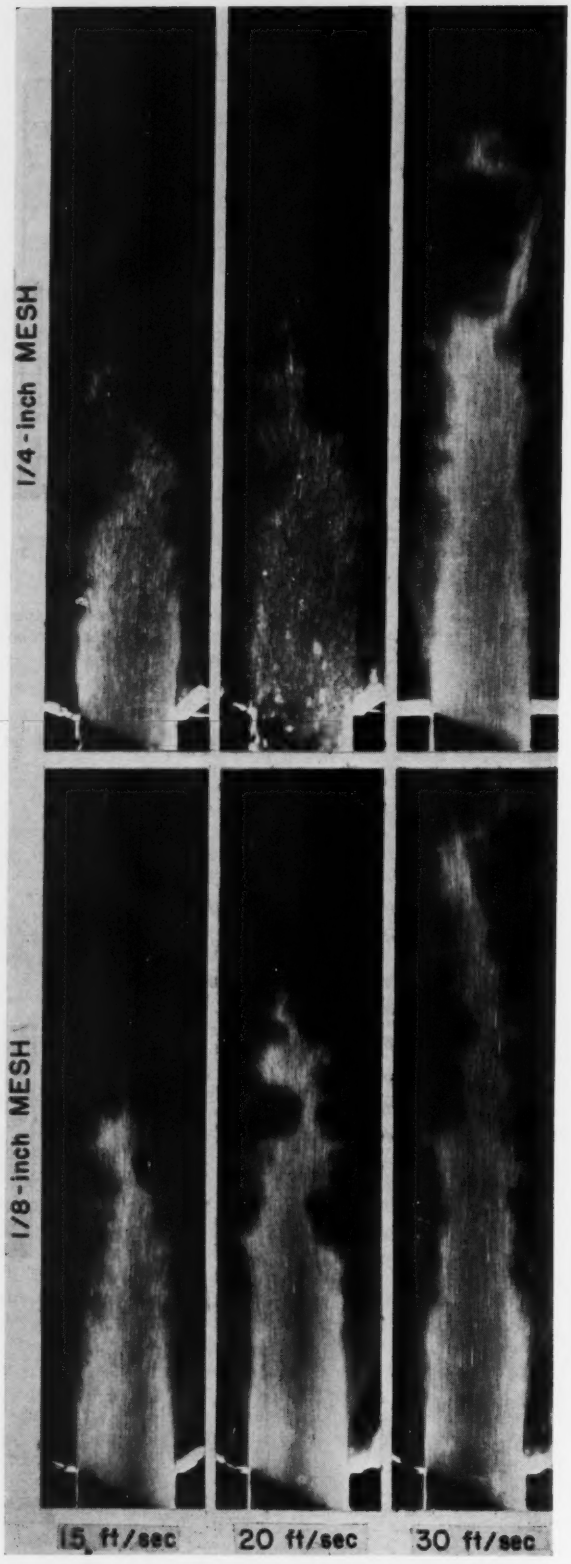

Fig. 10 Flash photographs of magnesium oxide particles in two-dimensional open burner flames at various flow velocities (stoichiometric natural gas-air mixture; screen 2 in. upstream of burner rim)

Instantaneous Flame Surface From Flash Tube Photographs

By further analysis of the flash tube photographs, an additional test of the wrinkled flame concept has been conducted. At flow velocities of both 20 and 40 ft per sec, and employing the same four-mesh turbulence generating screen as before, the mean instantaneous flame area has been approximated from flame perimeter measurements obtained from flash tube photographs taken at these two flow velocities. From these areas and the known mass flow at the inlet, laminar flame velocities have been calculated for comparison with the known value of 1.2 ft per sec. In order to convert the mean instantaneous flame perimeter, obtained by averaging the individual perimeter measurements from a set of flash photographs, into a mean instantaneous flame area, an assumption must be made in regard to flame wrinkling in the direction normal to the flame slice depicted in the photographs. It would seem reasonable, in the absence of other information, to assume that flame wrinkling in this direction is, on the average, the same as that in the plane of the photographs. This was the assumption chosen. Thus, to determine the mean instantaneous surface area per unit of flame depth, the mean instantaneous flame perimeter is multiplied by the ratio of mean instantaneous flame perimeter to perimeter of the mean flame front. The results of the analyses are given in Table 1. At an inlet velocity of 20 ft per sec, a flame velocity of 1.35 ft per sec based on the mean instantaneous flame area is obtained. At an inlet velocity of 40 ft per sec, the flame velocity similarly determined is 1.30 ft per sec. These compare well with the known laminar flame velocity of 1.2 ft per sec and indicate that, at least under the conditions of these experiments, the turbulent flame is nothing more than a randomly fluctuating wrinkled laminar flame.

Table 1 Flame velocity from mean instantaneous flame area

Inlet velocity, ft/sec	20	40
no. flash tube photographs analyzed	18	19
mean instantaneous flame perimeter, in.	10.8	19.13
standard deviation, in.	1.7	1.3
perimeter of mean flame front, in.	7.9	11.9
wrinkling factor = $\frac{\text{mean instantaneous flame perimeter}}{\text{perimeter of mean flame front}}$	1.36	1.61
mean instantaneous flame area per unit of flame depth, in.^{2}/in.	14.8	30.8
flame velocity based on mean instantaneous flame area, ft/sec	1.35	1.30
laminar flame velocity (9) S_L, ft/sec	1.2	1.2

Flame Photographs Over a Range of Flow Velocities

Shown in Fig. 10 are flash tube photographs taken at inlet velocities of 15, 20 and 30 ft per sec. In the top set of three photographs the four-mesh screen was employed for turbulence generation. An eight-mesh screen was used in the lower photographs. Flame height and turbulent flame velocity are found to increase with flow velocity. For a given flow velocity, flame height is always greater with the eight-mesh screen, and turbulent flame velocity is always found to be greater with the four-mesh screen. Qualitatively, these results are as would be expected and are consistent with those obtained previously by Wohl et al. (16).

Comparison With Theory

Scurlock and Grover (11, 12), in the development of their theory, consider an initially flat flame of infinite extent propagating into a combustible mixture agitated by isotropic

Table 2 Calculated values of l_2 and C_1

Distance above burner rim, in.	1.2	1.6	2.0	2.5	3.0	3.5
measured S_T, ft/sec	1.4	1.5	1.8	2.2	2.9	4.2
measured $(\overline{Y^2})^{1/2}$, in.	0.05	0.083	0.123	0.165	0.211	0.275
Dryden l_2, in.	0.0486	0.0493	0.0511	0.0526	0.0541	0.0556
calculated l_2 assuming $C_1 = 4$, in.	0.165	0.250	0.220	0.221	0.193	0.164
calculated C_1 using Dryden l_2	0.348	0.155	0.216	0.228	0.314	0.469

turbulence. Only turbulence with a scale very large relative to the thickness of the laminar flame front is considered, the turbulence assumed only to wrinkle and extend the flame surface, the laminar flame velocity remaining constant and unaffected either by any increase in transport properties or by flame curvature. It is proposed that as time passes the initially flat flame becomes more and more wrinkled by eddy diffusion of flame elements away from the mean position of the flame, and the flame area at first progressively increases. Assuming that the depth of the wrinkles is proportional to the rms displacement of a flame element from its mean position $(\overline{Y^2})^{1/2}$ and that the average base width of these wrinkles is proportional to the Eulerian scale of turbulence l_2, the following relation for the ratio of wrinkled to initially flat flame area A_T/A_L was obtained from simple geometric considerations

$$\frac{A_T}{A_L} = \frac{S_T}{S_L} = \left[1 + C_1\left(\frac{\overline{Y^2}}{l_2^2}\right)\right]^{1/2} \qquad [1]$$

where C_1 is a combined proportionality constant somewhat arbitrarily assigned a value of 4, based on the assumption that mean wrinkle depth equals $2(\overline{Y^2})^{1/2}$, and that the average base width of the turbulent flame wrinkles is about four times the scale of turbulence. Although neither of these assumptions can be considered quantitatively exact, geometric considerations and previous experimental results indicate that they should be fair approximations.

Indication That Scale of Flame Turbulence Is Substantially Larger Than Anticipated

Since experimental values of S_T and $(\overline{Y^2})^{1/2}$ are available from the present investigation, Equation [1] may be employed either:

1 With the constant C_1 assigned the value of 4, after Scurlock and Grover, to calculate the scale of turbulence l_2 at various points along the flame front for comparison with that predicted by the relation of Dryden et al. (5) for turbulence behind screens in cold flow.

2 With the values of l_2 predicted by the Dryden relation to calculate values of C_1.

The results of such calculations are shown in Table 2. For $C_1 = 4$, the calculated values of scale are approximately four times those predicted by the Dryden relation. Assuming values of scale from the Dryden relation, C_1 would have a value of approximately 0.25. Further work is necessary to determine where the truth lies, but one is left with the suggestion that the flame may be under the influence of turbulence with an effective scale larger than would be expected from the presence of the four-mesh screen.

Preliminary measurements of wrinkle base width from the Fig. 4 photographs yield values in the range of 0.4 to 0.8 in. compared with a wrinkle base width of 0.2 in. required for a $C_1 = 4$. This may be interpreted either as a further argument for the presence of a turbulence scale larger than that predicted by the Dryden relation, or as evidence, contradictory to (7), that average base width of the flame wrinkles is substantially greater than four times the turbulence scale. An increase in effective scale might result either from the divergence of the approach flow associated with the presence of the turbulent flame, or it might be attributed to the existence of flame-generated disturbances, the scale of which would not necessarily be the same as that generated by the screen.

High Effective Turbulence Intensity in Flame Suggests Presence of Flame Generated Turbulence

By modification of Taylor's (15) theory of eddy diffusion by continuous movements to take into account flame propagation, Scurlock and Grover arrived at the following relation for the effect of eddy diffusion on $(\overline{Y^2})$

$$\frac{d(\overline{Y^2})}{dt} = 2v'^2 \int_0^t R_t R_y dt \qquad [2]$$

where

v' = turbulence intensity (assumed to be isotropic and thus the same in all three directions)

R_t and R_y = the Lagrangian and Eulerian correlation coefficients of fluctuating velocity

t = the exposure time or age of the flame element under consideration

For short-time intervals, R_t and R_y may be assumed to equal 1, and Equation [2] may be integrated to obtain the following simple relationship

$$(\overline{Y^2})^{1/2} = v't \qquad [3]$$

For long-time intervals, R_t and R_y fall to zero, and the following relation may be obtained

$$(\overline{Y^2})^{1/2} = (2v'l_1't)^{1/2} \qquad [4]$$

where l_1' is a mixed scale.[10]

Thus assuming a constant v' in the vicinity of the flame, it would be anticipated from Equations [3 and 4] that $(\overline{Y^2})^{1/2}$ would rise linearly with exposure time for a short interval and would then increase at a lower rate proportional to the square root of exposure time. A more rapid increase in $(\overline{Y^2})^{1/2}$ would indicate that effective turbulence intensity was increasing with exposure time.

Using experimental values of $(\overline{Y^2})^{1/2}$ and t, Equation [3]

[10] Using Taylor's definition of Lagrangian scale

$$l_1 \equiv v' \int_0^\infty R_t dt$$

and Eulerian scale

$$l_2 \equiv \int_0^\infty R_y dy$$

and, accepting after Dryden (4) the approximations $R_t = \exp - v't/l_1$ and $R_y = \exp - S_T t/l_2$, the following relation may be obtained from the mixed scale l_1'

$$l_1' = v'\left(\frac{1}{v'/l_1 + S_L/l_2}\right) = v'T_0'$$

Equation [3] would apply when $t \ll T_0'$. Equation [4] applies when $t \gg T_0'$.

Table 3 Calculated values of v'

Distance above burner rim, in.	1.2	1.6	2.0	2.5	3.0	3.5
measured $(\overline{Y^2})^{1/2}$, in.	0.05	0.083	0.123	0.165	0.211	0.276
time (corrected for velocity reduction from flow divergence), sec	0.0052	0.0070	0.0088	0.0113	0.0142	0.017
v' (cold flow from Dryden (5)), ft/sec	1.3	1.2	1.11	1.00	0.88	0.80
v' (from Eq. [3]), ft/sec	0.80	0.99	1.16	1.22	1.24	1.31
v' (from Eq. [4]; l_2 Dryden from Table 1), ft/sec	1.22	2.14	3.30	4.30	5.16	7.03
v' (from Eq. [4]; l_2 from Eq. [1] and $C_1 = 4$), ft/sec	0.52	0.70	1.02	1.32	1.86	2.71

has been employed for computation of v'. Values of v' have also been calculated from the experimental quantities from Equation [4] assuming in one instance the l_2 predicted by the Dryden relation, and, in a second, that l_2 has the value obtained from Equation [1] assuming $C_1 = 4$. The results of these calculations are shown in Table 3 where they are compared with values of v' predicted by the relation of Dryden for turbulence intensity downstream of screens.

Equation [3] might be expected to apply fairly well for perhaps an inch or two downstream of the burner rim. Neither Equation [3] nor Equation [4], but something in between, should apply for the remainder of the distance to the flame tip.[11]

Although the Dryden relation predicts a slight decrease of v' with distance downstream due to decay, all of the calculated values of effective v' based on measured values of $(\overline{Y^2})^{1/2}$ show an increase. It is thus suggested that additional effective turbulence is being introduced into the flame over and above that generated by the screen. One explanation could be the appearance of flame generated turbulence.

Comparison of Experimentally Determined Curves of (S_T/S_L) vs. $(S_L t/l_2)$ With Those Obtained From the Theory

Scurlock and Grover in their theoretical development employed Equation [1], and, attempting to take into account the effects on the flames of eddy diffusion, flame propagation and flame generated turbulence, derived an approximate relation for $(\overline{Y^2})^{1/2}$ as a function of the dimensionless time $S_L t/l_2$, the ratio v'/S_L and the ratio of unburned to burned gas density ρ_u/ρ_b. Results of their theory presented as (S_T/S_L) vs. $(S_L t/l_2)$ for several values of v'/S_L, for density ratios of eight and ten, and with and without the presence of flame generated turbulence are shown in Fig. 11. All of the theoretical curves were computed using $C_1 = 4$. Superimposed for comparison are curves derived from the present experimental results. The first such curve is for the larger scale of turbulence obtained from Equation [1] and the assumption that $C_1 = 4$. The second assumes that the effective scale is that predicted by the Dryden relation. If, as has already been indicated by the experimental results, the correct value of C_1 is much lower than 4, then the first experimental curve is the one most directly comparable to the theoretical curves (since both are based on $C_1 = 4$). Based on the screen generated turbulence and the experimental density ratio, the theoretical curves most appropriate for comparison are those for $(v'/S_L) = 1$ and $(\rho_u/\rho_b) = 8$. The general shape of this experimentally derived curve is in reasonably good agreement with the theoretical. This lends support to the underlying physical picture upon which the theory is based. The experimental curve, however, rises well above those obtained from theory. The explanation of this deviation could be inadequacy of the theory in taking account of flame generated turbulence. Additional experimental results under other conditions should shed further light on this point and prove useful in assigning a more accurate value to the constant C_1.

[11] Taking $l_2 = 0.05$ ft, $v' = 1.2$ ft per sec, $l_1 = \frac{1}{4} l_2 = 0.025$ ft, and $S_L = 1.2$ ft per sec; T_0' for our experimental conditions is found to be 0.014 sec. For our flow velocity of 20 ft per sec, this corresponds to a distance of approximately 3.4 in. Flow divergence with the attendant reduction in flow velocity might reduce this value to about 3 in.

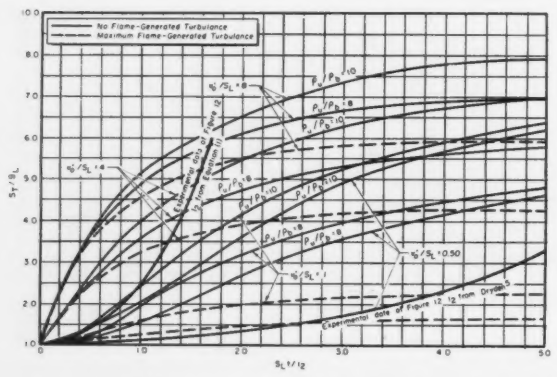

Fig. 11 Plots of S_T/S_L vs. $S_L t/l_2$ under different conditions

Conclusions

1 Under the experimental conditions of this study, the flame velocity increase in the presence of approach turbulence is, within experimental error, entirely accounted for by flame wrinkling. Both this result and the appearance of the flash tube photographs showing the instantaneous flame front (as denoted by the change in concentration of suspended particles) to be a thin wrinkled continuous boundary between unburned and burned gases, lend support to the wrinkled flame concept of turbulent flame propagation.

2 The turbulent flame velocity is found to increase rapidly with distance above the burner rim, this increase being somewhat greater than would be predicted by the Scurlock and Grover theory.

Comparison of theory with experiment indicates the presence of effective turbulence in excess of that in the approach flow. It is suggested that such additional turbulence might be flame generated. There is also evidence that the effective scale of the turbulence disturbing the flame is several times greater than that generated by the screen. This could be explained on the basis either that flame generated disturbances are present and that these would not necessarily have an effective scale equal to that in the approach flow, or that the flow divergence in the gases approaching the flame acts to increase the scale. Although the experimental values of turbulent flame velocity are somewhat greater than predicted by the Scurlock-Grover theory, the general shape of the experimental (S_T/S_L) vs. $(S_L t/l_2)$ curve is similar to that of the theoretical curves. This lends support to the general validity of the physical picture of the mechanism of turbulent flame propagation which underlies the theory. The experimental results suggest that the value of 4 previously assigned

to the constant C_1 for calculation of the theoretical curves is much too high.

3 A useful technique has been developed for determination for a turbulent flame of the mean flow field in the neighborhood of the flame, the mean flame front, the rms displacement of the mean flame front, the local turbulent flame velocity, and the position of the instantaneous flame front. The analysis of additional experimental results obtained over a range of conditions using this technique can be expected to provide further enlightenment regarding the mechanism of propagation of turbulent flames.

References

1 Bollinger, L. M. and Williams, D. T., "The Effect of Turbulence on Flame Speed of Burner Type Flames," NACA Tech. Note 1707, 1949, *also* "Third Symposium on Combustion, Flame, and Explosion Phenomena," Williams and Wilkins Co., Baltimore, 1949, p. 176.

2 Bolz, R. E. and Bunlage, Jr., H., "The Influence of Turbulence on Flame Propagation Rates," JET PROPULSION, vol. 25, 1955, p. 265.

3 Damkohler, G., "The Effect of Turbulence on the Flame Velocity in Gas Mixtures," *Z. Elektrochem.*, vol. 46, 1940, p. 610; English Translation: NACA Tech. Memo. 1112, 1947.

4 Dryden, H. L., "Turbulence and Diffusion," *Ind. & Eng. Chem. (Ind)*, vol. 31, 1939, p. 416; *see also* "A Review of the Statistical Theory of Turbulence," *Quart. Appl. Math.*, vol. 1, 1943, p. 7.

5 Dryden, H. L., Schubauer, G. B., Mock, Jr., W. C. and Skramstod, K. H., "Measurements of Intensity and Scale of Wind-Tunnel Turbulence and Their Relation to the Critical Reynolds Number of Spheres," NACA Report 581, 1937.

6 Gilbert, M., Davis, L. and Altman, D., "Velocity Log of Particles in Linearly Accelerated Combustion Gases," JET PROPULSION, vol. 25, 1955, p. 26.

7 Hottel, H. C., Williams, G. C. and Levine, R. S., "The Influence of Isotropic Turbulence on Flame Propagation," in "Fourth Symposium on Combustion," Williams and Wilkins Co., Baltimore, 1953, p. 636.

8 Karlovitz, B., Denniston, Jr., D. W. and Wells, F. E., "Investigation of Turbulent Flames," *J. Chem. Phys.*, vol. 19, 1951, p. 541.

9 Manton, J. and Millikan, B. B., "Study of Pressure Dependence of Burning Velocity by the Spherical Vessel Method," *Proc. Gas Dynamics Symposium, Aerothermochemistry*, Evanston, Illinois, p. 151, Aug. 1955.

10 Richmond, J. K., Singer, J. M., Cook, E. B., Oxendine, J. R., Grumsur, S. and Burgess, D. S., "Turbulent Burning Velocities of Natural Gas-Air Flames with Pipe-Flow Turbulence," in "Sixth Symposium on Combustion," Reinhold, New York, 1957, p. 303.

11 Scurlock, A. C. and Grover, J. H., "Propagation of Turbulent Flames," in "Fourth Symposiumon Combustion," Williams and Wilkins Co., Baltimore, 1953, p. 645.

12 Scurlock, A. C. and Grover, J. H., "Experimental Studies of Turbulent Flames," in "Selected Combustion Problems," Advisory Group for Aeronautical Research and Development, NATO, Butterworths Scientific Publications, 1954, p. 215.

13 Shelkin, K. I., "On Combustion in a Turbulent Flow," *J. Tech. Phys.*, (USSR), vol. 13, 1943, p. 520; English Translation: NACA Tech. Memo. No. 1110, 1947.

14 Summerfield, M., Reiter, S. H., Kebely, V. and Mascolo, R. W., "The Structure and Propagation Mechanism of Turbulent Flames in High Speed Flow" JET PROPULSION, vol. 25, 1955, p. 377.

15 Taylor, G. I., "Diffusion by Continuous Movements," *Proc. Lond. Math. Soc.*, vol. 20, 1921, p. 196.

16 Wohl, K., Shore, L., von Rosenberg, H. and Weil, C. W., "The Burning Velocity of Turbulent Flames," in "Fourth Symposium on Combustion," Williams and Wilkins Co., Baltimore, 1953, p. 620.

On-Off Control System for Attitude Stabilization of a Space Vehicle

JOSEF S. PISTINER[1]

The Martin Company
Denver, Colo.

This paper develops certain nonlinear analysis and synthesis techniques as applied to an on-off control system for attitude stabilization of a space vehicle. As an example of the possible applications of the theory, a hydrogen peroxide system is discussed. However, the analysis holds equally true for other gas systems, such as nitrogen, hydrazine, etc. It is shown how the analysis effort is simplified when vehicle attitude and attitude rate are represented by a set of nondimensional position-velocity coordinates defining a "phase plane." The requirement for compensation (lead) networks to achieve stable limit cycle operation is established, and the effect of time delays on system performance is discussed. Since fuel consumption is shown to be dependent on lead network configuration, a synthesis method for optimization of the compensation network to result in minimum fuel consumption is presented.

OUTSIDE of the Earth's atmosphere, the motion of a vehicle in coasting flight about its pitch, yaw or roll axes is determined by the respective angular rates existing at shutoff of the propulsion and control systems which put it into space; motion, about its body axes, of a vehicle in powered flight could be the result of misalignments of the propulsion system with respect to these axes.

Because of this motion, attitude stabilization and control of a satellite, or a space vehicle in general, may be required in some instances for short periods of time. These requirements, for example, may exist because of limitations on camera and antenna look angles or in gimbal travel of inertial platforms used for navigational purposes.

There are several known means of achieving the required results. The designer, for example, may select a proportional control system in which the applied correction force or moment is proportional to the attitude error sensed by some measuring device, or he may choose an on-off ("bang-bang") system in which a correction is applied only when the error exceeds a previously established value (dead zone).

Proportional systems have the disadvantage that they are elaborate and heavy because of the use of control vanes, gimballed thrust chambers or similar devices.

On-off systems, on the other hand, weigh appreciably less and are simple and reliable because they consist of relatively

Received April 18, 1958.

[1] Systems Analysis Section Staff, Denver Division.

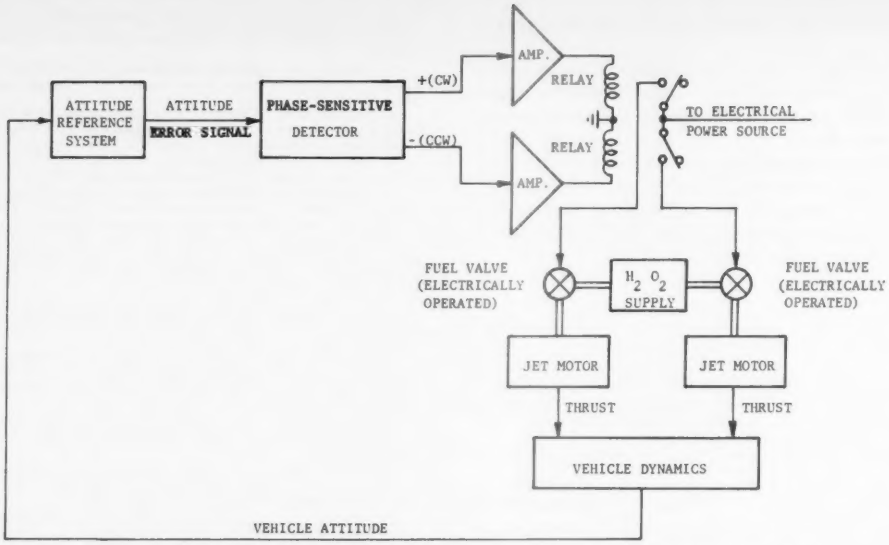

Fig. 1 Simplified block diagram of an on-off H_2O_2 control system (pitch axis shown only)

few components. For this application, hydrogen peroxide (H_2O_2) for example, is particularly well suited, although other gas systems, such as hydrazine, nitrogen, etc. are equally feasible.

Fig. 1 shows a simplified block diagram of a single channel (pitch axis) of a typical H_2O_2 on-off attitude stabilization and control system. The attitude reference system senses the pitch attitude of the vehicle, compares it with the reference attitude and feeds the difference or error signal into a phase-sensitive detector. Depending on the direction of the error, clockwise or counter-clockwise, the detector feeds the signal into the proper amplifier. When the amplifier output signal magnitude corresponds to the given dead zone value, the relay pulls in and the H_2O_2 control valve is electrically energized, allowing for flow of H_2O_2 to the proper jet motor. In the jet motor, the H_2O_2 passes over a suitable catalyst which changes the H_2O_2 into steam; thrust is developed by expansion of the steam through a nozzle. Corrective action stops upon de-energization of the control relay when the attitude error becomes less than the dead zone value.

Several analysis techniques for on-off control systems have been developed based on adaption of linear theory (see (1)[2] for example). However, it has been found that these methods do not lend themselves too well to the present application because of the very low limit cycle frequencies required to minimize fuel consumption.

In contrast, the phase plane technique, as will be shown in this paper, offers the designer the advantages of simplicity, flexibility and adequate accuracy in predicting the performance of the system.

Vehicle Dynamics*

This paper will discuss single axis vehicle motion only. This approach, although not providing a complete solution to the coupled equations of motion, permits a straightforward evaluation of those system characteristics which are required for the control system design.

Outside the Earth's atmosphere, the equations of motion of a vehicle with respect to any one of its principal axes become extremely simple.

During the "on" phase of the H_2O_2 (or N_2H_4, N_2, etc.) control system, when a correcting moment is applied about the pitch axis (identical analyses hold true for the yaw and roll axes), the vehicle dynamics are given by

$$\ddot{\theta} = \alpha = \frac{Fl}{I} = \text{constant} \qquad [1]$$

If the initial conditions at time $t = t_0$ are assumed to be $\theta = \theta(0)$, where $\theta(0) \geq$ dead zone and $\dot{\theta} = 0$, it immediately follows that at any time t

$$\theta = \theta(0) + \frac{1}{2}\alpha t^2 \qquad [2]$$

and

$$\dot{\theta} = \alpha t \qquad [3]$$

By elimination of time (t) between Equations [2 and 3], Equation [2] may then be written

$$\theta = \theta(0) + \frac{\dot{\theta}^2}{2\alpha} \qquad [4]$$

Equation [4] may be conveniently plotted on a position-velocity set of coordinates. This representation is called a phase plane (2). Inspection of Equation [4] shows that its phase plane trace will be a parabola with vertex at $\theta = \theta(0)$ and a latus rectum equal to 2α.

During the "off" phase of the control system, the vehicle will rotate at an angular pitching velocity equal to that when the thrust of the control system was reduced to zero. The vehicle dynamics, therefore, are given by

$$\dot{\theta} = \dot{\theta}(0) = \text{constant} \qquad [5]$$

On a phase plane plot, Equation [5] represents a straight line parallel to the displacement axis.

Introduction to Phase Plane Analysis Methods

If all quantities in Equation [4] are nondimensionalized, a considerable simplification in the analysis effort is accomplished. A parabolic template then can be constructed for analyzing the effect of system parameter variations.

[2] Numbers in parentheses indicate References at end of paper.
* A list of definitions of symbols is given at end of paper.

To nondimensionalize all quantities with dimensions containing time, a convenient time base, $t_b = 1$ sec is assumed. This defines a nondimensional time scale $\tau = t/t_b$. Angular position may be nondimensionalized by dividing θ by αt_b^2. Therefore, a dimensionless displacement Ω may be defined

$$\Omega = \frac{\theta}{\alpha t_b^2} \qquad [6]$$

Also

$$\dot{\Omega} = \frac{d\theta}{dt} \cdot \frac{dt}{d\tau} \div \alpha t_b^2$$

$$= \frac{\dot{\theta}}{\alpha t_b} \qquad [7]$$

and

$$\ddot{\Omega} = \frac{\ddot{\theta}}{\alpha} \qquad [8]$$

Inspection of Equation [8] shows that the dimensionless angular acceleration is of unity ($\ddot{\theta}$ = constant) or zero magnitude. When a correcting torque is applied, $\ddot{\Omega}$ may be positive or negative. Conventionally, a clockwise trajectory is assumed on a phase plane plot. $\ddot{\Omega}$ then is positive when the dimensionless rate $\dot{\Omega}$ is increasing in the positive direction, and $\ddot{\Omega}$ is negative when $\dot{\Omega}$ increases negatively.

By use of Equations [6, 7 and 8], Equation [4] can be rewritten in nondimensional form:

In left-hand plane where $\ddot{\Omega} = +1$

$$\Omega = \Omega(0) + \frac{1}{2}\dot{\Omega}^2 \qquad [9a]$$

In right-hand plane where $\ddot{\Omega} = -1$

$$\Omega = \Omega(0) - \frac{1}{2}\dot{\Omega}^2 \qquad [9b]$$

Parabolic templates to satisfy Equations [9] are easily constructed.

System dead zone and relay hysteresis may be shown on the phase plane as displacement boundaries at which relay pull-in and drop-out in either direction may occur.

Assuming, for the time being, instantaneous thrust buildup and decay, and neglecting any time delays, such as relay armature closing time, etc., which may be present in the system, it can be easily shown on a phase plane plot (Fig. 2a) that, with relay hysteresis, any disturbance would build up with time. That is, the system would hunt at an increasing amplitude and frequency. Such a system is dynamically unstable. If the relay hysteresis is reduced to zero, the system would hunt at constant frequency and at the amplitude of the transient displacement (Fig. 2b). However, in any physical system, time delays are always present. The assumption of instantaneous thrust buildup and decay also cannot be considered valid.

To include time delays in the analysis, it is necessary to be able to make time measurements on the phase plane plot. Along a constant velocity path [$\dot{\Omega} = \dot{\Omega}(0)$], the dimensionless time $\tau(= t/t_b)$ to move from one point Ω_1 to another Ω_2 is given by

$$\tau = \frac{|\Omega_2 - \Omega_1|}{|\dot{\Omega}(0)|} \qquad [10]$$

Along a constant acceleration (parabolic) path, the dimensionless time to travel from one point to another is given by the absolute value of the difference in ordinates $\dot{\Omega}$ of the starting and end points (see Appendix for derivation).

Comparison of Figs. 2a and 2c shows the system amplitude and frequency to increase more rapidly when a nominal time delay due to relay armature closing and opening time is considered.

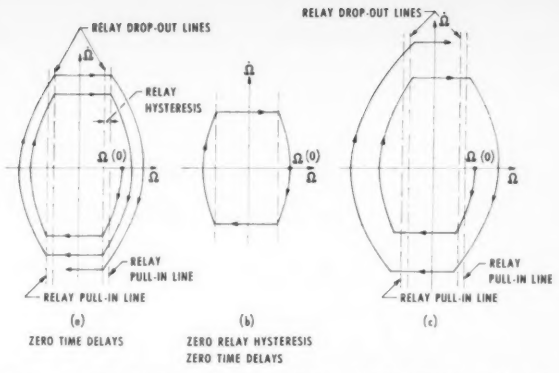

Fig. 2 Phase plane plot for an initial displacement $\Omega(0)$ and assumed instantaneous thrust buildup and decay

Therefore, some means for system stabilization and fuel conservation must be devised. Both of these requirements may be accomplished by incorporation of lead compensation in the system.

System Operation With Lead Compensation

Stable limit cycle operation can be achieved by incorporation of compensation (lead) networks in the system. It has been found that a single stage lead circuit, operating on the attitude error signal as represented by the amplifier output, is generally adequate when the angular acceleration during the system "on" mode is less than approximately 1 radian per sec^2. As will be shown later, fuel consumption as measured by limit cycle frequency, or more directly by thrust-on time per cycle, may be minimized by proper selection of lead circuit parameters.

The Laplace transform for the output $E_0(s)$ of a single lead circuit in response to an input $E_i(s)$ is given by

$$E_0(s) = \frac{(1 + Ts)}{\gamma[1 + (T/\gamma)s]} E_i(s) \qquad [11]$$

For a constant acceleration input, the complete solution for $E_0(t)$ is given by

$$E_0(t) = \frac{1}{\gamma}\left[E_i + \frac{T}{\gamma}(\gamma - 1)\dot{E}_i - \frac{T^2}{\gamma^2}(\gamma - 1)\ddot{E}_i\left(1 - \epsilon^{-\frac{\gamma}{T}t}\right)\right] \qquad [12]$$

whereas for a constant velocity input

$$E_0(t) = \frac{1}{\gamma}\left[E_i + \frac{T}{\gamma}(\gamma - 1)\dot{E}_i\left(1 - \epsilon^{-\frac{\gamma}{T}t}\right)\right] \qquad [13]$$

The input to the lead circuit is proportional to the vehicle attitude (provided the amplifier is not saturated), that is

$$E_i = K\theta$$

Equations [12 and 13], therefore, may be rewritten in terms of θ, i.e.

$$\frac{\gamma E_0(t)}{K} = \pm\theta_D = \theta + \frac{T}{\gamma}(\gamma - 1)\dot{\theta} - \frac{T^2}{\gamma^2}(\gamma - 1)\ddot{\theta}\left(1 - \epsilon^{-\frac{\gamma}{T}t}\right) \qquad [12a]$$

and

$$\frac{\gamma E_0(t)}{K} = \pm\theta_P = \theta + \frac{T}{\gamma}(\gamma - 1)\dot{\theta}\left(1 - \epsilon^{-\frac{\gamma}{T}t}\right) \qquad [13a]$$

where

θ_D = value of θ corresponding to the relay drop-out point in the uncompensated system

θ_P = value of θ corresponding to the relay pull-in point in the uncompensated system

Equations [12a and 13a] determine, respectively, actual relay drop-out and pull-in boundaries on either side of the zero displacement axis.

In nondimensional form, Equations [12a and 13a] are

$$\pm\Omega_D = \Omega + \frac{T}{\gamma}(\gamma - 1)\dot{\Omega} - \frac{T^2}{\gamma^2}(\gamma - 1)\ddot{\Omega}\left(1 - \epsilon^{-\frac{\gamma}{T}\tau_{db}}\right) \quad [14]$$

and

$$\pm\Omega_P = \Omega + \frac{T}{\gamma}(\gamma - 1)\dot{\Omega}\left(1 - \epsilon^{-\frac{\gamma}{T}\tau_{db}}\right) \quad [15]$$

For most practical applications, however, the exponential (transient) terms, as will be shown, may be neglected. When this is possible, the steady-state relay drop-out and pull-in boundaries become straight lines.

Then

$$\pm\Omega_D = \Omega + m\dot{\Omega} - mc\ddot{\Omega} \quad [16]$$

and

$$\pm\Omega_P = \Omega + m\dot{\Omega} \quad [17]$$

where

$$m = \frac{T}{\gamma}(\gamma - 1)$$

and

$$c = \frac{T}{\gamma}$$

The validity of the above assumption becomes apparent when the time interval τ between successive relay pull-in and drop-out or drop-out and pull-in points on the phase plane trajectory is considered to be large compared to the time constant c of the second break point of the lead circuit. In this paper, the effect of the transient terms will be neglected. However, if found necessary, the required correction to the steady-state pull-in and drop-out boundaries to account for the transient terms may be obtained by graphical methods developed by the author.

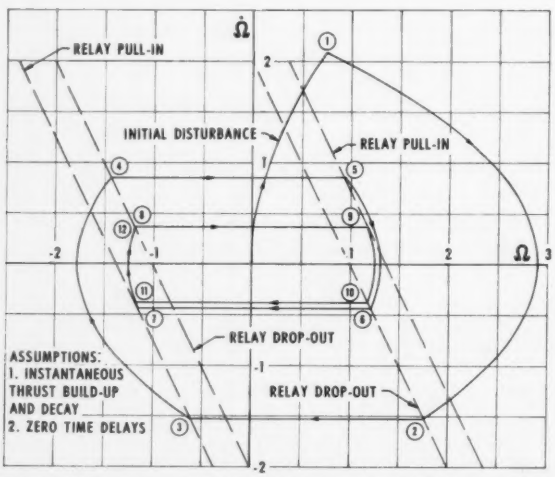

Fig. 3 Phase plane pitch trajectory of a lead-stabilized vehicle for an initial angular impulse (steady-state limit cycle period: 14.2 sec)

If thrust buildup and decay would be instantaneous and system time delays zero, then the intersections between the constant acceleration or velocity trajectory and the corresponding steady-state relay drop-out and pull-in lines would completely determine the system limit cycle. Fig. 3 shows a complete phase plane trajectory, defining the attitude and attitude rate of a hypothetical vehicle as a result of an initial angular disturbance impulse. The stabilizing effect of the lead circuit is clearly indicated. Steady-state operation is reached when successive trajectories fall on top of each other. The steady-state limit cycle trajectory is defined by the points 8, 9, 10, 11 and 12.

The analysis method, outlined above, has assumed instantaneous thrust build-up and decay and also zero system time delays. However, generally, these are not valid assumptions as will be shown.

Actual thrust build-up and decay characteristics of typical motors were determined by means of ground and flight tests on the Viking program in the early 1950's. They indicated the thrust buildup and decay essentially to be of exponential nature. After relay closure, when the system enters into its "on" phase, the vehicle dynamics, therefore, can be described by

$$\ddot{\theta} = c(1 - \epsilon^{-t/T_0}) \quad [18]$$

If the initial conditions at time $t = t_0$ (where t_0 corresponds to time of relay closure) are assumed to be $\theta = \theta(0)$, and $\dot{\theta} = 0$ at any other time t

$$\dot{\theta} = \alpha[t - T_0(1 - \epsilon^{-t/T_0})] \quad [19]$$

and

$$\theta = \theta(0) + \alpha\left[\frac{t^2}{2} + T_0^2(1 - \epsilon^{-t/T_0}) - T_0 t\right] \quad [20]$$

Inspection of Equations [19 and 20] shows that time t cannot any longer be eliminated from the equation for θ, as had been done previously (see Eq. [4]).

Similarly, after opening of the relay armature, when the system enters into its "off" phase, the vehicle dynamics are described by

$$\dot{\theta} = \dot{\theta}(0) - \alpha T_0(1 - \epsilon^{-t/T_0}) \quad [21]$$

assuming the thrust build-up and decay time constants to be identical.

Phase plane analyses of systems whose dynamics explicitly contain time t are difficult and laborious. However, a considerable reduction in analysis effort may be accomplished when it is assumed that the exponential thrust build-up and decay characteristics can be represented by simple time delays equal in length to the time constant T_0. This assumption is reasonable, since it is based on the equivalence of total impulse and the low frequency power spectrum distribution of the actual and assumed thrust characteristics.

By experiment, system designs based on phase plane analyses with assumed simple time delay thrust characteristics have been found to be conservative as far as actual fuel consumption and damping is concerned. Experimental data show that full thrust is generally not attained during steady-state operation; that is, relay drop-out and, as a consequence, fuel flow stoppage occur prior to achievement of full thrust. Actual fuel consumption, therefore, is somewhat less than predicted by the phase plane analysis method.

Experiments have also shown that there may be periods when simultaneous operation of opposing thrust motors could occur as a result of the exponential nature of the thrust buildup and decay. This results in a reduction of attitude rate; hence, transients are damped out somewhat faster than predicted by the phase plane analysis method.

The phase plane analyses must also consider the effect of system time delays. The more significant ones include those resulting from relay armature motion prior to actual relay

pull-in or drop-out. All of these time delays may be included in an equivalent time delay T_M.

Then, the total system time delay becomes

$$T_D = T_0 + T_M \qquad [22]$$

or, in nondimensional form

$$\tau_D = \tau_0 + \tau_M \qquad [23]$$

Equations [16 and 17] which defined the steady-state relay drop-out and pull-in lines respectively, can now be replaced by thrust-off and thrust-on lines, i.e.

$$\pm \Omega_D = \Omega + (m - \tau_D)\dot{\Omega} - \left[m(c + \tau_D) - \frac{\tau_D^2}{2}\right]\ddot{\Omega} \qquad [24]$$

and

$$\pm \Omega_P = \Omega + (m - \tau_D)\dot{\Omega} \qquad [25]$$

It is obvious that the thrust-on and thrust-off lines have a different slope than the relay pull-in and drop-out lines.

Fig. 4 shows a complete phase plane trajectory determined with the aid of thrust-off and thrust-on lines and with an assumed total system time delay of $\frac{1}{10}$ sec. The vehicle and lead circuit configuration as well as the initial conditions are identical to those used for the construction of Fig. 3 which demonstrated the use of relay pull-in and drop-out lines.

Selection of Lead Network Parameters

It has been shown that a stable limit cycle can be achieved by the insertion of a lead network into the control system. It is then quite apparent that the limit cycle characteristics strongly depend on the lead circuit parameters. On the other hand, total fuel consumption is a direct function of the limit cycle frequency and the thrust-on time per limit cycle. Therefore, to minimize fuel consumption, the limit cycle period should be as long as possible and the thrust-on time per limit cycle should be as short as possible.

It can be easily shown that the nondimensional thrust-on time per cycle τ_{on} is given by

$$\tau_{on} = 4\,|\Omega_J| \qquad [26]$$

where Ω_J = maximum positive or negative angular velocity during limit cycle operation (nondimensional).

Similarly, the nondimensional thrust-off time per cycle τ_{off} is given by

$$\tau_{off} = 4\left|\frac{\Omega_J}{\dot{\Omega}_J}\right| \qquad [27]$$

where Ω_J = angular displacement at end of each constant velocity portion of limit cycle (nondimensional).

In the right-hand side of the phase plane plot

$$\Omega_J = \frac{\Omega_P + (\Omega_D - m(c + \tau_D) + (\tau_D^2/2)}{2} \qquad [28]$$

and the maximum positive angular velocity during limit cycle operation is given by

$$\dot{\Omega}_J = \frac{\Omega_P - (\Omega_D + m(c + \tau_D) - (\tau_D^2/2)}{2(m - \tau_D)} \qquad [29]$$

But Ω_D may be expressed as a percentage of Ω_P. (This is true because Ω_D is a direct function of relay hysteresis and Ω_P.)

Therefore

$$r = \frac{\Omega_D}{\Omega_P} \qquad [30]$$

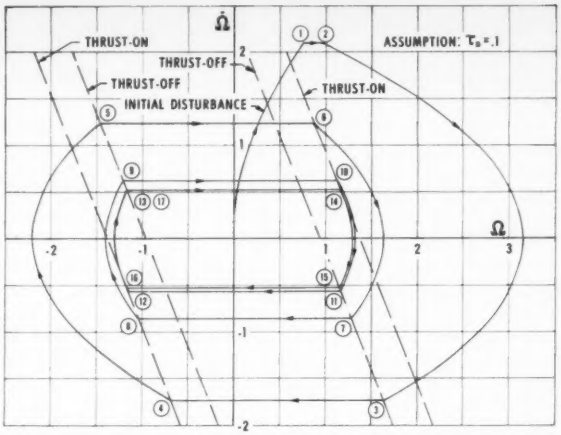

Fig. 4 Phase plane pitch trajectory of a lead-stabilized vehicle for an initial angular impulse (steady-state limit cycle period: 11.05 sec)

Then

$$\tau_{on} = 2\left[\frac{m(c + \tau_D) - (\tau_D^2/2)}{m - \tau_D}\right]\left[\frac{(\Omega_P(1 - r)}{m(c + \tau_D) - (\tau_D^2/2)} + 1\right] \qquad [31]$$

and

$$\tau_{off} = 4(m - \tau_D)\,\frac{\left[\dfrac{\Omega_P(1 + r)}{m(c + \tau_D) - (\tau_D^2/2)} - 1\right]}{\left[\dfrac{\Omega_P(1 - r)}{m(c + \tau_D) - (\tau_D^2/2)} + 1\right]} \qquad [32]$$

or, by letting

$$\left[m(c + \tau_D) - \frac{\tau_D^2}{2}\right] = f(m, c, \tau_D) = f$$

and

$$(m - \tau_D) = g(m, \tau_D) = g$$

$$\tau_{on} = 2\left(\frac{f}{g}\right)\left[\frac{\Omega_P(1 - r)}{f} + 1\right] \qquad [31a]$$

and

$$\tau_{off} = 4g\,\frac{\left[\dfrac{\Omega_P(1 + r)}{f} - 1\right]}{\left[\dfrac{\Omega_P(1 - r)}{f} + 1\right]} \qquad [32a]$$

Also

$$\frac{\tau_{on}}{\tau_{off}} = \frac{f}{2g^2}\,\frac{\left[\dfrac{\Omega_P(1 - r)}{f} + 1\right]^2}{\left[\dfrac{\Omega_P(1 + r)}{f} - 1\right]} \qquad [33]$$

Figs. 5, 6 and 7 show the significance of Equations [32a] and [33].

Inspection of Figs. 5 and 7 indicates that the ratio of τ_{on} to τ_{off} may be minimized (except for r equal to unity, i.e., zero relay hysteresis) by proper selection of lead circuit parameters. This minimum is given by

$$\left(\frac{\tau_{on}}{\tau_{off}}\right)_{min} = \frac{4\Omega_P(1 - r)^2}{[(T/\gamma)(\gamma - 1) - \tau_D]^2(1 + r)(3 - r)} \qquad [34]$$

Generally, Ω_P, r, and τ_D are known. In most cases, there is also an upper limit on the value of γ, the lead circuit attenuation factor, because of signal-to-noise ratio considerations in the design of electronic hardware. In a typical design, the maximum value of γ is usually taken to be equal to 10.

By use of the graphs or of Equation [34], it is therefore possible to minimize fuel consumption by selection of an optimum value for the lead circuit time constant T. Or, for a given set of system parameters, the limit cycle characteristics may be obtained directly without the plotting of phase plane trajectories or the use of other techniques.

Appendix Time Measurements Along a Constant Acceleration Path on a Phase Plane Plot

The equation of the parabolic phase plane trajectory determines the dimensionless time τ required to move from one point $(\dot{\Omega}_1, \Omega_1)$ to another $(\Omega_2, \dot{\Omega}_2)$.

The equation of the parabolic path is given by Equations [9a and 9b] or

$$\Omega - \Omega(0) = \pm \frac{1}{2}\left(\frac{d\Omega}{d\tau}\right)^2 \qquad [A\text{-}1]$$

Therefore, when the acceleration is negative

$$\frac{d\tau}{d\Omega} = \frac{1}{\sqrt{2[\Omega(0) - \Omega]}} \qquad [A\text{-}2]$$

or when the acceleration is positive

$$\frac{d\tau}{d\Omega} = \frac{1}{\sqrt{2[\Omega - \Omega(0)]}} \qquad [A\text{-}3]$$

Since the quantities under the radical signs in Equations [A-2 and A-3] are always positive, the time τ to go from $\Omega(0)$ to another point, $(\Omega_1, \dot{\Omega}_1)$, may be written as

$$\tau = \frac{1}{\sqrt{2}} \int_{\Omega(0)}^{\Omega_1} \frac{d\Omega}{\sqrt{|\Omega - \Omega(0)|}}$$

or

$$\tau_{\Omega(0)\to\Omega_1} = \sqrt{2}\left[\sqrt{|\Omega - \Omega(0)|}\right] \qquad [A\text{-}4]$$

But $|\Omega - \Omega(0)|$ is equal to $\dot{\Omega}^2/2$. Therefore

$$\tau_{\Omega(0)\to\Omega_1} = |\dot{\Omega}_1| \qquad [A\text{-}5]$$

Since the time τ required to move from $(\Omega_1, \dot{\Omega}_1)$ to $(\Omega_2, \dot{\Omega}_2)$ must be positive and is equal to the difference in time to go from $\Omega(0)$ to the points in question

$$\tau_{\Omega_1\to\Omega_2} = |\dot{\Omega}_1 - \dot{\Omega}_2| = |\Delta\dot{\Omega}| \qquad [A\text{-}6]$$

Also, since

$$\tau = \frac{t}{t_b} = \frac{t}{1} \qquad (t_b = 1 \text{ sec})$$

$$t_{\Omega_1\to\Omega_2} = |\Delta\dot{\Omega}| \qquad \text{(sec)} \qquad [A\text{-}7]$$

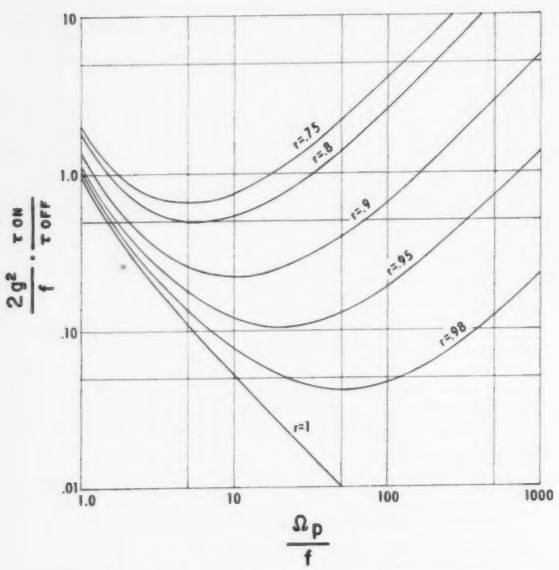

Fig. 5 τ_{on}/τ_{off} as a function of circuit parameters

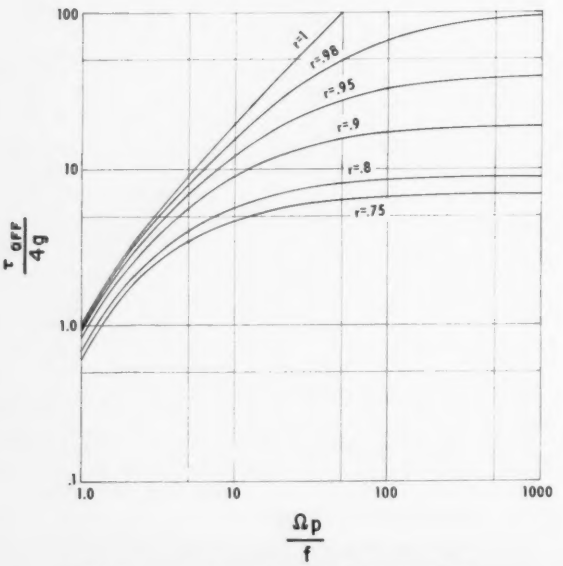

Fig. 6 τ_{off} as a function of circuit parameters

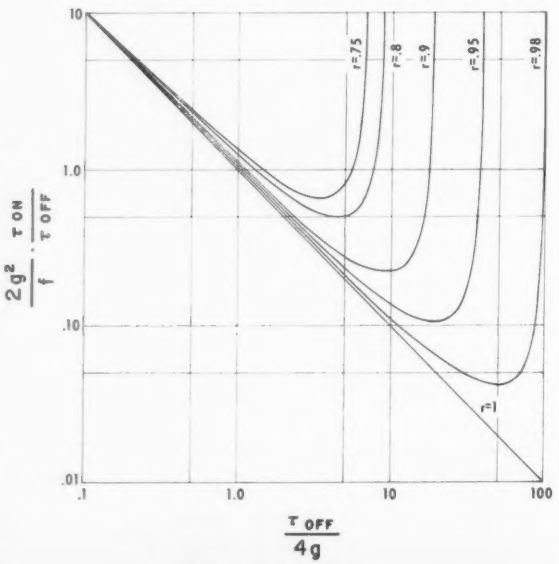

Fig. 7 τ_{on}/τ_{off} vs. τ_{off}

Acknowledgment

The author wishes to thank J. C. Goodwyn, Chief Engineer, Systems Analysis Section, The Martin Company for encouragement to write this paper. It should also be noted that due to the efforts of Mr. Goodwyn, phase plane techniques were used in the analysis of the Viking coasting flight control system as early as 1952.

Nomenclature

θ	= pitch attitude error, rad
$\dot{\theta}, \ddot{\theta}$	= first and second time derivatives of θ, respectively
$\theta(0), \dot{\theta}(0)$	= initial pitch attitude and rate, respectively
α	= Fl/I, angular acceleration about the pitch axis, rad/sec^2
F	= applied control (correcting) force, lb
l	= moment arm, ft
I	= pitch moment of inertia, slug-ft^2
t	= time, sec
t_0	= time of relay pull-in or drop-out
t_b	= 1, time base, sec
τ	= t/t_b, nondimensional time scale
Ω	= nondimensional angular displacement; nondimensional form of θ
$\dot{\Omega}, \ddot{\Omega}$	= nondimensional angular velocity and acceleration, respectively
$\Omega(0)$	= nondimensional form of $\theta(0)$; vertex of phase plane parabola or Ω-axis intercept
$\dot{\Omega}(0)$	= nondimensional form of $\dot{\theta}(0)$
s	= Laplace operator
$E_0(t)$	= lead circuit output
$E_0(s)$	= Laplace transform of $E_0(t)$
E_i	= lead circuit input
$E_i(s)$	= Laplace transform of E_i
T	= time constant of first break point of lead circuit, sec
γ	= lead network attenuation factor, nondimensional
$\dot{E}_i, \ddot{E}_i$	= first and second time derivatives of E_i, respectively
K	= proportionality constant
θ_D	= value of θ corresponding to relay drop-out point in the uncompensated system, rad
θ_P	= value of θ corresponding to relay pull-in point in the uncompensated system, rad
Ω_D	= nondimensional form of θ_D
Ω_P	= nondimensional form of θ_P
c	= T/γ, time constant of second break point of lead circuit, sec
m	= $(T/\gamma)(\gamma - 1)$
T_0	= thrust buildup and decay time constant, sec
T_D	= total system time delay, sec
T_M	= equivalent system time delay due to other causes than thrust buildup or decay, sec
τ_D	= nondimensional form of T_D
τ_M	= nondimensional form of T_M
τ_{on}	= total thrust-on time during each limit cycle, nondimensional
$\dot{\Omega}_J$	= maximum positive or negative angular velocity during limit cycle operation, nondimensional
τ_{off}	= total thrust-off time during each limit cycle, nondimensional
Ω_J	= angular displacement at end of each constant velocity portion of limit cycle, nondimensional
r	= relay hysteresis coefficient $= (\theta_D/\theta_P) = (\Omega_D/\Omega_P)$
f	= $m(c + \tau_D) - (\tau_D^2/2)$
g	= $m - \tau_D$

References

1 Kochenburger, R. J., "A Frequency Response Method for Analyzing and Synthesizing Contactor Servomechanisms," *Trans. AIEE*, vol. 69, 1950, part I, pp. 270–284.

2 Andronow, A. A. and Chaikin, C. E., "Theory of Oscillation," Princeton University Press, Princeton, 1949.

ARS CONTROLLABLE SATELLITES CONFERENCE

April 30 - May 1, 1959

MASSACHUSETTS INSTITUTE OF TECHNOLOGY

Cambridge, Mass.

GUIDANCE AND CONTROL — ELECTRICAL PROPULSION

VEHICLE DESIGN AND RECOVERY — EXTERNAL ENVIRONMENT

PHYSICS OF THE ATMOSPHERE

On the Use of Ionization Gage Devices at Very High Altitude[1]

N. W. SPENCER[2]
R. L. BOGGESS[3]
University of Michigan
Ann Arbor, Mich.

H. E. LAGOW[4]
R. HOROWITZ[5]
National Aeronautics and Space Administration
Washington, D. C.

The use of ionization gages and omegatrons in rockets and satellites at very high altitudes is considered. Appropriate instrumentation employing these devices is believed to offer good possibilities for the measurement of atmospheric pressure, temperature, density and composition.

THE MEASUREMENT of atmospheric pressure, temperature and density, in regions of the high atmosphere where the mean free path of typical particles is long compared with the dimensions of the instrument, has interested upper-air researchers for many years. Early attempts (1 to 4)[6] using V-2 rockets were largely inconclusive because of instrument contamination by rocket gas or because the altitudes attained were insufficient. Some significant measurements to 120 km were made, but could not be considered as entirely fulfilling desired conditions of a long mean free path environment. No further significant measurements were made until the Viking rocket, and still later the Aerobee-Hi rocket, became available (5 to 9).

The methods employed in these measurements have made use of local density determining devices which permit investigation of the pressure or density at selected points on the surface of a rocket. This allows interpretation in terms of ambient conditions, provided there is knowledge of rocket velocity, altitude, air composition and other such factors.

Advances in instrumentation, the availability of rockets with an increased capability for high altitudes, and the imminent availability of satellite vehicles have stirred a compelling new interest in these measurement areas.

Thus this paper considers the employment of ionization-type devices for performing measurements of ambient pressure, temperature, density and in addition, composition, in the light of the newer developments.

Measurements With a Single Ionization Gage

Each gas in a mixture of gases exerts a partial pressure upon the walls of the confining vessel in proportion to the gas concentration. Since pressure is defined in terms of the rate of momentum transfer, these partial pressures are also determined by the mass, velocity and, hence, temperature of the various constituents.

The presence of particles of different mass implies a velocity spectrum and thus suggests that some form of mass spectrometry approach is applicable to the measurement of structural parameters at altitudes where the mean free paths of various particles are large in comparison with the dimensions of an intruding object.

Consider a body moving in space at velocities comparable to the random molecular speeds of the constituent gases. Assume also that the body's velocity and orientation are known. If an orifice to a body-borne chamber is exposed to the outside, an interchange of particles will take place in a manner that is dependent upon the particle velocity distribution function, the body velocity, its orientation, the characteristic temperature, the composition and other effects.

If the body velocity V_c is reduced to zero, then the interchange will be altered only in degree. The relationship between the internal and external pressure will be governed by the thermal transpiration effect as investigated by Maxwell (10), Reynolds (11) and Knudsen (12). If the body velocity is not zero, then the pressure relationship is less easily stated, but readily so upon assumption of a velocity distribution function. Many experimenters (7,13,14,15) have derived a relation which is seen to be the transpiration equation modified by a factor dependent upon the ratio of body to particle velocity. Thus

$$\frac{P_i}{P_o} = \sqrt{\frac{T_i}{T_o}}\,[e^{-s^2} + s\sqrt{\pi}\ (1 - erf\ s)] \qquad [1]$$

where

$f(s)$ = $e^{-s^2} + s\sqrt{\pi}\ (1 - erf\ s)$
P_i = internal pressure
P_o = ambient pressure
T_i = internal temperature
T_o = external temperature
s = V_x/V_g,
component of body velocity normal to gage opening / most probable particle velocity

P_i was defined only as the pressure in the chamber, implying total pressure. It can be considered as the sum of the partial

Received Oct. 8, 1958.

[1] This paper has been written in large part as a result of research carried out by members of the Space Physics Research Laboratory of the Department of Electrical Engineering of The University of Michigan. The research was conducted under contract with the Geophysics Research Directorate of the Air Force Cambridge Research Center, administered by The University of Michigan Research Institute. Research of a similar nature conducted by members of the Planetary Atmosphere Branch of NASA, formerly of the Naval Research Laboratory, also contributed to the conclusions reported herein.

[2] Lecturer, Department of Electrical Engineering; Head, Space Physics Research Laboratory, Department of Electrical Engineering. Member ARS.

[3] Project Engineer, Space Physics Research Laboratory, Department of Electrical Engineering. Member ARS.

[4] Head, Planetary Atmospheres Branch, Space Services Division. Member ARS.

[5] Head, Aerometric Section, Planetary Atmospheres Branch.

[6] Numbers in parentheses indicate References at end of paper.

pressures of the component gases; thus

$$P_i = p(N_2) + p(N) + p(O_2) + p(O) + p(A) + p(H_2) + p(H) + p(He) + \ldots \quad [2]$$

considering some of the possibilities, including dissociation. Similarly, P_o may be considered as the sum of the external partial pressures, and accordingly an equation like [1] can be written for each component.

Since

$$V_g = \sqrt{\frac{2kT_o}{m_o}} \quad [3]$$

where

k = gas constant per molecule, 1.381×10^{-16} erg per deg K
T = temperature, K
m_o = mass per particle, gm

an $f(s)$ exists for each component. Thus, the internal partial pressure ratios will differ from the external ratios, the difference being a function of the body velocity component normal to the chamber opening.

Thermal equilibrium among gas particles can be assumed externally (16) as well as internally with small error. Internally, however, it is assumed that the particle temperatures will be set by the wall temperature, adopting a unity accommodation coefficient.[7] A Maxwellian velocity distribution in the region being sampled follows the equilibrium assumption.

These considerations suggest the possibility of composition measurement by observation of the change in pressure in a chamber as a function of V_z, the body velocity component normal to the chamber opening. As the relative velocity increases (or decreases), the total pressure will, in principle at least, increase (or decrease) gas by gas, so to speak, as required by the above considerations. The rate of change will be governed by the distribution function as well as by the normal acceleration component which presumably can be known. The maximum relative velocity must appreciably exceed the velocity of most of the particles to make this measurement possible. Expected relative values of the most probable external particle velocity corresponding to the various components are readily determined upon assumption of external temperature and temperature equilibrium. Typical values are presented in Table 1, which has been computed from Equation [3] for three temperatures. Since m can vary relatively from 1 (atomic hydrogen) to as much as perhaps 40 (argon), V_g can have a range of about 6.5 to 1 for a given temperature. For purposes of evaluating the feasibility of the experimental approach, the minimum expected particle velocity can be taken as 1300 fps (argon at approximately 400 K), and the maximum as 15,000 fps (hydrogen atom at 1200 K) for any particle except the electron. Considering both rockets and satellites as possible research vehicles, satellite velocities are adequate for all particles, whereas rocket velocities of present upper-air experimentation vehicles are adequate only for the more massive particles. Thus, in general, this procedure is discussed from the point of view of an orbiting vehicle.

[7] See (15) for discussion of exceptions to this assumption.

Consider application to a satellite, where the velocity may be taken as 26,000 fps. Thus, if the chamber opening is opposite to the direction of motion, only a few of the least massive components, as determined by the distribution function, could enter. On the other hand, if the opening is oriented in the forward direction, then all particles can be overtaken, again excepting a few of the lighter components. It follows that particular intermediate positions enable partial collection of the heavier atoms.

In the expected situation of rotation that would cyclically orient the opening in the direction of motion and then opposite to the direction of motion, velocity "scanning" would occur. The measured total pressure would, in principle, vary in accordance with the concentration of the various constituents and their associated velocities, thus offering the possibility of a particle velocity measurement.

The s function (Fig. 1) effect upon the internal partial pressure of a gas as compared with the external pressure is to reduce the internal pressure to zero as s approaches -1 or to increase the internal pressure significantly as s assumes larger positive values. Since s is greater for the more massive particles, contributions to total pressure from N_2, N, O_2 and O can, under high velocity conditions, tend to overwhelm the lighter and less plentiful components out of proportion to their ambient composition stature. For negative velocities, the effect is opposite, possibly enabling detection of the lighter components. This is illustrated in Fig. 2, which shows the ratios of internal to external partial pressures of nitrogen and hydrogen as functions of the angle of attack which is a measure of the normal velocity component. The curves are valid only for equal concentrations of the gases, a condition assumed for the sake of illustration. Some of the following data were used in computing the curves:

Altitude: 300 km
Pressure: 2.0×10^{-8} mb
Density: 5×10^{-12} kg/m^3
Temperature: 1000 K
Body velocity: 26,000 fps
Rotation: 1 rps with rotational axis perpendicular to plane of orbit
Internal temperature: 300 K
Most probable velocity:
atomic nitrogen at 1000 K = 3.56×10^3 fps
atomic hydrogen at 1000 K = 1.33×10^4 fps

Table 1 Most probable velocity of various atmospheric components as a function of the kinetic temperature

Component	300 K		600 K		1200 K	
	cm/sec	fps	cm/sec	fps	cm/sec	fps
air	4.17×10^4	1.36×10^3	5.9×10^4	1.93×10^3	8.34×10^4	2.75×10^3
N_2	4.2	1.38	5.95	1.95	8.4	2.77
N	5.95	1.95	8.4	2.77	11.9	3.9
O_2	3.95	1.3	5.58	1.83	8.0	2.62
O	5.56	1.82	7.9	2.6	1.11×10^5	3.65
He	1.12×10^5	3.7	1.58×10^5	5.2	2.24	7.39
H	2.23	7.3	3.15	1.04×10^4	4.46	1.47×10^4
H_2	1.58	5.2	2.23	7.3×10^3	3.01	9.9
A	3.52×10^4	1.16	5.0×10^4	1.65	7.04×10^4	2.3
e	5.18×10^7	1.7×10^6	7.3×10^7	2.4×10^6	1.03×10^8	3.4×10^6

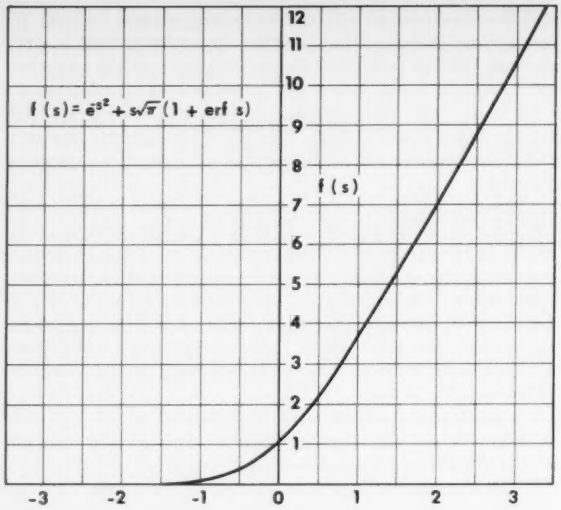

Fig. 1 Curve of $f(s)$ vs. s

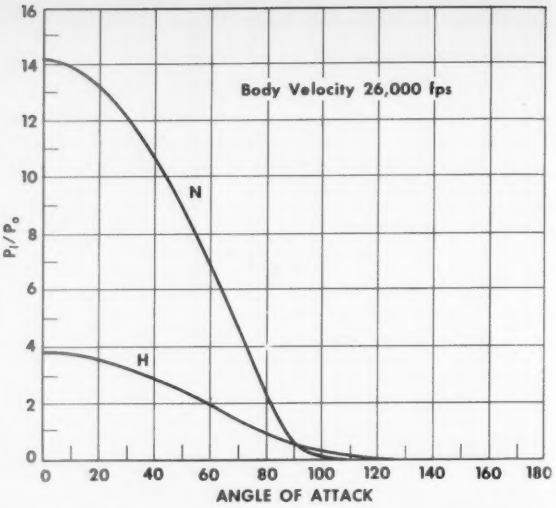

Fig. 2 Ratio of external to internal pressure for nitrogen and hydrogen as a function of angle of attack

Because the chamber wall temperature is likely to be substantially less than the external temperatures, the internal pressures can be less by as much as a factor of 2. However, the reduction will take place for all components and thus has a bearing on sensor sensitivity considerations rather than on relative partial pressures.

Although velocity scanning occurs as a result of rotational motion and in principle enables differentiation between the various component gases, as a practical matter there is a considerable overlap of the distribution functions primarily because the region is populated with gases of comparable mass. As a consequence, it is probably not possible to determine relative concentration by this method. It may be feasible, however, to determine the most probable velocity and hence the characteristic temperature. If the assumption of external thermal equilibrium is valid, or nearly so, the characteristic temperatures of the various gases should be the same. Thus determination of the most probable velocity for any component indicates the external temperature. Knowing the temperature, it is then possible to return to Equation [1] and compute the external pressure.

Summarizing, a pressure (or density) measuring device, such as an ionization gage in a body which is moving at an appropriate and known altitude and velocity, with a prescribed rotational rate, makes pressure and density measurements possible. Preferably, the maximum velocity should exceed, by an adequate margin, say 2:1, the most probable velocity of the lightest component to be measured, thus indicating the need for a vehicle of satellite capabilities, if the lighter gases are to be considered.

With such an arrangement, it appears that it may be feasible to measure the temperature directly, which would enable a check of the directly measured ambient pressure and density.

Ionization Gage Plus Omegatron

The addition of another instrument which permits an additional and independent measurement of the chamber gas offers considerably greater promise of fruitful experimentation. Assuming that a small mass spectrometer-type device is placed within the ionization chamber, so that the same gases measured by the ion gage are measured by the spectrometer. A less than ideal but more practical arrangement in which the spectrometer would be independently mounted within the same sphere is also suitable. An appropriate instrument is the omegatron, a device reported by Sommer, Thomas and Hipple (17) who were concerned primarily with measurements of charge to mass ratio. A version of the device applicable in the sense required here was later developed and reported by Alpert and Buritz (18) who suggested its usefulness as a pressure-measurement tool.[8] A "Diatron" is also suggested.[9]

The addition of such a device, which appears quite feasible, would enable determination of (a) the composition, (b) the shape of the distribution function and (c) the relative concentration of the constituent gases, provided the associated sensor had adequate sensitivity to detect the less plentiful gases. Thus, the "total" pressure determined by the ion gage could be resolved in terms of the various partial pressures.

Considering Equation [1] in partial pressure form

$$P_{ai} = P_{ao}\sqrt{\frac{T_i}{T_o}}\,f(s) \qquad [4]$$

where

$$f(s) = e^{-s^2} + s\sqrt{\pi}\,(1 + erf\ s) \qquad [5]$$

$$s = \frac{V_x}{V_a} \qquad [6]$$

$$V_a = \sqrt{\frac{2kT_o}{m_a}} \qquad [7]$$

P_{ai} = internal partial pressure of gas a
P_{ao} = external partial pressure of gas a

and

$$s = V_x\sqrt{\frac{m_a}{2kT_o}}$$

Substituting in Equation [4]

$$P_{ai} = P_{ao}\sqrt{\frac{T_i}{T_o}}\left[e^{-\left(V_x\sqrt{\frac{m_a}{2kT_o}}\right)^2} + V_x\sqrt{\frac{m_a\pi}{2kT_o}}\left(1 + erf\ V_x\sqrt{\frac{m_a}{2kT_o}}\right)\right] \qquad [8]$$

[8] Possible usefulness at high altitudes was suggested by H. S. Sicinski.

[9] Consolidated Electrodynamics Corp.

This is the general form for any value of V_x and hence any value of s. In simplification, as

$$s \rightarrow 2, \qquad erf \rightarrow 1$$

and

$$f(s) \cong 3.55 V_x \sqrt{\frac{m_a}{2kT_o}}$$

Thus Equation [8] becomes

$$P_{ai} = P_{ao} \sqrt{\frac{T_i}{T_o}} \left(3.55\ V_x \sqrt{\frac{m_a}{2kT_o}} \right) \qquad [9]$$

which, by combining, becomes

$$P_{ai} = 3.55\ V_x \sqrt{\frac{m_a T_i}{2k}} \cdot \frac{P_{ao}}{T_o} \qquad [10]$$

It is considered here that the only unknowns are P_{ao} and T_o, which appear as a ratio. Consequently, since the pressure can also be defined as

$$P_{ao} = n_a k T_o \qquad [11]$$

where n_a = number of particles of gas a, one can substitute

$$n_a k = \frac{P_{ao}}{T_o} \qquad [12]$$

Equation [10] becomes an expression for the number density in space of the gas a as a function of the internal partial pressure, the normal component of the body velocity, and the internal chamber temperature. Thus

$$n_a = \frac{1}{\sqrt{0.58 k m_a T_i}} \cdot \frac{P_{ai}}{V_x} \qquad [13]$$

It follows that the ambient number density of any constituent can be determined from the internal partial pressure. In addition, knowledge of the external temperature, so obtained from a characteristic velocity measurement with an ion gage or similarly with an omegatron, will permit computation of the external partial pressures.

Thus through employment of an ion gage and an omegatron, which admittedly involves redundancy, quantities can be evaluated, including: Pressure, temperature and density of ambient gas; type and concentration of the constituent gases.

Velocity Distribution Function

The preceding comments have been based upon the assumption of a Maxwellian distribution of velocities among the various gas particles. Although there is considerable evidence that this is true or very nearly so (15), it is of course desirable to obtain experimental verification, which the presence of the omegatron, or a similar instrument, makes possible.

Consider again the omegatron in the body whose orientation pattern is such as to bring the chamber opening cyclically into and away from the "stream." Assuming diffusive equilibrium between the chamber and the outside, the internal number density of a particular gas, which is the quantity measured by the omegatron, would vary as a function of the normal velocity component and the distribution function. Since the body velocity is known, determination of the distribution function becomes possible.

A plot of the change in internal number density (or partial pressure) as a function of angle of attack, or normal velocity component, should appear like Fig. 2, provided, of course, that the distribution is Maxwellian. Other distributions would alter the shape and would thus be definable.

Atmospheric Velocity

All previous considerations have assumed that the relative velocity between the body or chamber and the gas was due to (a) that characteristic of the gas and (b) that of the instrument-carrying body itself. Accordingly, the assumption is implied that the atmospheric velocity is negligible. This is not the case, for if one considers that the atmosphere moves with the Earth, the velocity in the equatorial plane at an altitude of 300 km is 1.6×10^3 fps.

This value is clearly significant in comparison with the most probable velocity of certain components (see Table 1). The effective value, insofar as possible measurements are concerned, is of course dependent upon the location of the plane of the orbit, and thus is maximum and nearly constant for passage near the equator and variable in magnitude and direction for polar orbits. In any case it can be considered as a definable perturbation on the body velocity.

Sensor Sensitivity

To employ fruitfully the above mentioned devices, it is of course necessary to arrange a sensor that will ideally have adequate sensitivity and time characteristics so as to permit detection and transmission to the recording device of signals corresponding to the least plentiful components.

The major constituents one expects at the higher altitudes are NO, O_2, O, N_2 and N, in both neutral and ion states. Speculation leads to consideration of hydrogen and helium as well, but in very small quantities. Detection of the various gases is dependent primarily upon their absolute abundance, and upon the sensitivity of the current-measuring instrument employed. Different elements in like concentration effect different responses in an ionization gage. In general, the apparent sensitivity is a function of the total number of electrons possessed by the molecule (19) rather than its ionization potential or atomic weight, and thus the ratio of sensitivities of helium and nitrogen is less than their mass ratio. The overall result, then, insofar as ion gage (or omegatron) sensitivity is concerned, is that the relative concentration is the more powerful factor.

Accordingly, in regard to gage sensitivity (S) to dissociated gases, one would expect the ion current resulting from dissociated or recombined gases to vary with the number of electrons per particle.

Ion gage sensitivities can be considered in terms of the ratio of collected ion current to ionization current at a given density. A typical value for present thermionic gage capability is $S = 100$ μa per microbar for an ionization current of 10 ma. Thus at this pressure each 100 electrons, on the average, emitted by the cathode produces one ion for collection. The density is such that it is unlikely one electron can generate more than one ion pair during transit. Thus the sensitivity factor indicates that an electron has, on the average, one chance in a hundred of producing an ion pair at one microbar of pressure.

Further, as long as the electron has sufficient energy to overcome the particle ionization potential, the energy level for typical thermionically-produced electrons is not of great consequence.

Similar sensitivity factors are appropriate for at least some radioactive ion gages, such as a radioactive ionization gage using a tritium source (20). However, the resulting ion currents are small compared with a thermionic gage, because the number of ionizing source electrons is very small. This factor, a limit imposed by practical considerations in the use of radioactive ionizing sources, in part precludes use of radioactive ion gages at very low densities. An additional factor that limits the usefulness of these devices is a dark current which overwhelms the ion current at densities that are relatively high in relation to this report. The dark current is a manifestation of collector-electron emission resulting from x-ray

emission caused by the high energy radioactive source electrons, ions or nuclei, as the case may be.

Phillips cold-cathode ionization gages are not useful at pressures less than 10^{-6} to 10^{-7} mb Hg for the reason that the gaseous conduction which underlies their operation cannot be sustained at the lower density values. Thus the thermionic ionization gage appears to be the only useful type at pressures to be encountered at very high altitudes.

At 300 km, and with an assumed pressure of 2×10^{-6} mb, the ion current, assuming ground air composition, can be determined from

$$i = 10^{-3} SP \qquad [14]$$

where

i = amp
S = sensitivity in μa per microbar
P = pressure in millibars

Thus, for this example one should expect

$$i = 100 \times 2 \times 10^{-6} \times 10^{-3}$$
$$= 2 \times 10^{-9} \text{ amp}$$

Currents of this magnitude do not pose difficult problems for instrumentation design, for currents as low as 10^{-12} amp are presently being successfully measured in upper atmosphere research program experiments.

The measurement of the ion current produced by an omegatron poses a somewhat more difficult problem. Although omegatron and ion gage sensitivities are comparable, the use of a relatively small ionizing beam, rather than the gross emission from a relatively long filament, as employed in ion gages, results in greatly reduced ion current. Generally speaking, the extent to which the beam current and resulting beam size may be increased is limited because of the difficulty of extracting the innermost ions from the beam. Excessive space charge is also a problem.

In addition to straightforward ion-current measurement, there are at least two other ways in which the low level output signal of the omegatron can be satisfactorily utilized. One of these involves use of an electron multiplier at the collector which can provide considerable amplification of the desired signal. The other method, also promising, involves detection of the resonant ions by measurement of the energy absorbed from the applied RF field (21).

Accordingly, because of these and other sensitive detecting devices certain to be developed, it is reasonable to conclude that the thermionic ion gage and the omegatron have adequate sensitive for use in measurements of the type discussed in this paper.

Difficulties To Be Anticipated in Use of Thermionic Ion Gages and Small Spectrometers

The problem of measuring very low pressures at very high altitudes is not different in principle from performing the measurements in the laboratory, with the major exception of unattended operation. Thus perturbations caused by outgassing of gage elements and the vehicle, pumping action by gage cathode, adsorption and absorption by gage elements, etc., must be considered. As the surfaces of the carrier become heated by solar radiation, they will produce quantities of gas which can perturb the measurement. Similarly, as they cool, gas will be sorbed. Data presented by Russian experimenters as measured on Sputnik III are of interest in this regard. At a recent conference[10] it was stated that the minimum pressure measured the first day in orbit was 10^{-7} mm Hg, the second day, 10^{-8} mm and the third, 10^{-9} mm.

The hot cathode of an ion gage or omegatron is a major offender in regard to absorption and particularly in regard to chemical reactions with the gas being measured. Thus steps to reduce cathode temperature and perhaps "on time" would be desirable from this standpoint. Specifically, it appears desirable to employ oxide-coated rather than pure tungsten cathodes to enable lower temperatures and to conserve power. The potential assumed by the vehicle can likewise conceivably cause perturbations upon the assumed environment. Some studies bearing on this problem are being made at present in connection with the application of Langmuir probe techniques to the measurement of various ionosphere characteristics.

[10] CSAGI, Moscow, Aug. 1958.

Concluding Remarks

This paper has presented a brief discussion of a measurement technique which seems to the authors to offer reasonable assurance of satisfactory measurements of pressure, temperature, density and composition at very high altitudes. Considerable development work leading first to use in vertical rocket soundings will of course be necessary prior to satellite use; however, the apparent promise of significant data will provide sufficient incentive for the development effort required.

References

1 Dow, W. G., and Reifman, A., "Technical Report on the Measurement of Temperature and Pressure in the Ionosphere," Univ. of Mich., Eng. Res. Inst. Report, Ann Arbor, July 1946.

2 Havens, R. J., Koll, R. T. and La Gow, H. E., "Pressures and Temperatures in the Earth's Upper Atmosphere," NRL Report, March 1950.

3 Best, N. R., Durand, E., Gale, D. I. and Havens, R. J., "Pressure and Temperature Measurements in the Upper Atmosphere," *Phys. Rev.*, vol. 70, 1946, p. 985.

4 Best, N. R., Havens, R. J. and La Gow, H. E., "Pressure and Temperature of the Atmosphere to 120 km," *Phys. Rev.*, vol. 71, 1947, pp. 915–916.

5 Havens, R. J., Koll, R. T. and La Gow, H. E., "Temperature of the Earth's Upper Atmosphere to 160 km," *J. Geophys. Res.*, vol. 57, March 1952, pp. 59–72.

6 Havens, R. J. and Berg, O., "Density of the Earth's Atmosphere at 219 km," *Trans. Amer. Geophys. Union*, vol. 33, 1952, p. 316.

7 Horowitz, R. and La Gow, H. E., "Upper Air Pressure and Density Measurements from 90 to 220 km with the Viking 7 Rocket," *J. Geophys. Res.*, vol. 62, March 1957, pp. 57–77.

8 La Gow, H. E., Horowitz, R. and Ainsworth, J., "Rocket Measurements of the Arctic Upper Atmosphere," *Annales de Geophysique*, vol. 14, April-June 1958, pp. 131–139.

9 Horowitz, R. and La Gow, H. E., "Summer Day Auroral Zone Atmospheric Structure Measurements from 100 to 210 Kilometers on an IGY Rocket," *J. Geophys. Res.*, Dec. 1958.

10 Maxwell, J. C., scientific papers.

11 Reynolds, O., "On Certain Dimensional Properties of Matter in the Gaseous State," *Trans. Phil. Soc.*, vol. 170, 1879, pp. 727–845.

12 Knudsen, M., "Ein absolutes Manometer," *Annalen Physik*, vol. 32, 1910, pp. 809–842.

13 Schultz, F. V., Spencer, N. W. and Reifman, A., "Atmospheric Pressure and Temperature Measurements Between the Altitudes of 40 and 110 km," Univ. of Mich., Eng. Res. Inst. Report no. 2, Ann Arbor, July 1948.

14 Horowitz, R. and Kleitman, D., "A Method for Determining Density in the Upper Atmosphere During Rocket Flight," NRL Report 4246, Oct. 1953.

15 Danilin, B. S., Mikhnevich, V. V., Repnev, A. I. and Shvidkovskii, E. G., "The Problem of Pressure and Density Measurements in the Upper Atmospheric Layers by Means of an Artificial Earth Satellite," in "The Russian Literature of Satellites, Part II," International Physical Index, Inc., New York, 1958, pp. 95–117.

16 Gerson, N. C., "Crtical Survey of Ionospheric Temperatures," *Reports on Progress in Physics*, vol. 14, 1951, pp. 316–365.

17 Sommer, H., Thomas, H. A. and Hipple, J. A., "The Measurement of e/m by Cyclotron Resonance," *Phys. Rev.*, vol. 82, June 1951, p. 697.

18 Alpert, D. and Buritz, R. S., "Ultra High Vacuum II. Limiting Factors in the Attainment of Very Low Pressures," *J. Appl. Phys.*, vol. 25, Feb. 1954, p. 202.

19 Dushman, S., "Vacuum Techniques," John Wiley & Sons, New York, 1949, p. 353.

20 Spencer, N. W. and Boggess, R. L., "Radioactive Ionization Gage Pressure Measurement System," ARS JOURNAL, vol. 29, no. 1, Jan. 1959, pp. 68–71.

21 Sommer, H. and Thomas, H. A., "Detection of Magnetic Resonance by Ion Resonance Absorption," *Phys. Rev.*, vol. 78, June 15, 1950, p. 806.

Technical Notes

Circular Orbit Stability in the Oblate Earth's Equatorial Plane

MARVIN H. HEWITT[1]

The Martin Company, Denver, Colo.

In the oblate Earth's field, circular equatorial orbits are stable for small planar perturbations. Disturbances causing orbital precession are not considered here since their effects require a consideration of the Earth's noncentral force field, which is outside the scope of the method used in this paper.

THE POTENTIAL function for the gravitational attraction of a solid homogeneous oblate spheroid upon a distant unit particle is, approximately[2]

$$V = -\frac{M}{r} + \frac{M}{5}\frac{(a^2 - b^2)}{r^3} P_2(\cos\theta) + \ldots \qquad [1]$$

where

$P_2(\cos\theta)$	=	Legendre coefficient
M	=	mass of the Earth
r	=	distance from center of Earth to satellite
a	=	semimajor axis of the Earth
b	=	semiminor axis of the Earth

In the equatorial plane the potential function reduces in approximation to

$$V = -\frac{M}{r} - \frac{M}{10}\frac{(a^2 - b^2)}{r^3} \qquad [2]$$

The corresponding acceleration g is given by the expression

$$g = -G \operatorname{grad} V = -G\left[\frac{M}{r^2} + \frac{3M}{10}\frac{(a^2 - b^2)}{r^4}\right] \qquad [3]$$

It is seen that this acceleration represents a central non-Newtonian force, and it is well-known that a circular orbit is always possible for central interaction. The following stability analysis will be restricted in application to perturbed motion confined to the equatorial plane. We define stability here in the sense of linearized perturbation theory. Perturbations that cause orbital precession will not be considered here. Satellite motion in a plane inclined to the equator involves a consideration of the Earth's noncentral force field which is outside the scope of the method used in this paper.

Let $u = 1/r$, where r is the orbital radius. Then the attraction on unit mass is a function of u, and we may write it in the form

$$P = ku^2 f(u) \qquad [4]$$

where

$$k = -GMm \qquad [5]$$

$$f(u) = 1 + \frac{3}{10}\,10\,(a^2 - b^2)u^2 \qquad [6]$$

m being the unit mass.

The differential equation of the orbit is

$$\frac{d^2u}{d\phi^2} + u = \frac{P}{h^2u^2} = \frac{k}{h^2} f(y) \qquad [7]$$

where h denotes, as usual, the constant moment of the velocity about the center of attraction, and ϕ is the orbital polar angle.

Let c be a constant given by the equation

$$c = \frac{k}{h^2} f(c) \qquad [8]$$

and note that $u = c$ satisfies Equation [7]. The orbit is now perturbed, and we set

$$u = c + x \qquad [9]$$

where x is initially small.

Substituting $c + x$ for u in Equation [7], we get

$$\frac{d^2x}{d\phi^2} + c + x = \frac{k}{h^2} f(c + x) \qquad [10]$$

For small x, we can expand the right-hand side of Equation [10] by Taylor's theorem and delete all powers of x higher than the first. Thus

$$\frac{d^2x}{d\phi^2} + c + x = \frac{k}{h^2}\,[f(c) + xf'(c)] \qquad [11]$$

Since c satisfies Equation [8], this last equation gives

$$\frac{d^2x}{d\phi^2} + x = \frac{k}{h^2}\,xf'(c) = \frac{c}{f(c)}\,xf'(c) \qquad [12]$$

or

$$\frac{d^2x}{d\phi^2} + x\left[1 - c\frac{f'(c)}{f(c)}\right] = 0 \qquad [13]$$

If the coefficient of x is positive in Equation [13], this takes the form

$$\frac{d^2x}{d\phi^2} + a_0^2 x = 0 \qquad [14]$$

the solution of which is

$$x = A\cos(a_0\phi + \beta) \qquad [15]$$

Therefore, if A is small, x is always small, and the orbit is therefore nearly circular. But if the coefficient of x in Equation [13] is positive, the equation has the form

$$\frac{d^2x}{d\phi^2} - b_0^2 x = 0 \qquad [16]$$

Received Jan. 15, 1959.

[1] Design Engineer, Applied Research Section. Member ARS.

[2] Webster, A. G., "Dynamics of Particles and of Rigid, Elastic, and Fluid Bodies," G. E. Stechert and Company, New York third ed., chapter VIII.

EDITOR'S NOTE: The Technical Notes and Technical Comments sections of ARS JOURNAL are open to short manuscripts describing new developments or offering comments on papers previously published. Such manuscripts are published without editorial review, usually within two months of the date of receipt. Requirements as to style are the same as for regular contributions (see masthead page).

the solution of which is

$$x = Ce^{b_0\phi} + De^{-b_0\phi} \qquad [17]$$

and thus x is large when ϕ is large (unless C is exactly zero) until the approximate Equation [13] is no longer applicable.

The conditions, therefore, that a satellite in a circular orbit should be stable, undetermined, or unstable are, respectively

$$1 - c\frac{f'(c)}{f(c)} \gtreqless 0 \qquad [18]$$

Substituting parametrically, we obtain Equation [18] in the form

$$1 - \frac{[(6/10)\ (a^2 - b^2)c^2]}{[1 + (3/10)\ (a^2 - b^2)c^2]} > 0 \qquad [19]$$

where satellite stability exclusively is realized. In the case where the equality holds, the corresponding orbital radius is given as

$$\left[\frac{3(a^2 - b^2)}{10}\right]^{1/2} \cong 134 \text{ nautical miles} = r \qquad [20]$$

We see that this orbit lies inside the Earth. And it is apparent that the unstable case requires a smaller orbit than that given by Equation [20].

Inequality [19] holds then for actual satellite orbits; we conclude that perturbed satellite orbits in the equatorial plane are stable for small perturbations in that plane.

Acknowledgment

The author wishes to express his thanks to Dr. W. H. Clohessy for his contributive suggestions.

Particle Impaction on Spheres at High Mach Numbers[1]

S. K. FRIEDLANDER[2]

The Johns Hopkins University, Baltimore, Md.

At high Mach numbers a detached shock wave is established upstream of the forward stagnation point of a blunt body. The equations of motion of a small particle in such a flow are set up, and deposition at the forward end by impaction is considered. An expression is derived for the impaction parameter, defined as in subsonic flow, at which the efficiency vanishes. This is applied to the high Mach number flow around a sphere, and it is found that the critical impaction parameter varies from 0.153 to 0.29 for density ratios from 4 to 14. A sample calculation is given. Possible applications are to high altitude sampling of particulates, to prediction of erosion and to the development of more efficient laboratory samplers.

WHEN a gas flows at a high Mach number over a blunt nosed body, a detached shock ("bow") wave is established upstream of the forward stagnation point. Between the shock and the stagnation point, the gas density is high and the flow subsonic. In this paper, the equations of motion of a small particle in such a flow are set up, and deposition at the forward end by impaction is considered. These calculations may have application to high altitude sampling, to predictions of erosion and to the development of more efficient laboratory samplers.

The calculation of the complete impaction efficiency curve would require a numerical solution to the equation of particle motion with varying drag coefficient in a manner similar to that for subsonic impaction (1).[3] At this point the uncertainty in the velocity distribution at high Mach numbers would not warrant such an effort. In the discussion which follows, a general limiting law is derived for the lower cut-off point of the impaction efficiency. This is then applied to the sphere, the blunt body for which the most theoretical and experimental information is available. Effects such as particle disintegration in the shock or melting at the surface are not considered. It is interesting to note that impaction calculations at high Mach numbers will in many cases be relatively simple (once the gas velocity distribution has been established), since the starting point for numerical calculations is well-defined compared with subsonic flows.

Lower Cut-off Point for the Impaction Efficiency

The equation of motion for a particle traveling along the stagnation streamline is given by

$$m\frac{dv}{dt} = -\frac{1}{2}C_D\rho_F A\,|v - v_F|\,(v - v_F) \qquad [1]$$

Immediately after the shock, the particle possesses its initial (supersonic) velocity while the gas velocity becomes subsonic. At low impaction efficiencies, however, the velocity of the particles near the forward stagnation point is small and the drag is given by Stokes law

$$m\frac{dv}{dt} = -f(v - v_F) \qquad [2]$$

The fluid velocity along the stagnation line can be expanded in a Taylor series around the stagnation point, $r = a$

$$v_F = \left(\frac{dv_F}{dr}\right)_{r=a}(r - a) + \left(\frac{d^2v_F}{dr^2}\right)_{r=a}\frac{(r - a)^2}{2!} + \ldots \qquad [3]$$

Substituting in Equation [2] with $v = dr/dt = dy/dt$, there results

$$mv\frac{dv}{dy} + fv = f(b_1y + b_2y^2 + \ldots) \qquad [4]$$

where the coefficients b_n represent the derivatives and numerical coefficients in Equation [3]. It has been shown by Poincaré (see, for example (2)) that the singularities of Equation [4] are the same as those of the first approximation

$$\frac{dv}{dy} = \frac{fb_1y - fv}{mv} \qquad [5]$$

The behavior of the v-y curve in the neighborhood of 0,0 can be determined (2) from Equation [5] by examining the roots of the characteristic equation

$$S^2 + fS - mfb_1 = 0 \qquad [6]$$

These are

$$S = \frac{-f \pm \sqrt{f^2 + 4mfb_1}}{2} \qquad [7]$$

When the discriminant $f^2 + 4mfb_1$ is negative, i.e., $(mV/fa) = N_I > -(V/4ab_1)$, the roots are complex conjugates, and the system has a focal or spiral point at 0,0 (Fig. 1a). The first intersection of the spiral with the v axis corresponds to finite

Received Jan. 13, 1959.

[1] This work was carried out at The Johns Hopkins University under the sponsorship of Atomic Energy Commission contract AT(30-1)-2165. Part of the analysis stems from the author's work with the Atlantic Research Corp., Alexandria, Va.

[2] Assistant Professor, Department of Chemical Engineering.

[3] Numbers in parentheses indicate References at end of paper.

velocity at the stagnation point. The rest of the spiral has no physical significance, since the particle cannot pass the surface of the sphere.

When the discriminant is positive, $N_I < -(V/4ab_1)$, the roots are real, and both are negative, since b_1 is a negative number. The system has a nodal point at 0,0 (Fig. 1b), which corresponds to zero particle velocity at the forward stagnation point and zero impaction efficiency. If the discriminant vanishes, the roots are equal, and the system again has a node as its singularity. Thus

$$N_I = -\frac{V}{4ab_1} \qquad [8]$$

represents a lower limit below which the impaction efficiency vanishes.

This analysis is an extension of one originally suggested by Taylor (3) for subsonic flows. It neglects boundary layer effects and is probably best applied when the particle diameter is larger than, or of the order of, the boundary layer thickness. For most real (viscous) flows, the first derivative of the velocity component normal to the surface with respect to the normal vanishes because of the no-slip boundary condition and the continuity relation. In this case, the equation of particle motion cannot be put into the form of Equation [5], and an analysis of the type developed above is not permissible.

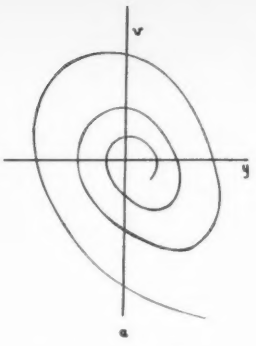

Fig. 1a Spiral point

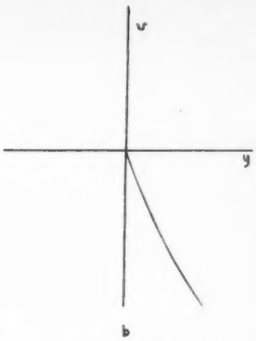

Fig. 1b Nodal point

Application to Flow Over a Sphere at High Mach Numbers

A number of investigators have chosen the sphere for theoretical or experimental studies of the fluid mechanics of high Mach number flow around blunt bodies. Lighthill (4) has developed a theory for the inviscid flow outside the laminar boundary layer assuming that near the forward stagnation point the shock front is spherical and concentric with the sphere, and that the flow between the shock and the surface is incompressible; this limits the analysis to the region within about 10 deg of the stagnation point. Although inviscid and incompressible, the flow is not irrotational because of the vorticity produced at the curved shock front. Using the strong shock approximation, Lighthill derived an expression for the vorticity at the shock surface. From the defining expression for the vorticity, he was able to calculate the stream function for the flow between the shock and the surface

$$\psi = \Psi(r) \sin^2 \theta \qquad [9]$$

where

$$\Psi(r) = \frac{Vc^2}{30K}\left[3(K-1)\left(\frac{r}{c}\right)^4 - 5K(K-4)\left(\frac{r}{c}\right)^2 + 2(K-1)(K-6)\left(\frac{r}{c}\right)^{-1}\right]$$

The position of the surface relative to the shock (and the detachment distance) is obtained by solving for the greatest root of $\Psi(r) = 0$ which is less than c.

The radial fluid velocity along the stagnation line is given by

$$v_F = -\frac{1}{r^2 \sin\theta}\frac{\partial\psi}{\partial\theta} = -\frac{2\Psi(r)}{r^2} \qquad (\theta = 0) \qquad [10]$$

and

$$b_1 = \left(\frac{dv_F}{dr}\right)_{r=a} = -2\left[\frac{d\Psi(r)/r^2}{dr}\right]_{r=a} \qquad (\theta = 0) \qquad [11]$$

$$= -\frac{V}{15Kc}\left[6(K-1)^2\left(\frac{a}{c}\right) - 6(K-1)(K-6)\left(\frac{a}{c}\right)^{-4}\right] \qquad [12]$$

This expression can be combined with $\Psi(a) = 0$ to give

$$b_1 = -\frac{V}{Ka}\left[(K-1)^2\left(\frac{a}{c}\right)^2 - K(K-4)\right] \qquad [13]$$

$$= -\frac{V}{Ka}\left[\frac{(K-1)^2}{(1+\delta/a)^2} - K(K-4)\right] \qquad [14]$$

Combining Equation [14] with [8], the critical impaction parameter becomes

$$N_I = \frac{K}{4\left[\dfrac{(K-1)^2}{(1+\delta/a)^2} - K(K-4)\right]} \qquad [15]$$

This is plotted in Fig. 2 as a function of K. The ratio of the detachment thickness to the radius of the sphere δ/a was taken from Lighthill's Fig. 6.

Sample Calculation

As an example of the application of these results, one may calculate the diameter of the smallest particle collectible by a sphere of radius 1 ft traveling at a velocity of 8000 ft per sec at an altitude of 36,000 ft. Under these conditions, according to the tables of normal shock parameters prepared by Huber (5), temperature and pressure before the shock are 217 K and 0.224 atm, and after the shock, 2600 K and 18.5 atm. The upstream Mach number is 8.25 and $K = 6.88$. From Fig. 1, the critical impaction parameter is 0.208. Assuming that the particles are spherical

$$N_I = \frac{mV}{fa} = \frac{\rho d^2 V}{18\,\mu a} = 0.208 \qquad [16]$$

The viscosity of the air can be calculated from Equation [10] and Fig. 12 of the review of the properties of high temperature air by Hansen and Heims (6). At 2600 K, the effect

Fig. 2 Critical impaction parameter as a function of density ratio

of dissociation on viscosity appears to be negligible, and μ is calculated to be 7.13 $(10)^{-4}$ gm/cm sec. For particles of unit density the minimum collectible diameter is

$$d = \sqrt{\frac{0.208(18)(7.13)(10)^{-4}(1)}{8000}} \qquad [17]$$

$$= 5.78 \text{ microns}$$

It is doubtful that particles this large exist at 36,000 ft, and thus no deposition would occur on the sphere. For a sphere one hundred times smaller, i.e., about $\frac{1}{4}$ in. in diameter, the minimum collectible particle would have a diameter of about 0.6 micron.

Nomenclature

a = radius of sphere
A = particle cross-sectional area
b_n = Taylor series expansion coefficients
c = radial position of shock
C_D = drag coefficient
d = particle diameter
f = coefficient of resistance in linear drag law
K = ratio of gas density downstream of shock to density upstream of shock
m = particle mass
N_I = impaction parameter
n = radial position from center of sphere
S = roots of the characteristic equation
t = time
v = particle velocity along stagnation line
v_F = gas velocity along stagnation line
V = velocity of gas at infinity relative to sphere
y = $r - a$
δ = shock detachment distance
θ = angle measured from forward stagnation point
μ = gas viscosity
ρ = particle density
ρ_F = gas density
ψ = stream function
Ψ = radial dependence of stream function

References

1 Brun, R. J. and Mergler, H. W., "Impingement of Water Droplets on a Cylinder in an Incompressible Flow Field and Evaluation of Rotating Multicylinder Method," NACA TN 2904, March 1953.

2 Ku, Y. H., "Analysis and Control of Nonlinear Systems," Ronald Press Co., N. Y., 1958, chap. 5.

3 Taylor, G. I., "Notes on Possible Equipment and Technique for Experiments on Icing on Aircraft," ARCR and M. no. 2024, 4350, Jan. 1940.

4 Lighthill, M. J., "Dynamics of a Dissociating Gas, Part I-Equilibrium Flow," *J. Fluid Mech.*, vol. 2, 1957, p. 1.

5 Huber, P. W., "Tables and Graphs of Normal-Shock Parameters at Hypersonic Mach Numbers and Selected Altitudes," NACA TN 4352, Sept. 1958.

6 Hansen, C. F. and Heims, S. P., "A Review of the Thermodynamic, Transport, and Chemical Reaction Rate Properties of High-Temperature Air," NACA TN 4359, July 1958.

Simple Analytical Approximation to the Equation of State of Dissociated Air[1]

W. L. BADE[2]

Avco Research and Advanced Development Division, Wilmington, Mass.

A NUMBER of investigators (1 to 4)[3] have calculated the thermodynamic properties of equilibrium air to 10,000 K or higher. At temperatures exceeding about 2000 K, the density is found to be a rather complicated function of temperature and pressure. The compressibility factor $Z(p, T) = pM_0/\rho RT$ increases rapidly with temperature in regions where O_2 or N_2 molecules dissociate into atoms, and varies slowly in intermediate regions. The equation of state has been available only in tabular and graphical forms and in terms of fairly complicated approximate analytical representations.

A simple analytical approximation to the equation of state of equilibrium air would be useful in many types of calculations pertaining to boundary layers, aerodynamic heating, skin friction, inviscid flow problems, etc. Such a simple approximation may be found by noting that, in regions where the density changes rapidly with temperature owing to occurrence of dissociation, the specific enthalpy h also changes rapidly with temperature because of increase of enthalpy of dissociation. This crude argument makes it plausible that density should be a simpler function of enthalpy and pressure than of temperature and pressure. Such is indeed the case. Fig. 1 is a logarithmic plot of ρ/p vs. h/RT_0 for the four pressures 0.1, 1, 10 and 100 atm. The data are from Hansen[4] (4). It is seen that the points for each pressure are fitted rather well by a straight line, that the four lines corresponding to the different pressures can be drawn so as to pass through a single point at

$$h_1 = 31.9RT_0 = 1080 \text{ Btu/lb} = 600 \text{ cal/gm}$$
$$\rho_1 = 0.124\rho_0 = 0.0100 \text{ lb/ft}^3 = 1.60 \times 10^{-4} \text{ gm/cm}^3 \qquad [1]$$

and that the slopes of the lines vary in a regular way with the logarithm of the pressure. A simple curve-fitting operation leads to the formulas

$$\rho/\rho_1 = (p/p_1)(h/h_1)^{-x} \qquad [2]$$

$$x = 0.70 + 0.04 \log_{10}(p/p_1) \qquad [3]$$

Received Jan. 15, 1959.

[1] This work was supported by the U. S. Air Force, Ballistic Missile Division, under Contract no. AF 04(645)-30.

[2] Senior Scientist, Physics Section.

[3] Numbers in parentheses indicate References at end of paper.

[4] Hansen's tables provide the most convenient basis for seeking a correlation of this type, because they give the thermodynamic functions with pressure as an independent variable from 0.0001 to 100 atm.

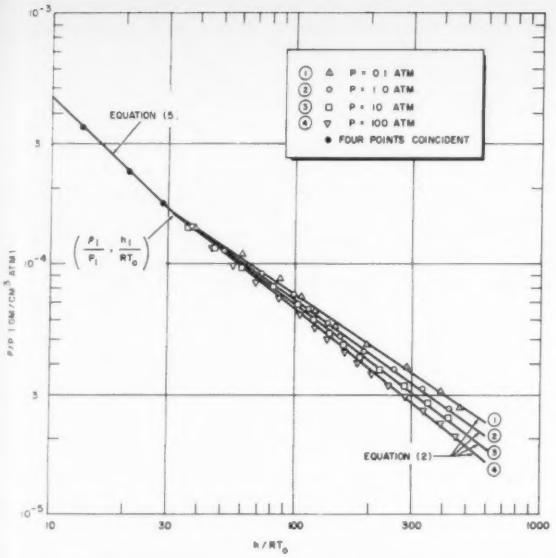

Fig. 1 Density (ρ) of equilibrium air as a function of pressure (p) and enthalpy (h/RT_0)

where ρ_1 and h_1 are given by Equation [1], and $p_1 = 1$ atm. Within the range of conditions

$$31.9 \leq h/RT_0 \leq 480 \qquad 0.1 \text{ atm} \leq p \leq 100 \text{ atm} \qquad [4]$$

Equation [2] agrees with Hansen's results to within 5 per cent. In the same range, Equation [2] also[5] agrees with the results of Logan and Treanor (3) to within 5 per cent, except in the region $0.1 \leq p \leq 1$ atm, $60 \leq h/RT_0 \leq 100$, where the error rises to 8 per cent. In addition, Equation [2] is valid to within 5 per cent at pressures considerably greater than 100 atm over the full enthalpy range indicated in Equation [4], and at pressures smaller than 0.1 atm over a reduced enthalpy range ($120 \leq h/RT_0 \leq 400$ down to 0.001 atm).

Below the enthalpy $h_1 = 31.9\ RT_0$, the ratio ρ/p is nearly independent of pressure and can be represented readily in various ways as a simple function of temperature or enthalpy. It may be convenient, for some applications, to represent the density in this low temperature region by a function similar in form to Equation [2] and joining onto [2] at the point $h = h_1$. Such a function is

$$\rho/\rho_1 = (p/p_1)(h/h_1)^{-0.94} \qquad [5]$$

which agrees with the results of Hilsenrath et al. (5) to within 7 per cent in the range $3.8 \leq h/RT_0 \leq 31.9$, 0.1 atm $\leq p \leq 100$ atm.

The dependence of ρ upon p through the $\log_{10}(p/p_1)$ term in the exponent of (h/h_1) in Equation [2] is weak, so that, for processes not involving excessively large changes in pressure, the exponent can be replaced, to a close approximation, by a fixed value $x = x(\bar{p}) =$ constant, where p is a mean or typical pressure. For example, by differentiating Equation [2], with $x =$ constant, and employing the equation

$$DQ = dh - dp/\rho = 0 \qquad [6]$$

defining an adiabatic process, one readily obtains an approximate expression for the velocity of sound in dissociated air

$$a \equiv \left[\left(\frac{\partial p}{\partial \rho}\right)_s\right]^{1/2} = \left[\frac{\rho_1}{p_1}\left(\frac{h}{h_1}\right)^{-x(\bar{p})} - \frac{x(\bar{p})}{h}\right]^{-1/2} \qquad [7]$$

Within the range of enthalpy and pressure defined by Equation [4], Equation [7] agrees with Hansen's results to within 7 per cent.

The constant-exponent approximation to Equation [2] can also be used in the integration of Equation [6] to obtain a real air analog

$$p \exp\left[-\frac{\rho_1}{p_1}\left(\frac{h}{h_1}\right)^{-x}\frac{h}{1-x}\right] = \text{constant} \qquad [8]$$

of the ideal gas adiabatic equation of state $p/T^{\gamma/(\gamma-1)} =$ constant. Equation [8] leads to an analog of the Bernoulli equation, for the compressible flow of dissociated air

$$p_s = p \exp\left\{\frac{h}{1-x}\frac{\rho}{p}\left[\left(1+\frac{u^2}{2h}\right)^{1-x} - 1\right]\right\}$$
$$= p \exp\left\{\frac{\rho u^2}{2p}\left[1 - \frac{x}{2}\frac{u^2}{2h} + \frac{x(1-x)}{6}\left(\frac{u^2}{2h}\right)^2 - \cdots\right]\right\} \qquad [9]$$

where p_s is the stagnation pressure and (p, ρ, h) is the state of the air at a point where the velocity is u.

A further application of Equation [2] is in calculations of aerodynamic heat flux. For example, Fay and Riddell's (6) expression for the laminar heat transfer rate at the stagnation point of a blunt body in dissociated air may be written, for the case of a strongly cooled surface, in the form

$$q_s = F(p_s, h_s)(du_e/dx)_s^{1/2}(h_s - h_w) \qquad [10a]$$

where h_w represents the wall enthalpy, $(du_e/dx)_s$ is the stagnation point velocity gradient, and $F(p_s, h_s)$ depends upon the Prandtl and Lewis numbers and the density, viscosity, stagnation enthalpy and dissociation enthalpy of the air at the edge of the boundary layer. Equation [2], together with a crude fit to the temperature of equilibrium air as a function of enthalpy, provides an approximate analytical expression for this function F

$$F(p_s, h_s) \simeq$$
$$7.68 \times 10^{-4}\left(\frac{p_s}{p_1}\right)^{1/2}\left(\frac{h_s}{h_1}\right)^{-[0.19 + 0.016 \log_{10}(p_s/p_1)]} \qquad [10b]$$

in lb/ft^2 sec$^{1/2}$. Equation [10] agrees with the Fay-Riddell formula to within 5 per cent in the range of conditions $100 \leq h_s/RT_0 \leq 400$, 0.1 atm $\leq p_s \leq 100$ atm.

Acknowledgment is made to Martin Zlotnick, who read this Note in manuscript and made helpful comments, and to Leonard Comeau, who carried out many of the numerical calculations.

References

1 Gilmore, F. R., "Equilibrium Composition and Thermodynamic Properties of Air to 24,000°K," U. S. Air Force Project RAND, Research Memo 1543, Aug. 1955.

2 Hilsenrath, J. and Beckett, C. W., "Tables of Thermodynamic Properties of Argon-Free Air to 15,000°K.," Arnold Engineering Development Center, AEDC-TN-56-12, Sept. 1956.

3 Logan, J. G., Jr. and Treanor, C. E., "Tables of Thermodynamic Properties of Air from 3000°K to 10,000°K at Intervals of 100°K," Cornell Aeronautical Laboratory, Report no. BE-1007-A-3, Jan. 1957.

4 Hansen, C. F., "Approximations for the Thermodynamic and Transport Properties of High-Temperature Air," NACA TN 4150, March 1958.

5 Hilsenrath, J. et al., "Tables of Thermal Properties of Gases," Nat. Bur. Standards, Circular 564, Nov. 1955.

6 Fay, J. A. and Riddell, F. R., "Theory of Stagnation Point Heat Transfer in Dissociated Air," *J. Aeron. Sci.*, vol. 25. 1958, pp. 73–85.

[5] It was considered necessary to check Equation [2] against the accurate tabulation of Logan and Treanor as well as against Hansen's tables, because the latter are based upon an approximate method which leads to errors (<5 per cent) of the same general size as those being sought in Equation [2].

Minor Circle Flight for Boost Glide Vehicles

W. H. T. LOH[1]

Chance Vought Aircraft, Dallas, Texas

HYPERSONIC gliders designed to strike targets located halfway around the Earth will fly great circle paths in reaching these targets and returning to the launch area. Great circle paths are also used in striking targets at shorter ranges. However, the possibility of reaching these shorter range targets by flying paths other than great circles (minor circle paths) may be of interest. Recognizing that the great circle path is the shortest path between any two given points and recognizing that the great circle path is also the glider's natural automatic gliding path (in contrast to the minor circle path which needs continuous accurate aerodynamic control to force the glider on the desired path) nevertheless, one might use a minor circle path simply for strategic reasons. The approximate range equation of such a glider flying along a great circle path, derived recently by Eggers and Allen[2] is

$$R = \left(\frac{R_0}{2}\right)\left(\frac{L}{D}\right)\ln\left[\frac{1-(V_F^2/gR_0)}{1-(V_i^2/gR_0)}\right]$$

or

$$R \cong \left(\frac{R_0}{2}\right)\left(\frac{L}{D}\right)\ln\left[\frac{1}{1-(V_i^2/gR_0)}\right]$$

On deriving the equation, they used the following assumptions:

1 Flight is in planes containing the great circle arc between takeoff and landing.

2 Small inclination angle to the horizontal, i.e., $\cos\theta \cong 1$, and $\sin\theta \cong \theta$.

3 Constant gravity acceleration, i.e., $R_e \cong R_0$.

4 Constant L/D flight.

5 Rotation of Earth is neglected.

6 Since $(L/D)\,\theta \ll 1$, and $V^2\,d\theta/ds \ll 1/2(L/D)(dV^2/ds)$, both small terms are neglected in the basic equations.

7 Contribution to range of powered phase of flight is neglected.

Similar assumptions for minor circle flight may be written here:

1 Flight is in planes containing the minor circle arc between takeoff and landing.

2 Small inclination angle to the minor circle plane horizontal, i.e., $\cos\theta \cong 1$, and $\sin\theta \cong \theta$.

3 Constant gravity acceleration, i.e., $R_e \cong R_0$. Note that this implies here that the altitude of the glider when compared with Earth radius is negligible. Therefore $R_e \cong R_0$; $r \cong r_0$, and $\lambda \cong \lambda_0$ (see Figs. 1 and 2).

4 Constant L/D flight.

5 Rotation of Earth is neglected.

6 Since $(L/D)\,\theta \sin\alpha \ll 1$, and $V^2\,d\theta/ds \ll 1/2(L/D) \times (dV^2/ds)\sin\alpha$, both small terms are neglected in the basic equation (provided α is not too small).

7 Contribution to range of powered phase of flight is neglected.

With these assumptions and referring to Figs. 1 and 2, one obtains immediately the following three equations of motion normal and parallel to the direction of flight

$$L\cos\alpha = mg\cos\lambda \qquad [1a]$$

$$L\sin\alpha - mg\sin\lambda\cos\theta = -m\frac{V^2}{r_c} \qquad [1b]$$

$$-D + mg\sin\lambda\sin\theta = m\frac{dV}{dt} = \frac{1}{2}m\frac{dV^2}{ds} \qquad [1c]$$

$$\frac{1}{r_c} = \frac{d(\Psi-\theta)}{ds} \qquad \frac{d\Psi}{ds} = \frac{\cos\theta}{r} \cong \frac{1}{r_0} \qquad [1d]$$

Combining Equations [1b, 1c and 1d] and using the approximations as listed, one obtains after simplification

$$g\sin\lambda_0\left(1-\frac{L}{D}\theta\sin\alpha\right) + \left(\frac{1}{2}\frac{L}{D}\sin\alpha\frac{dV^2}{ds} + V^2\frac{d\theta}{ds}\right) - \frac{V^2}{R_0\sin\lambda_0} = 0 \qquad [2a]$$

Since $(L/D)\theta\sin\alpha \ll 1$, and $V^2(d\theta/ds) \ll 1/2(L/D) \times (dV^2/ds)\sin\alpha$, they may be dropped out. Equation [2a] therefore simplifies to

$$\frac{dV^2}{ds} - \left[\frac{2}{R_0\,(L/D)\sin\lambda_0\sin\alpha}\right]V^2 + \frac{2g\sin\lambda_0}{(L/D)\sin\alpha} = 0 \qquad [2b]$$

Combining Equations [1a and 1b] and using the approximations as listed, one obtains after simplification

$$\sin\alpha \cong \sin\lambda_0\,\frac{1-\dfrac{V^2}{gR_0\sin^2\lambda_0}}{\sqrt{\left(1-\dfrac{V^2}{gR_0}\right)^2 + \left(\dfrac{V^2}{gR_0}\right)^2\cot^2\lambda_0}} \qquad [3]$$

Substituting Equation [3] into [2b] and integrating it between initial and final conditions, one obtains

$$R = \left(\frac{R_0}{2}\right)\left(\frac{L}{D}\right)\sin\lambda_0\ln\left[\frac{\left(1-\dfrac{V_F^2}{gR_0\sin^2\lambda_0}\right) - \dfrac{1}{\sin\lambda_0}\sqrt{\left(\dfrac{V_F^2}{gR_0\sin\lambda_0}\right)^2 - 2\left(\dfrac{V_F^2}{gR_0}\right)+1}}{\left(1-\dfrac{V_i^2}{gR_0\sin^2\lambda_0}\right) - \dfrac{1}{\sin\lambda_0}\sqrt{\left(\dfrac{V_i^2}{gR_0\sin\lambda_0}\right)^2 - 2\left(\dfrac{V_i^2}{gR_0}\right)+1}}\right] \qquad [4a]$$

As maximum range is approached $L/W \cong 1$, $V_F^2/gR_0\sin^2\lambda_0$ then is small compared to one, and it may be neglected in Equation [4a] without much loss of accuracy. In this case, the maximum range for the glider flying along a minor circle path becomes simply

$$R \cong \left(\frac{R_0}{2}\right)\left(\frac{L}{D}\right)\sin\lambda_0\ln\left\{\frac{1}{\left[1-\dfrac{V_i^2}{gR_0\sin^2\lambda_0}\right]}\,\frac{\left[1-\dfrac{1}{\sin\lambda_0}\right]}{\left[1-\dfrac{1}{\sin\lambda_0}\dfrac{\sqrt{1-2\left(\dfrac{V_i^2}{gR_0}\right)+\left(\dfrac{V_i^2}{gR_0\sin\lambda_0}\right)^2}}{\left(1-\dfrac{V_i^2}{gR_0\sin^2\lambda_0}\right)}\right]}\right\} \qquad [4b]$$

Received Jan. 27, 1959.

[1] Staff Engineer to Assistant Chief Engineer, Technical.

[2] Eggers, A. J. and Allen, H. J., "A Comparative Analysis of the Performance of Long-Range Hypervelocity Vehicles," NACA TN 4046, Oct. 1957.

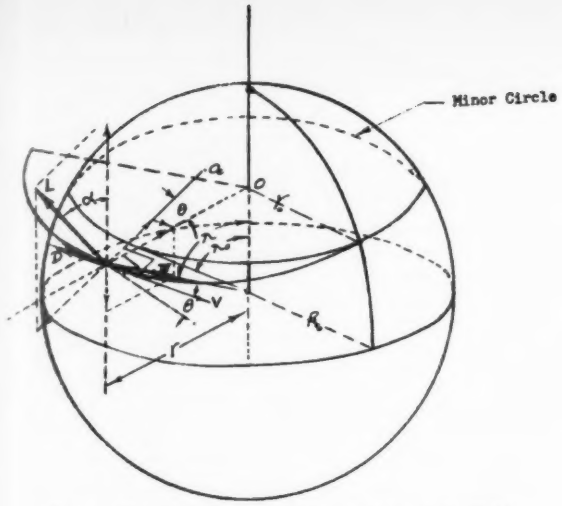

Fig. 1 Three-dimensional view on minor circle flight

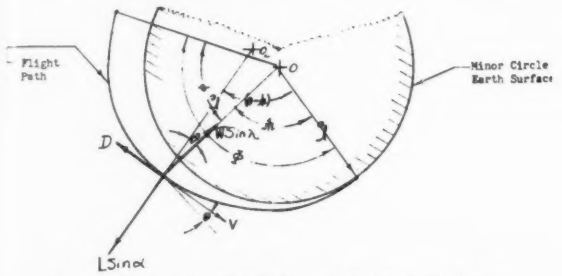

Fig. 2 Two-dimensional view on minor circle flight

When $\lambda_0 = (\pi/2)$, the minor circle becomes a great circle, and the present range of Equations [4a and 4b] are reduced to the range equation derived for great circle paths by Eggers and Allen. Consequently, the great circle range equation may be considered as a special case of the range equation derived here. The reduction of range on minor circle path is mainly due to the fact that part of the dynamical energy possessed by the glider is now used to control and force the glider in and within the minor circle path being particularly specified; consequently, this dynamical energy is simply dissipated without accomplishing any useful range.

Nomenclature

D = drag
g = acceleration due to force of gravity
L = lift
m = mass
r = distance shown in Figs. 1 and 2
r_0 = distance shown in Figs. 1 and 2
r_c = radius of curvature of flight path, shown in Fig. 2
R_0 = radius of Earth
R_g = glider distance from center of Earth
R = flight range, measured along surface of the Earth
s = distance along flight path
t = time
V = velocity
W = weight
θ = angle of flight path to horizontal
ϕ = partial range angle, rad
Φ = total range angle, rad
Ψ = remaining range angle, rad
λ_0 = angle defined in Fig. 1
λ = angle defined in Fig. 1
α = angle defined in Fig. 1

Subscripts

i = initial conditions
F = final conditions

Aerodynamic Moment on Bodies Moving at High Speed in the Upper Atmosphere

W. A. GUSTAFSON[1]

Lockheed Aircraft Corp., Sunnyvale, Calif.

THE ATTITUDE control of vehicles traveling in the upper atmosphere is of considerable importance and requires a knowledge of the aerodynamic characteristics of various body shapes. At sufficiently high altitudes and correspondingly low densities, the aerodynamic and gravitational moments acting on a body may be of similar magnitude, thereby making an analytical expression for the aerodynamic moment useful for an investigation of the dynamics of the vehicle about its center of gravity.

In the following discussion, only altitudes above 100 statute miles are considered, and consequently free molecular flow theory is applicable. It is assumed that the surface temperature is primarily controlled by thermal radiation phenomena, and thus T_r can be determined by a separate analysis.

The three body shapes of greatest practical interest are the cylinder, the cone or cone frustum, and the spherical segment. Applying free molecular theory to these shapes for the purpose of determining the aerodynamic moment results in integrals which apparently must be evaluated numerically except for the case of the cylinder. However, analytical expressions for the moment on a cone and on a spherical segment can be obtained by neglecting the free stream thermal motion. This is a good approximation as long as the molecular speed ratio is not too low. In the following paragraphs, the static aerodynamic pitching moment is determined about an arbitrary point on the body axis and for any angle of attack. It is assumed that the free stream strikes the body surface and gives up its total momentum, and that diffuse reflection then takes place with the atmospheric particles leaving the surface possessing a Maxwellian distribution corresponding to the surface temperature. It is also assumed that the mass of particles striking a unit of surface area per unit of time is equal to the mass leaving that area in a unit of time. Based on these assumptions, the forces acting on an element of area can be described and the moment arm determined. Thus, integrating over the body surface exposed to the free stream provides the desired result. Since the method is straightforward, only the final results are given below. A more detailed description of the derivation of the results is presented in (1).[2]

Received Dec. 22, 1958.

[1] Associate Research Scientist, Aerodynamics Department, Missile Systems Division.

[2] Numbers in parentheses indicate References at end of paper.

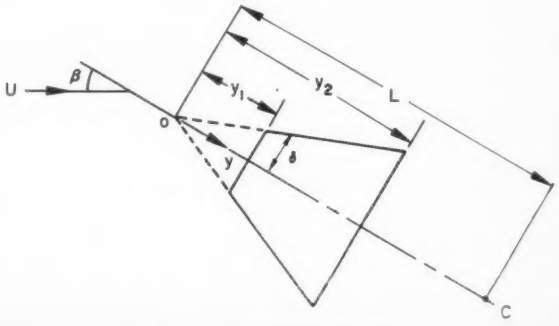

Fig. 1. Geometry of cone

Cone

The moment M_c about the point C is given below, corresponding to the notation in Fig. 1. However, when the angle of attack is greater than the semi-vertex angle, part of the cone is shielded from the free stream. Hence, this area is not included in the integration. The final result is given in two parts.

(a) $\beta \leq \delta$

$$\frac{M_c}{(1/2)\,\rho U^2} = \pi \tan\delta \sin\beta \left\{ 2 \tan\delta \cos\beta \left[L(y_2^2 - y_1^2) - (y_2^3 - y_1^3) \right] + \sqrt{\pi T_r/T_i}\, \frac{H}{S} \right\} \quad [1]$$

(b) $\beta \geq \delta$

$$\frac{M_c}{(1/2)\,\rho U^2} = \frac{\tan\delta}{\cos\delta} \left\{ 2(y_2^2 - y_1^2)\, LA \sin\beta - \frac{4}{3}(y_2^3 - y_1^3)(A \sin\beta + B \cos\beta \tan\delta) + \sqrt{\pi T_r/T_i}\, \frac{2BH}{S} \right\} \quad [2]$$

where

$y_1 \neq 0$ for a cone frustum

$$A = \cos\beta \sin\delta \left[\pi - \cos^{-1}(\cot\beta \tan\delta) \right] + \sin\beta \cos\delta \sin\left[\cos^{-1}(\cot\beta \tan\delta) \right]$$

$$H = \frac{L}{2} \cos\delta\,(y_2^2 - y_1^2) - \frac{1}{3\cos\delta}(y_2^3 - y_1^3)$$

$$B = \cos\beta \sin\delta \sin\left[\cos^{-1}(\cot\beta \tan\delta) \right] + \frac{1}{2} \sin\beta \cos\delta \left\{ \pi - \cos^{-1}(\cot\beta \tan\delta) - \frac{1}{2} \sin\left[2 \cos^{-1}(\cot\beta \tan\delta) \right] \right\}$$

Sphere

On a complete sphere, the total force is only a drag force so that the moment of a sphere about any point is easily determined. However, in some cases it may be required to cap a cylinder or a cone frustum by a hemisphere or a spherical segment, respectively. According to Fig. 2, θ_1 is the angle which specifies the size of the spherical segment. If a spherical cap for a cone frustum is required, then θ_1 is determined by the cone geometry, since $\delta = \pi/2 - \theta_1$. In a manner similar to that for the cone, the analysis is done in two parts, since for angles of attack greater than $\pi/2 - \theta_1$, part of the surface is shielded, and the limit of the ϕ integration then depends both on θ_1 and β.

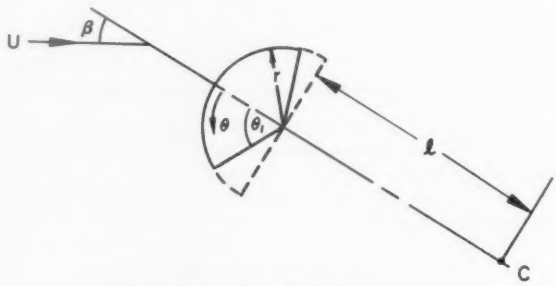

Fig. 2. Geometry of spherical segment

(a) $\beta \leq \pi/2 - \theta_1$

$$\frac{M_c}{(1/2)\,\rho U^2} = \pi r^2 \sin\beta \left\{ 2 \cos\beta \sin^2\theta_1 (l + r\cos\theta_1) + \frac{l}{S} \sqrt{\pi T_r/T_i} \left[\frac{2}{3} - \frac{1}{3} \cos\theta_1 (\sin^2\theta_1 + 2) \right] \right\} \quad [3]$$

(b) $\beta \geq \pi/2 - \theta_1$

$$\frac{M_c}{(1/2)\,\rho U^2} = 4r^2 \left\{ \frac{\pi}{4} \sin\beta \cos\beta \left[-\frac{r}{3} + 2r \sin^2\theta_1 \cos\theta_1 + \frac{l}{2} \cos\beta + 2l \sin^2\theta_1 \right] + \frac{r}{2} \sin\beta \cos^3\beta \sqrt{Q} - \frac{r}{3} \sin\beta \cos\beta \tan^{-1}\sqrt{Q} + \right.$$

$$\frac{l\pi}{4} \sin^3\beta + \frac{1}{6} \sin\beta \cos\beta \cos^{-1}(\cot\beta \cot\theta_1) \left[-3l \sin^2\theta_1 + 2r \cos^3\theta_1 - 3r \cos\theta_1 \left(1 - \frac{1}{3}\cos^2\theta_1 \right) \right] -$$

$$\frac{l}{2} \sin^2\beta \cos\theta_1 \sqrt{P} - \frac{l}{4} \sin\beta \cos^2\beta \sin^{-1}[1 + 2\cot^2\beta - 2\csc^2\beta \sin^2\theta_1] + \frac{r}{6} \sin^2\beta (2\sin^2\beta - \cos^2\beta) \sqrt{P^3} + \quad [4]$$

$$\left. \frac{l}{2} \sin^3\beta \tan^{-1} \sqrt{\cos^2\theta_1/(\sin^2\theta_1 - \cos^2\beta)} - \frac{r}{6} \sin\beta \cos\beta \sin^{-1}[-2\cos^2\beta \csc^2\theta_1 + 1] \right\} +$$

$$\frac{2lr^2}{S} \sqrt{\pi T_r/T_i} \left\{ \frac{\pi}{3} \sin\beta \left[1 - \frac{1}{2} \cos\theta_1 (\sin^2\theta_1 + 2) \right] + \frac{1}{6} \sin^2\beta \cos\beta \sqrt{P^3} + \frac{1}{3} \sin\beta \tan^{-1}\sqrt{Q} - \right.$$

$$\left. \frac{1}{6} \sin\beta \cos^2\beta \sqrt{Q} + \frac{1}{2} \sin\beta \cos\theta_1 \left(1 - \frac{1}{3}\cos^2\theta_1 \right) \cos^{-1}(\cot\beta \cot\theta_1) \right\}$$

In Equation [4]

$$P = \sin^2 \theta_1 \csc^2 \beta - \cot^2 \beta$$

$$Q = \frac{1 - \cot^2 \beta \cot^2 \theta_1}{\cot^2 \beta \csc^2 \theta_1}$$

The principal values of the arc sine terms between $-\pi/2$ and $\pi/2$ are to be taken in the preceding expression. The negative root of the radical in the arc tangent terms should be used, and the corresponding angle between $-\pi/2$ and 0 should be selected. The positive root of all other radicals is retained. Equation [4] is valid only to $\beta = \pi/2$, although an equation for $\beta > \pi/2$ can be derived in a similar manner.

Cylinder—Free Molecular Theory

The analysis of the cylinder based on free molecular flow is given below using the notation and local coordinate system of Talbot (2), except that his T-axis is reversed in direction. The components of the pressure and shear forces acting on an element of area in the N and T directions for $\alpha = \sigma = \sigma' = 1$ are

$$\frac{p_N}{(1/2)\,\rho U^2} = \left(\frac{1}{S\sqrt{\pi}} \sin \beta \sin \phi + \frac{1}{2S^2}\sqrt{\frac{T_r}{T_i}}\right) \sin \phi\, e^{-\xi^2 \sin^2 \phi} + \sin^2 \phi \left(\frac{1}{2S^2} + \sin^2 \beta \sin \phi + \frac{\sqrt{\pi}}{2S} \sin \beta \sqrt{\frac{T_r}{T_i}}\right) \times$$
$$[1 + erf\,(\xi \sin \phi)] \quad [5]$$

$$\frac{\tau_N}{(1/2)\,\rho U^2} = -\frac{1}{S\sqrt{\pi}} \sin \beta \cos^2 \phi \left\{e^{-\xi^2 \sin^2 \phi} + \sqrt{\pi}\, \xi \sin \phi\, [1 + erf\,(\xi \sin \phi)]\right\} \quad [6]$$

$$\frac{\tau_T}{(1/2)\,\rho U^2} = \frac{1}{S\sqrt{\pi}} \cos \beta \left\{e^{-\xi^2 \sin^2 \phi} + \sqrt{\pi}\, \xi \sin \phi\, [1 + erf(\xi \sin \phi)]\right\} \quad [7]$$

where

$\xi = S \sin \beta$
β = the angle of attack of the cylinder

Hence, the pitching moment about a point on the cylinder axis a distance L from the origin of the y coordinate (see Fig. 3) is given by

$$M_c = 2 \int_{-\pi/2}^{\pi/2} \int_0^{y_2} [(p_N - \tau_N)(y + L) - \tau_T r \sin \phi] r dy d\phi \quad [8]$$

Evaluating the integrals gives

$$\frac{M_c}{(1/2)\,\rho U^2} = 2ry_2\sqrt{\pi}\left(\frac{y_2}{2} + L\right)\left\{\frac{\pi}{4S}\sqrt{\frac{T_r}{T_i}} \sin \beta + 3 \sin^2 \beta e^{-\xi^2/2}\left[\left(\frac{1}{2\xi} + \frac{\xi}{3}\right) I_0\left(\frac{\xi^2}{2}\right) + \left(\frac{\xi}{3} + \frac{1}{6\xi}\right) I_1\left(\frac{\xi^2}{2}\right)\right]\right\} -$$
$$\pi r^2 y_2 \sin \beta \cos \beta \quad [9]$$

where $I_0(\xi^2/2)$ and $I_1(\xi^2/2)$ are modified Bessel functions of the first kind and of zero and first order, respectively. The ends of the cylinder have been neglected in determining Equation [9].

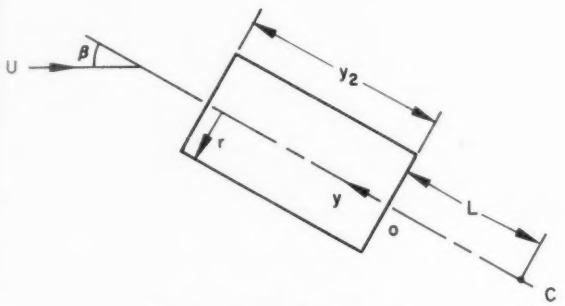

Fig. 3. Geometry of cylinder

Nomenclature

ρ = atmospheric density
U = flight velocity
T_i = ambient temperature
T_r = surface temperature
R = gas constant
S = molecular speed ratio = $U/\sqrt{2RT_i}$

References

1 Gustafson, W. A., "The Newtonian-Diffuse Method for Computing Aerodynamic Forces," Technical Memorandum LMSD-5132, Lockheed Aircraft Corp., Aug. 28, 1958.

2 Talbot, L., "Free Molecular Flow Forces and Heat Transfer for an Infinite Circular Cylinder at Angle of Attack," *J. Aeron. Sci.*, vol. 24, 1957, p. 458.

Book Reviews

Ali Bulent Cambel, Northwestern University, *Associate Editor*

Turbojet Fundamentals, by Howard E. Morgan, McGraw-Hill Book Co., Inc., New York, 1958, 104 pp. $4.00.

Reviewed by P. Roy Choudhury
University of Southern California

The very elementary nature of this book makes it suitable for those aircraft technicians and mechanics who have little preliminary fundamental technical training.

Having had occasion to lecture on afterburners and flame stabilization to groups of high school students who had no previous training in thermodynamics, fluid mechanics, etc, the reviewer fully appreciates the problems faced by the author in writing the book. As a matter of fact, the author has done a commendable job in explaining the operating principles of the various components of a jet engine. The use of numerous appropriate sketches and figures makes the subject matter easily readable. In some instances, however, the author fails to stimulate the interest of a somewhat brighter student by not adding a note of explanation to various topics. The omission of the variable stator type of compressor is rather unfortunate. The author defines isentropic as "inactive or static condition," and because of the unorthodox nature of this definition an explanation is certainly justified.

Jet Engine Manual, by E. Mangham and A. Peace, Philosophical Library, Inc., New York, 1955, 133 pp.

Reviewed by P. Roy Choudhury
University of Southern California

Unlike "Turbojet Fundamentals," "Jet Engine Manual" gives a detailed description of the components of a jet engine. The authors have discussed the operation of the fuel, lubrication, starter and control systems of turbojet and turboprop engines. In addition to these, the construction and functional details of the two types of engines are discussed. This manual will be very useful to those who are concerned with the maintenance and operation of turbojet and turboprop engines.

The lack of adequate sketches and figures, in many sections, makes it rather difficult to visualize the working of various small components. The addition of appropriate figures will greatly improve the utility of this manual.

Pumps, Fans, and Compressors, by A. de Kováts and G. Desmur, Blackie and Son, Ltd., Glasgow, 1958, xii + 327 pp. 45s.

Reviewed by R. C. Binder
Purdue University

This book is an English translation (by R. S. Eaton of Manchester College) of the original French work "Pompes, Ventilateurs, Compresseurs" (published by Dunod, Paris, 1953). This book discusses the design, construction and operation of centrifugal and axial flow pumps, fans and compressors. It has a practical industrial viewpoint and assumes some knowledge of basic fluid mechanics. In making design studies, some engineers rely heavily on purely theoretical relations. As a contrast, this book by Kováts and Desmur does not follow this purely analytical approach; rather it relies directly on experimental data and empirical relations in many cases.

The book is divided into seven parts with a total of 34 chapters. Some of the chapters are short, but the authors manage to bring out pertinent main topics in a book of moderate size. Part 1, on fundamentals, treats incompressible flow in channels, the flow around blades and through cascades, and fluid power losses. Part 2, on the design and construction of impellers and diffusers, covers performance characteristics, velocity triangles, specific speed, energy losses, cavitation, operation of a pump as a turbine, problems affecting the choice of a machine, impeller design, diffuser, volutes, and axial thrust and balancing devices. Part 3, construction of pumps and fans, describes mechanical details, such as casings, impellers, shafts, bearings and stuffing boxes. Part 4 describes pumps for such special duties as boiler feed, condensate, sewage, dredging and chemical applications. Part 5 gives some examples of the calculation of the principal dimensions of various types of pumps and fans. The various numerical examples and illustrations are very helpful to one interested in learning something about design. Part 6 covers briefly the operation of pumps and fans, along with the selection of type. Parts 1 through 6 are primarily for incompressible flow. Part 7, on turbo-compressors, includes a treatment of basic thermodynamics, the calculation of losses, the selection of compressor type, compressor characteristics, the mechanical details of compressors, and an example of the thermodynamic calculation of a compressor.

This book is more of the practical reference type of book rather than a college text. It should be useful to the engineer who may be concerned with practical problems involving the design, construction and operation of these machines.

Fundamentals of Gas Dynamics, edited by Howard W. Emmons, Vol. III of "High Speed Aerodynamics and Jet Propulsion," Princeton University Press, Princeton, 749 pp. $20.00

Reviewed by Robert A. Gross
Fairchild Engine Division

This book, the sixth to be published in what will be a twelve volume series, is a valuable addition to the aerodynamics literature. Gas dynamics is treated here as a branch of physics and applied mathematics, and this volume reflects the recent rapid growth and increasing breadth of this subject. It contains eight major sections each written by persons well-known for their original contributions to the subject. Because each section of this book strongly reflects its author, each is treated separately in this review.

A Equations of Gas Dynamics; H. S. Tsien, pp. 3–63. This section presents a classical continuum approach to the basic equations of gas dynamics. Equations are developed for quite general flows, and kinetics are discussed only as they effect relaxation times. The equations of motion are expressed finally in general orthogonal coordinates. It is unfortunate this work was completed before the current interest in magnetohydrodynamics, since this subject may well be considered as a domain in gas dynamics.

B One-Dimensional Treatment of Steady Gas Dynamics; L. Crocco, pp. 64–349. This section is nearly a book in itself. It treats many interesting and important subjects from an engineering point of view. Although correction coefficients are frequently employed, the difficult subjects which are discussed require occasional empirical treatment. Some of the topics covered are: Thermodynamics of real substances, shock waves and "pseudo-shocks" (boundary layer-shock interaction in one dimension), nozzle flow, supersonic diffusers, friction in long ducts, heat exchange and combustion, flows with piecewise uniformity, and mixing. The analysis and physical descriptions are coupled with frequent graphs and 67 references.

C One-Dimensional Treatment of Nonsteady Gas Dynamics; A. Kantrowitz, pp. 350–415. This section reflects activity in this field up to about 1952. The fundamental equations are again derived. Plane isentropic waves of large amplitude and weak and strong shocks are discussed. The formation of shocks in channels and nozzles are analyzed along with their stability. Intense explosions and implosions are briefly treated, and, finally, a very short section on the application of pressure waves to heat engines is presented.

D The Basic Theory of Gasdynamic Discontinuities; W. D. Hayes, pp. 416–481. This section presents a theoretical introduction to gasdynamic discontinuities from a quite general point of view, and appears to contain much original work. The basic conservation laws are presented. The existence of various solutions is explored using thermodynamic and stability arguments. Normal shocks, exothermic discontinuities and Chapman-Jouguet conditions are examined. The internal structure of a wave is examined for stability with regard to its ability to jump to another condition. The Navier-Stokes structure of shocks and exothermic discontinuities are treated, and, finally, some physics of shocks, such as radiation, ionization and relaxation are briefly mentioned. Fifty-one references are cited.

E Shock Wave Interaction; H. Polachek and R. Seeger, pp. 482–525. Shock waves are again treated as discontinuities with emphasis on normal and oblique re-

(*Continued on page 308.*)

MISSILE TRACKING

SEA-LAB

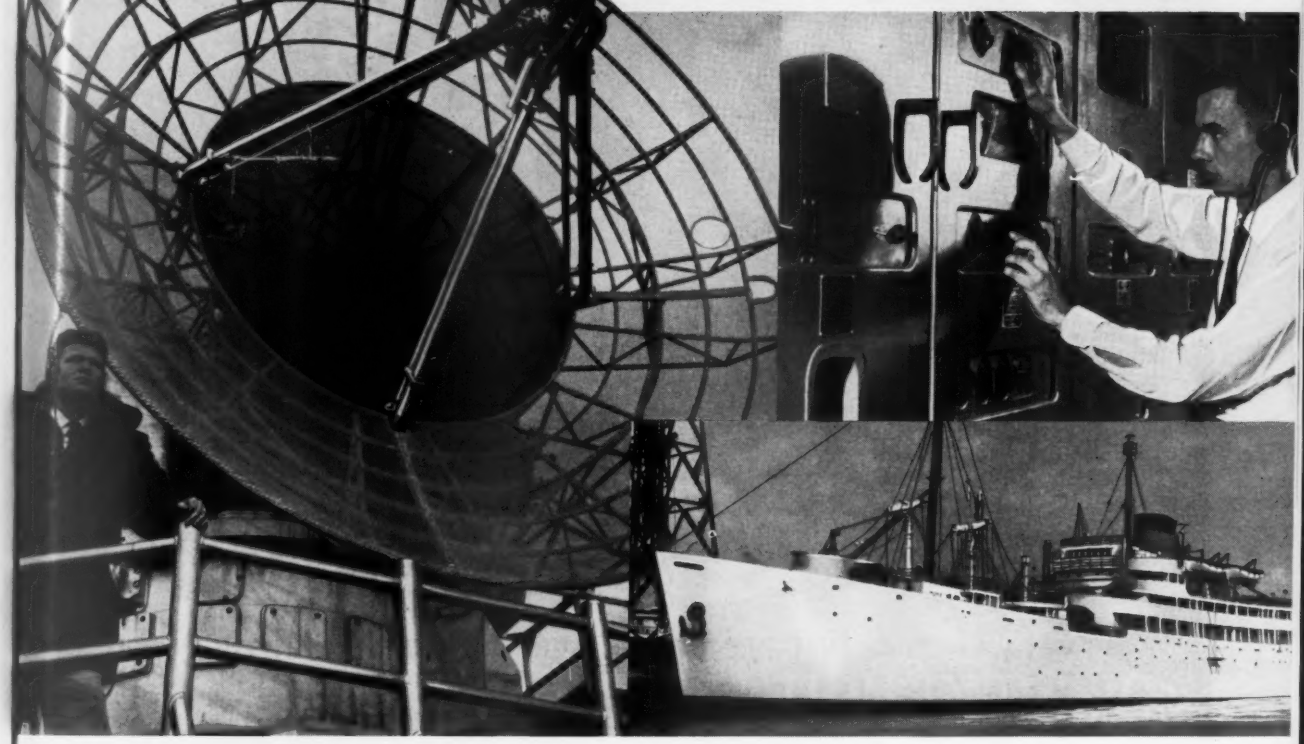

This huge antenna is part of an electronic and optical system that RCA installed and is operating on the S.S. American Mariner. The purpose of the equipment, for which the ship has been refitted, is to provide the most precise data yet obtained at sea on missile flights over a range extending from Cape Canaveral, Fla., to the area of Ascension Island. The project is sponsored jointly by the Advanced Research Projects Agency, Department of Defense and the Army Ordnance Command. A scientific staff—most of them RCA personnel—will operate the equipment and report on missile performance from descent from space to final plunge, the data to be shared by all branches of the armed services.

RCA Tmk(s) ®

RADIO CORPORATION of AMERICA

DEFENSE ELECTRONIC PRODUCTS

CAMDEN, N. J.

STORABILITY

Just one of the many outstanding attributes of

DIMAZINE®

unsym-Dimethylhydrazine

DIMAZINE has many characteristics that make it excel as a storable fuel.

Its remarkable stability has been proven in tests of more than two years' duration, even in mild-steel vessels. Its high thermal stability and low freezing point permit wide variations of storage temperatures. It is not shock sensitive and is unaffected by many types of accidental contamination. It is highly compatible with most metals and appropriate sealant materials.

Excellent storability, high performance, ease of handling, ample availability . . . these and many other advantages are combined in DIMAZINE, the outstanding storable fuel.

We will be pleased to assist in your evaluation of DIMAZINE and to supply detailed data on its properties and handling.

fmc
FOOD MACHINERY AND CHEMICAL CORPORATION ®

Putting Ideas to Work

FOOD MACHINERY AND CHEMICAL CORPORATION

Westvaco Chlor-Alkali Division

General Sales Offices:
161 E. 42nd STREET, NEW YORK 17

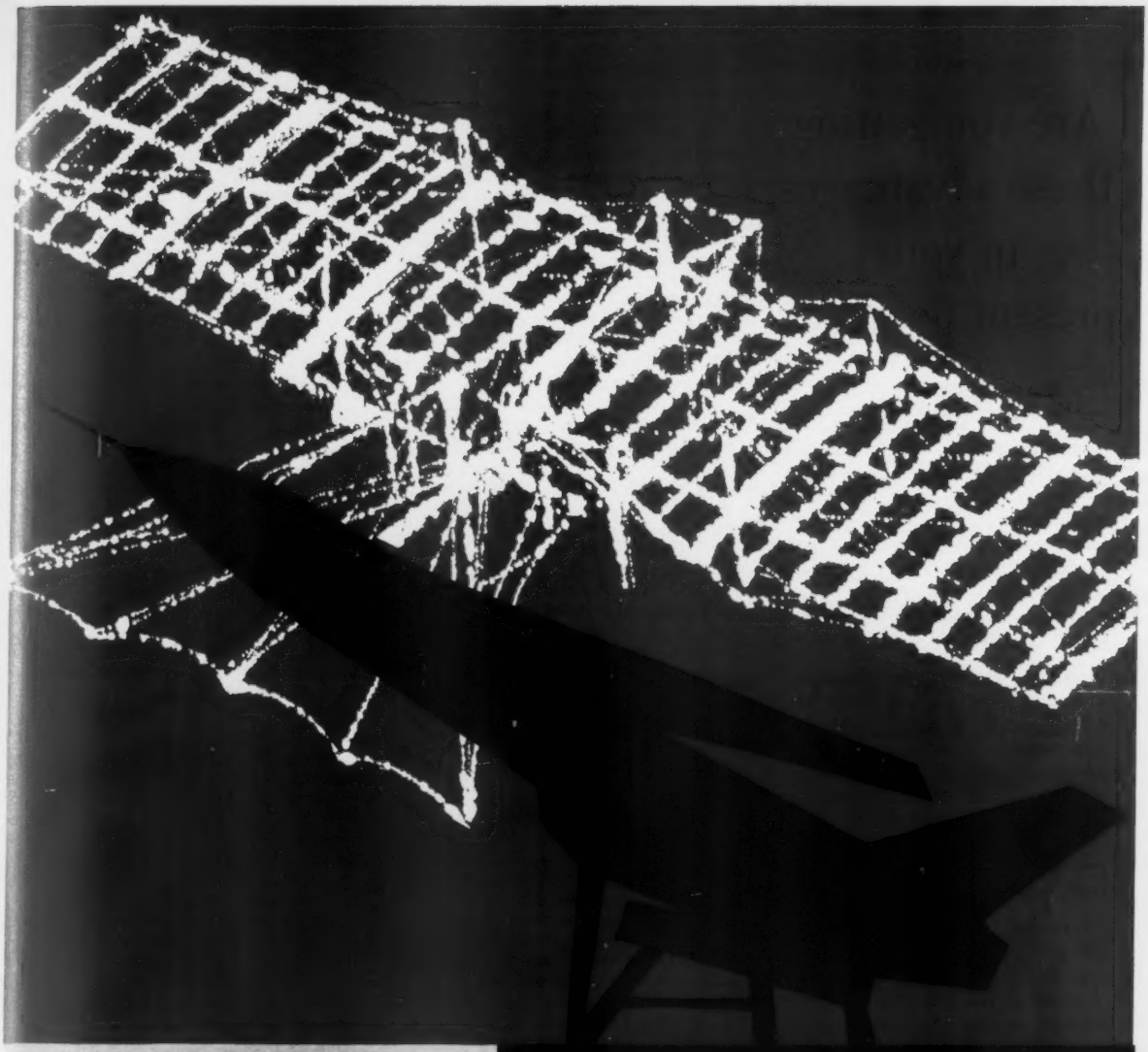

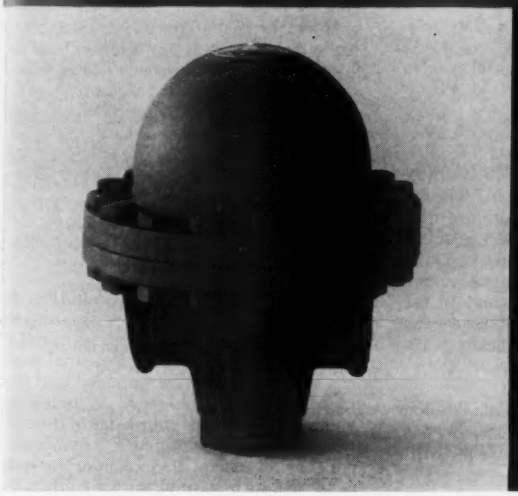

REVOLUTION IN DESIGN

As revolutionary in design and engineering as the technological transition from flying machine to space vehicle... Achieved a quarter of a century ago, the only regulators which could be used for the first missile experiments in the Navy Experimental Station at Annapolis ...still today the standard for the critical control of high pressure fluids... Now on the threshold of space, Grove is uniquely prepared—through advance research and development—to meet the challenge of even higher pressures ahead.

GROVE POWREACTOR DOME REGULATOR MODEL GH-408–50-6000 PSI INLET...5-3000 PSI REDUCED PRESSURE

GROVE VALVE and REGULATOR COMPANY

6529 Hollis St., Oakland 8, California • 2559 W. Olympic Blvd., Los Angeles 6, California

Offices in other principal cities

Subsidiary of Walworth

ENGINEERS · SCIENTISTS

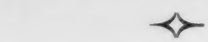

Are you getting these advantages in your present position?

☐ **Space-Age Assignments**

Advanced studies at Boeing include boost-glide vehicles, anti-ballistic missile area defense systems, supersonic missiles, interplanetary systems, and manned and unmanned space vehicles.

☐ **Advanced Research Facilities**

Boeing's research, development and engineering facilities are among the most varied, extensive and complete in the industry. Your progress is faster. And you work with men who have "written the book" on the state-of-the-art.

☐ **Opportunity for Advancement**

At Boeing, you work with small, integrated teams where initiative and ability get plenty of visibility. A personal merit review every six months assures continuing opportunity for individual recognition. And you are eligible for advancement to a higher level at any time.

☐ **Better Family Living**

There's a real bonus of better living in the heart of the evergreen Puget Sound country. Four full seasons of comfortable moderation in an area where scenery and outdoor recreation are nation-famed. To give you an idea: per capita ownership of sail and power boats in Seattle is the highest in America.

Write *today* for your free copy of the 24-page book "Environment for Dynamic Career Growth." Indicate your degree(s) and field of interest. Address: Mr. Stanley M. Little, Boeing Airplane Co., P.O. Box 3822 - JPA, Seattle 24, Washington.

BOEING

flections. Some excellent photographs of such waves are presented. Some mention of detonation, refraction of shocks and particle models of continuum are made. Sixty-one references are cited.

F Condensation Phenomena in High Speed Flow; H. G. Stever, pp. 526–573. Condensing vapors are first treated as an equilibrium problem. The kinetics of condensation are theoretically treated and then applied to high speed flow. Some experimental techniques are outlined; their results presented and compared with theory. It is concluded that the phenomena are well understood, but thermodynamic data and more precise and usable calculations are needed.

G Gas Dynamics of Combustion and Detonation:

1 Aerothermodynamic Problems of Combustion; T. von Kármán, pp. 574–584. The case of one-dimensional flow of a gas mixture in which chemical reactions take place is formulated. Approximations are made and the eigenvalue flame speed problem is discussed.

2 Flow Discontinuities Associated with Combustion; H. W. Emmons, pp. 584–621. The theoretical formulation of the flame speed problem is presented along with a discussion of its inadequacies. The flame front is then treated as a discontinuity in one- and two-dimensional flows. Flame generated vorticity is discussed. Finally, the stability of flame discontinuities is treated analytically.

3 Gas Dynamical Aspects of Detonation; G. I. Taylor and R. S. Tankin, pp. 622–686. The Chapman-Jouguet theory of detonation is presented along with several numerical examples. The possibility of strong and weak detonations is discussed in some detail, and the transformation from deflagration to detonation is examined for some particular cases. Interesting sections on spherical detonation, spinning detonation and explosions in solids and liquids are presented.

H Flow of Rarified Gases; S. Schaaf and P. Chambré, pp. 687–739. This section gives a modern summary of this subject including free molecular flow, heat transfer, aerodynamic forces, nonsteady flows, slip flow and experimental results.

This book despite its size, does not attempt to treat all of gas dynamics. Transonics, mixed flow problems and boundary layers are not included in this volume. It suffers somewhat from repetition, resulting from the numerous contributors. The fine photographs are often located far from their associated text. These are minor distractions however, and this undoubtedly is an outstanding work in gasdynamic fundamentals and will be a standard reference for future research efforts in this fascinating and still growing field.

Principles and Applications of Random Noise Theory, by Julius S. Bendat, John Wiley and Sons, Inc., New York, 1958, ix+ 422 pp. $11.00.

Reviewed by G. J. MURPHY
Northwestern University

According to the author, this book was written for advanced senior students and graduate students in engineering, applied mathematics, or physics. The author's purpose is to "present a systematic development of topics deemed to be most fundamental in random noise theory, and show how to apply the theory in certain areas of far-reaching importance which are not covered elsewhere."

His primary objective in the first four chapters is "to explain principles of random noise analysis and optimum filtering techniques in understandable engineering language, emphasizing physical meanings and mathematical expressions." In the opinion of this reviewer he has partially succeeded, in that he does discuss, in "engineering language," the principles of random noise analysis and optimum filtering techniques, and he does emphasize physical significance.

However, his attention to mathematical detail is far from adequate. For example, on page 21, in making the transition from (1–60) to (1–69) he neglects to mention that the conditions under which one may change the order of differentiation and integration are restricted. As a result of his failure to recognize this restriction, he concludes that for all stationary random processes the slope of the autocorrelation function is zero for zero argument. Then on the next page he presents an example in which this conclusion is contradicted, and on pages 204 through 206 he attempts at great length to force an (unjustifiable) agreement of that example with the incorrect conclusion.

In the remaining six chapters of the book, the author's objectives are "to show how: (a) to formulate certain difficult noise problems; (b) to obtain their mathematical solutions, and (c) to draw proper physical designs and interpretations." Particularly noteworthy inclusions are the work of S. O. Rice on the distribution of a fixed sine wave plus random noise, a chapter on envelope detection, a chapter on analogue computer techniques, and a liberal discussion of time-varying filters.

The book is enhanced by the use of chapter summaries, immediately following the table of contents, giving the reader a concise statement of the scope of each chapter, and by the effective use of modern techniques of layout, printing and binding.

This book is recommended to both the university student and the research worker interested in random noise theory.

Nuclear Rocket Propulsion, by R. W. Bussard and R. D. De Lauer, McGraw-Hill Book Co., New York, 1958, 370 pp.

Reviewed by DONALD H. LOUGHRIDGE
General Motors Corp.

The title of this book will doubtless attract much attention, since the subject matter has at present so much technical as well as political glamor. Potential readers, however, should be reminded that due to existing military secrecy, a complete review of present U. S. knowledge of the subject cannot be expected. Accordingly, only overall general discussions of the state of the art are presented, with no direct discussion of the KIWI or SNAP projects. Chapters on basic rocket performance and system analysis contain much engineering data and formulas which have been collected and are useful for the design en-

(*Continued on page 311.*)

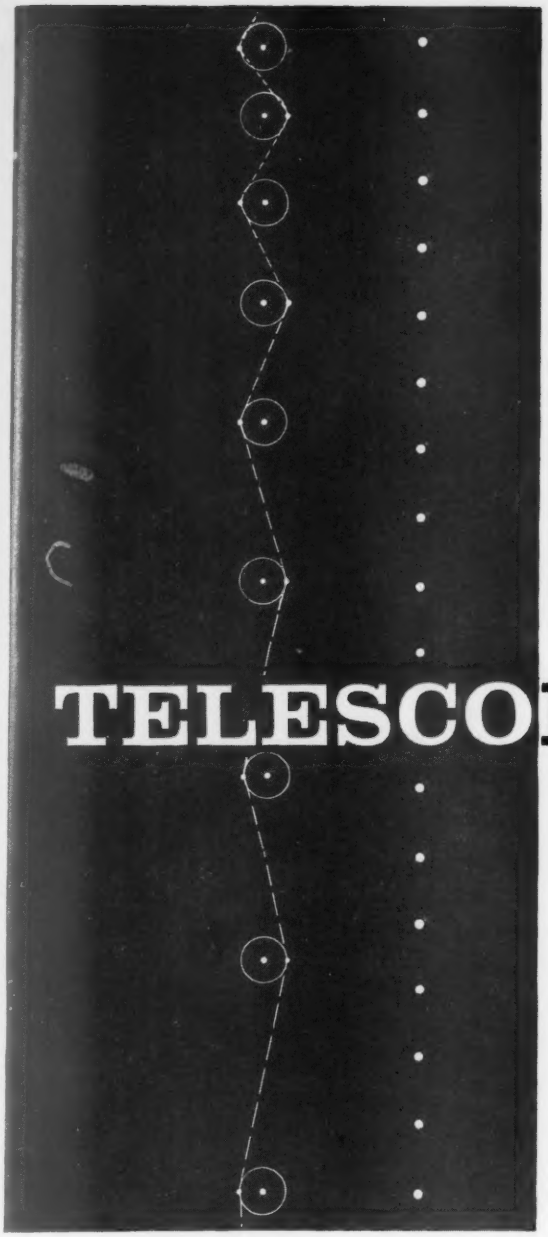

ENGINEERS–SCIENTISTS

Engineers and Scientists at Republic Aviation—with a turn for dry professional humor—say that they're asked to solve every problem of upper atmosphere and space flight with the factor

$$\sqrt{1-\frac{v^2}{c^2}}$$

This human application of the relativistic theory of space-time relationships is predicated on the conviction that the creative content of technological thinking can be immeasurably expanded and enriched—given a propitious environment.

That the environment at Republic *is* propitious, is evident from the results.

Engineers and scientists like it. They thrive on it. Technical ideas of a "revolutionary" character—rather than "evolutionary"—are appearing at a rate that exceeds the norm of even 5 years ago.

In every professional area—research, development, experimental engineering—*the goal is the same:*

TELESCOPING TIME

in terms of technological progress

▶ *in exotic propulsion systems for space operation—plasma propulsion...advanced nuclear power applications...*

▶ *in integrated electronic systems for flight vehicles to operate at every altitude*

▶ *in supersonic and hypersonic weapons systems, both manned and unmanned*

For an invigorating environment, where new ideas flourish, look at the range of opportunities at Republic

ELECTRONICS
Inertial Guidance & Navigation • Digital Computer Development • Systems Engineering • Information Theory • Telemetry-SSB Technique • Doppler Radar • Countermeasures • Radome & Antenna Design • Microwave Circuitry & Components • Receiver & Transmitter Design • Airborne Navigational Systems • Jamming & Anti-Jamming • Miniaturization-Transistorization • Ranging Systems • Propagation Studies • Ground Support Equipment

THERMO, AERODYNAMICS
Theoretical Gasdynamics • Hyper-Velocity Studies • Astronautics Precision Trajectories • Airplane/Missile Performance • Air Load and Aeroelasticity • Stability and Controls • Flutter & Vibration • Vehicle Dynamics & System Designs • High Altitude Atmosphere Physics • Re-entry Heat Transfer • Hydromagnetics • Ground Support Equipment

PLASMA PROPULSION
Plasma Physics • Gaseous Electronics • Hypersonics and Shock Phenomena • Hydromagnetics • Physical Chemistry • Combustion and Detonation • Instrumentation • High Power Pulse Electronics

NUCLEAR PROPULSION & RADIATION PHENOMENA
Nuclear Weapons Effects • Radiation Environment in Space • Nuclear Power & Propulsion Applications • Nuclear Radiation Laboratories

A new $14,000,000 Research Center—to be completed this year—is part of Republic's far-ranging R&D programs aimed at major state-of-the-art breakthroughs in every flight regime and environment.

Send resume in complete confidence to:
Mr. George R. Hickman, Engineering Employment Mgr. Dept. 10D

REPUBLIC AVIATION
Farmingdale, Long Island, New York

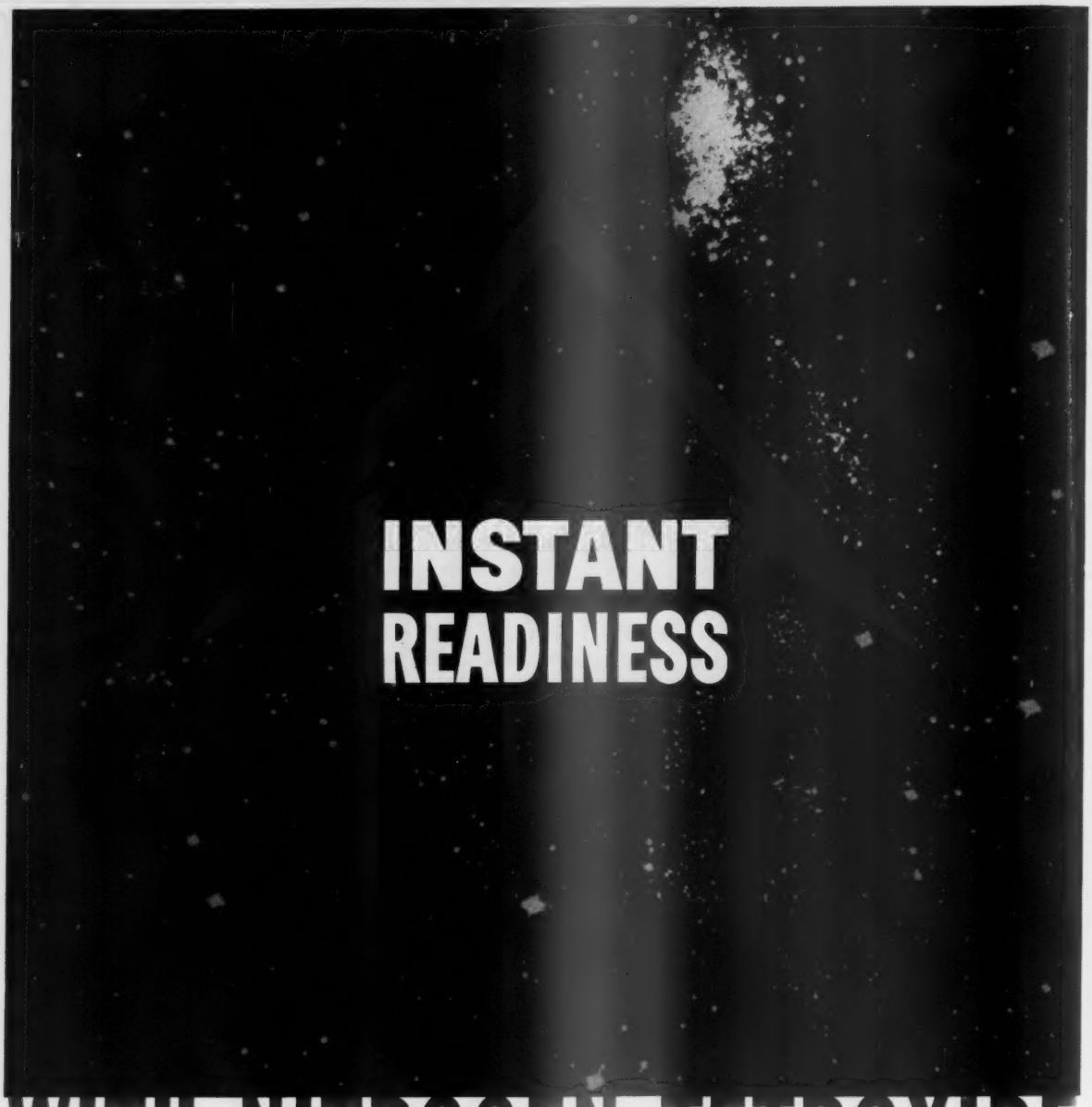

INSTANT READINESS

WITH NITROGEN TETROXIDE

. . . Requires no refrigeration . . . Easier to store than liquid oxygen

Performance of Nitrogen Tetroxide as an oxidizer for many fuels is comparable to that of liquid oxygen. In convenience it is far superior to liquid oxygen.

N_2O_4 can be shipped easily and stored indefinitely without refrigeration in ordinary carbon steel containers. It is a dense, mobile liquid that is noncorrosive if kept dry. The quantity of oxygen contained per unit volume of N_2O_4 is 1.01 Kg/liter at 20°C.

N_2O_4 is available in tank car quantities from Allied's Hopewell, Virginia plant. For experimental purposes, N_2O_4 is available in 125 lb. cylinders and 2000 lb. containers. Write for technical data, and information on prices and delivery.

N_2O_4 Oxidant for liquid rocket propellants

Molecular weight	92.02
Boiling Point	21°C
Freezing Point	−11.3°C
Latent Heat of Vaporization	99 cal/gm @ 21°C
Critical Temp.	158°C
Critical Pressure	99 atm
Specific Heat of Liquid	0.36 cal/gm −10 to 20°C
Density of Liquid	1.45 gm/ml at 20°C
Density of Gas	3.3 gm/liter 21°C, at 1 atm
Vapor Pressure	2 atm at 35°C

"Basic To America's Progress"

Allied Chemical

NITROGEN DIVISION

Dept. NT 4A-12-5, 40 Rector St., New York 6, N. Y.

gineer working in this field. References to original papers are given at the end of each chapter. However, for the technical reader who may be interested in more basic concepts and their interrelationships, such a purely engineering approach is never very satisfying. A chapter on heat transfer and fluid flow and the following one on materials constitute about a third of the book and proved, to the present reviewer, to be the most useful and convincing part of the text. The following chapter on nucleonics depends upon a previous knowledge of elementary reactor theory, and without such, a reader would find little usefulness in this cursory survey. The treatments of system control and testing could just as well apply to any power reactor as to the particular application to nuclear rockets. The last chapter on advanced and exotic systems gives a short discussion of gaseous-fission, thermomechanical and accelerator systems which are under such wide study at present.

It is to be regretted that with such a great deal of work as has evidently been expended by the authors in collecting the wide range of engineering data here presented, more direct reference to the work of the Los Alamos and Livermore Laboratories in the field of nuclear rockets was not apparently cleared for publication. It is to be hoped that within a year or so a second edition of this book can be produced, the contents of which will more closely conform to the title of the book.

Technical Literature Digest

M. H. Smith, *Associate Editor,* **and M. H. Fisher,** *Contributor*
The James Forrestal Research Center, Princeton University

Jet Propulsion Engines

TRIDAC Flight Simulator for Missiles, by J. J. Gait, *Fusées et Recherche Aeron.*, vol. 3, April 1958, pp. 10–19. (In French.)

British Rockets and Missiles, by J. Pellandini, *Fusées et Recherche Aeron.*, vol. 3, April 1958, pp. 29–33. (In French.)

A Theoretical and Experimental Investigation of the Aerothermopressor Process, by Alve J. Erickson, *MIT, Dept. Mech. Engng., Gas Turbine Lab.*, May 1958, 171 pp.

A Simplified Method for Estimating the Performance of Supersonic Ram-jets, by B. P. Beeton, *Aeron. Quart.*, vol. 9, Aug. 1958, pp. 195–212.

Theoretical Investigation on the Fluidodynamics of "Wave-engines" Operating According to the Principle of the "Comprex," by Dino Dini, *L'Aerotecnica*, vol. 38, Feb. 1958, pp. 8–18. (In Italian.)

DeHavilland Dual Spectra Rocket, *Aviation Week*, vol. 69, Aug. 25, 1958, p. 25.

Engineering Method of Ram-jet Thrust Determination Based on Experimentally Obtained Combustor Parameters, by H. Rudolph Dettwyler and Maxime A. Faget, *NACA Res. Mem.* L53E21, Aug. 1953, 44 pp., diagrs., tab. (Declassified from Confidential by authority of *NACA Res. Abstr.* 128, 7/28/58.)

Military Studies Rocket Test Chamber, by Michael Yaffee, *Aviation Week*, vol. 69, Aug. 4, 1958, pp. 51, 53, 55.

Aerodynamics of Jet Propelled Missiles

Effects of Boundary-layer Displacement and Leading-edge Bluntness on Pressure Distribution, Skin Friction, and Heat Transfer of Bodies at Hypersonic Speeds, by Mitchel H. Bertram and Arthur Henderson Jr., *NACA TN* 4301, July 1958, 33 pp.

Laminar Incompressible Boundary Layer Flow over the Cylindrical Portion of Slender Bodies of Revolution at Small Angles of Attack, by John C. Martin and Nathan Gerber, *Aberdeen Proving Ground, Ball. Res. Labs., Rep.* 1038, Nov. 1957, 54 pp.

An Experimental Investigation of the Stability of the Hypersonic Laminar Boundary Layer, by Anthony Demetriades, *Calif. Inst. Tech., Guggenheim Aeron. Lab., Hypersonic Res. Proj., Mem.* 43, May 1958, 85 pp.

An Experimental Investigation of the Turbulent Boundary Layer behind a Forward Facing Step in Supersonic Flow, by Dave Robert Moore, *Univ. of Texas, Defense Res. Lab.* CF 2707, (*DRL*-425), April 1958, 27 pp., 3 tabs., 25 figs.

Dynamic Stability of Vehicles Traversing Ascending or Descending Paths through the Atmosphere, by Murray Tobak and H. Julian Allen, *NACA TN* 4275, July 1958, 35 pp.

Inviscid Hypersonic Flow Near the Stagnation Point of Oblate Ellipsoidal Noses, by Marcel Vinokur, *J. Aero/-Space Sci.*, vol. 25, July 1958, pp. 469–470.

Flight Measurements of Average Skin-friction Coefficients on a Parabolic Body of Revolution (NACA RM-10) at Mach Numbers from 1.0 to 3.7, by J. Dan Loposer and Charles B. Rumsey, *NACA Res. Mem.* L54G14, Aug. 1954, 32 pp. (Declassified from Confidential by authority of *NACA Res. Abstr.* 129, 7/17/58.)

Flow Around a Cone at Angle of Attack at High Supersonic Speeds, by A. L. Gonor, *Akademii Nauk SSSR, Izvestiia, Otdelenie Tekhnicheskikh Nauk*, no. 7, July 1958, pp. 102–105. (In Russian.)

An Estimate of the Fluctuating Surface Pressures Encountered in the Reentry of a Ballistic Missile, by Edmund E. Callaghan, *NACA TN* 4315, July 1958, 18 pp., diagrs.

Wind Tunnel Investigation at Mach Numbers of 2.0 and 2.9 of Several Configurations of a Supersonic Ram-jet Test

EDITOR'S NOTE: Contributions from Professors E. R. G. Eckert, J. P. Hartnett, T. F. Irvine Jr. and P. J. Schneider of the Heat Transfer Laboratory, University of Minnesota, are gratefully acknowledged.

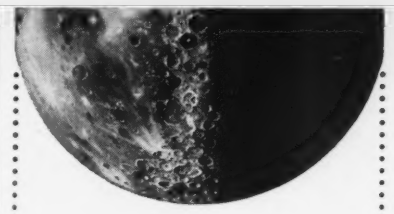

Our Advanced Design Group is at work on

NUCLEAR ROCKET ENGINES

and needs the help of the following men

Senior Engineer. MS or PhD. He will study nuclear engine applications, determine the most suitable missions, correlate engine thrust requirements with vehicle performance, and evaluate vehicle and engine system design problems peculiar to the thermal, nuclear, and space environment of nuclear missile systems.

Senior Engineer. MS or PhD. He will make system dynamic studies of nuclear rocket engine systems to determine system stability and operational characteristics, establish control system requirements to obtain required accuracy and response characteristics, and synthesize new methods of control required by thermal and nuclear radiation environment.

Senior Design Engineers or Specialists. BA or MS or equivalent. These men should be conceptual rocket engine designers with experience in turbopump or high speed rotating machinery layouts and familiarity with combustion devices. They should be creative designers, oriented toward preliminary design.

Please write to Mr. A. D. Jamieson, Engineering Personnel Dept., 6633 Canoga Avenue, Canoga Park, Calif.

ROCKETDYNE

A DIVISION OF NORTH AMERICAN AVIATION, INC.

FIRST WITH POWER FOR OUTER SPACE

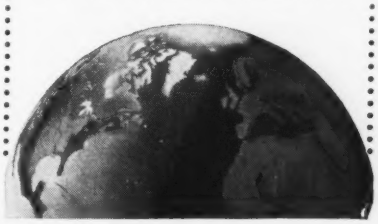

AEROJET...
for engineering careers

STRESS ANALYSTS

1. Experience and/or training in *analytical* stress computations, with emphasis on structural and pressure vessel applications. B.S. required; graduate work desirable.

2. Experience and/or training in *experimental* stress analysis. Familiarity with advanced experimental techniques and expedient methods of stress analysis. B.S. required; graduate work desirable.

GAS DYNAMICIST

M.S. or Ph.D. in engineering, physics or applied mechanics. Five to ten years' experience in analytical and experimental work in the fields of boundary layer studies, supersonic and hypersonic flows, or application of non-ideal-gas theories.

AERODYNAMICIST

M.S. or Ph.D. in aeronautical or mechanical engineering or applied mechanics. Five to ten years' experience in the field of advanced aerothermodynamics, missile aerodynamics, heat transfer in rockets, missiles, etc.

MISSILE SYSTEMS ANALYST

B.S., M.S. or Ph.D. in engineering, physics or applied mechanics. Five to ten years' experience in analysis and evaluation of interactions between propellant systems and other missile components. Capable of developing optimum vehicle configurations from the standpoint of the propulsion system.

U.S. Citizenship Required

Resumes cordially invited. Write:

E. P. JAMES
AEROJET-GENERAL CORPORATION
P.O. BOX 1947
SACRAMENTO, CALIFORNIA

Vehicle, by J. Richard Spahr and Robert A. Robinson, *NACA Res Mem.* A50C20, Aug. 18, 1950, 61 pp. (Declassified by authority of *NACA Res. Abstr.* 126, 6/24/58.)

Heat Transfer and Fluid Flow

Flow of Conducting Fluids Past Magnetized Bodies, by A. Kulikovskii, *Doklady Akad. Nauk SSSR,* vol. 117, no. 2, Nov. 11, 1957, pp. 199–202. (In Russian.)

Some Investigations on Arc Discharges in Helium and Hydrogen at High Pressures, by A. Michels, H. Tjin, A. Djie, H. DeKluiver and C. A. Ten Seldam, *Physica,* vol. 23, no. 12, Dec. 1957, pp. 1115–1125.

Plasma Jet: Research at 25,000 F, by J. W. Reid, *Machine Design,* vol. 30, no. 3, Feb. 6, 1958, pp. 22–24.

On the Visualization of Laminar Boundary Layer Oscillations and the Transition to Turbulent Flow, by H. Bergh and B. Van Den Berg, *Zeitschrift fur Angewandte Mathematik und Physik,* vol. 9, 1958, pp. 97–104.

Influence of Free-Stream Turbulence on Heat Transfer by Convection from Isolated Region of Plane Surface in Parallel Air Flow, by A. Edwards and B. N. Furber, *Proc. Inst. Mech. Engrs.,* vol. 170, no. 28, 1956, pp. 941–954.

Heat Transfer in a Laminar Boundary Layer with Constant Fluid Properties and Constant Wall Temperature, by A. Smith and D. Spalding, *J. Roy. Aeron. Soc.,* vol. 62, Jan. 1958, pp. 60–64.

Heat Transfer from Surfaces of Nonuniform Temperature, by D. Spalding, *J. Fluid Mech.,* vol. 4, May 1958, pp. 22–32.

A Boundary-layer Treatment of Laminar-film Condensation, by E. Sparrow and J. Gregg, *ASME Paper* 58-SA-2, June 1958.

On the Aerodynamic Heating of Blunt Bodies, by E. Van Driest, *ZAMP,* vol. 9, 1958 pp. 233–248.

Prediction of Flashing Water Flow through Fine Annular Clearances, by A. Agostinelli and V. Salemann, *ASME Paper* 57–A–78, Dec. 1–6, 1957, 5 pp.

Heat-transfer and Pressure-drop Characteristic of Internal Finned Tubes, by E. C. Brouillette, T. R. Mifflin and J. E. Myers, *ASME Paper* 57–A–47, Dec. 1–6, 1957, 9 pp.

Subcritical and Critical Flow through Strain-through Elbow, and Tee A-N Fittings and Sharp-edged Orifices at Elevated Temperatures, by A. L. Ducoffe, J. R. Bennett and C. G. Ray, *ASME Paper* 57–A–60, Dec. 1–6, 1957, 8 pp.

Local Laminar Heat Transfer in Wedge-shaped Passages, by E. R. G. Eckert, T. F. Irvine Jr. and J. T. Yen, *ASME Paper* 57-A-133, Dec. 1-6, 1957, 6 pp.

Effect of Heat Transfer on Flow Field at Low Reynolds Numbers in Vertical Tubes, by T. J. Hanratty, E. M. Rosen and R. L. Kabel, *Ind. & Engng. Chem.,* vol. 50, no. 5, May 1958, pp. 815–820.

Heat Transfer in Fully Developed Flow between Parallel Plates with Variable Heat Sources, by A. L. Loeffler Jr., *Nuclear Sci. & Engng.,* vol. 2, no. 5, Sept. 1957, pp. 547–566.

Non-Newtonian Flow, by W. L. Wilkinson, *Indust. Chemist,* vol. 34, Feb. 1958, pp. 79–84.

Investigation of Effective Thermal Conductivities of Powders in Various Gases, by R. G. Deissler and J. S. Boegli, *ASME Paper* 57–A–110, Dec. 1–6, 1957, 7 pp.

Prismatic Fin with Non-linear Heat Loss Analyzed by Resistance Network and Iterative Analogue Computer, by M. Hutcheon and D. Spalding, *Brit. J. Appl. Phys.,* vol. 9, 1958, pp. 185–191.

Heat Transfer from Rods Normal to Subcooled Water Flow for Non-boiling and Surface-boiling Conditions up to and including Burnout, by S. P. Kezios and R. K. Lo, *Argonne Nat. Lab.* (*U.S. AEC*) ANL-5822, Jan. 1958, 12 pp.

On the Uniqueness of the Solution of Stephan's One-dimensional Problem for a Heat Conducting Medium in One-phase Initial State, by L. I. Rubinshtein, *Doklady Akad. Nauk SSSR,* vol. 117, no. 3, Nov. 21, 1957, pp. 387–390. (In Russian.)

Heat and Mass Exchange in Forced Flow around Bodies of Various Shapes, by O. Krischer and G. Loos, *Chemie-Ingenieur-Technik,* vol. 30, no. 2, Feb. 1958, pp. 69–74. (In German.)

Mass Transfer in Liquid Metal Systems, II: Isothermal Transfer, by J. W. Taylor, and A. G. Ward, *Nuclear Power,* vol. 3, no. 23, March 1958, pp. 101–105.

Measurement of Intense Beams of Thermal Radiation, by A. Broida and A. B. Willoughby, *J. Optical Soc. Amer.,* vol. 48, no. 5, May 1958, pp. 344–350.

Some High-pressure, High-temperature Apparatus Design Considerations: Equipment for Use at 100,000 Atmospheres and 3000°C, by H. T. Hall, *Rev. Sci. Instr.,* vol. 29, no. 4, April 1958, pp. 267–275.

Apparatus for Precision Flash Radiography of Shock and Detonation Waves in Gases, by H. T. Knight and D. Venable, *Rev. Sci. Instr.,* vol. 29, no. 2, Feb. 1958, pp. 92–98.

Combustion, Fuels and Propellants

Combustion—an Aeronautical Science, by H. W. Emmons, (The 1958 Minta Martin Aeron. Lecture), *Inst. Aeron. Sci., SMF Fund Paper* FF19, 1958, 36 pp.

Aerodynamics of Flame Stabilization; Experimental Procedures, by A. Sherman, *Princeton Univ., Dept. Aeron. Engng., Rep.* 426, July 1958, 23 pp.

Effect of Pressure on Turbulent Burning Velocity, by B. Fine, *Combustion and Flame,* vol. 11, June 1958, pp. 109–116.

Separation of the Products of Cool Flame Oxidation of Propane, by C. R. Yokley and R. E. Ferguson. *Combustion and Flame,* vol. 11, June 1958, pp. 117–128.

The Detonability Envelope of Gaseous Fuming Nitric Acid-*n*-Heptane-Nitrogen Mixtures as a Function of Initial Pressure, by R. L. Potter and D. H. Wayman, *Combustion and Flame,* vol. 11, June 1958, pp. 129–136.

The Hydrazine Flame, by M. Gilbert, *Combustion and Flame,* vol. 11, June 1958, pp. 137–148.

Kinetics of Hydrazine Decomposition in a Laminar Non-isothermal Flow, by M. Gilbert, *Combustion and Flame,* vol. 11, June 1958, pp. 149–156.

Gaseous Nitric Acid - Hydrocarbon Flames, by J. Mertens and R. L. Potter, *Combustion and Flame,* vol. 11, June 1958, pp. 181–192.

Some Recent Developments Concerning Free Radicals (A Review), by G. J. Min-

CHEMISTRY

Expanding the Frontiers of Space Technology

Research and Development facilities in the Stanford Industrial Park at Palo Alto, California, provide the latest in technical equipment.

(above) Synthesizing high-energy propellant in development of new and exotic fuels in propulsion chemistry laboratory.

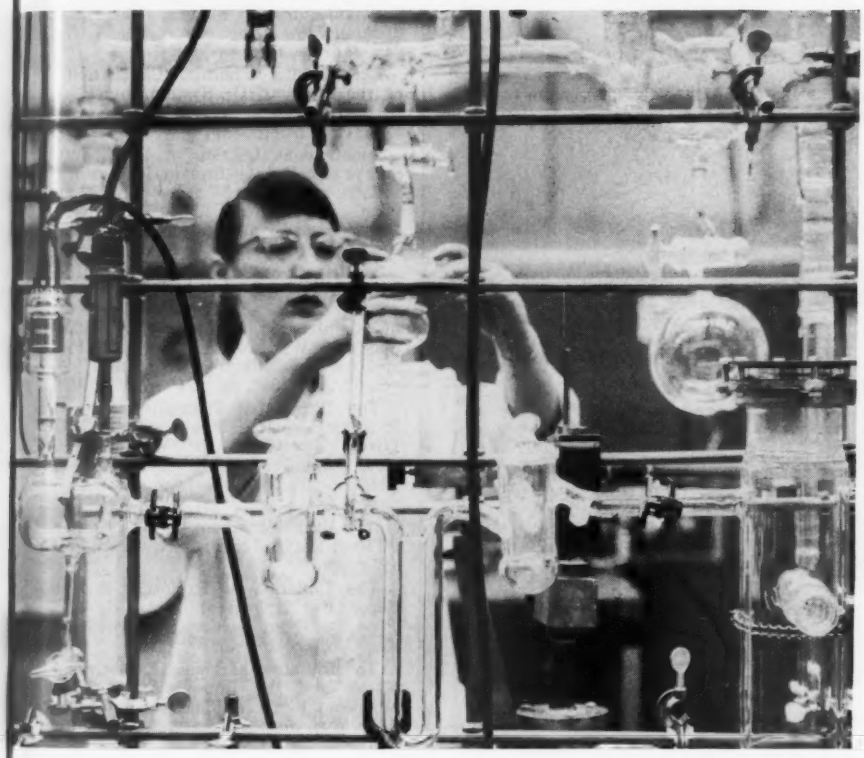

(left) Vacuum systems used in study of gas metal reactions at elevated temperatures – one of many studies in materials research program.

At Lockheed, chemistry plays a highly important role in materials, research, metallurgy, solid state electronics, ordnance, propulsion and test. Applications are for advanced missile, spacecraft and nuclear projects.

Special programs include: research in high and low temperature materials; radio-active and toxic materials; pure metals; properties of beryllium and the alloys and the development of refractory and special-purpose metals, cermets and ceramics.

Other chemical studies embrace reaction kinetics and thermodynamics, and the development of new and exotic fuels, high-energy batteries and fuel cells, and explosives. In electrochemistry, solid state work is directed to related fuel research in electrode reaction kinetics and materials synthesis by electrochemical methods and vacuum deposition.

The test laboratories assay raw materials, evaluate materials and components and assist in design and development.

Scientists and engineers of outstanding talent and inquiring mind are invited to join us in the nation's most interesting and challenging basic research programs. Write: Research and Development Staff, Dept. D-25, 962 W. El Camino Real, Sunnyvale, California.

"The organization that contributed most in the past year to the advancement of the art of missiles and astronautics." NATIONAL MISSILE INDUSTRY CONFERENCE AWARD

Lockheed / **MISSILES AND SPACE DIVISION** / SUNNYVALE, PALO ALTO, VAN NUYS, SANTA CRUZ, SANTA MARIA, CALIFORNIA
CAPE CANAVERAL, FLORIDA
ALAMOGORDO, NEW MEXICO

HAWS DRENCH SHOWERS

RID THE BODY OF CAUSTICS and CHEMICALS
Instantly! Thoroughly!

ACCIDENTS with caustic chemicals strike with shocking swiftness—and HAWS Drench Showers are instantly ready to deliver relief just as fast! A solid downpour washes away destructive materials—saving seconds until medical aid arrives, possibly averting serious injury and excessive compensation claims. HAWS Drench Showers can help you! Write for details and illustrated literature.

MODEL 8935—Drench shower augmented by HAWS eye-wash fountain. A complete safety station—always ready!

HAWS **DRINKING FAUCET CO.**
(Since 1909)
1443 FOURTH STREET · BERKELEY 10, CALIFORNIA

SOUTHWEST
"Monoball"®
SELF-ALIGNING BEARINGS

CHARACTERISTICS

	ANALYSIS	RECOMMENDED USE
1	Stainless Steel Ball and Race	For types operating under high temperature (800-1200 degrees F.).
2	Chrome Alloy Steel Ball and Race	For types operating under high radial ultimate loads (3000-893,000 lbs.).
3	Bronze Race and Chrome Steel Ball	For types operating under normal loads with minimum friction requirements.

Thousands in use. Backed by years of service life. Wide variety of Plain Types in bore sizes 3/16" to 6" Dia. Rod end types in similar size range with externally or internally threaded shanks. Our Engineers welcome an opportunity of studying individual requirements and prescribing a type or types which will serve under your demanding conditions. Southwest can design special types to fit individual specifications. As a result of thorough study of different operating conditions, various steel alloys have been used to meet specific needs. Write for Engineering Manual No. 551. Address Dept. JP-59.

SOUTHWEST PRODUCTS CO.
1705 SO. MOUNTAIN AVE., MONROVIA, CALIFORNIA

koff, *Combustion and Flame*, vol. 11, June 1958, pp. 193–207.

Theory of Detonations, I: Irreversible Unimolecular Reaction, by Joseph O. Hirschfelder and Charles F. Curtiss, *J. Chem. Phys.*, vol. 28, June 1958, pp. 1130–1146.

Theory of Detonations, II: Reversible Unimolecular Reaction, by B. Linder, C. F. Curtiss and J. O. Hirschfelder, *J. Chem. Phys.*, vol. 28, June 1958, pp. 1147–1151.

Specific Heat of Liquid Ozone, by Robert I. Brabets and Thomas E. Waterman, *J. Chem. Phys.*, vol. 28, June 1958, pp. 1212–1214.

Determination of Hydrogen Atoms in Rich, Flat, Premixed Flames by Reaction with Heavy Water, by C. P. Fenimore and G. W. Jones, *J. Phys. Chem.*, vol. 62, June 1958, pp. 693–697.

Approximate Solutions of Transient and Two-dimensional Flame Phenomena: Constant-enthalpy Flames, by D. B. Spalding, *Proc. Roy. Soc.*, Series A., vol. 245, June 24, 1958, pp. 352–372.

Experimental Thermal Conductivities of the $N_2O_4 \rightleftarrows 2NO_2$ System, by K. P. Coffin and C. O'Neal Jr., *NACA TN* 4209, Feb. 1958, 22 pp.

Spontaneous Ignition of Pentaborane Sprays in a Hot-Air Stream, by Erwin A. Lezberg and Albert M. Lord, *NACA Res. Mem.* E55F29a, Nov. 1956, 26 pp., diagrs. (Declassified by authority of *NACA Res. Abstr.* 128, 6/24/58.)

The Heats of Combustion and Formation of Hexacyclo $(7:2:1:0^{2,5}:0^{3,10}:0^{4,8}:0^{6,12})$ dodecane; Two Techniques for the Combustion Calorimetry of Volatile Solids, by Ward N. Hubbard, F. R. Frow and Guy Waddington, *J. Phys. Chem.*, vol. 62, July 1958, pp. 821–823.

The Differential Thermal Analysis of Perchlorates, II: The System $LiClO_4$-$LiNO_3$, by Meyer M. Markowitz, *J. Phys. Chem.*, vol. 62, July 1958, pp. 827–829.

Measurement of Flame Speeds by a Nozzle Burner Method, by Carl Halpern. *J. Res., Nat. Bur. Standards*, vol. 60, June 1958, pp. 535–546.

The Initiation of Explosion in Solid Secondary Explosives, by G. B. Cook, *Proc. Roy. Soc., London*, vol. A 246, July 29, 1958, pp. 154–159.

The Initiation of Liquid Explosives by Shock and the Importance of Liquid Break-up, by G. H. Johansson and others, *Proc. Roy. Soc., London*, vol. A 246, July 29, 1958, pp. 160–166.

Materials of Construction

Compatibility of Metals with Liquid Fluorine at High Pressures and Flow Velocities, by Harold W. Schmidt, *NACA Res. Mem.* E58D11, July 1958, 15 pp.

Compressive Strength and Creep of 17-7 PH Stainless-steel Plates at Elevated Temperatures, by Bland A. Stein, *NACA TN* 4296, July 1958, 33 pp.

A Review of Seal Materials for Guided Missile Applications, by Robert J. Berg, *Calif. Inst. Tech., Jet Prop. Lab., Progr. Rep.* 20-340, March 1958, 16 pp.

Dynamic Response of Cylindrical Tanks, by F. L. DiMaggio, *Columbia Univ., Dept. Civil Engng. and Engng. Mech., Rep.* CU-1-58 DA XZ 554 (CE), (*Armed Forces Special Weapons Proj.* 1075), May 1958, 24 pp., 17 figs.

Plastics in the Space Age, by John H.

Lux, *J. Franklin Inst.*, vol. 266, July 1958, pp. 21–26.

Wires and Cables: Vital to Missiles, by Peer Fossen, Raymond M. Nolan, *Missiles and Rockets*, vol. 4, Sept. 8, 1958, pp. 23–25.

Magnesium: Will It Find Biggest Market in Missiles, by Carl N. Mortenson, *Missiles and Rockets*, vol. 4, Sept. 8, 1958, pp. 46–49.

Effect of Temperature on Dynamic Modulus of Elasticity of Some Structural Alloys, by Louis F. Vosteen, *NACA TN* 4348, Aug. 1958, 19 pp., diagrs., tabs.

Influence of Not-working Conditions on High-temperature Properties of a Heat-resistant Alloy, by John F. Ewing and J. W. Freeman, *NACA Rep.* 1341, 1957, 42 pp. (Formerly *TN* 3727.)

Surface Tension at Elevated Temperatures, IV: Surface Tension of Fe-Se and Fe-Te Alloys, by W. D. Kingery, *J. Phys. Chem.*, vol. 62, July 1958, pp. 878–879.

Instrumentation, Data Recording, Telemetering

Theory of Construction of High-speed Automatic Regulating Systems, by M. V. Meerov, *Automatika i Telemekhanika*, vol. 19, no. 7, July 1958, pp. 621–633. (In Russian.)

On the Speediest Transient Process in Servo Systems with Power, Torque and Rate Limitations of the Power Unit, by E. A. Rosenman, *Automatika i Telemekhanika*, vol. 19, no. 7, July 1958, pp. 633–653. (In Russian.)

New Principles for the Design of Telemetering Systems with Time and Width Pulse Modulation, by B. A. Il'in and A. I. Novikov, *Automatika i Telemekhanika*, vol. 19, no. 8, 1958, pp. 757–761. (In Russian.)

Noise Stability of Telemetering Signal Transmission along a Channel, with Fluctuation Noise, by V. A. Kashiriu and G. A. Shastova, *Automatika i Telemekhanika*, vol. 19, no. 8, 1958, pp. 762–775. (In Russian.)

A Constant Liquid Flow Device, by G. H. Laycock, *Brit. J. Appl. Phys.*, vol. 9, Aug. 1958, pp. 333–335.

Pressure Measurement in Armament Research, by A. J. Cable, *NATO, AGARD, Rep.* 177, March 1958, 10 pp., 6 figs.

Simple Surface Thermometer, by C. F. Rothe, *Rev. Sci. Instr.*, vol. 29, no. 5, May 1958, pp. 436–437.

Experimental Studies on the Initiation of Electric Arcs, by T. Yamaguti, *J. Phys. Soc. Japan*, vol. 13, no. 5, May 1958, pp. 520–525.

A Method for the Measurement of Heat Conductivity at 1100°C, by K. Schafer and F. W. Reiter, *Zeitschr. f. Elektrochemie*, vol. 61, no. 9, 1957, pp. 1230–1235. (In German.)

Stabilization of Energy Transfer at Long Distances, by Rene Perret, *France, Ministere de l'Air, Publications Sci. et Tech., Note Tech.* 74, 1958, 104 pp. (In French.)

A Thermistorized Apparatus for Differential Thermal Analyisis, by Jack M. Pakulak Jr. and Guy William Leonard, *NAVORD Rep.* 5829 (*NOTS* 1920), June 1958, 15 pp.

Telemetry Looks into the Future, *Aviation Age*, vol. 30, Aug. 1958, pp. 20–24.

Design Digest: Missile Telemeter

The challenge of outer space has created the need for a man. **Space flight** is his business. **Recognition** is his goal. He'll find it at Martin. He will make decisions, move up as quickly as his abilities take him. If your interests lie in **Astrophysics, Space Mechanics, Systems Dynamics, Magneto Hydrodynamics** or **Aerophysics,** this man could be **you.** Write or phone William Spangler, Manager, Professional Employment, Dept.A-4, The Martin Company, Baltimore 3, Md.

where the North meets the South **MARTIN BALTIMORE**

Nuclear Scientists

Steadily advancing programs at this leading Nuclear firm have created several entirely new positions on the professional staff.

PhD PHYSICIST

Salary range: **$10,000 to $15,000**

—to develop theory, analyze phenomena and predict performance and characteristics of nuclear reactors, and/or recommend experimental research programs.

PhD MATHEMATICIAN

Salary range: **$10,000 to $15,000**

—to deal with advanced problems arising in the design of nuclear reactors and powerplants.

PhD METALLURGIST

Salary range: **$10,000 to $15,000**

—to initiate and evaluate experiments in materials and process development; study irradiation effects.

Inquiries will be held in confidence. Forward complete résumé, including salary requirement, to:

Box 1001
AMERICAN ROCKET SOCIETY
500 Fifth Ave.
New York 36, New York

Mates PDM-FM with FM-PM, *Aviation Age*, vol. 30, Aug. 1958, pp. 126–127.

New Missiles and Spacecraft Challenge Telemetry Technology, *Aviation Age*, vol. 30, Aug. 1958, pp. 128–133.

Lockheed Switches to PAM-FM, *Aviation Age*, vol. 30, Aug. 1958, p. 138.

Light Modulator Records Airborne Radar Displays, by Leo Levi, *Electronics*, vol. 31, Aug. 1, 1958, pp. 80–83.

Guidance Systems and Components

Rocket Guidance as a Problem of Enslaving, by E. Perret, *Fusées et Recherche Aeron.*, vol. 3, April 1958, pp. 21–25. (In French.)

Servomechanisms and Controls

Analytical Method of Synthesis of Linear Control Systems in the Presence of Noise, when Dynamic Precision is Specified, by K. I. Kurakin, *Automatika i Telemekhanika*, vol. 19, no. 5, 1958, pp. 408–417. (In Russian.)

On Improving the Quality of On-Off Control, by A. I. Cherepanov, *Automatika i Telemekhanika*, vol. 19, no. 5, 1958, pp. 471–474. (In Russian.)

Stable Receiving Circuits for Remote Control, by S. J. Neshyba and F. E. Brooks Jr., *Electronics*, vol. 31, Aug. 1, 1958, pp. 74–76.

Flight Vehicle Design and Testing

Stationary Conditions for Problems Involving Time Associated with Vertical Rocket Trajectories, by Angelo Miele, *J. Aero/Space Sci.*, vol. 25, July 1958, pp. 467–469.

Guided Weapons and Aeronautics, by R. Cockburn, *J. Roy. Aeron. Soc.*, vol. 62, Aug. 1958, pp. 539–558.

Solving Missile Problems, *Ordnance*, vol. 43, July-Aug. 1958, p. 149.

Talos Land-based System, by D. B. Holmes, *Ordnance*, vol. 43, July-Aug. 1958, p. 156.

Space Flight

Study of the Vital Activity of Animals in Flight in Rockets in the Upper Atmosphere, by Pokrovski, *Fusées et Recherche Aeron.*, vol. 3, April 1958, pp. 5–9. (In French.)

Regulation of Sovereignty in the Very High Atmosphere and the Law of Space Ships, by E. B. Winandy, *Fusées et Recherche Aeron.*, vol. 3, April 1958, pp. 34–39. (In French.)

Problems Posed by the Law of Astronautics and Atomic Power in Space Flight, by E. B. Winandy, *Fusées et Recherche Aeron.*, vol. 3, April 1958, pp. 40–43. (In French.)

Air Drag Effect on a Satellite Orbit Described by Difference Equations in the Revolution Number, by R. E. Roberson, *Quart. Appl. Math.*, vol. 16, July 1958, pp. 131–136.

Earth-Moon Rocket Trajectories, by Louis Gold, *J. Franklin Inst.*, vol. 266, July 1958, pp. 1–8.

The Human System in Space, by C. Wright Reininger, *Missiles and Rockets*, vol. 4, Sept. 8, 1958, pp. 33–34.

Soviets Certain They'll Be First on Moon, by Dr. Victor P. Petrov, *Missiles and Rockets*, vol. 4, Sept. 8, 1958, pp. 50, 55–58.

An Analytical Solution for Flight Time of Satellites in Eccentiric and Circular Orbits, by F. M. Perkins, *Astronautica Acta*, vol. 4, no. 2, 1958, pp. 113–134.

Orbit Determination from the Vector of Orbit Velocity, by M. Vertregt, *Astronautica Acta*, vol. 4, no. 2, 1958, pp. 135–137. (In German.)

Moon Refueling for Interplanetary Vehicles, *Aviation Age*, vol. 30, Aug. 1958, pp. 22–24.

Design Progress: Missile-launched Manned Space Capsule, *Aviation Age*, vol. 30, Aug. 1958, pp. 172–173.

How to Find Thermal Equilibrium in Space, *Aviation Age*, vol. 30, Aug. 1958, pp. 174–176.

Army Explorer IV Satellite Reports Corpuscular Radiation Intensity, by Evert Clark, *Aviation Week*, vol. 69, Aug. 4, 1958, pp. 30–31.

Ground Testing May Ease Space Problems, by Richard Sweeney, *Aviation Week*, vol. 69, Aug. 4, 1958, pp. 59, 61.

Aerophysics, Astrophysics

High-altitude Atmospheric Density, by Theodore E. Sterne, *Phys. Fluids*, vol. 1, May-June, 1958, pp. 165–170.

Interaction of the Solar Wind with the Geomagnetic Field, by E. N. Parker, *Phys. Fluids*, vol. 1, May-June 1958, pp. 171–187.

The Statistics of Meteors in the Earth's Atmosphere, by Gerald S. Hawkins and Richard B. Southworth, *Smithsonian Contrib. to Astrophys.*, vol. 2, no. 11, 1958, pp. 349–364.

Granulation and Oscillations of the Solar Atmosphere, by Charles Whitney, *Smithsonian Contrib. to Astrophys.*, vol. 2, no. 12, 1958, pp. 365–376.

A Cosmic Ray Increase Related to Solar Activity, by J. Katzman, *Canadian J. Phys.*, vol. 36, July 1958, pp. 807–815.

Analysis of Meteoric Body Doppler Radar Records Taken during a Geminid Shower Period, by M. Srimama Rao, *Canadian J. Phys.*, vol. 36, July 1958, pp. 840–848.

On the Fluorescence of Air, Excited by Fast Electrons: Light Yield as a Function of Pressure, by A. E. Grün, *Canadian J. Phys.*, vol. 36, July 1958, pp. 858–870.

Photon Correlation in Coherent Light Beams, by E. Brannen, H. I. S. Ferguson and W. Wehlau, *Canadian J. Phys.*, vol. 36, July 1958, pp. 871-879.

Cosmic-ray Modulation by Solar Wind, by E. N. Parker, *Phys. Rev.*, vol. 110, June 15, 1958, pp. 1445–1448.

Nature of the Current Reduction in the Primary Cosmic-ray Intensity, by M. A. Pomerantz, S. P. Agarwal and V. R. Potnis, *Phys. Rev. Letters*, vol. 1, no. 2, July 15, 1958, p. 65.

Large-amplitude Hydromagnetic Waves Above the Ionosphere, by A. J. Dessler, *Phys. Rev. Letters*, vol. 1, no. 2, July 15, 1958, p. 68.

Atomic Energy

New Batteries for the Space Age, by D. Linden and A. F. Daniel, *Electronics, Engng. Ed.*, vol. 31, July 18, 1958, pp. 59–65.

Stability of the Pinch, by S. Chandrasekhar, A. N. Kaufman and K. M. Watson.

Proc. Roy. Soc., London, vol. A 245, July 8, 1958, pp. 435–455.

Nuclear Fuels for Hydromagnetic Shock Engine, by C. F. Johnson, *Aviation Age*, vol. 30, Sept. 1958, pp. 118–124.

Stabilized Pinch and Controlled Fusion Power, by S. A. Colgate and H. P. Furth, *Science*, vol. 128, Aug 15, 1958, pp. 337–343, 29 refs.

The Ion Rocket Engine, by R. H. Boden, *N. A. Aviation, Rocketdyne Div., Rep.* R-645, Aug. 26, 1957, 40 pp. (*AFOSR TN-57,573; ASTIA AD* 136,558.)

Outer Space Propulsion by Nuclear Energy: Hearings before Subcommittees . . . Jan. 22, 23, Feb. 6, 1958, *Congress, 85th, 2nd Session, Joint Comm. on Atomic Energy*, Washington, Govt. Print. Off., 1958, 232 pp.

Neutron Generation from Straight Pinches, by R. E. Dunway and J. A. Phillips. *J. Appl. Phys.*, vol. 29, Aug. 1958, pp. 1137–1143.

Supersonic Motion of Vacuum Spark Plasmas along Magnetic Fields, by D. Finkelstein, G. A. Sawyer and T. F. Stratton, *Phys. Fluids*, vol. 1, May-June 1958, pp. 188–192.

Effect of Charge Separation on Plasma Diffusion in a Strong Magnetic Field, by A. N. Kaufman, *Phys. Fluids*. vol. 1, May-June 1958, p. 252.

Containment of a Fully-ionised Plasma by Radio-frequency Fields, by H. A. H. Boot, S. A. Self, and R. B. R. Shersby-Harvie, *SERL Tech. J.*, vol. 8, no. 3, May 1958, pp. 107–131. (Gt. Brit. Services Electronics Res. Lab.)

The Thermodynamic Properties of Hydrogen and Water as Possible Working Fluids for Nuclear Rockets, by I. Sänger-Bredt, *Forschungsinstitut für Physik der Strahlantriebe*, Stuttgart, Mitt. 16, May 1958, 58 pp. (In English.)

Stochastic Theory of Transport Phenomena in a Reacting Plasma at Extreme Temperatures, by H. J. Kaeppler, *Forschungsinst. f. Phys. der Strahlantriebe*, Stuttgart, Mitt. 15, March 1958, 115 pp., (In English.)

Russian Technical Articles*

Perturbation Method for Problems of Strong Detonations, by E. I. Andrianikin, *Izvestiia Akad. Nauk SSSR, Otdelenie Tekhnicheskikh Nauk*, no. 12, Dec. 1958, pp. 5–14. (In Russian.)

Absorption and Dispersion of Infinitesimal Force Plane Waves of Very Small or Very Large Frequency under the Influence of Radiative Heat Transfer, by V. A. Prokoph'ev, *Izvestiia Akad. Nauk SSSR, Otdel. Tekh. Nauk*, no. 12, Dec. 1958, pp. 15–23. (In Russian.)

On the Stability of Permanent Rotations of a Body Around a Fixed Point, by V. V. Rumyantsev, *Prikladnaya Matematika i Mekhanika*, vol. 21, no. 3, 1957, pp. 339–346. (In Russian.)

Calculation of Some Gas Flows for Sonic Velocity, by P. I. Chuskin, *Priklad. Mate-*

* The editors of Technical Literature Digest are making a systematic search for pertinent Russian articles, both in the original Russian and in translated form. For the balance of 1959, these will appear in a separate section with this heading, mainly to draw the readers' attention to the new listing. After that, they will appear item by item under the proper subject headings.

MISSILE HARDWARE by NEWBROOK

Specializing in

- **MOTOR CASES** Solid and Liquid Propellants
- **JATO CASES**
- **NOZZLES**
- **PLENUM CHAMBERS**
- **BLAST TUBES**
- **FUEL INJECTORS**

Finest Welding Facilities
Certified Welders

We have the "KNOW-HOW"

We have developed new techniques, new methods, new processes that effect production economy so necessary to a successful missile program.

Here at Newbrook you will find men with experience gained from doing... a modern plant with up-to-date equipment... precision inspection to meet your most exacting quality control requirements.

And most important, Newbrook specialization results in strict reliability! Let us help you with your Missile Hardware problems.

Machining Nozzles

X-Ray Inspection

Below: Machining Motor Cases

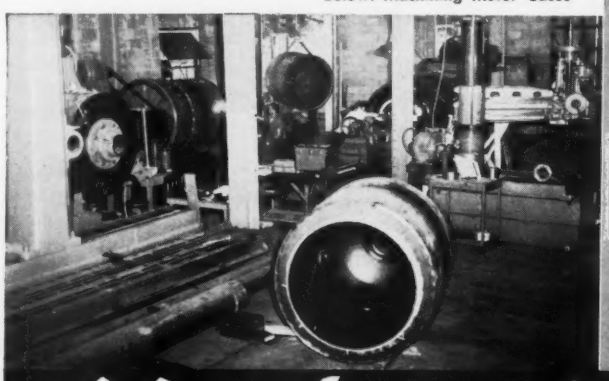

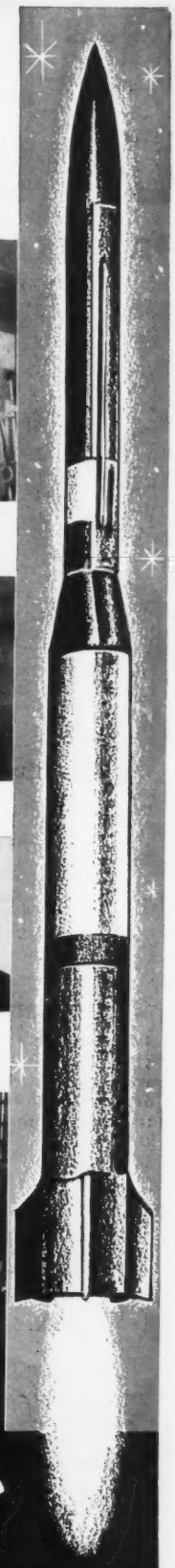

Newbrook
MACHINE CORPORATION

45 MECHANIC ST. PHONE 45 SILVER CREEK, N. Y.

CAE...

PRODUCERS OF SPECIALIZED POWER

Announces two new turbines

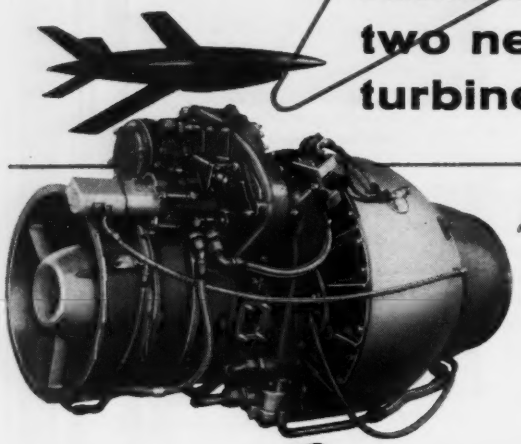

J69-T-29A

1,700 lb.-thrust model for drone applications. The new engine has 60% more thrust with only a 6% increase in weight. It is presently powering the Ryan Q-2C target drone which recently underwent successful flight tests.

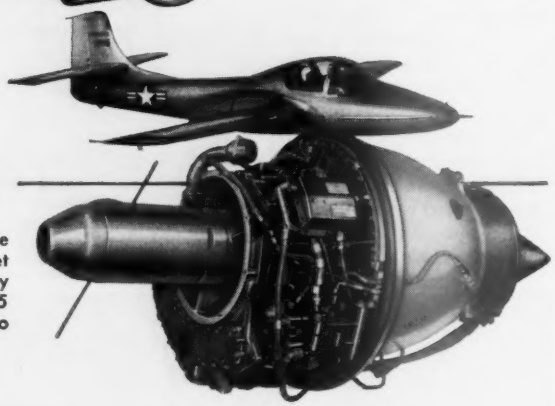

J69-T-25

Latest power plant for the Air Force T-37A twin-jet trainer manufactured by Cessna, the J69-T-25 has increased thrust to 1,025 lbs.

CAE has more than 10 years of turbine engine experience in the medium and low power range. The Air Force MA-1A trailer-mounted turbine air generator manufactured by CAE is on duty at air bases the world over, demonstrating outstanding performance and reliability.

CONTINENTAL AVIATION

CONTINENTAL AVIATION & ENGINEERING CORPORATION

12700 KERCHEVAL, DETROIT 15, MICHIGAN

SUBSIDIARY OF CONTINENTAL MOTORS CORPORATION

mat. i Mekhan., vol. 21, no. 3, 1957, pp. 353–360. (In Russian.)

Zempleri's Theorem in Magnetohydrodynamics, by S. V. Iordansky (translated from *Doklady Akad. Nauk SSSR*, vol. 121, Aug. 1, 1958, pp. 610–612). Morris D. Friedman, Inc., Needham Heights 94, Mass., Translation no. I-117.

The Stability of an Elastic Plate in a Supersonic Flow, by Tung Ming-teh, *Doklady Akad. Nauk SSSR*, vol. 120, June 1, 1958, pp. 726–729. (In Russian.)

The Spread of Perturbations in Media with a Non-linear Dependence of Stresses on Strains and Temperatures, by G. J. Galin, *Doklady Akad. Nauk SSSR*, vol. 120, June 1, 1958, pp. 734–738. (In Russian.)

Aerodynamics of High Speeds, *Grazhdanskaia Aviatsiia*, no. 6, June 1958, pp. 17–20. (In Russian.)

Some Remarks on the High Speed Motion of Bodies in a Weak Gravitational Field, by K. P. Stanukovich, *Doklady Akad. Nauk SSSR.*, vol. 120, May 11, 1958, pp. 277–280. (In Russian.)

Hypersonic Flow Around a Cone at an Angle of Attack, by A. L. Gonor (translated from *Izvestiia Akad. Nauk SSSR. Otdel. Tekh. Nauk*, no. 7, 1958, pp. 102–105). Morris D. Friedman, Inc., Needham Heights 94, Mass., Translation no. G-154, 1958, 6 pp.

Three-dimensional Streamline Flow Around Slender Bodies, by M. D. Khaskind (translated from *Priklad. Matemat. i Mekhan.*, vol. 20, no. 3, 1956, pp. 203–210). Morris D. Friedman, Inc., Needham Heights, 94, Mass., Translation no. K-165, 1958, 12 pp.

On Minimum Drag Bodies at Hypersonic Speeds, by A. L. Gonor and G. G. Chernyi (translated from *Izvestiia Akad. Nauk SSSR Otdel. Tekh. Nauk*, no. 7, 1957, pp. 89–93). Morris D. Friedman, Inc., Needham Heights 94, Mass., Translation no. G-141, 1958, 6 pp.

Certain Peculiarities of the Flow around Bodies at High Supersonic Velocities, by G. L. Grodzovskii (translated from *Izvestiia Akad. Nauk SSSR, Otdel. Tekh. Nauk*, no. 6, 1957, pp. 86–92). Morris D. Friedman, Inc., Needham Heights 94, Mass., Translation no. G-140, 1958, 11 pp.

An Experimental Investigation of the Specific Heat of Water and Steam at High Parameters, by D. S. Rasskazov and A. E. Sheindlin, *Doklady Akad. Nauk SSSR*, vol. 120, June 1, 1958, pp. 771–774. (In Russian.)

Motions with Homogeneous Deformation in Magnetohydrodynamics, by A. G. Kulikovsky, *Doklady Akad. Nauk SSSR*, vol. 120, June 11, 1958, pp. 984–986. (In Russian.)

An Investigation of the Oxygen Dissociation Process Behind a Strong Shock Wave, by S. A. Losev, *Doklady Akad. Nauk SSSR*, vol. 120, July 21, 1958, pp. 1291–1293. (In Russian.)

Plane Problems in Magnetohydrodynamics, by G. S. Golytzin, *Zhur. Eksper. Teor. Fiziki*, vol. 34, March 1958, pp. 688–693. (In Russian.)

A Determination of Molecular Dissociation Energy Based on Equilibrium Studies of Dissociation in Flames, by L. V. Gurvich and I. V. Veits, *Izvestiia Akad. Nauk SSSR, Ser. Fiz.*, vol. 22, June 1958, pp. 673–676. (In Russian.)

A Study of the Burning of Hydrogen with Oxygen Above the Lower Ignition Limit, by A. V. Karmilova and others, *Zhur. Fiz. Khim.*, vol. 32, June 1958, pp. 1193–1204. (In Russian.)

THERMODYNAMICISTS

with ME, ChE or Nuclear Engineering Degrees (BS, MS)

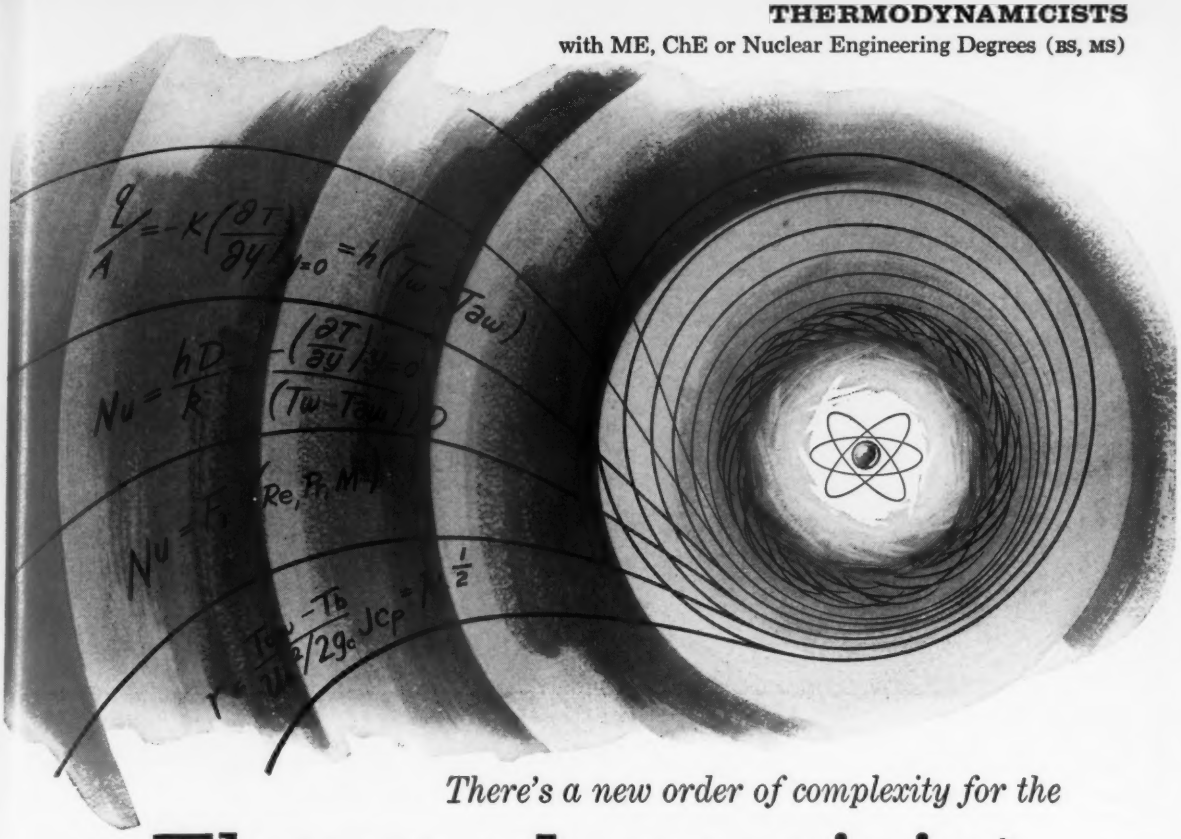

There's a new order of complexity for the

Thermodynamicist

in developing the nuclear propulsion system for aircraft

The requirements for small-size, coupled with high-power density in a reactor for flight propulsion, raise problems in heat transfer never faced before.

As an indication of the technical difficulty of these problems, consider the fact that the reactor now being developed by General Electric for flight propulsion must generate more power than a submarine reactor, though it is only a fraction of the size.

If problems "of this order" attract you, and you have had 3 to 8 years relative experience, your inquiry on any of the following assignments will be welcomed:

- EXPERIMENTAL FLUID DYNAMICS & THERMODYNAMICS ANALYSIS OF REACTOR PERFORMANCE.
- HEAT TRANSFER AND FLUID FLOW DESIGN CALCULATIONS FOR NUCLEAR REACTORS.
- CALCULATIONS ON NUCLEAR DESIGN PARAMETERS OF EXISTING OR PROPOSED REACTOR COMPONENTS AS BASIS FOR CRITICAL EVALUATION.
- DEVELOPMENT TESTING OF HEAT TRANSFER & FLUID FLOW DESIGN OF REACTOR COMPONENTS.
- DEVELOPMENT TESTING OF REACTOR CORE COMPONENTS.
- MECHANICAL DEVELOPMENT OF POWER PLANT COMPONENTS. ALSO OF REACTOR STRUCTURAL COMPONENTS. *(Includes devising and conducting laboratory tests.)*

Assignments are at several levels

Write in confidence, including salary requirement.
Mr. P. W. Christos, Div. 35-MD
AIRCRAFT NUCLEAR PROPULSION DEPARTMENT

GENERAL ELECTRIC

P.O. Box 132 CINCINNATI 15, OHIO

CHEMISTS

- **ANALYTICAL** PhD or equivalent to perform research on new analytical methods and techniques.
- **INORGANIC—ORGANIC** PhD or equivalent for synthetic chemistry. Industrial experience required—preferably in fuels, oxidizers and propellant technology.
- **PHYSICAL**—PhD or M.S. Supervisory experience and background in experimental and theoretical thermodynamics and cybernetics required. To supervise research programs in evaluation of physical and ballistic properties of liquid and solid propellants.
- **PHYSICAL**—B.S. with education or experience emphasis on experimental thermodynamics, particularly heat capacity measurements.

CHEMICAL ENGINEERS

- **DEVELOPMENT ENGINEERS** with experience in design analysis, and operation of bench scale units and pilot plants.
- **SENIOR PROCESS ENGINEER** with broad rather than specialized pilot plant and production experience including design and economic studies. Technical supervisory experience required.

OTHER

- **APPLICATIONS RESEARCH CHEMIST** or **ENGINEER** with industrial experience and interest in several technological fields. To explore new industrial products or applications of existing products.
- **PROPELLANT TESTING SPECIALIST**—Chemist, Physicist or Engineer, B.S., M.S. or PhD with a minimum of 3 years' experience in small scale testing and evaluation of liquid and solid propellants. To organize and coordinate programs for broadened utilization of high energy fuels.

Permanent positions with producer of Boron chemicals and high energy fuels located 25 miles north of Pittsburgh's Golden Triangle.

Please send resume including salary requirements in confidence to:

PERSONNEL MANAGER

CALLERY CHEMICAL COMPANY

Callery
Pennsylvania

RESEARCH ENGINEERS

Stimulating and creative research positions are open at ARMOUR RESEARCH FOUNDATION in the fields of:

Hypersonic Flight Problems
Hydrodynamics
Cavitation Problems
Gas Dynamics

Boundary layer investigations and wake flow problems of high speed flight are some of the programs and concepts you will work on.
M.S. to Ph.D. in Aerodynamics or Mechanical Engineering required with good theoretical background in compressible flow, heat transfer and thermodynamics. We offer outstanding employment benefits including liberal vacation policy. If you would like to work in a well known research organization with some of the leading engineers in this field, please write to:

E. P. Bloch

ARMOUR RESEARCH FOUNDATION

of

Illinois Institute of Technology
10 West 35th Street
Chicago 16, Illinois

Index to Advertisers

AEROJET-GENERAL CORP. ..... 312, Back Cover
D'Arcy Adv. Co., Los Angeles, Calif.

ALLIED CHEMICAL CORP., GENERAL CHEMICAL DIVISION. 243
Kastor, Hilton, Chesley, Clifford & Atherton, Inc., New York, N.Y.

ALLIED CHEMICAL CORP., NITROGEN DIVISION 310
G. M. Basford Co., New York, N. Y.

ARMOUR RESEARCH FOUNDATION OF ILLINOIS INSTITUTE OF TECHNOLOGY 320

BOEING AIRPLANE CO. 308
Calkins & Holden Adv., Seattle, Wash.

BULOVA WATCH CO. 241
Duncan-Brooks, Inc., Garden City, N. Y.

CALLERY CHEMICAL CO. 320
Commerce Adv. Agency, New York, N. Y.

CONTINENTAL AVIATION & ENGINEERING CORP. 318
The Hopkins Agency, Detroit, Mich.

CONVAIR, A DIVISION OF GENERAL DYNAMICS CORP. ..... Third Cover
Lennen & Newell, Inc., Los Angeles, Calif.

THE DECKER CORP. 244
The Harry P. Bridge Co., Philadelphia, Pa.

GENERAL ELECTRIC CO., AIRCRAFT NUCLEAR PROPULSION DEPT. 319
Deutsch & Shea, Inc., New York, N. Y.

GROVE VALVE & REGULATOR CO. 307
L. C. Cole Co., Inc., San Francisco, Calif.

HAWS DRINKING FAUCET CO. 314
Pacific Advertising Staff, Oakland, Calif.

LOCKHEED AIRCRAFT CO. 313
Hal Stebbins, Inc., Los Angeles, Calif.

THE MARTIN CO. 315
VanSant Dugdale & Co., Inc., Baltimore, Md.

NEWBROOK MACHINE CORP. 317
Melvin F. Hall Agency, Inc., Buffalo, N. Y.

RADIO CORPORATION OF AMERICA 305
Al Paul Lefton Co., Inc., Philadelphia, Pa.

REPUBLIC AVIATION CORP. 309
Deutsch & Shea, Inc., New York, N. Y.

ROCKETDYNE, A DIVISION OF NORTH AMERICAN AVIATION, INC. 311
Batten, Barton, Durstine & Osborn, Inc., Los Angeles, Calif.

SOUTHWEST PRODUCTS CO. 314
O. K. Fegan Adv. Agency, Los Angeles, Calif.

THIOKOL CHEMICAL CORP. ..... Second Cover
Dancer-Fitzgerald-Sample, Inc., New York, N. Y.

WESTVACO CHLOR-ALKALI DIVISION, FOOD MACHINERY & CHEMICAL CORP. 306
James J. McMahon, Inc., New York, N. Y.